

Francisco João Anastácio Duarte

PAVEMENT ENERGY HARVESTING SYSTEM TO CONVERT VEHICLES KINETIC ENERGY INTO ELECTRICITY

PhD Thesis in Doctoral Program in Transport Systems, supervised by Professor Adelino Ferreira, presented to the
Department of Civil Engineering of the Faculty of Sciences and Technology of the University of Coimbra

August 2017



UNIVERSIDADE DE COIMBRA

Francisco João Anastácio Duarte

PAVEMENT ENERGY HARVESTING SYSTEM TO CONVERT VEHICLES KINETIC ENERGY INTO ELECTRICITY

PhD Thesis in Doctoral Program in Transport Systems supervised by Professor Adelino Ferreira, presented to the
Department of Civil Engineering of the Faculty of Sciences and Technology of the University of Coimbra

August 2017



UNIVERSIDADE DE COIMBRA

To Silvia and my parents

Financial support

This research work was financed by “Fundação para a Ciência e a Tecnologia” (FCT, Portugal) through the Ph.D. grant with reference SFRH / BD / 95018 / 2013, and was co-financed by the European Social Fund (ESF) within the “Programa Operacional Potencial Humano” (POPH). The POPH research program is integrated in the “National Strategic Reference Framework 2007-2013 - Tipologia 4.1 – Formação Avançada” (QREN 2007-2013).

Several developments of the present research work has been carried out in the framework of project PAVENERGY – Pavement Energy Harvest Solutions (PTDC/ECM-TRA/3423/2014), co-financed by the European Regional Development Fund (POCI-01-0145-FEDER-016676) through the Operational Programme for Competitiveness Factors (COMPETE) and by national funds through “Fundação para a Ciência e a Tecnologia” (FCT, Portugal).

FCT Fundação para a Ciência e a Tecnologia
MINISTÉRIO DA CIÊNCIA, TECNOLOGIA E ENSINO SUPERIOR Portugal



Acknowledgements

The work developed for this thesis could not have been developed and concluded without the support of several people and organizations, to which I would like to express my gratitude.

In first place I would like to express my gratitude to Professor Adelino Ferreira. Firstly, I thank for the invitation and incentive to apply for the Doctoral Program in Transportation Systems, which has led me to start this adventure. Initially this was an area somehow out of my scope and I was not able to perceive all the value of developing the research project within the scope of transportation systems. However, in the course of the PhD work I was able to understand that this project is totally related to transportation system and the PhD, both the doctoral program and the thesis work, has brought an immense value to the project, with a completely new approach that was only possible through this process. I would also want to thank for the continuous mentoring, support and knowledge transmitted through all the research activities, essential to develop this research project successfully.

I would also like to express my gratitude to Professor Paulo Fael, who was my mentor in the final project in electromechanical engineering degree, then in my MSc thesis, and now, once again, he has supported me through the PhD work. His support has been very important during all these stages, but in particular during the PhD work, where his contribution was very important and essential to develop this project. His vision and knowledge in the mechanical engineering area was decisive in many stages of the project. Many thanks for everything!

To Professor António Pais Antunes, I would like to thank for the way he received me in the PhD and in the Civil Engineering Department of the FCTUC, which has facilitated my integration and adaptation to a new environment.

Acknowledgements

To all the professors from the Transportation Systems Doctoral Program of the MIT-Portugal Program I would like to thank for all the knowledge and learning transmitted which, in a way or another, I've used during the developments of my thesis and allowed me to see the project with different perspectives. In particular to Professor Luís Picado Santos, I would like to thank for the perspectives he gave regarding this project, which has challenged me to think differently regarding its practical implementation and allowed me to make some developments that I haven't considered initially.

To Professors Carlos Cabrita and Davide Fonseca, from University of Beira Interior, I would like to thank for the support during the development of the electrical components of the project, which has allowed me to develop these with more confidence and knowledge.

I would like to thank to the companies and their responsible that were involved in the prototype development and experimental validation, as their knowledge and know-how was very important to the results achieved with the developed solution. In particular, I would like to thank to Eng. Santiago Monteiro and Eng. Jorge Silva for the support in the hydraulic project development, and to Eng. Fernando Dias for the support in the mechanical parts development. Their industrial know-how was determinant to adjust the initial version of the prototype to an industrial model. Also, to Eng. Alfredo Amaral for the support in the prototype implementation and for let me test it in his company facilities, which was important to have a test in a relevant environment.

I would also like to express my gratitude to all the Waydip team members who have worked with me in the Waynergy project. They all have played an important role not only in the project development, but also in my professional development and, for that, I thank them all. In particular to João Paulo Champalimaud, for always believe in the project and for the continuous incentive to pursuit its development, my sincere thank you.

To "Fundação para a Ciência e Tecnologia" (FCT), I express my gratitude for the financial support, which allowed me to continue my studies and project development.

Acknowledgements

I would like to thank to Automóvel Cub de Portugal, BP Portugal, Agência Nacional de Inovação and to the CRUP (Conselho de Reitores das Universidades Portuguesas) for the distinction with the Road Safety Innovation Award 2016 (Prémio Inovação Segurança Rodoviária 2016), due to the potential of this project in the contribution to the reduction of road accidents.

Also to Vodafone Portugal, Ericsson and Universidade Nova de Lisboa, for the distinction with the BIG Smart Cities 2017 innovation award, due to the potential contribution of this project in turning cities safer, smarter and sustainable, many thanks!

In the same manner, many thanks to Climate-KIC, the most important European program and competition tackling climate change, for the distinction with the Climate LaunchPad innovation award and selection to represent Portugal in the European final of the competition, for the potential of this project in tackling climate change.

To my family, for always be there in the good and not so good moments and for the continuous motivation to develop this project, I also express my gratitude. In particular to my father, mother and my cousin Henrique, for supporting me during the prototype development and experimental validation, thank you!

Finally, I would like to express my profound and sincere gratitude to my wife, Sílvia, for all the support during the development of this work. It has been quite a journey and she has been always there for me. There are no words to express my gratitude for all the support she gave me during the last years. Thank you so much!

Contents

FINANCIAL SUPPORT.....	VII
ACKNOWLEDGEMENTS.....	IX
CONTENTS	XIII
LIST OF FIGURES.....	XXI
LIST OF TABLES	XXVII
LIST OF ABBREVIATIONS.....	XXXIII
LIST OF NOTATIONS	XXXV
ABSTRACT	XLI
RESUMO.....	XLVII
CHAPTER 1	1
INTRODUCTION	1
1.1 GLOBAL PROBLEM.....	1
1.2 RESEARCH PROBLEM AND OPPORTUNITY FOR INVESTIGATION	4
1.3 MOTIVATION	6
1.4 RESEARCH OBJECTIVES.....	7
1.5 RESEARCH METHODOLOGY	10
1.6 RESEARCH DESIGN.....	13
1.7 STRUCTURE OF THE THESIS.....	17
1.8 PUBLICATIONS.....	20

1.9	REFERENCES.....	25
CHAPTER 2		29
ENERGY HARVESTING IN TRANSPORTATION INFRASTRUCTURES: STATE-OF-THE-ART		29
2.1	INTRODUCTION.....	29
2.2	ENERGY HARVESTING ON ROAD PAVEMENTS.....	30
2.2.1	Introduction	30
2.2.2	Solar energy harvesting on road pavements.....	31
2.2.2.1	Photovoltaic technology.....	31
2.2.2.2	Thermoelectric technology	32
2.2.2.3	Asphalt solar collector technology.....	33
2.2.3	Vehicle mechanical energy harvesting on road pavements.....	34
2.2.3.1	Piezoelectric technology	35
2.2.3.2	Electromagnetic technology.....	36
2.2.4	Technical analysis.....	41
2.3	ENERGY HARVESTING ON RAILWAYS.....	44
2.3.1	Introduction	44
2.3.2	Piezoelectric technologies.....	45
2.3.3	Electromagnetic technologies	46
2.3.3.1	Electromechanical actuation	47
2.3.3.2	Hydraulic actuation.....	49
2.3.3.3	Other actuation types	50
2.3.4	Technical analysis.....	50
2.4	SUMMARY AND CONCLUSIONS.....	52
2.4.1	Road pavement technologies	52
2.4.2	Railway technologies.....	54
2.5	REFERENCES.....	56
CHAPTER 3		67

DEVELOPMENT OF A SOFTWARE TOOL TO EVALUATE THE VEHICLE-ROAD INTERACTION	67
.....	
3.1 INTRODUCTION	67
3.2 VEHICLE DYNAMICS.....	70
3.2.1 Introduction	70
3.2.2 Vehicle forces distribution.....	72
3.2.3 Vehicle dynamics models	73
3.2.4 Vehicle-road interaction models.....	76
3.2.5 Energetic analysis	79
3.3 ROAD PAVEMENT DEVICES	80
3.3.1 Introduction	80
3.3.2 Speed reducers.....	80
3.3.3 Energy harvesting devices	81
3.3.4 Energy captured	84
3.4 SIMULATION SOFTWARE TOOL	85
3.4.1 Introduction	85
3.4.2 Inputs and outputs.....	86
3.4.3 Models	89
3.4.4 Flowchart.....	90
3.5 TECHNICAL ANALYSIS	90
3.5.1 Introduction	90
3.5.2 Simulations and results analysis	92
3.5.2.1 Scenario 1 - Different vehicle models.....	94
3.5.2.2 Scenario 2 - Different interaction models	95
3.5.2.3 Scenario 3 - Different surface profile and displacement	97
3.6 SUMMARY AND CONCLUSIONS	99
3.7 REFERENCES.....	101
CHAPTER 4	105

ROAD PAVEMENT ENERGY HARVESTING: OPTIMIZING THE ENERGY EXTRACTION FROM VEHICLES TO PROMOTE ROAD SAFETY.....	105
4.1 INTRODUCTION	105
4.2 SPEED REDUCTION EQUIPMENT	108
4.2.1 Introduction	108
4.2.2 Existing equipment analysis	109
4.2.3 Energetic analysis	111
4.3 ROAD PAVEMENT ENERGY HARVESTING DEVICE FOR SPEED REDUCTION PURPOSES	112
4.3.1 Introduction	112
4.3.2 Surface profile	112
4.3.3 VRI models with movable surface.....	114
4.3.4 Mechanical system modelling.....	114
4.3.5 Energetic analysis	118
4.4 TECHNICAL ANALYSIS	118
4.4.1 Introduction	118
4.4.2 Comparison between typical SRE and the proposed solution	119
4.4.2.1 Scenario 1 - Standard SRE.....	120
4.4.2.2 Scenario 2 - New device with movable surface	122
4.4.3 Potential contribution to road safety	125
4.5 EXPERIMENTAL VALIDATION.....	127
4.5.1 Introduction	127
4.5.2 Prototype.....	128
4.5.3 Test scenarios.....	130
4.5.4 Computational simulations	132
4.5.5 Experimental results	136
4.5.6 Discussion.....	140
4.6 SUMMARY AND CONCLUSIONS	143
4.7 REFERENCES.....	145

CHAPTER 5	149
ROAD PAVEMENT ENERGY HARVESTING: A NEW ELECTROMECHANICAL DEVICE TO CONVERT VEHICLES MECHANICAL ENERGY INTO ELECTRICAL ENERGY.....	149
5.1 INTRODUCTION.....	149
5.2 RPEH ELECTROMECHANICAL SYSTEM DEVELOPMENT	151
5.2.1 Introduction	151
5.2.2 Existing systems	151
5.2.3 New mechanical system.....	156
5.2.4 Energetic analysis	159
5.3 ELECTRICAL SYSTEM	160
5.3.1 Introduction	160
5.3.2 Electrical generator.....	161
5.3.3 Electric load.....	162
5.3.4 Energetic analysis	163
5.4 TECHNICAL ANALYSIS	164
5.4.1 Introduction	164
5.4.2 Simulation software tool.....	166
5.4.2.1 Software inputs.....	166
5.4.2.2 Software outputs	168
5.4.2.3 Models	169
5.4.3 Computational simulations	171
5.4.3.1 System 1 - RAP	171
5.4.3.2 System 2 - Lever.....	171
5.4.3.3 System 3 - CTS.....	174
5.4.4 Results analysis.....	176
5.5 EXPERIMENTAL VALIDATION.....	178
5.5.1 Introduction	178
5.5.2 Prototype.....	179
5.5.3 Test scenarios.....	182

5.5.4	Computational simulations	183
5.5.5	Experimental results	187
5.5.6	Discussion.....	191
5.6	SUMMARY AND CONCLUSIONS	195
5.7	REFERENCES.....	196
CHAPTER 6	199
ROAD PAVEMENT ENERGY HARVESTING: A NEW HYDRAULIC DEVICE TO CONVERT VEHICLES MECHANICAL ENERGY INTO ELECTRICAL ENERGY	199
6.1	INTRODUCTION.....	199
6.2	RPEH HYDRAULIC SYSTEM DEVELOPMENT.....	201
6.2.1	Introduction	201
6.2.2	Existing systems	201
6.2.3	New hydraulic system with mechanical actuation	206
6.2.4	Electrical system.....	209
6.2.5	Energetic analysis	210
6.3	TECHNICAL ANALYSIS	211
6.3.1	Introduction	211
6.3.2	Typical hydraulic system	213
6.3.3	Hydraulic system with mechanical actuation.....	215
6.3.4	Results analysis.....	216
6.4	SUMMARY AND CONCLUSIONS	218
6.5	REFERENCES.....	220
CHAPTER 7	223
INTEGRATION OF A MECHANICAL ENERGY STORAGE SYSTEM IN A ROAD PAVEMENT ENERGY HARVESTING HYDRAULIC DEVICE	223
7.1	INTRODUCTION.....	223

7.2 MECHANICAL ENERGY STORAGE SYSTEM FOR HYDRAULIC DEVICES.....	225
7.2.1 Introduction	225
7.2.2 Hydraulic pressure storage.....	225
7.2.3 Standard RPEH device with hydraulic system with integrated mechanical energy storage	228
7.2.4 New RPEH device with hydraulic system with integrated mechanical energy storage	233
7.2.5 Energetic analysis	235
7.3 TECHNICAL ANALYSIS	238
7.3.1 Introduction	238
7.3.2 Standard hydraulic system	239
7.3.3 Hydraulic system with mechanical actuation.....	247
7.3.4 Results analysis.....	253
7.3.4.1 Standard hydraulic system	253
7.3.4.2 Hydraulic system with mechanical actuation.....	255
7.4 SUMMARY AND CONCLUSIONS	257
7.5 REFERENCES.....	259
CHAPTER 8	261
A METHODOLOGY FOR TECHNICAL AND ECONOMIC EVALUATION OF ROAD PAVEMENT	
ENERGY HARVESTING DEVICES	261
8.1 INTRODUCTION.....	261
8.2 EVALUATION MODEL DESCRIPTION.....	266
8.2.1 Introduction	266
8.2.2 Technical and economic analysis.....	267
8.2.3 Cost benefit analysis	271
8.3 SOFTWARE TOOL FOR TECHNICAL AND ECONOMICAL EVALUATION OF RPEH	
APPLICATIONS.....	274
8.3.1 Introduction	274
8.3.2 Inputs and calculations.....	275
8.3.3 Outputs and results presentation	278

8.3.4	Sensitivity analysis	281
8.4	CASE STUDIES AND RESULTS	284
8.4.1	Introduction	284
8.4.2	Technical and economic analysis.....	286
8.4.3	Cost benefit analysis	292
8.5	SUMMARY AND CONCLUSIONS	298
8.6	REFERENCES.....	300
CHAPTER 9	305
SUMMARY, CONCLUSIONS AND FUTURE WORK.....		305
9.1	SUMMARY AND CONCLUSIONS	305
9.2	FUTURE WORK	316
9.3	REFERENCES.....	319

List of Figures

Figure 1.1- Diagram showing the components of the proposed solution.....	12
Figure 1.2- Schematic diagram of the research design framework.....	16
Figure 1.3- Schematic diagram of the thesis outline.....	18
Figure 2.1- Road pavement energy harvesting technologies.....	31
Figure 2.2- Railway EH and EG technologies.....	45
Figure 3.1- (a) Quarter car model and (b) bicycle car model (adapted from Jazar, 2008).....	74
Figure 3.2- (a) Quarter car model with a harvester surface on the pavement; and (b) bicycle car model with a harvester surface on the pavement.....	75
Figure 3.3- (a) Perpendicular force distribution; and (b) longitudinal force distribution.....	76
Figure 3.4- Contact patch pressure and resultant distribution of forces.....	78
Figure 3.5- Speed reducer or EHD surface profiles.....	82
Figure 3.6- GUI to select the inputs for the computational model.....	86
Figure 3.7- GUI to present the outputs for the computational model.....	88
Figure 3.8- Simulation software flowchart.....	91
Figure 3.9- Graphical user interface with the standard inputs.....	92
Figure 4.1- Typical SRE surface profiles.....	110
Figure 4.2- New SRE surface profiles for a one degree of freedom movable surface.....	113
Figure 4.3- SRE mechanical system.....	115

Figure 4.4- Force diagrams for the downward motion of the surface.....	116
Figure 4.5- Force diagrams for the upward motion of the surface.....	117
Figure 4.6- SRE with two CTS mechanical systems connected to the surface.....	117
Figure 4.7- Prototype design without sensors and instrumentation components.....	129
Figure 4.8- (a) Prototype system fully assembled with sensors, trimetric view; (b) data logger with instrumentation.	130
Figure 4.9- Prototype installed in a road pavement.	131
Figure 4.10- Simulation results of the total energy harvested for VE_1	135
Figure 4.11- Simulation results of the total energy harvested for VE_2	135
Figure 4.12- Experimental results of the total energy harvested for VE_1	139
Figure 4.13- Experimental results of the total energy harvested for VE_2	139
Figure 5.1- Typical RAP system connected to an IW.....	152
Figure 5.2- Forces distribution for the RAP system, (a) for the vehicle wheel - device surface interaction; and (b) for the upward motion of the device surface without vehicle wheel interaction.....	153
Figure 5.3- Lever system connected to an IW.	154
Figure 5.4- Forces distribution for the lever system, (a) for the vehicle wheel - device surface interaction; and (b) for the upward motion of the device surface without vehicle wheel interaction.....	154
Figure 5.5- Crank to slider system connected to a RAP system and an IW.....	157

Figure 5.6- Forces distribution for the CTS system, (a) for the vehicle wheel - device surface interaction; and (b) for the upward motion of the device surface without vehicle wheel interaction.....	158
Figure 5.7- Purely DC electric circuit with a DC electric generator and a resistive load.	161
Figure 5.8- GUI to select the inputs of the upgraded software tool.	166
Figure 5.9- GUI to select the outputs of the upgraded software tool.	169
Figure 5.10- Mechanical system using two CTS systems and one RAP system.	180
Figure 5.11- Prototype design without sensors and instrumentation components.	181
Figure 5.12- Fully assembled prototype system with sensors.	182
Figure 5.13- Simulation results for VE_1	187
Figure 5.14- Simulation results for VE_2	187
Figure 5.15- Experimental results for VE_1	190
Figure 5.16- Experimental results for VE_2	190
Figure 6.1- Hydraulic system with a DAC connected to a RAP mechanical system.	202
Figure 6.2- Hydraulic system with a mechanical actuation, connected to a double cylinder and a rack and pinion mechanical system.	207
Figure 7.1- Representation of a spring-loaded hydraulic accumulator.	226
Figure 7.2- Representation of a gas-loaded hydraulic accumulator.	227
Figure 7.3- Representation of a RPEH device with a hydraulic transmission system, using a MES unit based on a hydraulic accumulator, spring-loaded type.	229
Figure 7.4- Representation of a RPEH device with a hydraulic transmission system, using a MES unit based on a hydraulic accumulator, gas-loaded type.	229

Figure 7.5- Representation of a RPEH device with a mechanically actuated hydraulic transmission system, using a MES unit based on a hydraulic accumulator, spring-loaded type.	233
Figure 7.6- Representation of a RPEH device with a mechanically actuated hydraulic transmission system, using a MES unit based on a hydraulic accumulator, gas-loaded type... ..	233
Figure 8.1- Schematic representation of RETEES.....	275
Figure 8.2- RETEES GUI to select the inputs for the computational model.	276
Figure 8.3- RETEES flowcharts from Inputs GUI actions and buttons: (a) fill input data action; (b) press "Default values" button; (c) press "Clear all" button; (d) press "Technical & Economic Analysis" button; (e) press "Cost Benefit Analysis" button.....	277
Figure 8.4- RETEES GUI to present the outputs for the TEA.....	279
Figure 8.5- RETEES graphical user interface to present the outputs for the cost benefit analysis.	280
Figure 8.6- RETEES flowcharts from output GUI buttons: (a) press "Sensitivity Analysis" button; (b) press "Print Sens Analysis Results" button; (c) press "Close" button; (d) press "Print Graphics" button.	281
Figure 8.7- RETEES output GUI filled with TEA numerical and graphical results and with the SA graphical results.	282
Figure 8.8- RETEES output GUI filled with CBA numerical and graphical results and with the SA graphical results.	283
Figure 8.9- Sensitivity analysis results for the variation of the (a) <i>AADT</i> ; (b) η ; (c) <i>PPM</i> ; (d) <i>YMP</i>	289

Figure 8.10- SA results for the simultaneous variation of the <i>AADT</i> and η to determine the: (a) <i>LCOE</i> and the (b) <i>CF</i>	291
Figure 8.11- SA results of a CBA for a GI application, for the variation of the (a) <i>AADT</i> ; (b) η ; (c) <i>PPM</i> ; (d) <i>YMP</i> ; (e) <i>GIEP</i>	294
Figure 8.12- Results of a multi-variable SA for a CBA to a RPEH system with a GI application, for the (a) <i>ROC</i> ; (b) <i>NPV</i> ; (c) <i>IRR</i>	296

List of Tables

Table 2.1- Patents related to electromechanical systems.	39
Table 2.2- Parameters for performing a technical analysis.	42
Table 2.3- Technical analysis of different road pavement energy harvesting technologies.	43
Table 2.4- Technical analysis of different railway energy harvesting technologies.	51
Table 3.1- Vehicle perpendicular force distribution on level and inclined pavements.	72
Table 3.2- Vehicle longitudinal force distribution on level and inclined pavements.	73
Table 3.3- Perpendicular and longitudinal wheel forces on an inclined surface.	77
Table 3.4- Speed reducer or EHD surface profile's equations.	83
Table 3.5- Fixed and initial values for the simulation variables.	93
Table 3.6- Scenario 1 results.	94
Table 3.7- Scenario 2 results.	96
Table 3.8- Scenario 3 results.	98
Table 4.1- Levels of acceptability of ride quality (ISO, 1997).	119
Table 4.2- Fixed and initial values for the simulation variables.	120
Table 4.3- Standard SRE simulation results.	121
Table 4.4- New SRE with movable surface simulation results.	124
Table 4.5- Speed reduction case study.	126
Table 4.6- Test scenarios for the system prototype.	131

Table 4.7- Fixed and initial values for the simulation variables.	132
Table 4.8- Simulation results of the new SRE with movable surface for VE_1	133
Table 4.9- Simulation results of the new SRE with movable surface for VE_2	134
Table 4.10- Prototype test results for VE_1	137
Table 4.11- Prototype test results for VE_2	138
Table 4.12- Difference between the simulations and experimental results for tested scenarios using VE_1	141
Table 4.13- Difference between the simulations and experimental results for tested scenarios using VE_2	142
Table 5.1- RAP system modelling.	155
Table 5.2- Lever system modelling.	156
Table 5.3- CTS system modelling using a RAP and an IW.	159
Table 5.4- Input data for the computational simulations of the three systems.	165
Table 5.5- Simulation results for the energy outputs of the RPEH device components using the RAP mechanical system.	172
Table 5.6- Simulation results for the efficiencies of the RPEH device components using the RAP mechanical system.	172
Table 5.7- Simulation results for the energy outputs of the RPEH device components using the lever mechanical system.	173
Table 5.8- Simulation results for the efficiencies of the RPEH device components using the lever mechanical system.	174

Table 5.9- Simulation results for the energy outputs of the RPEH device components using the CTS mechanical system.	175
Table 5.10- Simulation results for the efficiencies of the RPEH device components using the CTS mechanical system.	176
Table 5.11- Test scenarios for the system prototype.....	183
Table 5.12- Fixed and initial values for the simulation variables.	184
Table 5.13- Simulation results of the new RPEH system for VE_1	185
Table 5.14- Simulation results of the new RPEH system for VE_2	186
Table 5.15- Prototype test results for VE_1	188
Table 5.16- Prototype test results for VE_2	189
Table 5.17- Difference between the simulations and experimental results for tested scenarios using VE_1	193
Table 5.18- Difference between the simulations and experimental results for tested scenarios using VE_2	194
Table 6.1- Force diagrams for the RPEH DS, hydraulic circuit and DAC piston.....	203
Table 6.2- RPEH DS physical modelling.	204
Table 6.3- RPEH hydraulic circuit with a DAC connected to a RAP system physical modelling.	204
Table 6.4- Force diagrams for the RPEH DS, mechanical system, hydraulic circuit and DAC piston.	207
Table 6.5- RPEH DS and mechanical system physical modelling.....	208

Table 6.6- RPEH mechanically actuated hydraulic circuit with a DAC connected to a RAP system physical modelling.....	209
Table 6.7- Input data for the computational simulations of the hydraulic systems.....	212
Table 6.8- Simulation results for the energy outputs of the RPEH device components using a standard hydraulic system.....	213
Table 6.9- Simulation results for the efficiencies of the RPEH device components using a standard hydraulic system.....	214
Table 6.10- Simulation results for the energy outputs of the RPEH device components using a hydraulic system with mechanical actuation.....	215
Table 6.11- Simulation results for the efficiencies of the RPEH device components using a hydraulic system with mechanical actuation.....	216
Table 7.1- Force diagrams for the RPEH DS, MES system and DAC piston.....	230
Table 7.2- System modelling for the RPEH DS charging the MES device (spring loaded).....	231
Table 7.3- System modelling for the MES device (spring loaded) releasing stored energy to the hydraulic and mechanical system.....	232
Table 7.4- Force diagrams for the RPEH DS, mechanical system, MES system and DAC piston.....	235
Table 7.5- System modelling for the RPEH hydraulic circuit with a mechanical actuation charging the MES device (spring-loaded).....	236
Table 7.6- System modelling for the MES device (spring-loaded) releasing the stored energy for the hydraulic and mechanical system.....	237
Table 7.7- Input data for the computational simulations of the three systems.....	240

Table 7.8- Simulation results for the energy outputs of the RPEH device components using a standard hydraulic system, without MES.....	241
Table 7.9- Simulation results for the efficiencies of the RPEH device components using a standard hydraulic system, without MES.....	242
Table 7.10- Simulation results for the energy outputs of the RPEH device components using a spring-loaded hydraulic accumulator connected to a standard hydraulic system.	243
Table 7.11- Simulation results for the efficiencies of the RPEH device components using a spring-loaded hydraulic accumulator connected to a standard hydraulic system.	244
Table 7.12- Simulation results for the energy outputs of the RPEH device components using a gas-loaded hydraulic accumulator connected to a standard hydraulic system.	245
Table 7.13- Simulation results for the efficiencies of the RPEH device components using a gas-loaded hydraulic accumulator connected to a standard hydraulic system.....	246
Table 7.14- Simulation results for the energy output of the RPEH device using a mechanically actuated hydraulic system without MES.....	248
Table 7.15- Simulation results for the efficiencies of the RPEH device using a mechanically actuated hydraulic system without MES.....	248
Table 7.16- Simulation results for the energy outputs of the RPEH device components using a spring-loaded hydraulic accumulator connected to a mechanically actuated hydraulic system.	249
Table 7.17- Simulation results for the efficiencies of the RPEH device components using a spring-loaded hydraulic accumulator connected to a mechanically actuated hydraulic system.	250

Table 7.18- Simulation results for the energy outputs of the RPEH device components using a gas-loaded hydraulic accumulator connected to a mechanically actuated hydraulic system. ...	251
Table 7.19- Simulation results for the efficiencies of the RPEH device components using a gas-loaded hydraulic accumulator connected to a mechanically actuated hydraulic system.....	252
Table 8.1- Average energy released by vehicle category in relation to the vehicle speed ($E_{HW} = 0.25$ m).	285
Table 8.2- Initial values for the simulation variables.....	287
Table 8.3- Results for a TEA to a RPEH application.....	288
Table 8.4- Results of a multi-variable SA for a TEA to a RPEH application.....	290
Table 8.5- Simulation results for a CBA on a GI application.	293
Table 8.6- Results of a multi-variable SA for a CBA to a RPEH system with a GI application.	295
Table 8.7- Simulation results for a CBA on a SC application.	298

List of Abbreviations

AC	Alternating Current
ACV	Accumulator Control Valve
ASC	Asphalt Solar Collector
CBA	Cost Benefit Analysis
CF	Capacity Factor
CG	Centre of Gravity
CO ₂	Carbon Dioxide
CPA	Contact Patch Analysis
CTS	Crank to Slider
CV	Control Valve
DAC	Double Acting Cylinder
DC	Direct Current
EA	Energy Application
EG	Energy Generation
EH	Energy Harvesting
EHD	Energy Harvesting Device
EL	Electric Load
EU	European Union
FW	Front Wheel
GI	Grid Injection
GUI	Graphical User Interface
ICT	Information and Communications Technologies
IM	Installation Method
INPI	Instituto Português de Propriedade Industrial
IPEG	Innowattech Piezo Electric Generator
IRR	Internal Rate of Return
IT	Information Technologies
IW	Inertia Wheel
LCOE	Levelized Cost of Electricity
MEMS	Micro Electromechanical Systems
MES	Mechanical Energy Storage
NPV	Net Present Value
OECD	Organization for Economic Co-operation and Development
PPW	Price Per installed Watt

PRV	Pressure Relief Valve
PV	Photovoltaic
QW	Quantum Well structured
RAP	Rack and Pinion
RES	Hydraulic Reservoir
RETEES	Road Energy Technical and Economic Evaluation Software
RoadVISS	Road Vehicle Interaction Simulation Software
ROC	Return of Capital
RPEH	Road Pavement Energy Harvesting
RPEH DS	Road Pavement Energy Harvesting Device Surface
RW	Rear Wheel
SA	Sensitivity Analysis
SAC	Single Acting Cylinder
SERSO	Solar Energy Recuperation from the Road Pavement
SFA	Single Force Analysis
SP	Surface Profile
SRE	Speed Reducer Equipment
SC	Self Consumption
TEA	Technical and Economic Analysis
TEG	Thermoelectric Generator
TNO	Toegepast Natuurwetenschappelijk Onderzoek
TRL	Technology Readiness Level
TUB	Hydraulic Tube
UK	United Kingdom
USA	United States of America
VRI	Vehicle-Road Interaction
WHO	World Health Organization

List of Notations

a	Vehicle acceleration (m/s^2)
a_1	Vehicle geometry - A1 (CG-FW) (m)
a_2	Vehicle geometry - A2 (CG-RW) (m)
A	Area (m^2)
A_{cp}	Area of the DAC piston (m^2)
A_h	Area of the contact point between the RPEH DS and the TUB (m^2)
A_{ha}	Pavement or harvester surface area (m^2)
A_{rod}	Area of the DAC rod (m^2)
A_{sp}	Area of the SAC piston (m^2)
A_{sto}	Area of the MES hydraulic accumulator (m^2)
A_{tub}	Area of the hydraulic circuit tube (m^2)
AADT	Annual average daily traffic (vehicles/day)
AEG	Annual energy generated (kWh)
ATE	Annual traffic evolution (%)
b	Friction coefficient
b_{cb}	Mechanical system clutch bearing friction coefficient
b_{gen}	Electrical generator friction coefficient
cp_a	Contact patch half length (m)
C_d	Hydraulic valves discharge coefficient
C_s	Vehicle suspension damping (Ns/m)
C_u	Vehicle unsprung mass damping (Ns/m)
CAPEX	Initial capital invested (€)
CCF	CO ₂ conversion factor (kWh to g CO ₂)
CF	Capacity factor (%)
CFLO	Cash-flow (€)
CFLOU	Updated Cash-flow (€)
COY	CO ₂ avoided per year (ton)
COP	Total CO ₂ avoided - period (ton)
CP_A	Contact patch area (m^2)
CVT	CO ₂ value per ton (€/ton)
d_{tub}	Hydraulic tube inner diameter (m)
d_1	Distance from the lever axes to the force actuation point (m)
d_2	Distance from the lever axes to the rack / lever total length (m)
DT_{cat}	Daily traffic by vehicle category (vehicles/day)

DTEG	Daily energy generated (kWh)
E	Energy (J)
E_a	Electric generator armature induced voltage (V)
E_{De}	Energy delivered by the mechanical system (J)
E_{Ge}	Energy generated by the electric system (J)
E_{Ha}	Energy harvested (J)
E_{Lo}	Energy consumed by the electric load (J)
E_{sto}	Energy stored by the mechanical system (J)
E_{Su}	Energy absorbed by the road pavement/EHD surface material (J)
E_{Tr}	Energy transmitted by the mechanical system (J)
E_v	Energy released from the vehicle (J)
E'	Elasticity modulus (Pa)
EEP	Extra equipment cost (€)
EG_{cat}	Total energy generated by each vehicle category (kWh)
EGV_{cat}	Average energy generated by vehicle category (cat), per module (J)
EHW	RPEH device' surface width (m)
ERV_{cat}	Average energy released by vehicle category (J)
ET	Electric torque (N.m)
F	Force (N)
F_a	Acceleration force (N)
F_d	Drag force (N)
F_{hl}	Force related to the hydraulic circuit losses (N)
F_k	Mechanical system spring force (N)
F_l	Lift force (N)
F_{los}	Force losses due to friction (N)
F_{sto}	MES piston force (N)
F_{SMj}	Force transmitted by the mechanical system element j (N)
F_{SMjs}	Opposition force from the mechanical system element j (N)
F_{SHj}	Force transmitted by the hydraulic system element j (N)
F_{SHjs}	Opposition force from the hydraulic system element j (N)
F_x	Vehicle wheel longitudinal force (N)
$F_{x.f}$	Vehicle front wheel longitudinal force (N)
$F_{x.r}$	Vehicle rear wheel longitudinal force (N)
F_z	Vehicle wheel perpendicular force (N)
$F_{z.f}$	Vehicle front wheel perpendicular force (N)
$F_{z.r}$	Vehicle rear wheel perpendicular force (N)
g	Gravitational acceleration (m/s^2)
GIAEP	GI - Annual energy price (€/kWh)
GIAI	GI - Annual income (€)
GIEP	GI - Energy price - initial (€/kWh)

GIPI	GI - Total income - period (€)
GIYE	GI - Annual price evolution (%)
h	Height (m)
h_{CG}	Height of the vehicle' centre of gravity (m)
h_{cr}	Mechanical system crank height between axes (m)
h_{cr-in}	Initial crank height between axes (m)
h_{max}	Surface maximum height (m)
h_t	Device surface height, related to its base (m)
i	Iteration
I_a	Electric generator armature current (A)
I_{Lo}	Electric circuit load current (A)
I_y	Vehicle inertia moment ($kg.m^2$)
ICPM	Installation cost per RPEH unit (€)
INF	Annual price inflation (%)
IPM	Installed power per module (W)
J_{gen}	Moment of inertia of the electric generator ($kg.m^2$)
J_{iw}	Moment of inertia of the inertia wheel ($kg.m^2$)
J_l	Moment of inertia of the mechanical system lever ($kg.m^2$)
J_p	Moment of inertia of the mechanical system pinion ($kg.m^2$)
J_{ra}	Moment of inertia of the mechanical system rack ($kg.m^2$)
J_{sh}	Moment of inertia of the mechanical system shaft ($kg.m^2$)
k_a	Electric generator constant
K_h	EH device (spring) stiffness (N/m)
K_s	Vehicle suspension stiffness (N/m)
K_{sto}	Spring-loaded hydraulic accumulator stiffness (N/m)
K_t	Vehicle tire stiffness (N/m)
K_u	Vehicle unsprung mass stiffness (N/m)
KH	Loss coefficient for hydraulic elements
l	Length (m)
l_{cr}	Crank length (m)
l_{tub}	Hydraulic circuit tube length (m)
l_v	Vehicle length (m)
l_0	Pavement or harvest surface thickness (m)
L_a	Electric generator armature inductance (H)
L_{max}	EH device surface' maximum length (m)
LAT	Lane annual traffic - average (vehicles)
LCOE	Levelized cost of electricity (€/kWh)
LDT	Lane daily traffic - average (vehicles)
LMT	Lane monthly traffic - average (vehicles)
m_{cp}	DAC piston mass (kg)

m_h	RPEH DS mass (kg)
m_{iw}	Mechanical system inertia wheel mass (kg)
m_s	Vehicle sprung mass (kg)
m_{SP}	Mechanical system piston mass (kg)
m_{sto}	MES piston mass (kg)
m_u	Vehicle unsprung mass (kg)
m_v	Vehicle mass (kg)
NL	Number of road lanes
NMI	Number of installed RPEH units
NMP	Number of RPEH devices installed meters
NPV	Net present value (€)
OCI	Other costs involved (€)
OPEX	Annual operational costs (€)
p_{atm}	Atmospheric pressure (Pa)
P_{gas}	MES gas pressure (Pa)
p_{sto}	MES hydraulic fluid pressure (Pa)
P_{Ge}	Power produced by the electric generator (W)
P_{Lo}	Power consumed by the electric load (W)
PPM	Price per RPEH module (€)
PPW	Price per installed Watt (€/W)
$q(x)$	Pressure distribution on the contact patch (N/m ²)
q_0	Tire maximum normal pressure (N/m ²)
r_p	Mechanical system pinion radius (m)
r_1	Mechanical system gear 1 radius (m)
r_2	Mechanical system gear 2 radius (m)
R_a	Electric generator armature resistance (Ω)
R_{Lo}	Electric circuit load resistance (Ω)
R_x	Tire rolling resistance (N)
$R_{x.f}$	FW tire rolling resistance (N)
$R_{x.r}$	RW tire rolling resistance (N)
ROC	Return of capital payback (years)
SCAH	SC - Daily average consumption hours (h/day)
SCAS	SC - Annual savings (€)
SCECP	SC - Total energy costs - period (€)
SCEI	SC - Energy price annual inflation (%)
SCEP	SC - Energy price - initial (€/kWh)
SCEPY	SC - Annual energy price (€/kWh)
SCIP	SC - Installed power (W)
SCPC	SC - Generated energy contribution (%)
SCPCE	SC - Total consumed energy - period (kWh)

SCYCE	SC - Annual consumed energy (kWh)
t	Time (s)
T_{SM}	Mechanical system torque (N.m)
TAS	Traffic average speed (km/h)
TD_{cat}	Traffic distribution by vehicle category (%)
TE_{Ge}	Total energy generated - period (kWh)
TIP	Total installed power (W)
TINV	Total investment - period (€)
U_a	Electric voltage generated (V)
U_{Lo}	Electric circuit load voltage (V)
v	Vehicle speed (m/s)
v_{ini}	Vehicle initial speed (km/h)
v_{red}	Vehicle speed reduction (km/h)
V_{gas}	MES gas volume (m ³)
V_{sto}	MES hydraulic fluid volume (m ³)
VCP	Total avoided CO ₂ valuation - period (€)
VCY	Avoided CO ₂ valuation per year (€)
x	Vehicle body vertical displacement (m) / motion coordinate
x_{CP}	Contact patch position (m)
x_{cp}	DAC piston displacement (m) / motion coordinate
x_{cr}	Mechanical system crank axes horizontal distance (m)
x_h	EH device' surface vertical displacement (m) / motion coordinate
x_{h-max}	Maximum displacement of the RPEH DS (m)
x_{hf}	Hydraulic fluid displacement (m) / motion coordinate
x_K	Mechanical system spring displacement (m) / motion coordinate
x_{l1}	Mechanical system lever displacement (m) / motion coordinate (in d_1)
x_{l2}	Mechanical system lever displacement (m) / motion coordinate (in d_2)
x_{ra}	Mechanical system rack displacement (m) / motion coordinate
x_s	Vehicle sprung mass vertical displacement (m) / motion coordinate
x_{sp}	Mechanical system / SAC piston displacement (m) / motion coordinate
x_{sp-in}	Initial position of the mechanical system piston / SAC piston (m)
x_{sto}	MES piston displacement (m) / motion coordinate
x_u	Vehicle unsprung mass vertical displacement (m) / motion coordinate
x_1	Front wheel vertical displacement (m) / motion coordinate
x_2	Rear wheel vertical displacement (m) / motion coordinate
y_1	Road excitation at the front wheel (m)
y_2	Road excitation at the rear wheel (m)
YMP	Yearly maintenance cost per unit (€)
YRS	Number of years (years)
ΔCP_A	Variation of the contact patch area (m ²)

Δl	Material deflection (m)
Δp	Hydraulic pressure variation / drop (Pa)
Δt	Time variation for each iteration (s)
ΔT	Thermal gradient of the road pavement ($^{\circ}\text{C}$)
ΔV_{sto}	Variation of the MES hydraulic fluid volume (m^3)
Δx_i	Position variation for the variable i (m)
θ	Vehicle body pitch angle (rad) / motion coordinate
θ_{cr}	Mechanical system crank angle (rad) / angular motion coordinate
$\theta_{\text{cr-in}}$	Initial angle of the mechanical system crank (rad)
θ_{iw}	Mechanical system IW angle (rad) / angular motion coordinate
θ_l	Mechanical system lever angle (rad) / angular motion coordinate
θ_p	Mechanical system pinion angle (rad) / angular motion coordinate
θ_{ra}	Mechanical system lever' rack angle (rad) / angular motion coordinate
φ	Road pavement / EH device surface angle (longitudinal direction) (rad)
η	Energy conversion efficiency (%)
η_{Co}	Energy conversion efficiency from the E_{Ge} to the E_{Lo} (%)
η_{De}	Energy conversion efficiency from the E_{Tr} to the E_{De} (%)
η_{Ele}	Energy conversion efficiency from the E_{De} to the E_{Lo} (%)
η_{Ge}	Energy conversion efficiency from the E_{De} to the E_{Ge} (%)
η_{Ha}	Energy conversion efficiency from the E_v to the E_{Ha} (%)
η_{Mec}	Energy conversion efficiency from the E_{Ha} to the E_{De} (%)
η_{RPEH}	Energy conversion efficiency from the E_{Ha} to the E_{Lo} (%)
η_{sto}	Energy conversion efficiency from the E_{Tr} to the E_{sto} (%)
η_{Tot}	Energy conversion efficiency from the E_v to the E_{Lo} (%)
η_{Tr}	Energy conversion efficiency from the E_{Ha} to the E_{Tr} (%)
μ	Kinematic viscosity (St)
ρ	Hydraulic fluid density (kg/m^3)

Abstract

The increasing movement of human beings from rural areas to the city, known as urbanization, the lifestyle changes and the increase in use of new technologies have led to an exponential increase in the consumption of the planet's resources in recent years. Demand for energy and in particular electric energy has increased immensely. Change is urgently required to the current paradigm, in which energy is produced in large power plants outside cities, consuming non-renewable resources and inducing energy loss from production to final consumption. Energy production must use renewable resources, be decentralized, be done near to where the energy is consumed and, preferably, when needed.

Within renewable energies, the concept of energy harvesting on a micro scale has recently been adopted, where, from small energy variations, it is possible to generate electrical energy. The road surface is continuously exposed to vehicle loads from which it is possible to extract energy, which, using specific technologies, may be transformed into electrical energy.

This thesis starts by evaluating the existing solutions in the road pavement energy harvesting (RPEH) field, allowing us to draw conclusions regarding the efficiency of each system, its working principle, its stage of development and method of installation.

Then, a new methodology is defined to develop a new RPEH system, in which an energetic analysis is conducted, quantifying the energy delivered from a vehicle's wheels to the surface of the device, the energy transmitted by the mechanical system and delivered to an electromechanical converter, the electrical energy generated and consumed. This methodology will allow us to understand and quantify the efficiency of each component and optimize it, allowing us to achieve a maximum energy conversion efficiency for the proposed and evaluated systems.

Abstract

Based on this methodology, a software tool is developed, to simulate and study vehicle–road interaction (VRI) to quantify the forces induced and energy released from vehicles to the road pavement, in different vehicle motion scenarios, and the energy absorbed by the road surface, speed reducers or a specific RPEH device. The software tool also enables users to quantify the energy efficiency of the process. The developed software tool was called RoadVISS and it allows us to study VRI with greater precision than existing tools, especially when energetic analyses are performed and when speed reduction or RPEH devices are applied on the pavement.

Based on this tool, a study on speed reducer equipment optimization was performed, and a new solution to promote more effective speed reduction without any driver action was proposed. Through computational simulations it was concluded that the proposed solution is able to extract 81.0% more energy than standard speed reducers, with 87.0% less impact on the vehicle body for similar scenarios. A prototype was developed and tested, which allowed us to validate most of the computational simulation results. This solution has a great potential to contribute to road safety, as it is more effective than existing solutions.

After this, new solutions to convert the vehicle's mechanical energy into electrical energy were developed, one based on an electromechanical system, another based on a hydraulic system with mechanical actuation without mechanical energy storage, and another, similar to the previous one, using mechanical energy storage. All systems were developed using the defined methodology. The physical models of each system were defined and incorporated in the RoadVISS software tool, allowing us to develop a new software tool directed at the development of RPEH devices. Through computational simulations it was proved that all systems are more efficient than all existing solutions studied in the state-of-the-art. The electromechanical device was also subjected to an experimental validation and, for specific scenarios, it proved to have a conversion efficiency of 60.5%, a higher value than current state-of-the-art, making it the most efficient system validated through experimental tests. This system should be optimized so that full validations are achieved for other test scenarios. The hydraulic systems

Abstract

should also be subjected to experimental validations to compare experimental data with the computational simulation results.

Finally, evaluation models were developed to perform the technical and economical analysis of RPEH systems, as well as performing a cost benefit analysis for the application of this type of energy generation solution as an energy source for different applications. The models also allow a sensitivity analysis to be performed, meaning each parameter value is optimized to determine the best conditions for achieving economic viability. Some case studies are presented and conclusions are drawn about the required conditions for these systems to be economically viable.

Keywords

Road Pavement

Energy Harvesting

Road Safety

Vehicle-Road Interaction

System Modelling

Experimental Validation

Cost-Benefit Analysis

Resumo

A crescente mobilização do ser humano para as cidades, as mudanças no estilo de vida e a crescente adoção de novas tecnologias, levaram a um aumento exponencial do consumo de recursos do planeta nos últimos anos, sendo a energia um dos recursos em que o consumo aumentou muito significativamente, com ênfase especial na energia elétrica. Nesta área, urge mudar o paradigma atual em que a produção é feita em grandes centrais, fora das cidades, consumindo recursos não renováveis e induzindo perdas de energia desde a produção até ao local de consumo final. A produção de energia elétrica deverá ser feita a partir de recursos renováveis, de forma descentralizada, próximo dos locais onde esta energia é consumida e, preferencialmente, no momento em que é necessário consumir essa energia.

Na área das energias renováveis foi adotado recentemente o conceito de *energy harvesting*, vulgarmente traduzido para "colheita de energia", sendo novidade quando aplicado a uma escala "micro" em que, a partir de pequenas variações de energia é possível gerar energia elétrica. A superfície do pavimento rodoviário está continuamente exposta às cargas de veículos que se deslocam sobre a mesma, a partir das quais é possível captar energia que, através da utilização de tecnologias específicas, pode ser transformada em energia elétrica.

Esta tese começa pela avaliação das soluções existentes na área da "colheita de energia" em pavimentos rodoviários (RPEH), permitindo tirar conclusões acerca da eficiência de cada sistema, do seu princípio de funcionamento, estado de desenvolvimento e do método de instalação no pavimento rodoviário.

É de seguida definida uma metodologia para desenvolver um novo sistema de RPEH, na qual é realizada uma análise energética, quantificando a energia entregue pelas rodas do veículo para a superfície do equipamento de RPEH, a energia transmitida pelo sistema mecânico e entregue a um conversor eletromecânico, a energia elétrica gerada e também

consumida. Esta metodologia irá permitir compreender e quantificar a eficiência de cada componente e otimizá-lo, permitindo assim alcançar a máxima eficiência de conversão de energia possível para cada sistema proposto e avaliado.

Com base nesta metodologia foi desenvolvido um *software* para simular e estudar a interação veículo-pavimento (VRI), de modo a quantificar as forças induzidas e a energia libertada de um veículo para o pavimento rodoviário para diferentes cenários de movimento do veículo, e ainda a energia absorvida pela superfície do pavimento, ou por equipamentos redutores de velocidade ou equipamentos de RPEH. Esta ferramenta permite também aos seus utilizadores quantificar a eficiência energética deste processo. Este *software*, denominado RoadVISS, permite estudar a VRI com uma precisão superior às ferramentas existentes, especialmente quando são realizadas análises energéticas e quando o estudo é relativo a equipamentos de redução de velocidade ou de RPEH.

Utilizando este *software*, foi realizado um estudo para otimização de equipamentos redutores de velocidade, sendo proposta uma nova solução para promover uma redução de velocidade mais eficaz, sem qualquer ação dos condutores de veículos. Através das simulações computacionais realizadas concluiu-se que a solução proposta é capaz de extrair 81,0% mais energia dos veículos em relação aos sistemas redutores de velocidade normalmente utilizados, com um impacto 87,0% menor no *chassi* do veículo, em cenários semelhantes. Foi desenvolvido e testado um protótipo da solução proposta, que nos permitiu validar a maioria dos resultados obtidos a partir das simulações computacionais. Esta solução apresenta um grande potencial para contribuir para a promoção da segurança rodoviária, sendo mais eficaz do que as soluções existentes.

De seguida foram desenvolvidas novas soluções para converter a energia mecânica de veículos em energia elétrica, a primeira baseada num sistema eletromecânico, a segunda baseada num sistema hidráulico com atuação mecânica, sem armazenamento de energia mecânica, e a terceira semelhante à segunda, mas utilizando um acumulador de energia mecânica. Os modelos físicos de cada sistema foram definidos e incorporados no *software* RoadVISS, o que nos permitiu desenvolver uma nova ferramenta direcionada

Resumo

para o desenvolvimento de equipamentos de RPEH. Através das simulações computacionais realizadas foi possível verificar que todos os sistemas propostos são mais eficientes que as várias soluções existentes, previamente estudadas no estado-da-arte. O equipamento eletromecânico foi submetido a uma validação experimental e, em cenários específicos, provou ter uma eficiência de conversão de 60,5%, um valor superior ao atual estado-da-arte, passando assim a ser o sistema mais eficiente validado através de testes experimentais na literatura. Este sistema deve ainda ser otimizado, de modo que se alcance uma validação completa para todos os cenários de teste. Os sistemas hidráulicos propostos e estudados devem também ser submetidos a validações experimentais de forma a comparar os dados experimentais com os resultados obtidos a partir das simulações computacionais.

Finalmente, foram desenvolvidos modelos de avaliação para realizar a análise técnica e económica dos equipamentos de RPEH, bem como para realizar análises de custo-benefício para a aplicação deste tipo de solução de geração de energia como fonte energética para diferentes aplicações. Os modelos propostos permitem também a realização de análises de sensibilidade, permitindo assim otimizar o valor de cada parâmetro de modo a definir as condições ótimas para que um sistema de RPEH tenha viabilidade económica. Alguns estudos de caso são apresentados, permitindo tirar conclusões acerca das condições necessárias para que estes sistemas sejam economicamente viáveis.

Palavras-chave

Pavimento Rodoviário

Energy Harvesting

Segurança Rodoviária

Interação Veículo-Pavimento

Modelação de Sistemas

Validação Experimental

Análise Custo-Benefício

*"Action without vision is only passing time,
vision without action is merely day dreaming,
but vision with action can change the world"*

Nelson Mandela

**PAVEMENT ENERGY HARVESTING
SYSTEM TO CONVERT VEHICLES
KINETIC ENERGY INTO
ELECTRICITY**

Chapter 1

Introduction

1.1 Global problem

The increasing movement of human beings from rural areas to the city has led to an exponential increase in the consumption of the planet's resources in recent years. Energy, and in particular electrical energy, is one of the resources for which there has been great increase in demand (IEA, 2016a). Currently, and for the first time in history, approximately 54% of the world's population lives in cities (Buhaug and Urdal, 2013; WHO, 2016; UN, 2016) and, by 2050, this number will increase by more than 3 billion people, reaching almost 70% (WHO, 2016; UN, 2016) and leading to global urbanization, which will lead to further increases in energy consumption, especially in cities.

Making cities “smart” is emerging as a strategy to mitigate the problems generated by the urban population growth and fast urbanization. There are various different definitions of the smart city concept in the literature, which can be summarised as follows:

- A city performing well in a forward-looking way in terms of its economy, people, governance, mobility, environment and living, built on the smart

combination of endowments and activities of decisive, independent and aware citizens (Giffinger *et al.*, 2007);

- A city that monitors and integrates conditions of all of its critical infrastructures, including roads, bridges, tunnels, railways, subways, airports, seaports, communications, water, power, even major buildings, can better optimize its resources, plan its preventive maintenance activities, and monitor security while maximizing services to its citizens (Hall, 2000);
- A city “connecting the physical infrastructure, the IT infrastructure, the social infrastructure, and the business infrastructure to leverage the collective intelligence of the city” (Harrison *et al.*, 2010);
- A city “combining ICT and Web 2.0 technology with other organizational, design and planning efforts to dematerialize and speed up bureaucratic processes and help to identify new, innovative solutions for complex city management, in order to improve sustainability and liveability.” (Toppeta, 2010);
- “The use of Smart Computing technologies to make the critical infrastructure components and services of a city – which include city administration, education, healthcare, public safety, real estate, transportation, and utilities – more intelligent, interconnected and efficient” (Whashburn *et al.*, 2010).

For all the "smart cities" concepts presented an increase in the use of electrical equipment is implicit, which, if any optimization is performed, will lead to an increase in the consumption of electrical energy, justifying the need for new and more efficient renewable energy sources that are able to generate electrical energy near the place of consumption, i.e., inside cities.

Also, mobility increasingly uses electrical energy, and it is expected that this could be the main source of energy by 2050 (Arthur D. Little, 2014). In 2015 the market share of electric vehicles was only 0.1% on a global level, when compared with the total number of passenger cars on the road worldwide, but this is expected to reach 1.7% by 2020,

showing the fast adoption of these vehicles (IEA, 2016b). This transition implies an increase in the demand of electrical energy, especially in the urban environments where mobility is greater, leading to the need to increase the levels of electrical energy production. If production continues to be from fossil fuels, electric mobility will not be sustainable. To change the paradigm and have a really sustainable concept of mobility with the use of electric vehicles, electrical energy production must be done using renewable energy sources (Garcia-Valle and Lopes, 2012).

With the present energetic paradigm, most electrical energy production uses fossil fuel combustion, which makes economies dependent on fuel costs. This is also leading to irreversible environmental damage, with growing levels of CO₂ emissions. According to International Energy Agency (IEA, 2016a), in 2014, globally, more than 80% of energy production came from fossil fuels. Urgent action is required to change the paradigm of electrical energy generation as, presently, energy is mostly produced outside cities, consuming non-renewable resources and inducing energy losses between the point of production and the point of consumption. Energy production must be based on renewable resources, decentralized, happen near to the point of consumption and, preferably, when it is needed.

However, renewable energy sources are not fully effective, as they do not allow electrical energy to be produced when it is needed, but only when the resources are available. These energy sources do not allow electrical energy to be produced where this is needed either, but only where the resources are available and the installation of the technologies is feasible and viable. New ways of generating electric energy are needed, especially to generate energy when and where consumption is required.

In the area of renewable energies, besides the major energy sources (hydro, solar, wind, waves), energy harvesting has recently been adopted in a micro-scale concept, where it is possible to generate electrical energy from small energy variations, such as thermal gradients, pressure, vibrations, radiofrequency or electromagnetic radiation, among others (Khaligh and Onar, 2010). Road surfaces are continuously exposed to two phenomena: solar radiation and vehicle loads. From both of these it is possible to extract

energy, which, using specific technologies, can be transformed into electrical energy (Andriopoulou, 2012).

Within cities, there are roads that carry vehicles, the main option for mobility. Vehicles consume energy to work their engines and release energy in different ways, by way of different components. Part of the energy released by vehicles goes into the road pavement. 15% to 21% of the energy is transferred to the vehicle's wheels (IEA, 2012; Hendrowati *et al.*, 2012). As vehicles abound in all cities in developed countries, this means that a considerable amount of energy is transferred to road pavements without ever being used. Roads are also exposed to solar radiation, which induces thermal gradients between its layers. This solar radiation and the resulting thermal gradients can also be transformed into useful energy. So, road pavements represent a considerable source of energy ready to be harvested and converted into useful forms of energy, such as electrical energy, at the same time reducing the need to "import" energy from distant places.

Considering this, infrastructure managers such as municipalities and motorway operators have on their own road pavements a possible source of energy for harvesting and conversion into useful energy such as electrical energy, allowing the need to "import" energy from distant places to be reduced. Also, by harvesting typically wasted energy and converting it into electrical energy, it allows energy to be produced without polluting the environment, reducing the CO₂ emissions associated to the energy produced by fossil fuel combustion. In order to turn this into a viable process, the infrastructure managers need a technology (or set of technologies) that allows this conversion process to work in an efficient and cost effective way.

1.2 Research Problem and Opportunity for Investigation

With the growing energy demand in cities and knowing that road pavements are permanently exposed to great amounts of energy, there is an opportunity to investigate

and develop a technology that allows a significant part of that wasted energy to be converted into electrical energy.

Energy is transferred to the road pavement mainly in two different ways. The first is by the pressure induced by the vehicles loads and the second is by the solar radiation that reaches the road pavement surface. In recent years, some research has been done in this area in order to develop technologies that can harvest this energy and transform it into a useful energy, such as electrical energy. However, none of the developed systems have presented a level of conversion efficiency or a technical-economic ratio to make the solution cost-effective.

The research problem consists of the need for a technology to convert a typically wasted energy delivered to the road pavements into electrical energy, with high conversion and storage efficiencies, and in a cost-effective way, contributing to the supply of the electrical network, mainly inside cities, as well as supplying specific electric applications without the need to be connected to the electric grid system.

However, the traditional practice of developing energy harvesting devices based only on the system itself without considering the road and traffic conditions has led to unsuccessful projects. It is therefore clear that the development of a road pavement energy harvesting (RPEH) device should be started by studying the vehicle-road interaction (VRI) with a detailed analysis of forces, kinematics, dynamics and, finally, an energetic analysis, so that the RPEH device can be modelled with complete understanding of the loads and the energy delivered by each vehicle type and the motion conditions. This study should include the complete VRI models and also the development of a software tool, where the user can define the vehicle and the RPEH device parameters and, based on it, perform computational simulations to understand the impact of each variable in the end result. Then, different elements and systems can be modelled as part of the RPEH device and added to the software tool, so that their performance can be evaluated and the most efficient solution can be identified. After this, an experimental validation should be performed, so that experimental results can be compared with the computational simulations and conclusions can be drawn. Finally,

a complete Technical and Economic Analysis (TEA) should be performed, with the definition of the complete models for such analysis and their integration in a software tool which would allow detailed studies to be performed on each variable influence in the viability of RPEH devices.

Therefore, to enable such a holistic approach, different techniques need to be used and properly combined to enable the appropriate development of an efficient and cost-effective RPEH device.

1.3 Motivation

Considering all the aforementioned facts, there is an awareness that to meet the sustainability challenges of the near future, new efficient and cost-effective energy generation technologies are needed and the development of a technology that makes use of energy released by vehicle into road pavements, converting this typically wasted energy into electrical energy, could play a very important role in the sustainability of our cities, by reducing the need to import energy from the outside.

Previous to this doctoral research, a technology to convert the kinetic energy from the movement of people into electrical energy was developed by a Portuguese start-up, where the author was one of the promoters. This technology was called *Waynergy*[®] *People* and its working principle was based on an electromechanical system that was patented (Duarte and Casimiro, 2011) and experimentally validated (Duarte *et al.*, 2013) using a pre-industrial prototype. The system has achieved a conversion efficiency of almost 60%, a higher value than all the existing pavement energy harvesting devices, creating an expectation for a high potential technology.

It was identified that the energy generation depends greatly on the load applied over the system surface and, since vehicles deliver a much higher load to the pavement than people, the system was adapted to convert the kinetic energy released from vehicles to the pavement into electrical energy (Duarte and Casimiro, 2013) and the system was

experimentally validated using a prototype (Duarte *et al.*, 2014). This system was named *Waynergy[®] Vehicles*. Although the results were satisfactory, the need for further research was identified, as the system did not support the vehicle loads properly, it was extremely complex to install in the pavement infrastructure and the production cost was too high.

Considering the technology previously developed for *Waynergy[®] People* with a conversion efficiency of almost 60% and the knowledge acquired in the development and experimental validation of *Waynergy[®] Vehicles*, I am led to believe that using the scientific method in the development of a new RPEH system, using similar energy conversion principles but with a redesigned system, integrated with the road pavement engineering and traffic engineering rules, it is possible to achieve the goal of finding an efficient and cost-effective solution to produce electrical energy in the road pavement, which can make an impact on the sustainability challenges facing cities.

1.4 Research Objectives

Recently, some investigation has been done on road pavement energy harvesting, mostly focused on the pavement's thermal gradients and the vehicle load induced on the pavement surface. This research has been performed both by academia and industry. Despite the various attempts to develop a new set of products in this field, none of the research projects has originated a successful product. The main reasons for the failure are related to the low energy conversion efficiency of the technologies and also to the difficulty integrating the systems in the road pavement infrastructure. The product's cost of production is also a challenge, but this should only be considered after the first two challenges are solved.

Therefore, the main objective of this research work is the development of a new system to convert the energy released by vehicles to the road pavement into electrical energy with a higher conversion efficiency than the current state-of-the-art. As well as the

conversion efficiency, the system should be designed so that a simple method of installing it in the road pavement infrastructure could be developed.

As the goal is to develop a new technology to implement in a place where there are not any products or enough experiments conducted worldwide, there is a need to perform several studies, developments and experiments during the development of this research project. So, the fulfilment of the main objective of this research requires the following research tasks to be conducted, which correspond to individual objectives:

1. To evaluate the state-of-the-art relating to infrastructure energy harvesting, both related to the road pavement and railway tracks, so that each technology can be identified in terms of conversion efficiency, energy generation potential, current development stage and installation method. With this analysis, the best practices can be defined and detailed guidelines for the development of the research can be defined as well;
2. To develop a software tool to quantify the forces delivered from each vehicle tyre to the pavement or to a RPEH device's surface, as well as the energy released from the vehicle to the road pavement or to the device, considering different vehicle weights and speeds, as well as different vehicle parameters, and depending on the pavement shape, slope and material properties and other technical features of the RPEH device. Such a tool is fundamental for the development of the project and to perform computational simulations during the development of the RPEH device, as this will allow us to quantify the forces and energy inputs of the system;
3. To evaluate the impact of the RPEH device in the vehicle body in terms of ride comfort, so that this is not affected or, at least, it is minimized, which would allow RPEH devices to be applied in a wide range of places. Combining this evaluation with the energy harvested from vehicles and the vehicle speed reduction, the impact of RPEH devices on road safety can also be studied, as they work as a speed reducer. For this, an energy harvesting system can be modelled and

integrated in the software tool so that computational simulations can be performed and evaluated;

4. To model existing RPEH device systems and incorporate the models in the software tool, so that computational simulations can be performed and the behaviour of existing systems can be evaluated;
5. To develop and model new systems for RPEH and incorporate them in the software tool, so that computational simulations can be performed and the performance of the new systems can be evaluated and compared to the performance of existing systems;
6. To evaluate the inclusion of a mechanical energy storage unit in the developed RPEH systems, model the proposed solutions and determine their impact on the efficiency of the systems;
7. To perform an experimental validation of the developed solutions using a prototype developed for this purpose, so that data can be collected and compared with the computational simulation results, allowing us to make conclusions about the precision of the models. At this stage, the installation method of the prototype in the pavement should be addressed, so that the process can be simple;
8. To develop a complete model and a software tool to perform a TEA of RPEH devices, as well as *Cost-Benefit Analysis* (CBA), considering different variables as inputs and presenting the outputs numerically and graphically. This tool should also allow a *Sensitivity Analysis* (SA) to be performed to evaluate the impact of one or multiple variables in the technical and economic performance of the system, so that the most critical variables can be identified.

To sum up, this thesis provides a scientifically-based development of a RPEH system that, without affecting ride comfort, is able to efficiently convert the energy released from vehicles to the device's surface into electrical energy, with the option of also being able to store the harvested energy. Guidelines to develop a viable product should be

defined through a CBA. Beside the system and models development, at the end of the research project it is expected that two software tools will be finished that can support other research projects to evaluate and develop RPEH devices, both technically and economically.

1.5 Research Methodology

The research will start with an extensive literature review and state-of-the-art analysis related to energy harvesting technologies, with special emphasis on one which can be applied in transportation infrastructures such as road pavements and railways and that are able to convert the vehicle released energy into electrical energy. This will allow us to identify the positive aspects of each solution and also the main failures and disadvantages of the existing technologies.

Prior to the development of the energy harvesting unit, a study of the VRI will be performed, including the main vehicle dynamics models and the road pavement parameters, so that this interaction can be properly evaluated depending on the vehicle characteristics and actions (acceleration, braking, free rolling) and considering the road pavement characteristics (materials, slope, shape, among others), in order to quantify the energy released from vehicles to the road pavement precisely, the energy absorbed by the road pavement material and the energy delivered to the conversion system. None of the existing research projects within the field of RPEH have presented a complete model for the energy released from vehicles with vehicle and road pavement characteristics as inputs of the RPEH system. This research aims to develop and validate such a model.

Looking at a typical energy harvesting system, it usually has three different units: harvesting, conversion and storage. The harvesting component is always the first, as this is responsible for capturing energy from the external sources. In most cases, the conversion unit is the second and the storage is the third. However, in some specific

cases, storage is included between the harvesting and the conversion units, working as a buffer of the harvested energy and allowing the global efficiency of the system to be maximized. In the energy harvesting from vehicles mechanical energy, this approach has never been reported and one of the goals of this research is to evaluate the best combination of these different components of the global system, by studying the efficiency of different combinations.

Following the development of the computational model, the energy conversion unit will be developed, including four major components: energy harvesting, energy conversion, energy storage, and the energy storage controller units. Each unit represents a different component of the system, but the model combines them so that all can work as a single unit. Each component will be physically and computationally modelled, using different systems in the conversion and storage units. The performance of each component will be evaluated considering the energy received and delivered or converted, allowing the efficiency of each component and of the complete system to be determined. Using this approach, it will be possible to identify the inefficiencies of each component of the system and, consequently, the parts that need to be optimized to increase the global efficiency of the complete system.

After these models are validated, the energy delivery model will be developed, while studying different possible uses of the electrical energy that will be generated, such as delivery to the electric grid or to an end application, both in DC or AC.

The different components of the research project are presented in Figure 1.1.

After concluding the physical and computational models and performing the computational simulations and identifying the most efficient solutions, prototypes will be developed to validate the models and the computational simulations using experimental data. This step will be useful to calibrate the models and optimize the achieved results.

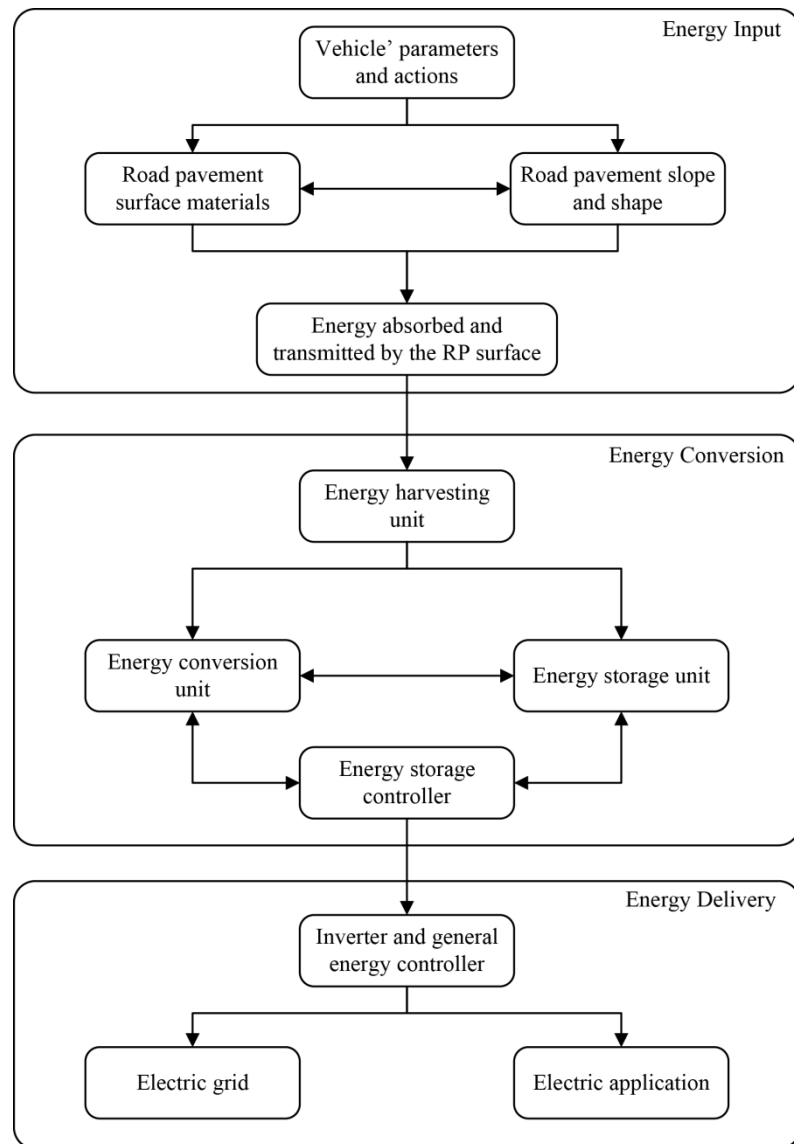


Figure 1.1- Diagram showing the components of the proposed solution.

RPEH is a recent research area and the economic viability of the proposed solution will be evaluated, as well as the technical validation. To do this, a model and a software tool will be developed, which consider different inputs such as traffic distribution, vehicle characteristics (including average weight, speed, among others), technical and economic aspects of the RPEH installation and the application and price of electric energy. This tool will calculate the electrical energy output of the application as well as the economic

outputs, such as the cost per installed watt, cost of the generated energy, net present value of the investment and return on the investment, among other relevant technical and economic parameters. This software tool will also allow a SA to be performed to identify the parameters that can be optimized to maximise output.

1.6 Research Design

For the initial data collection of existing technologies, a literature review will be performed for the different areas related to the research, including road pavement, railway infrastructure, energy harvesting methods and technologies (general), focusing then on the particular cases of road pavement energy harvesting and railway infrastructure energy harvesting technologies. This will allow us to fully characterize the state-of-the-art, by analysing papers and patents about existing technologies, their efficiencies, technical characteristics, experiments performed and achieved results, current development stage and installation method. A performance analysis will be used as a quantitative method to evaluate each system and technology identified, both technically and economically.

After this phase, experimental research will be carried out, focusing on the development and testing of a new RPEH system. This will be performed using the scientific method, with the following steps:

- 1- Formulation of hypothesis;
- 2- Project, modelling, simulation and testing of the hypothesis;
- 3- Application of inductive and deductive logic on the analysis of the obtained results;
- 4- Prototyping and experimental tests;
- 5- Results analysis and comparison between theoretical and experimental data and results;
- 6- Conclusions (and optimization).

During the different system modelling stages the *System Dynamics* technique will be used, in order to optimize the performance of each component and obtain the maximum theoretical efficiency of the system. *Iterative Analysis* will also be used, as multiple simulations will be performed to optimize the different RPEH device characteristics in order to obtain the most efficient combination and parameters. The methodologies previously mentioned allow iterative steps to be taken, as with the results of the computational simulations and experimental tests it is possible to perform changes to the system and perform new tests, allowing new data and new conclusions to be obtained.

An *Experimental Development* will be performed with the development of prototypes, in order to evaluate different solutions in the laboratory environment and in an operational environment, with experimental tests. This will allow us to collect data and to make conclusions about the system's efficiency and achieved results.

Scenarios will be performed, both during the technology development and modelling, to compare and analyze different computational simulations results, as well as in the evaluation of the prototype results. Also, *Scenarios* will be used during the technical and economic evaluation of the system.

Finally, a *Cost-Benefit Analysis* will be performed, where the impact of the project and its performance in terms of economic outputs will be evaluated. Different economic variables such as the net present value and the internal rate of return will be evaluated for different *Scenarios* and *Case Studies*, and a sensitivity analysis will be performed. During this stage, the environmental impact of the application of the system in different places will also be considered, as well as the costs associated with it.

Figure 1.2 presents the research design framework in a schematic diagram. As explained, initially evidence will be collected through a literature review and state-of-the-art techniques, in order to make a performance analysis, and define the research problems and questions. The second step is the development of physical and computational models for all the main components of the RPEH system, starting with the evaluation of the energy released from vehicles to the road pavement surface or to

the RPEH device surface, followed by the models of the energy harvesting system, including all its components, and finishing with the electrical energy management and application models. These models will be developed using the *System Dynamics* technique and simulations will be performed to evaluate each component both individually and together. Different components will be considered for each model in order to evaluate the most efficient combination.

The third step consists of the *Experimental Development*, with experimental tests being performed on the system prototype, both in laboratory and tests in a relevant environment. These will allow us to acquire experimental data and compare it to the simulation results, which will allow us to calibrate and optimize the computational models with an iterative analysis. During the prototype development stage the installation of the system in the road pavement and the production costs of the system will be evaluated, so that all the costs involved in real implementation can be defined for the CBA.

The fourth step consists of a CBA with the development of a model and a software tool where all the input variables can be defined using both the traffic and road parameters as inputs, as well as the technical and economic characteristics of the RPEH system and the electrical energy application. This will allow us to define multiple scenarios and evaluate the technical and economic performance of each application, providing important data for an end user to evaluate the benefits of the implementation of a RPEH solution for a real case scenario. Also, this model will allow us to perform a SA in order to identify the impact of each variable in the system performance. The results of the SA will provide important information that can be used to enhance the models outputs by focusing on adjusting and improving the system components that are identified as having the greatest impact on the model outputs. Moreover, the SA provides insights to the users of the system regarding the different types of data that need to be collected for precise evaluation of the system performance.

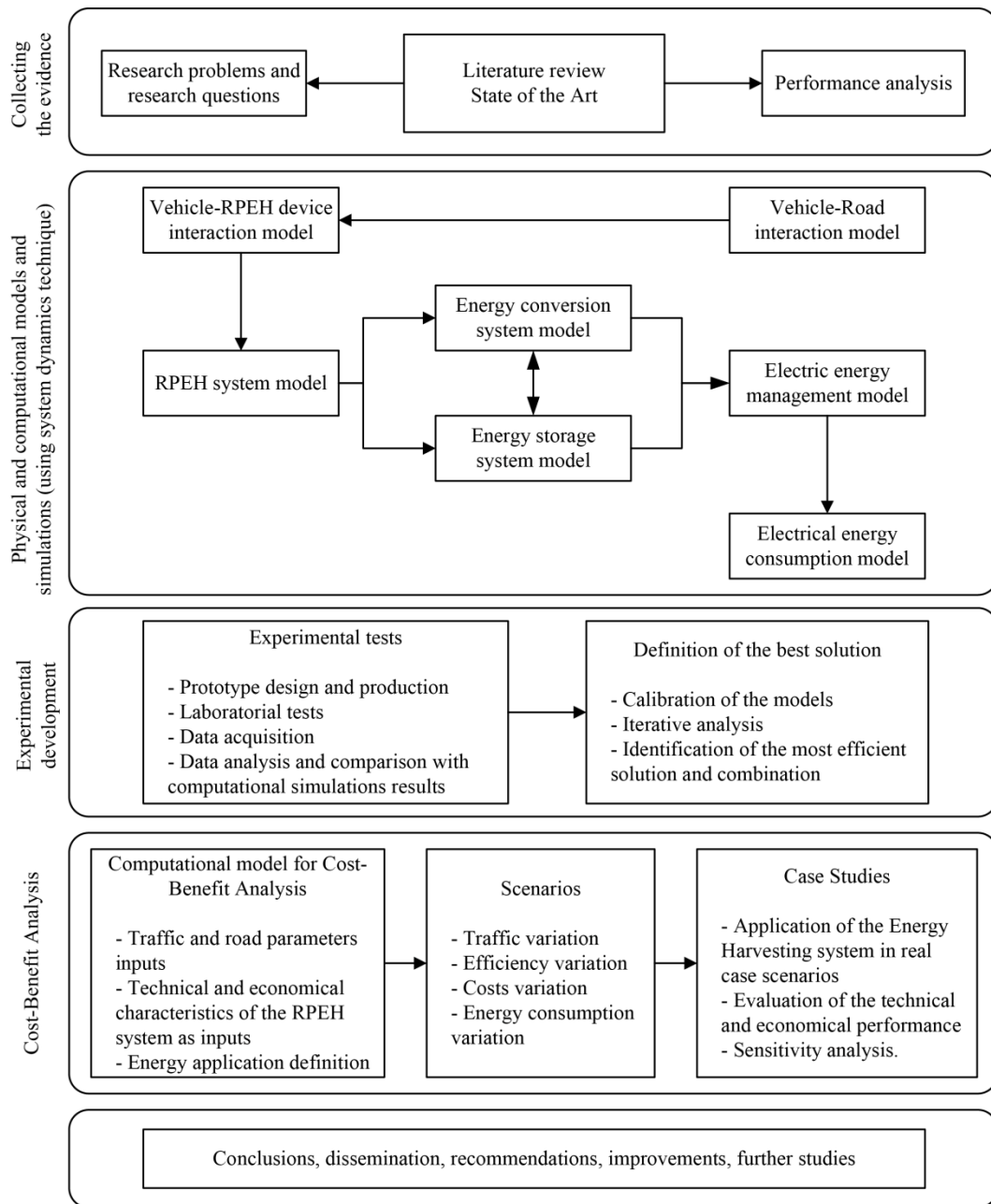


Figure 1.2- Schematic diagram of the research design framework.

1.7 Structure of the Thesis

This thesis is organized into nine chapters. Excluding Chapters 1 and 9, the remaining chapters of the thesis are based on the scientific papers produced during the development of the present research work. The contents of each chapter do not correspond to the exact text and structure of each scientific paper to avoid repetition and to facilitate the reading of the thesis.

Although each chapter can be considered as an independent subject and related to a specific scientific article, this thesis does not intend to represent a chain of scientific articles, but a planned evolution of the research work developed during the research activities. The relationship between the thesis chapters is presented in Figure 1.3, through a schematic diagram of the outline of the thesis.

Chapter 1 provides an introduction to the thesis. It presents the global problem statement, the research problem and opportunity for investigation, the motivation, the research objectives, research methodology, research design and the organization of the thesis.

Chapter 2 presents the state-of-the-art regarding infrastructure energy harvesting systems, relating both to the road pavement and to the railway, as both infrastructure types have similarities, but different energy harvesting technologies are being developed for each. Each existing technology will be evaluated in terms of its energy generation potential and energy conversion efficiency, current stage of development and the installation mode in the infrastructure, allowing us to make conclusions about its viability. Finally, conclusions will be drawn about the most promising technologies and guidelines for the research to perform.

Chapter 3 describes the VRI in terms of a forces analysis, kinematic analysis and dynamic analysis, allowing an energetic analysis of the interaction to be performed. A detailed study regarding vehicle dynamics is presented, including the tyre contact patch in the vehicle models, allowing a more detailed and complete model to be developed to evaluate the interaction. Also, a movable surface in the pavement is considered and

modelled. A software tool is developed based on the presented models and the simulation results are presented and discussed, allowing conclusions to be made about more precise models.

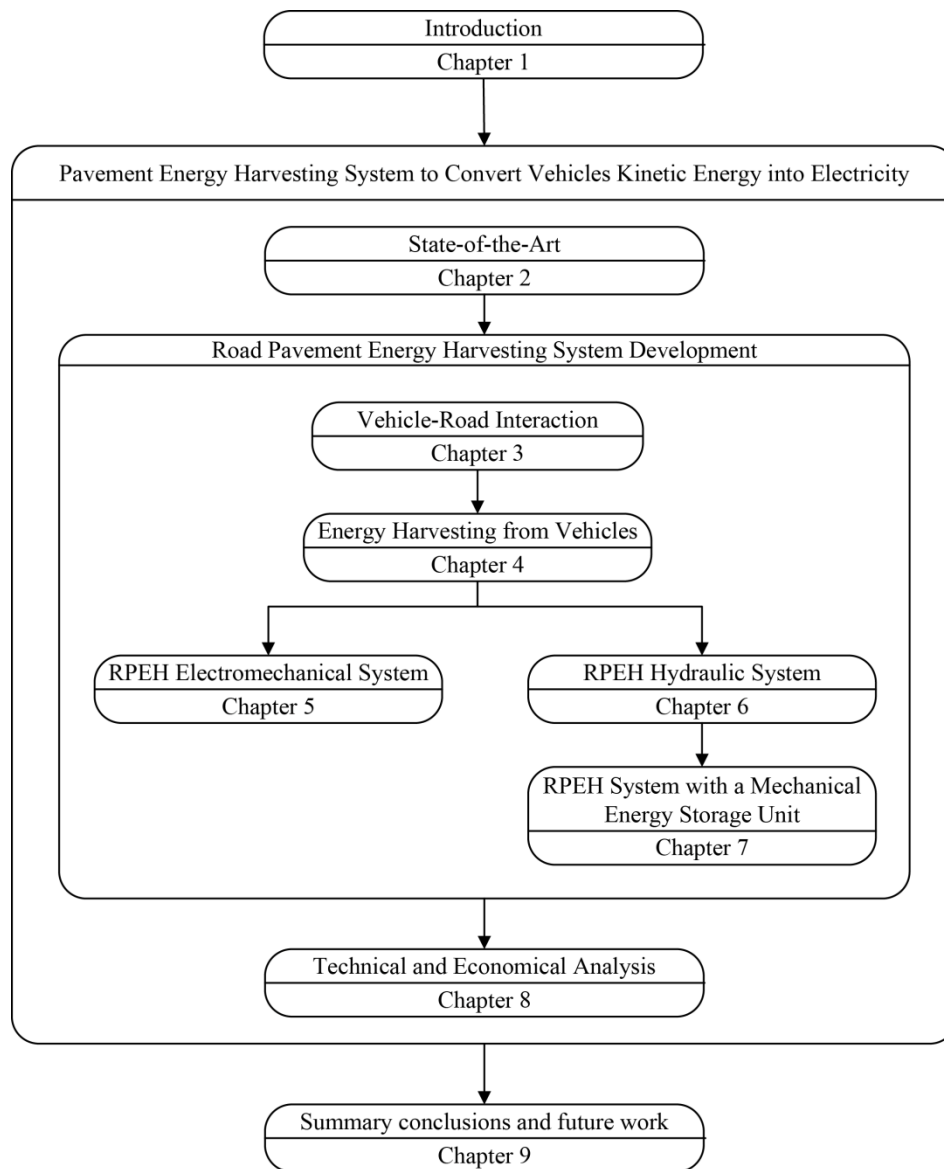


Figure 1.3- Schematic diagram of the thesis outline.

Chapter 4 presents a study of the potential for energy harvesting from vehicles using a RPEH device with a movable surface and the impact of such device in the ride comfort and its contribution to promote road safety. The software tool developed in the previous Chapter is used and simulations are performed evaluating not only the energy harvested but also the ride quality and the vehicle's speed reduction. Following this analysis, an experimental evaluation is performed using a prototype of the proposed system and the experimental results are compared to the computational simulation results, allowing conclusions to be drawn about the precision of the model.

Chapter 5 presents the development of a RPEH device using an electromechanical system. The two most common electromechanical devices are presented and modelled and a new proposed device is then presented. The developed models are integrated into the software tool developed in Chapter 3 and, using the upgraded tool, new computational simulations are performed to evaluate the different electromechanical systems and draw some conclusions. Following this analysis, an experimental evaluation is performed using a prototype of the new electromechanical system and the experimental results are compared to the computational simulation results, allowing us to make conclusions about the model's precision and system's performance, as well as making comparisons with the present state-of-the-art.

Chapter 6 presents the development of a RPEH device using a new hydraulic system with a mechanical actuation, which is presented and modelled. First, the most common hydraulic device is presented and modelled and both models are included in the software tool previously developed. Based on the upgraded tool, computational simulations are performed and some conclusions regarding each system's efficiency and behaviour are presented. Also, a comparison with electromechanical devices is performed, as well as with the current state-of-the-art.

Chapter 7 describes the adoption of a mechanical energy storage unit in RPEH devices, with emphasis on hydraulic devices. Different solutions are presented and modelled and these are included in the software tool developed previously. The computational

simulations results are presented for different scenarios and conclusions regarding the efficiency and effectiveness of these systems are presented.

Chapter 8 presents a technical and economical evaluation of RPEH devices, defining the main equations to evaluate such devices. A computational model is developed based on the presented equations and an analysis is performed for different scenarios, including a SA for specific key variables. Based on this, several conclusions are made in order to evaluate these devices and the conditions necessary for positive viability are defined.

Chapter 9 summarizes the research work described in this thesis, highlights its contributions and main achievements, and establishes a set of research guidelines and improvements for future work.

1.8 Publications

As mentioned in the previous section, this thesis is based on the scientific articles written about the research work developed during the doctoral studies. Most of the scientific articles have been submitted to international peer-reviewed journals and are either published or under review, and others are about to be submitted. Below is the list of references for the thesis chapters, in the sequence in which they are presented.

1) Scientific articles already published

Chapter 2:

Duarte, F. and Ferreira, A. (2016). Energy harvesting on road pavements: state of the art. *Proceedings of the Institution of Civil Engineers – Energy*, 169(2): 79-90. DOI: 10.1680/jener.15.00005.

Duarte, F. and Ferreira, A. (2017). Energy harvesting on railway tracks: state of the art. *Transport, Institution of Civil Engineers*, 170(3): 123-130. DOI: 10.1680/jtran.16.00016.

Chapter 3:

Duarte, F., Ferreira, A. and Fael, P. (2016). Software for simulation of vehicle-road interaction. *New Advances in Information Systems and Technologies*, Vol. 444 of the *Series Advances in Intelligent Systems and Computing*, Springer International Publishing, Switzerland, pp. 681-690. DOI: 10.1007/978-3-319-31232-3_64.

Duarte, F., Ferreira, A. and Fael, P. (2017). Software tool for simulation of vehicle-road interaction. *Engineering Computations Journal*, 34(5): 1501-1526. DOI: 10.1108/EC-07-2016-0273.

Chapter 5:

Duarte, F., Ferreira, A. and Fael, P. (2017). Software to Support the Development of Road Pavement Energy Harvesting Devices. *Recent Advances in Information Systems and Technologies*, Vol. 569 of the *Series Advances in Intelligent Systems and Computing*, Springer International Publishing, Switzerland, pp. 807-817. DOI: 10.1007/978-3-319-56535-4_79.

Chapter 6:

Duarte, F., Ferreira, A. and Fael, P. (2017). Road pavement energy harvesting: an evaluation methodology for new and existing vehicle-derived mechanical energy collectors. *Journal of Renewable and Sustainable Energy*, 9(3): 1-22. DOI: 10.1063/1.4982795.

2) Scientific articles submitted and under review/accepted for publication

Chapter 4:

Duarte, F., Ferreira, A. and Fael, P. Contribution of a novel speed reduction equipment to promote road safety. *International Journal of Pavement Engineering*.

Duarte, F., Ferreira, A. and Fael, P. Experimental validation of a new speed reduction equipment to promote road safety. *Accident Analysis and Prevention*.

Chapter 5:

Duarte, F., Ferreira, A. and Fael, P. Road pavement energy harvesting: a new electromechanical device to convert vehicles mechanical energy into electrical energy. *Journal of Energy Engineering*, American Society of Civil Engineers. Accepted for publication.

Chapter 7:

Duarte, F., Ferreira, A. and Fael, P. Integration of a mechanical energy storage system on a road pavement energy harvesting device. *Proceedings of the Institution of Civil Engineers – Energy*.

Duarte, F., Ferreira, A. and Fael, P. Integration of a mechanical energy storage system on a road pavement energy harvesting hydraulic device with mechanical actuation. *Journal of Renewable and Sustainable Energy*, American Institute of Physics. Accepted for publication.

Chapter 8:

Duarte, F., Ferreira, A. and Fael, P. Software tool for technical and economical evaluation of road pavement energy harvesting devices. *Advances in Engineering Software*.

Duarte, F., Ferreira, A. and Fael, P. A technical and economic evaluation of road pavement energy harvesting devices applied in urban environment. *Journal of Renewable and Sustainable Energy*.

3) Scientific article to be submitted soon

Chapter 5:

Duarte, F., Ferreira, A. and Fael, P. Experimental validation of a new electromechanical road pavement energy harvesting device. The submission to *Journal of Energy Engineering* is currently being considered.

Besides the scientific articles, two patent requests were submitted to the Portuguese Institute for Intellectual Property (INPI - Instituto Português de Propriedade Industrial), regarding the systems presented in Chapters 4, 5, 6 and 7, with the following description:

4) Patent requests submitted

Chapters 4 and 5:

Duarte, F., Ferreira, A. and Fael, P. Equipamento de Aplicação em Pavimentos que Integra um Sistema para Captação de Energia Mecânica de Veículos e Conversão em Energia Elétrica. *Instituto Nacional da Propriedade Industrial (INPI)*, Portuguese Patent Request 109935 P (*in Portuguese*).

Chapters 6 and 7:

Duarte, F., Ferreira, A. and Fael, P. Equipamento de Aplicação em Pavimentos que Integra um Sistema Hidráulico com Atuação Mecânica para Geração de Energia Elétrica a partir do Movimento de Veículos. *Instituto Nacional da Propriedade Industrial (INPI)*, Portuguese Patent Request 109936 R (*in Portuguese*).

Complementarily, some scientific articles have been presented and discussed in different international conferences, with the complete list of conferences presented below.

5) Conference articles

Chapter 2:

Duarte, F. and Ferreira, A. (2015). Energy harvesting on road pavements. *Proceedings of the Third International Conference on Advances in Civil, Structural and Environmental Engineering - ACSEE 2015*, CD Ed., paper ACSEE-15-535, pp. 126-130, Zurich, Switzerland.

Duarte, F., Ferreira, A., Paiva, C. (2016). Energy harvesting on transport infrastructures: the particular case of railways. *Proceedings of the 4th International Conference on Road and Rail Infrastructure*, CD Ed., pp. 811-816, Sibenik, Croatia.

Chapter 3:

Duarte, F., Ferreira, A. and Fael, P. (2017). A new decision-aid tool for simulation of tire-pavement interaction and for quantification of energy harvesting on pavements. *Proceedings of The World Conference on Pavements and Assets Management*, CD Ed., 02d05.pdf, pp. 1-10, Milan, Italy.

Chapter 4:

Duarte, F., Ferreira, A. and Fael, P. (2016). Optimization of the shape of road speed reducers. *Proceedings of the International Conference on Traffic and Transport Engineering - ICTTE 2016*, pp. 608-615, Belgrade, Serbia.

The work developed and presented in the present thesis was developed following previous research project in which the author had been involved. Both the previous project and the achieved results have made an important contribution to the work developed during this thesis and the achieved results were recently published, both in scientific articles and in conference papers:

6) Scientific articles published

Duarte, F., Champalimaud, J. and Ferreira, A. (2016). Waynergy Vehicles: an innovative pavement energy harvest system. *Municipal Engineer, Institution of Civil Engineers*, 169(1): 13-18.
DOI: 10.1680/muen.14.00021.

Duarte, F., Ferreira, A. and Champalimaud, J. (2016). Waynergy People - application in an operational environment. *Proceedings of the Institution of Civil Engineers – Energy*, pp. 1-8. DOI: 10.1680/jener.16.00010.

Duarte, F., Champalimaud, J. and Ferreira, A. (2017). Waynergy vehicles: system prototype demonstration in an operational environment. *Municipal Engineering - Institution of Civil Engineers*, pp. 1-8. DOI: 10.1680/jmuen.16.00071.

7) Conference articles

Duarte, F., Champalimaud, J. and Ferreira, A (2014). Waynergy Vehicles: an innovative pavement energy harvest system. *Proceedings of the 2nd International Congress on Energy Efficiency and Energy Related Materials*, CD Ed., pp. 343-348, Oludeniz, Turkey.

Duarte, F., Ferreira, A. and Champalimaud, J. (2015). Waynergy Vehicles: a road pavement energy harvest system application. *Proceedings of the conference Energy for Sustainability 2015 - Sustainable Cities: Designing for People and the Planet*, CD Ed., ID25, pp. 1-5, Coimbra, Portugal.

Duarte, F., Ferreira, A. and Champalimaud, J. (2016). Waynergy Vehicles: system prototype demonstration in an operational environment. *Proceedings of the Transport Research Arena*, CD Ed., Contribution10157.pdf, pp. 1-10, Warsaw, Poland.

1.9 References

Andriopoulou, S. (2012). *A review on energy harvesting from roads*. KTH, Stockholm, Sweden.

Arthur D. Little (2014). *The Future of Urban Mobility 2.0, Imperatives to shape extended mobility ecosystems of tomorrow*. Available from <http://www.adlittle.com/future-of-urban-mobility.html>. Accessed in October, 2015.

Buhaug, H., and Urdal, H. (2013). An urbanization bomb? Population growth and social disorder in cities. *Global Environmental Change*, 23(1): 1-10.

- Duarte, F. and Casimiro, F. (2011). *Pavement Module for Generating Electric Energy from the Movement of People and Vehicles*. International Patent Application PCT/IB2011/052164, Patent WO2011145057 A2, Nov.
- Duarte, F. and Casimiro, F. (2013). *Electromechanical System for Electric Energy Generation and Storage Using a Surface Motion*. International Patent Application PCT/IB2013/050616, Patent WO2013114253 A1, Aug.
- Duarte, F., Casimiro, F., Correia, D., Mendes, R. and Ferreira, A. (2013). Waynergy people: a new pavement energy harvest system. *Proceedings of the Institution of Civil Engineers – Municipal Engineer*, 166(4): 250–256. <http://dx.doi.org/10.1680/muen.12.00049>.
- Duarte, F., Champalimaud, J. and Ferreira, A. (2014). Waynergy vehicles: an innovative pavement energy harvest system. *Proceedings of the 2nd International Congress on Energy Efficiency and Energy Related Materials, Oludeniz, Turkey*. Springer, London, UK.
- Garcia-Valle, R., and Lopes, J. A. P. (Eds.) (2012). *Electric vehicle integration into modern power networks*. Springer Science & Business Media, Berlin, Germany.
- Giffinger, R., Fertner, C., Kramar, H., Kalasek, R., Pichler-Milanović, N., and Meijers, E. (2007). *Smart Cities: Ranking of European Medium-Sized Cities*. Vienna, Austria: Centre of Regional Science (SRF), Vienna University of Technology. Available from: http://www.smartcities.eu/download/smart_cities_final_report.pdf. Accessed in October, 2015.
- Hall, R. E. (2000). The vision of a smart city. In *Proceedings of the 2nd International Life Extension Technology Workshop*, Paris, France. Available from: <http://www.osti.gov/bridge/servlets/purl/773961-oyxp82/webviewable/773961.pdf>. Accessed in October, 2015.
- Harrison, C., Eckman, B., Hamilton, R., Hartswick, P., Kalagnanam, J., Paraszczak, J., and Williams, P. (2010). Foundations for Smarter Cities. *IBM Journal of Research and Development*, 54(4).

- Hendrowati, W., Guntur, H. and Sutantra, I. (2012). Design, modelling and analysis of implementing a multilayer piezoelectric vibration energy harvesting mechanism in the vehicle suspension. *Engineering*, 4(11): 728–738.
- IEA (2012). *Technology Roadmap: Fuel Economy of Road Vehicles*, International Energy Agency, Paris, France. Available from:
http://www.iea.org/publications/freepublications/publication/Fuel_Economy_2012_WEB.pdf. Accessed in September, 2015.
- IEA (2016a). *Key world energy statistics 2016*, International Energy Agency, Paris, France. Available from:
<https://www.iea.org/publications/freepublications/publication/KeyWorld2016.pdf>. Accessed in June, 2017.
- IEA (2016b). *Global EV Outlook 2016*, International Energy Agency, Paris, France. Available from:
https://www.iea.org/publications/freepublications/publication/Global_EV_Outlook_2016.pdf. Accessed in June, 2017.
- Khaligh, A. and Onar, O.C. (2010). *Energy Harvesting: Solar, Wind, and Ocean Energy Conversion Systems*. CRC Press Inc, Boca Raton, FL, USA.
- Toppeta, D. (2010). *The Smart City Vision: How Innovation and ICT Can Build Smart, “Livable”, Sustainable Cities*. The Innovation Knowledge Foundation. Available from:
http://www.thinkinovation.org/file/research/23/en/Toppeta_Report_005_2010.pdf. Accessed in October, 2015.
- UN (2016). *The World's Cities in 2016*. United Nations - Department of Economic and Social Affairs, New York, NY, USA. Available from:
http://www.un.org/en/development/desa/population/publications/pdf/urbanization/the_worlds_cities_in_2016_data_booklet.pdf. Accessed in July, 2017.

Washburn, D., Sindhu, U., Balaouras, S., Dines, R. A., Hayes, N. M., and Nelson, L. E. (2010). *Helping CIOs Understand "Smart City" Initiatives: Defining the Smart City, Its Drivers, and the Role of the CIO*. Cambridge, MA: Forrester Research, Inc. Available from: http://public.dhe.ibm.com/partnerworld/pub/smb/smarterplanet/forr_help_cios_und_smart_city_initiatives.pdf. Accessed in September, 2015.

WHO (2016). *Global report on urban health: equitable, healthier cities for sustainable development*. World Health Organization, Geneva, Switzerland. Available from: http://www.who.int/kobe_centre/publications/urban-global-report/en/. Accessed in June, 2017.

Chapter 2

Energy Harvesting in Transportation Infrastructures: State-of-the-art

2.1 Introduction

Energy Harvesting is described as a concept by which energy is captured, converted, stored, and utilised using various sources, by employing interfaces, storage devices, and other units (Khaligh and Onar, 2010; Priya and Inman, 2009). Simplified, energy harvesting is the conversion of ambient energy present in the environment into other useful means of energy, as for example, in electrical energy (Kazmierski and Beeby, 2009).

Energy harvesting is divided into two main groups: macro-energy harvesting sources, associated with solar, wind, hydro and ocean energy; and micro-energy harvesting, associated with electromagnetic, electrostatic, heat, thermal variations, mechanical vibrations, acoustic and human body motion as energy sources (Harb, 2011; Khaligh and Onar, 2010; Yildiz, 2009). Macro-energy harvesting is related to large-scale energy harvesting, usually in the order of kilojoules or more. Micro-energy harvesting is related to small-scale energy harvesting, usually in the order of a joule or less.

Different transportation infrastructures are continuously exposed to different energy sources. From these it is possible to extract energy, which, using specific technologies, can be transformed into electrical energy. This Chapter aims to review the energy harvesting technologies with possible implementation on the major transportation infrastructures in which some research has been developed in recent years, namely in road pavements and railways.

2.2 Energy Harvesting on Road Pavements

2.2.1 Introduction

From the energy harvesting technologies identified by Harb (2011), two groups of technologies have a great potential for implementation on pavements: one uses solar radiation as an energy source and the other uses the mechanical energy from vehicle loads. Considering these energy sources, different technologies and systems have been developed and tested in recent years. The main energy harvesting technologies applicable on road pavement can be divided into two main groups, as presented in Figure 2.1. The first group is related to technologies that make use of the solar exposure on the road pavement. Solar radiation can be directly harvested by photovoltaic (PV) cells and transformed into electrical energy; it can induce thermal gradients between the road pavement layers, which can be used to power thermoelectric generators (TEGs), which produce electrical energy, or be harvested by asphalt solar collectors (ASC), which extract the temperature accumulated on the road pavement. Induction heating is a concept in which introducing conductive particles in the asphalt mixture provides self-healing capacities autonomously at high temperatures by harvesting solar radiation. The second group is related to technologies that make use of the mechanical energy transferred from vehicles to the road surface. This can be harvested directly by piezoelectric harvesters, which generate electrical energy; or it can be harvested by hydraulic, pneumatic, electromechanical or micro-electromechanical systems (MEMS) that transfer the harvested energy to electromagnetic generators, which produce

electrical energy. In the case of MEMS, they can also transfer the harvested energy to piezoelectric generators.

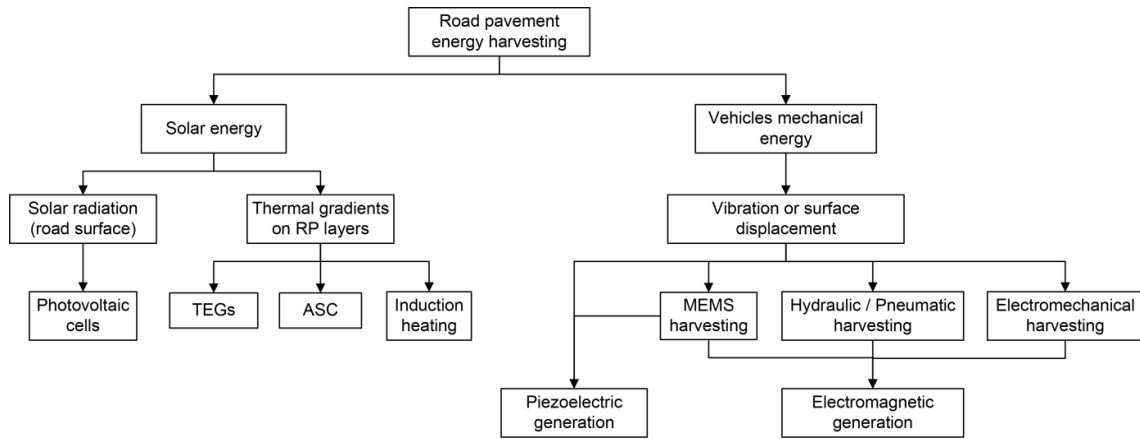


Figure 2.1- Road pavement energy harvesting technologies.

2.2.2 Solar energy harvesting on road pavements

2.2.2.1 Photovoltaic technology

Researchers from the Korea Institute (Kang-Won and Correia, 2010) have investigated the possibility of harvesting solar energy from road pavements, using solar cells embedded into the pavement infrastructure. They have concluded that the current thin-film solar cells are difficult to use on surfaces that receive mechanical loads and environmental conditions can cause premature corrosion and wear. For these reasons, the researchers are developing new thin-film solar cells that meet the requirements for use on road surfaces.

Julie and Scott Brusaw proposed a solar collector system to replace the upper layer of the road pavement, called Solar Roadway (SR, 2015). The Solar Roadway is a series of structurally engineered solar panels that are able to support traffic loads and are applied on the road surface transforming solar radiation into electrical energy. Each panel has

an installed power of 36W and measures 0.37 m². They have patented the upper layer of the product with a design patent (Brusaw and Brusaw, 2014). The Brusaws indicate a conversion efficiency of the system of 11.2% (SR, 2015), a value that cannot be confirmed in any scientific publication or product certification. One of the major challenges of this project is to offer safety and the appropriate conditions for the mobility of the vehicles passing over the panels. At the same time, the upper layer needs to guarantee the transmission of the solar radiation to the PV cells beneath it in order to present good conversion efficiency.

In the Netherlands, Toegepast Natuurwetenschappelijk Onderzoek (TNO), along with other technological partners, have developed a pilot project consisting of a modular cycle path system, named SolaRoad (SolaRoad, 2014; TNO, 2014). The cycle path is constructed of concrete elements which are covered by a 1.0 cm thick glass top layer. Underneath this glass layer, crystal silicon solar cells are laid, although the values of the installed power and energy conversion efficiency are not presented. The modules are embedded in concrete slabs and applied on the base layer of the pavement. The authors of the project indicate that the next step will be to adapt the system for application on roads (SolaRoad, 2014).

2.2.2.2 Thermoelectric technology

TEGs produce electrical energy due to the Seebeck effect, described by Schreier *et al.* (2013) as a voltage difference on a material, resulting from a temperature gradient imposed between its surfaces. The greater the temperature gradient, the more energy is generated.

Hasebe *et al.* (2006) developed a pavement-cooling system using a TEG incorporated into the pavement. Solar heat is collected by a water piping system embedded in the road pavement, and this water is cooled by river water. The water first passes on the hot side of the TEG, and then on the cold side of the TEG, installed under the road. The maximum power output of the prototype tested was 5 W, using 19 Bi-Te cells (1.23 cm³ each), for a ΔT of 40.5 °C. For a ΔT of 25.9 °C, the maximum output power was 2.9 W,

and for a ΔT of 11.5 °C, the maximum output power was 0.9 W. The conversion efficiency of the system was not presented.

Wu and Yu (2012) studied the implementation of TEGs on the surface of pavements. They propose the connection of the lower part of the module with the sub-grade soil via highly thermal conductive materials in order to facilitate heat conduction and thus increase electrical energy production. They have concluded that its maximum efficiency reached 4% using Quantum Well structured (QW) materials, instead of Bi-Te cells, but the problem was the storage of that energy. Tests were performed with a pavement ΔT of 50 °C, which generated 300 mV with one TEG cell. They have concluded that the efficiency of the electronic system was 41.3%, which results in a global efficiency of the TEG system of 1.6%. The prototype, which used a 7.7 cm³ TEG unit, was able to produce a maximum output power of 0.02 W, for a thermal gradient of 6.44 K on the TEG (Wu and Yu, 2013).

Due to their low conversion efficiency, none of these studies have led to a product available on the market. Kelk (2015), a Japanese company, have different products based on TEGs, and sell the TEG cells individually, but none of their available products have been developed to implement on road pavements so far.

2.2.2.3 Asphalt solar collector technology

An alternative way of using the thermal gradients between the road pavement layers is to transform the pavement into a solar collector, using pipes and pumps, arranged specifically in order to capture solar energy and convert it into thermal energy. This is a method that has been studied in recent years by different authors, called ASC (Bobes-Jesus *et al.*, 2013).

Sullivan *et al.* (2007) proposed an ASC system for heating and cooling road pavements and other infrastructures, using the heat-absorbing property of asphalt concrete applied on the construction of flexible pavements. The ASC system consists of an asphalt pavement layer with water pipes in it. The ASC system is linked to two underground

water storage reservoirs, one for cold water and another for warm water (RES, 2007), involving seasonal storage. Solar radiation induces an increase in the temperature of the road surface, which is absorbed by the road pavement materials and transferred to a water piping system applied under the road surface and is then stored in the soil or other storage tanks (Sullivan *et al.*, 2007).

The real-world performance of ASCs has been demonstrated by systems installed in different places around the world, working in different climatic conditions. In Switzerland, the Solar Energy Recuperation from the Road Pavement (SERSO) system, presented by Lund (2000), was successfully installed with the main purpose of melting ice on roads. In the Netherlands, Road Energy Systems[®], developed by Ooms (Sullivan *et al.*, 2007) and TNO (Loomans *et al.*, 2003), has been commercialized in recent years, with the main advantages presented by the company being a focus on increased road safety (RES, 2007).

In the UK, ICAX[™] (ICAX, 2014) develops and implements ASC solutions. In Japan, the Gaia system has been developed during the last decade, with different studies being performed focused more on the snow melting heat storage capacity (Morita and Tago, 2000; Gao *et al.*, 2010). The authors say that the heat collecting capacity is between 150 and 250 W/m² under normal summer weather conditions (Gao *et al.*, 2010). Other applications have been developed in China (Tu *et al.*, 2010) and the USA (Mallick *et al.*, 2009).

2.2.3 Vehicle mechanical energy harvesting on road pavements

The mechanical energy transmitted by vehicle wheels to the road surface can induce two types of action on the road pavement: vibrations or surface displacement. This energy can be harvested using different methods and different technologies.

2.2.3.1 Piezoelectric technology

Pierre and Jacques Curie, in 1880, were the first individuals to develop an energy harvesting method from pressure. They successfully predicted and proved experimentally that certain crystals would exhibit a surface charge when subjected to mechanical stress. This phenomenon was given the name piezoelectricity (Harb, 2011), after the Greek word *piezo*, meaning "to press".

Piezoelectric materials fall within a class of multiple solid-state materials that can generate electrical energy with the application of pressure or vibrations (Beeby *et al.*, 2006). Both vehicle pressure and vibrations induced on the road pavement can be used to actuate piezoelectric transducers, in order to convert mechanical energy into electrical energy (Xiang *et al.*, 2013).

Zhao *et al.* (2010) proposed and studied the application of cymbal piezoelectric transducers on road pavements. The amount of generated energy was of 1.2 mW at 20 Hz for one vehicle passage. This was equivalent to 0.06 J per vehicle passage and a conversion efficiency of lower than 15%.

Zhao *et al.* (2013) studied different piezoelectric materials in order to determine how to adapt them for use on road pavements. They have identified that none of the typical piezoelectric transducers made of lead zirconate titanate were suitable for the asphalt pavement environment. They suggest a specific design and optimisation process to adapt the piezoelectric materials for road pavement application.

Xiong *et al.* (2012) have defined two coupling modes of piezoelectric components: 31-mode and 33-mode. With 31-mode, the piezoelectric material generates electrical energy from transverse displacement. On the 33-mode, the power output of the system increases linearly with the deflection of the pavement or the stress along the poling direction of the material. They have stated that the usual power generation capacity of piezoelectric transducers is about $300 \mu\text{W}/\text{cm}^3$.

Wischke *et al.* (2011) studied the application of piezoelectric modules in road pavements in tunnels. They concluded that the vibrations caused by vehicles were small due to vehicle suspension.

The patent applications US20050127677 (Luttrull, 2005) and US20100045111 A1 (Abramovich *et al.*, 2010a) relate to systems that make use of piezoelectric transducers on road pavements that produce electrical energy while being deformed due to the passage of vehicles.. The system presented by Abramovich *et al.* (2010a) was tested in a real environment by Innovattech on a product called Innovattech Piezo Electric Generator (IPEG) (Innovattech, 2014). There are no published results for the generated energy, or for the conversion efficiency of this product.

Abramovich *et al.* (2010b, 2012) have developed a system with new methodologies to increase energy generation and simplified the installation process, as well as using a new methodology to multiply the forces of the vehicles delivered to the piezoelectric transducers (Klein *et al.*, 2012). Nevertheless, there were no scientific results presented for any of these systems.

Bowen and Near (2000) have patented a piezoelectric actuator for road pavements, which was developed recently (Near, 2013), presenting an energy harvesting product based on piezoelectric components for use on road pavements. With this product, Near (2013) created the Genziko company in the USA (Genziko, 2014).

Hill *et al.* (2014) have compared the products developed by Innovattech and Genziko using data provided by both companies. From Innovattech, they present an energy generation per module, per vehicle, of 5.76 J, while Genziko have presented an energy generation per module, per vehicle, of 40 J, almost seven times more than that of Innovattech. However, the authors of the study have concluded that none of these companies have enough real-environment validations to support the presented energy generation values.

2.2.3.2 Electromagnetic technology

Electromagnetic generators operate based on electromagnetic induction, known as Faraday's law, where, if an electric conductor is moved in relation to a magnetic field, electric current will be induced in the conductor (Beeby *et al.*, 2006). These generators

are mostly used in big power plants, based on both non-renewable and renewable sources. In energy harvesting, smaller electromagnetic generators have been developed over the last decade in order to convert environmental energy sources (mechanical vibrations, mostly) into electrical energy (Beeby *et al.*, 2007; Saha, 2011; Arroyo and Badel, 2011; Munaz *et al.*, 2013; Peralta *et al.*, 2014; Elliot and Zilletti, 2014).

Electromagnetic generators are different from piezoelectric systems in that they are not actuated directly by the mechanical energy of vehicles. Interfaces are applied where the harvester units are based on hydraulic or pneumatic systems, electromechanical systems or MEMS, which will be presented following.

2.2.3.2.1 Hydraulic and pneumatic harvesting systems

A hydraulic system consists of a drive or transmission system that uses a pressurized hydraulic fluid to transmit forces and actuate mechanical components, which are usually actuated by electric machines. In the case of pneumatic systems, the difference is in the working fluid; air is used instead of liquid (Parr, 2011). In road pavements, hydraulic systems can be used in the opposite way, transmitting the mechanical energy of the vehicles to actuate electric machines.

Some companies and individual inventors have registered patents where they use hydraulic or pneumatic mechanisms to harvest energy released from vehicles and convert it into electrical energy. These systems are designed to be implemented on roads, as are related patent applications US5634774 (Angel and Gomez, 1997), GB2290115A (Nakatsu, 1994), US6376925B1 (Galich, 2002), US20040130158A1 (Kenney, 2004), US20070246940A1 (Valon, 2007), WO2007045087 (Horianopoulos and Horianopoulos, 2007), US20100192561A1 (Hendrickson, 2010a), WO2010081113A1 (Hendrickson, 2010b), US20110215593A1 (Chang and Lee, 2011) and GB2476826A (Houghton, 2011) for hydraulic systems, and US4173431 (Smith, 1979) and GB2408074A (Morley *et al.*, 2005) for pneumatic systems.

Horianopoulos and Horianopoulos (2007) developed a hydraulic device that harvests energy on road pavements, claiming an energy generation capacity of 51 kWh with

10,000 vehicles passages along 50 meters (Kinergy Power, 2014). This is proportional to 367 (J/m)/vehicle, an average of 91.8 J/wheel, which is a very high value. However, this value is not supported by any scientific evidence, and the average vehicle weight used in the study is not presented. In their patent (Horianopoulos and Horianopoulos, 2007), the working principles of the technology are described without reference to the conversion efficiency. On the basis of this system, they have created the product KinerBump, and the company KinergyPower International Corporation (Kinergy Power, 2014) in the USA.

Moreover, Hendrickson (2010a, 2010b) has created the company New Energy Technologies with a product line called MotionPower™ (NewEnergyTechnologies, 2015), based on his patents. Real-environment tests were performed with this technology but the company has not published the results.

2.2.3.2.2 Electromechanical harvesting systems

In electromechanical systems, electrical devices are operated by mechanical components or vice versa. In the case of electromechanical energy harvesting systems, mechanical energy is used to actuate an electrical machine, which produces electrical energy.

In the case of road pavement energy harvesting, the electromechanical systems can be divided into four classes:

- 1) Conversion of rotational motion of a surface into a rotational motion of an electric generator (Rot-Rot);
- 2) Conversion of linear motion of a surface into a rotational motion of an electric generator (Lin-Rot);
- 3) Conversion of linear motion of a surface into a linear motion of an electric generator (Lin-Lin);
- 4) Conversion of rotational motion of a surface into a linear motion of an electric generator (Rot-Lin).

Table 2.1 summarises the electromechanical systems that are being developed according to the motion conversion principle. From this table, it can be seen that most of the systems have a rotational output motion.

Table 2.1- Patents related to electromechanical systems.

		Input motion	
		Rotational	Linear
Output motion	Rotational	US4238687 (Martinez, 1980), US6767161B1 (Calvo and Calvo, 2004), US7102244B2 (Hunter, 2006), US20090315334A1 (Chen, 2009), US7714456B1 (Daya, 2010), US20110187125A1 (Jang, 2011) and WO2012099706A2 (Mansfield <i>et al.</i> , 2012)	US4434374 (Lundgren, 1984), US20070181372A1 (Davis, 2007), WO2009101448A1 (Hughes <i>et al.</i> , 2009), WO2011145057A2 (Duarte and Casimiro, 2011) and WO2013114253A1 (Duarte and Casimiro, 2013)
	Linear	US20120248788A1 (Pirisi, 2012)	WO2004067850A1 (Hughes <i>et al.</i> , 2004)

On the basis of the systems presented in the patents WO2004067850A1 (Hughes *et al.*, 2004) and WO2009101448A1 (Hughes *et al.*, 2009), the company Highway Energy Services was created (HES, 2015), in the UK. Besides the information presented in their patents, no technical data is available on these systems.

Pirisi (2012), following his patent, has developed a prototype of the technology which, together with researchers from Politecnico di Milano, he has tested and presented the results (Pirisi *et al.*, 2012a, 2012b, 2013). The generator is described as a tubular permanent magnet linear generator, an electromechanical device able to convert linear motion into electrical energy; using a 1:10 scale prototype in the laboratory, they claim a conversion efficiency of 85% (Pirisi *et al.*, 2013) between the mechanical energy applied to the slider of the generator and the electrical output efficiency. This value does not include power electronics, but presents only the conversion efficiency of the generator. In laboratory tests, the system was applied on the top of the road surface. The

authors of this system have created the company Underground Power, which is developing a product called "LYBRA" (Underground Power, 2014).

In the USA, the authors of the patent WO2012099706A2 (Mansfield *et al.*, 2012), a class-1 system, have created the company Energy Intelligence. So far, there have been no scientific results presented for the project. The authors maintain that the system will be embedded in the road surface, replacing the upper layers of the road pavement (EnergyIntelligence, 2014).

Following the development of a suitable system to convert people-released energy into electrical energy (Duarte and Casimiro, 2011), with a 60% conversion efficiency (Duarte *et al.*, 2013a, 2013b), Duarte and co-authors have developed the system presented in the patent WO2013114253A1 (Duarte and Casimiro, 2013), with a class-2 system, suited for application on roads. The authors, together with the company Waydip, have tested a real-scale prototype, naming the project Waynergy[®] Vehicles (Waydip, 2015). Laboratory tests with the prototype obtained experimental energy generation data, achieving a conversion efficiency of about 50% for the mechanical energy delivered to the system and the electrical energy output delivered to an electric load (Duarte *et al.*, 2014, 2016). The system was applied on the upper layer of the road pavement.

2.2.3.2.3 MEMS harvesting systems

MEMS is a technology that is usually defined as miniaturised mechanical and electromechanical elements, made using the techniques of micro-fabrication, which can vary from relatively simple structures having no moving parts to extremely complex electromechanical systems with multiple moving parts, usually under the control of integrated microelectronics. There has been much recent interest in using MEMS to harvest energy from ambient vibration and transform it into electrical energy (Stephen, 2006).

To find optimal architectures for maximal power generation under the different operating constraints, analysis and verification by simulation of three classes of MEMS-

based vibration-driven microgenerator architectures were presented by Mitcheson *et al.* (2004).

Harb (2011) studied and tested different MEMS systems in laboratory, actuating electromagnetic microgenerators. These generators presented a maximum energy conversion efficiency of 18%, with ten cells and a buck converter.

Zorlu and Külah (2013) developed a MEMS-based energy harvesting device to generate electrical energy from vibrations, with implementation on road pavements being one of the possible applications. In laboratory tests with a prototype, a maximum output of 3.2 mW/cm^3 was achieved, which is a high power density for this type of application. However, when a prototype was developed to be tested in a real environment, the energy generation was $6.0 \text{ }\mu\text{W/cm}^3$, 500 times lower than in laboratory tests. So, the technology presents some potential but, when applied in a real environment, its efficiency decreased considerably.

The patent US20130193930A1 (Baugher, 2013) presents a system consisting of a microstructure for implementation under the road surface, which uses vibrations to actuate piezoelectric materials to generate electrical energy. No commercial application of this system has been developed so far, nor have technical results of experiments been published, as the system is under development.

2.2.4 Technical analysis

To perform a technical analysis and evaluate an energy generation technology, the most commonly used parameters are the installed power (per area or volume), conversion efficiency, power density and the energy generation of the technology in normal operating conditions (Table 2.2). In the specific case of road pavement energy harvesting, it is also important to classify the technologies according to the installation method (IM), as this is an important issue regarding the final cost of the solution, the driving and safety conditions and the maintenance operations of the equipment. Finally,

as these are mostly new technologies, it is important to classify them regarding their development status – in this case, using technology readiness levels (TRLs).

Table 2.2- Parameters for performing a technical analysis.

Parameter	Description
Installed power	The installed power of an electrical energy generation device is its energy generation capacity in nominal conditions – that is, the maximum theoretical power it can generate. It is related to the output power and is expressed in watts (W). In many cases, it is expressed by comparing the installed power with the occupied area of the device (W/m^2), or with the occupied volume of the device (W/m^3). In micro-energy harvesting devices, the analysis is usually done in regard to volume
Conversion efficiency	Energy conversion efficiency (η) is the ratio between the useful output of an energy conversion device and the energy input. In the case of electrical machines, the output is electrical energy measured in joules (J), or electrical power measured in watts (W). The energy conversion efficiency is a dimensionless parameter, usually expressed as a percentage
Energy generation	Energy generation is used to quantify the amount of electrical energy generated under the operating conditions. It gives the energy input of the system, its efficiency and the installed power. Usually, it is expressed in joules, but in some micro-energy harvesting devices it can also be related to the volume (J/m^3). In the analysis of energy harvesting devices, sometimes power generation is also presented, related to the volume of the device (W/m^3)
IM	The different energy harvesting devices can be installed in the road pavement using different techniques and in different layers of the road pavement. Four main installation methods were identified
TRL	TRLs are measures used to evaluate the maturity of a technology during its developmental stages. These levels were initially defined by NASA (Mankins, 1995), but are now commonly used in project evaluations

Following the analysis of the different technologies presented in this study, the main characteristics of each one are presented in Table 2.3. For this analysis, the technologies that convert both solar and vehicle mechanical energy into useful electrical energy and which have been tested on road pavements were considered. So, ASC, induction heating and MEMS technologies were excluded from the analysis.

Table 2.3- Technical analysis of different road pavement energy harvesting technologies.

Technology	Company/ R&D institute	Installed power (W/m ²)	Conversion efficiency (%)	Energy generation	IM ^a	TRL ^b
PV	Solar Roadways	97.3	11.2%	Not reported	1	4
	TNO	Not reported	Not reported	Not reported	2	7 ^c
TEG	Hasabe <i>et al.</i>	Not reported	Not reported	38.0 mW/cm ³	3	3
	Wu and Yu	Not reported	1.6%	2.6 mW/cm ³	3	3
Piezoelectric	Innowattech	Not reported	Not reported	5.8 J/veh m	3	4
	Genziko	1942.0	Not reported	40.0 J/veh m	3	4
Hydraulic	Kinergy	Not reported	Not reported	188.0 J/veh m	1/2	4
	New Energy Technologies	Not reported	Not reported	Not reported	1/2	4
Electro-mechanical	Waydip	833.0	50.0%	680.0 μ W/cm ³ 180.0 J/veh m	2	4
	Underground Power	Not reported	85.0% ^d	Not reported	1/2	4
	HES	Not reported	Not reported	Not reported	2	3
	Energy Intelligence	Not reported	Not reported	Not reported	2	3

a – IM 1 - on the road pavement surface, fixed to the upper layer (the device surface becomes the new road surface); IM 2 - embedded in the road pavement, upper layer, surface exposed (the device surface becomes the new road surface); IM 3 - embedded in the road pavement, upper layer, surface covered by road pavement material; IM 4 - embedded in the road pavement, lower layer, surface covered by road pavement material

b - TRL 1 - basic principles observed and reported; TRL 2 - technology concept and/or application formulated; TRL 3 - analytical and experimental critical function and/or characteristic proof-of-concept; TRL 4 - component validation in laboratory environment; TRL 5 - component validation in relevant environment; TRL 6 - system/subsystem model or prototype demonstration in a relevant environment; TRL 7 - system prototype demonstration in an operational environment; TRL 8 - actual system completed and qualified through tests and demonstration; TRL 9 - actual system proven in operational environment

c - For cycle lanes. For road pavements it has only been conceptualized, not prototyped (TRL 1/2)

d - Efficiency on a 1:10 scale and not considering the losses of control, storage and deliver energy to an electrical load

From Table 2.3, it may be seen that most of the studies do not meet all the parameters required to perform a complete technical analysis, hindering a more detailed and direct comparison of all the technologies. Most researchers or companies present only the energy generation capacity and IM of the developed devices and only a few studies present the installed power and the conversion efficiency of the technologies. From this analysis, one can conclude that the systems that make use of vehicle mechanical energy have a higher conversion efficiency and energy generation capacity than the systems

that make use of solar radiation. In terms of energy generation, hydraulic and electromechanical systems present higher capacities.

In terms of IMs, PV systems are mainly applied using IM 1, while TEG systems are applied under the road surface, using IMs 3 and 4. Piezoelectric systems are also applied using IM 3, while hydraulic and electromechanical systems can both be installed using methods 1 or 2, with their surface in direct contact with vehicle wheels, to maximise the energy input to the system.

In terms of development status, one can conclude that none of these devices are fully validated and available on the market; they are generally at TRL 3 or 4. The TNO system is on TRL 7, but this is for cycle path application and does not present any evidence of application on roads.

To determine fully whether any technology is viable, an economic analysis should also be performed. In such an analysis, the most important factor is the levelized cost of electricity (LCOE), which determines the cost per watt produced, relating the total economic investment in a technology to the energy generated (EIA, 2014). However, no technology is fully developed and available on the market. So, no economic data of any product are yet available and such an analysis cannot be performed at this stage.

2.3 Energy Harvesting on Railways

2.3.1 Introduction

The concept of energy harvesting in the railways industry has started with the goal of directly supplying trackside electrical infrastructure used for safety and monitoring purposes (e.g. electric and electronic equipment such as sensors, cameras, electric panels, etc.). These devices typically have a power consumption of 10–100 W (Lin *et al.*, 2014), so this was set as the energy generation goal in several research projects (Lin *et al.*, 2014; Phillips, 2011; Pourghodrat, 2011).

Different systems were developed for this purpose, both for harvesting the mechanical vibrations induced by trains into the railway track, as well as converting these into electricity. Energy conversion (or energy generation) technologies are mostly electromagnetic and piezoelectric but, in the case of electromagnetic technology, the systems to actuate the energy generation components can be electromechanical, hydraulic, pneumatic or other specific systems. Electromagnetic generators can be linear or rotational. Figure 2.2 illustrates the segmentation of the developed systems, with EH representing energy harvesting and EG representing energy generation.

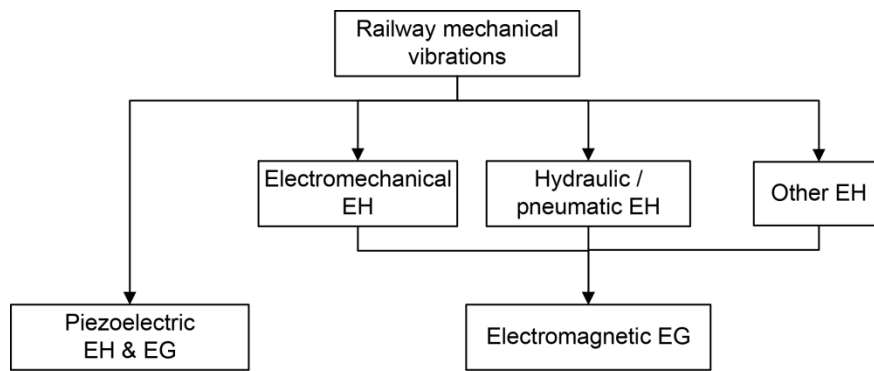


Figure 2.2- Railway EH and EG technologies.

2.3.2 Piezoelectric technologies

In the case of railways, Nelson *et al.* (2007) initially developed a system based on piezoelectric technology to harvest the mechanical energy provided by moving trains to the rail, in the form of mechanical vibrations and pressure, and to convert it into electricity. They concluded that the maximum power generation with this technology was about 0.05 mW per each train passage, a very small value that is insufficient to supply electric equipment by itself.

The Israeli company Innowattech has also developed a system based on piezoelectric technology to harvest the mechanical energy of moving trains and convert it into

electricity (Innowattech, 2014). The company has registered three different patents. Under the patent WO2009098673 A1 (Abramovich *et al.*, 2009), a piezoelectric generator (IPEG) is applied under the railroad fixation to the sleeper, producing electrical energy when compressed by a moving train. Also based on piezoelectric technology, alternative energy harvesting devices are presented in patents US20100045111 A1 (Abramovich *et al.*, 2010a) and US20110291526 A1 (Abramovich *et al.*, 2011); these consist of piezoelectric cells in a stack using the same installation methodology as patent WO2009098673 A1 (Abramovich *et al.*, 2009). However, no prototype tests or results have been published about the systems presented in these patents.

Wischke *et al.* (2011) tested the IPEG system developed by Innowattech in a laboratory and in a real environment. They concluded that with one piezoelectric cell, the maximum energy generation with a passing train was 0.26 mJ, a very small value to fully supply electric or electronic equipment near the railway track. A huge number of cells would be required to acquire acceptable values of energy generation with this technology.

2.3.3 Electromagnetic technologies

Some researchers are investigating energy harvesting techniques on railway tracks using electromagnetic generators as the energy generation component of the system. Electromagnetic generators are different from piezoelectric systems, as they are not actuated directly by the mechanical energy of moving trains. Interfaces are applied between the energy source and the energy generator in order to maximise the harvested energy, supply the electromagnetic generators with the appropriate characteristics of mechanical energy, exploit their maximum efficiency, guarantee best performance and protect them from high loads that could incur damage. The harvesting units are based on electromechanical systems, hydraulic or pneumatic systems, or MEMS. The technologies that have been developed for this purpose are now presented.

2.3.3.1 Electromechanical actuation

Nelson *et al.* (2009) were the first to present an electromechanical system for implementation on railway tracks to convert the mechanical vibrations induced by trains into electrical energy. Their initial approach consisted of a mechanical system making use of railway track vibrations to actuate a shaft, via a rack–pinion system, converting the linear motion of the railway track into rotational motion of the shaft. The shaft, in turn, was connected to an electromagnetic generator, through a gearbox and a flywheel. The developed prototype was tested in a laboratory and achieved an energy generation of 10.05 W for a load identical to a train in motion. This result was considered very positive, being much higher than all other published results at the time (Nelson *et al.*, 2009).

Following Nelson's research, Penamalli (2011) tried to optimise the electromechanical system with a mechanical approach that increases the number of rotations in the shaft of the electromagnetic generator, leading to higher generation. This was achieved with a mechanical system called a "mechanical motion rectifier". The system was also based on the rack and pinion methodology of Nelson *et al.* (2009), but it increased the number of rotations on the shaft, with constant values, turning the irregular upward and downward track vibrations into a unidirectional motion and used a flywheel to stabilise the generator speed by storing energy during the high-speed vibration pulse and then releasing the stored energy to rotate the generator during low-speed vibration. The prototype was tested in a laboratory with loads emulating a moving train, and achieved a global energy conversion of 22.0%. The results in terms of energy generation were not higher than 3.00 W, but the author offered several recommendations for improvements to the system to increase its efficiency and energy generation (Penamalli, 2011).

Also following the research of Nelson *et al.* (2009), Pourghodrat (2011) optimised the electromechanical system, keeping the rack and pinion system, but with a different approach: the system was actuated in both the downward and upward motion of the railway track, increasing the rotation of the generator. Computational simulations of the system presented a potential average output power of 41.82 W, much higher than the system developed by Nelson's team. The difference was mainly due to the higher

rotation of the generator shaft and the new electromagnetic generator integrated in the system. In extreme conditions (a loaded train and 60 mph (≈ 97 km/h) travelling speed), the Nelson' project achieved 10.05 W. Pourghodrat intended to achieve, theoretically, 306.28 W of average output power. However, when the prototype was tested in the laboratory, only 4.24 W of average output power was achieved (Pourghodrat, 2011).

After failing to improve on Nelson's system output, Pourghodrat proposed a new electromechanical system with a new actuation principle – actuated directly by the train wheels instead of using only the mechanical vibrations of the railway track (Pourghodrat, 2011). To develop the system, Pourghodrat used the principle of the mechanical wayside lubrication system. In this system, each train wheel actuates a lever that, through the cam-follower mechanical system, actuates the gearbox shaft, which in turn actuates the electromagnetic generator. The development or testing of a prototype has not been reported, but Pourghodrat estimates, theoretically, that the system could produce four times more power than the system developed by Nelson *et al.* (2009).

Following the research of Nelson *et al.* (2009) and combining it with the work of Pourghodrat (2011), Phillips (2011) has modelled and computationally simulated the potential of both systems. Phillips concluded that Pourghodrat's system presents the greater potential for generating electrical energy, achieving a theoretical value of 276.87 W, which is enough to supply most of the electric devices used near railway tracks. Phillips also tested the system proposed by Pourghodrat (2011) in a laboratory, achieving an average power output of 5.29 W. It was concluded that the problem was in the generator shaft speed, which did not reach the theoretical speeds, leading to much lower power generation in practice.

Following on from the research of Nelson *et al.* (2009) and Penamalli (2011), Lin *et al.* (2014) optimised the electromechanical system, based on the double rack and pinion proposed by Penamalli (2011), with a new mechanical approach. Lin *et al.* aimed to reduce friction, which was the main cause of the low experimental results achieved with the prototype developed by Penamalli (2011), and so used a single shaft, doubly actuated (downward and upward motion of the railway track), with one flywheel and a gearbox, connecting the shaft to the generator. The prototype was tested in the

laboratory and in a real environment, and managed an average power output of 49.80 W, almost five times higher than the Nelson *et al.* (2009) prototype under the same test conditions. This system achieved an overall conversion efficiency of 45.60%, the highest value achieved with a prototype when comparing all the devices.

2.3.3.2 Hydraulic actuation

In railways, mechanical energy is delivered from train loads to the railway track so hydraulic systems can be used in the opposite way to their common use: transmitting the mechanical energy of the train to actuate electric machines.

Oxtoby (2010) developed a hydraulic system that makes use of the weight of a train to actuate a turbine. In this system, a passing train compresses a pad on the railway track, which produces a flow of air that in turn actuates a turbine. However, no technical results of this system were presented and no commercial application of the system was found.

Besides the two electromechanical systems described earlier, Pourghodrat (2011) also came up with a hydraulic energy harvesting system to actuate an electromagnetic generator using a train's mechanical energy. The goal with this system was to amplify the vertical deflection of the rail using a hydraulic actuator. This system was expected to achieve 40.00 W of power output for each loaded train passage, and a prototype was tested in the laboratory. Under the same test conditions used for the two electromechanical systems proposed by Pourghodrat (2011), the hydraulic system achieved an average power output of 11.08 W in the best case scenario. This is a promising result because several hydraulic energy harvesters can be connected to the same electromagnetic generator, multiplying the power output for the same train passage, without additional electromagnetic generators.

2.3.3.3 Other actuation types

Nelson *et al.* (2007) originally started the concept of harvesting a train's mechanical energy on a railway track by using an electromagnetic device, a simple electromagnetic linear generator, directly driven by the vertical displacement of the rail. The generator was called the 'inductive coil' electromagnetic generator. This system, tested in the laboratory, achieved an average power output of 0.15 mW. Mian (2013a, 2013b), representing the US International Electronic Machines Corporation (IEM, 2015), developed a similar concept but, instead of using an inductive coil, used a magnetic coil actuated by the train wheel pressure. This system was patented (Mian, 2013a, 2013b), but technical results of the prototype have not been published. On the IEM website, this technology is presented as a module of a multi-energy harvesting technology that is part of the solution called RailPower Suite, which comprises several technologies for harvesting energy on or nearby railroads and converting it into electrical energy. However, with no technical results reported, it is not possible to compare this technology with the other systems discussed.

2.3.4 Technical analysis

To perform a technical analysis and evaluate an energy generation technology, the most commonly used parameters were presented in Table 2.2. For the particular case of the railway energy harvesting systems, the IM is different when compared with the road pavement energy harvesting systems, as different energy harvesting devices can be installed on railway track using different techniques and in different zones of the railway track. Three main IMs were identified:

- IM 1: fixed on the rail lateral area, harvesting the rail vibrations;
- IM 2: fixed on the rail base, between the rail and the sleeper;
- IM 3: fixed on the railway track, harvesting the train's wheel mechanical pressure.

Following the analysis of the different technologies previously presented, the main characteristics of each are presented in Table 2.4. For this analysis, only technologies with results published in scientific papers were considered. Table 2.4 reveals that most of the reported studies do not quantify the conversion efficiency of the technologies, but almost all reveal the power/energy generation, the IM and identify the TRL. From this analysis, one can conclude that most current research is based on electromechanical systems and these are the ones that permit higher values in terms of electrical energy production.

Table 2.4- Technical analysis of different railway energy harvesting technologies.

Technology	Reference	Conversion efficiency (%)	Power/energy generation	IM	TRL
Piezoelectric	Nelson <i>et al.</i> (2007)	Not reported	0.05×10^{-3} W	1	5
	Abramovich <i>et al.</i> (2009, 2010a, 2011)	Not reported	Not reported	2	3
	Wischke <i>et al.</i> (2011)	Not reported	0.26×10^{-3} W.s (J)	2	5
Hydraulic	Oxtoby (2010)	Not reported	Not reported	3	2
	Pourghodrat (2011)	Not reported	11.08 W	1	4
Electro-mechanical	Nelson <i>et al.</i> (2009)	Not reported	10.05 W	1	4
	Penamalli (2011)	22.0%	2.50 W	1	4
	Pourghodrat (2011)	Not reported	4.24 W	1	4
	Pourghodrat (2011)	Not reported	50.00 W ^a	3	2
	Philips (2011)	Not reported	5.29 W	1	4
	Lin <i>et al.</i> (2014)	45.6%	49.8 W	1	5
Other	Nelson <i>et al.</i> (2007)	Not reported	0.15 W	1	3
	Mian (2013a, 2013b)	Not reported	Not reported	3	-

a – Theoretical value

The system developed by Lin *et al.* (2014), resulting from an optimisation of two previous studies (Nelson *et al.*, 2009; Penamalli, 2011), presents the highest value in terms of energy generation (proved experimentally) and is one of the most advanced in terms of TRL. Piezoelectric technology, besides being on an advanced TRL, presents very low energy production values, making it a technology with low technical and economic viability for generating electrical energy. Hydraulic systems, especially the system developed by Pourghodrat (2011), present an interesting potential: with one unit

a good value was achieved in terms of energy production (the second highest experimentally proven value) and this could be multiplied with the use of more hydraulic units connected to the same electromagnetic generator.

In terms of IM, most of the technologies are fixed on the rail lateral area, harvesting the mechanical vibrations of the railway. The exceptions are the piezoelectric systems installed between the rail and the sleepers and some other systems that use the pressure of the train's wheels to harvest mechanical energy directly from the train's weight.

In terms of TRL, the system developed by Mian (2013a, 2013b) is already commercially available (IEM, 2015), but no values regarding energy production or conversion efficiency have been published. Innowattech (2014) also presents some piezoelectric solutions in its portfolio, but again with no reported values for energy generation or energy conversion efficiency of the systems. Apart from these two systems, which are related to the R&D of the companies, the electromechanical system presented by Lin *et al.* (2014) is at the most advanced stage as it has been tested and validated in a real environment. Most of the other solutions analysed have only been tested in laboratory conditions.

2.4 Summary and conclusions

2.4.1 Road pavement technologies

The concept of road pavement energy harvesting has become increasingly popular over the last few years. Unlike the case of wind energy, the present situation shows a wide variety of energy harvesting systems, at several stages of development, competing against each other to get an opportunity in the market. In the last 15 years or so, the research and development activity in road pavement energy harvesting has been developed more by companies than by universities, leading to a lack of scientific evidence being available on the developed technologies. The tests performed were not fully characterised in the literature, making very limited information available about the experimental tests and results obtained. It is clear that none of the developed

technologies have been fully developed and validated, as none of them have entered the market with a finished and certified product (with the exception of ASC, which is an energy harvesting system, but not to generate electrical energy). In the road pavement energy harvesting field, most of the technologies are at a laboratorial and prototyping validation stage.

Comparing the technologies that make use of solar energy as their energy source with the technologies that make use of vehicle mechanical energy, the former is at a more advanced developmental stage, as it makes use of more mature systems and technologies. However, presently, most research and development is being performed on the latter, mainly due to the higher potential that these systems present, in terms of energy conversion efficiency, energy generation and adaptability to road pavement conditions.

Comparing the technologies that make use of solar energy as an energy source, PV systems are the most efficient and mature. However, the implementation on road pavements is still a challenge, as glass has been used on the PV cells, causing difficulties for vehicle adherence, which is essential to guarantee rolling capacity and safety conditions. Systems that make use of TEGs are easier to install on the road pavement; however, efficiency is considerably reduced.

Comparing the technologies that make use of vehicle mechanical energy as an energy source, piezoelectric technology was the first to get the attention of researchers. However, due to its lower energy conversion efficiency, the developments with this technology have decreased in the last 4 or 5 years. On the other hand, there has been an increase in research and development of electromechanical systems that harvest vehicle mechanical energy and, using electromagnetic generators, generate electrical energy. These, together with hydraulic systems, have registered the highest energy generation values in experimental tests. Their installation is also simpler than the installation of piezoelectric devices and they currently present a higher likelihood of success as an effective solution to transform vehicle mechanical energy into electrical energy effectively.

MEMS also present potential in this field since they have been successful in other applications. However, in the case of road pavement energy harvesting, they have been applied to harvesting pavement vibrations instead of directly harvesting vehicle mechanical energy. Pavement vibrations represent a small amount of the available energy, leading to a low level of energy generation. In the future, these systems should also be developed to harvest vehicle mechanical energy in order to maximise energy generation.

2.4.2 Railway technologies

The concept of railway energy harvesting is a very recent area of research, which has only taken off in the last five years. Unlike wind energy, the present situation shows a wide variety of energy harvesting systems at several stages of development and competing with each other to obtain an opportunity in the market. Different technologies are being investigated in order to convert the mechanical energy induced by trains on railway tracks into electrical energy. Piezoelectric and electromagnetic technologies are dominant, with electromagnetic generators being actuated by different harvesting systems.

In terms of systems/technologies validated in a real environment and with published results, only one system is available. This system, developed by Lin *et al.* (2014), achieved a power production of 49.80 W for each train passage. Higher values of energy production can be achieved for each train passage by multiplying the number of devices, but investment in the solution would clearly be multiplied by the number of devices. In that sense, the hydraulic system proposed by Pourghodrat (2011) could be a very interesting solution. With one hydraulic energy harvester and one electromagnetic generator, a power production of 11.08 W for one train passage was achieved in the laboratory; as this system allows multiplication of the number of hydraulic harvesters for the same electromagnetic generator, the harvested energy (and consequently the electrical energy produced) can be multiplied without the need to multiply the number of generators. Energy production could thus be greatly increased with a lower

investment increase than required for the electromechanical system proposed by Lin *et al.* (2014).

In terms of energy application, most researchers have targeted the electric and electronic devices used to monitor railway tracks and guarantee user safety; these devices have power consumptions of 10.00–100.00 W (Zuo and Tang, 2013). To supply these electric and electronic devices, the systems proposed by Lin *et al.* (2014) and Pourghodrat (2011) offer potential. These devices are the most targeted solutions, mainly due to the fact that there are many areas on railway lines with no electricity, making it a challenge to supply electric devices in those areas. The use of generated electrical energy to directly supply electrical equipment near the railway is, at the present time, the most interesting application for energy harvesting equipment.

However, by multiplying the number of energy harvesters and generators, higher values of energy production could be achieved and the concept of railway energy harvesting could increase its potential by injecting the produced energy into the national grid. Considering the available power from a railway track over long distances, the extraction and generation of a great amount of energy is possible (Zuo and Tang, 2013). These two major applications should be considered when the technical and economic viability of the developed technologies is studied: the cost of each solution needs to be considered to analyse the return on investment.

In terms of future directions, the developed systems should be optimised and tested in real environments, using the generated electrical energy to supply electrical equipment used near railways or, if high energy generation values were achieved, to inject energy into the electrical grid. New devices should also be developed using different technologies that allow the conversion of mechanical energy into electrical energy, such as pneumatic devices and other hydraulic systems, different from the system developed by Pourghodrat (2011). Energy storage also needs to be analysed: these systems capture mechanical energy, which can be more easily and efficiently stored than electrical energy and then converted into electrical energy only when needed. The simultaneous use of harvesting, storage and converting systems could be a key factor for the success of mechanical energy harvesting and should be one of the key research areas in the

future. Finally, the effect of railway dynamics on the developed systems needs to be analysed to guarantee that a sufficient period of in-service time is available to make this new technology viable as an alternative power source in economic terms.

2.5 References

- Abramovich, H., Harash, E., Milgrom, C. and Amit, U. (2009). *Power Harvesting from Railways; Apparatus System and Method*. Patent WO2009098673 A1, Aug.
- Abramovich, H., Milgrom, C., Harash, E., Azulay, L. and Amit, U. (2010a). *Multi-layer modular energy harvesting apparatus, system and method*. US Patent US20100045111 A1, Feb.
- Abramovich, H., Harash, E., Milgrom, C., Azulay, L., Tsikhotsky, E. and Amit, U. (2010b). *Modular Piezoelectric Generators*. International Patent Application PCT/IL2009/000365, Patent WO2010116348 A1, Oct.
- Abramovich, H., Milgrom, C., Harash, E., Azulay, L. and Amit, U. (2011). *Piezoelectric Stack Compression Generator*. US Patent US20110291526 A1, Dec.
- Abramovich, H., Milgrom, C., Harash, E., Azulay, L., Amit, U. and Klein, G. (2012). *Piezoelectric-based weight in motion system and method for moving vehicles*. International Patent Application PCT/IL2011/000741, Patent WO2012038955 A1, Mar.
- Angel, R. and Gomez, J. (1997). *Road vehicle-actuated air compressor*. US Patent US5634774, Jun.
- Arroyo, E. and Badel, A. (2011). Electromagnetic vibration energy harvesting device optimization by synchronous energy extraction. *Sensors and Actuators A: Physical*, 171(2): 266-273.
- Baughner, J.P. (2013). *Energy Harvesting with a Mico-Electro-Mechanical System (MEMS)*. US Patent US20130193930 A1, Aug.

- Beeby, S. P., Tudor, M. J. and White, N. M., (2006). Energy harvesting vibration sources for Microsystems applications. *Journal of Measurement Science and Technology*, 17(12): R175.
- Beeby, S. P., Torah, R. N., Tudor, M. J., Glynne-Jones, P., O'Donnell, T., Saha, C. R. and Roy, S. (2007). A micro electromagnetic generator for vibration energy harvesting. *Journal of Micromechanics and microengineering*, 17(7): 1257.
- Bobes-Jesus, V., Pascual-Muñoz, P. and Castro-Fresno, D. (2013). Asphalt solar collectors: A literature review. *Applied Energy* 102: 962-970.
- Bowen, L. and Near, C (2000). *Low voltage piezoelectric actuator*. US Patent 6,111,818, Aug.
- Brusaw, S. and Brusaw, J. (2014). *Solar Roadway Panel*. Design Patent US D712822S, Set.
- Calvo, R. and Calvo, J. (2004). *Highway electric power generator*. US Patent US6767161 B1, Jul.
- Chang, H. and Lee, C. (2011). *On-road energy conversion and vibration absorber apparatus*. US Patent US20110215593 A1, Sep.
- Chen, R. (2009). *Vehicular Movement Electricity Converter Embedded Within A Road Bumb*. US Patent US20090315334 A1, Dec.
- Davis, C.R. (2007). *Roadway power generating system*. US Patent US20070181372 A1, Aug.
- Daya, A. (2010). *Road vehicle actuated energy device*. US Patent US7714456 B1, May.
- Duarte, F. and Casimiro, F. (2011). *Pavement module for generating electric energy from the movement of people and vehicles*. International Patent Application PCT/IB2011/052164, Patent WO2011145057 A2, Nov.
- Duarte, F. and Casimiro, F. (2013). *Electromechanical system for electric energy generation and storage using a surface motion*. International Patent Application PCT/IB2013/050616, Patent WO2013114253 A1, Aug.

- Duarte, F., Casimiro, F., Correia, D., Mendes, R. and Ferreira, A. (2013a). Waynergy People: a new pavement energy harvest system. *Proceedings of the Institution of Civil Engineers – Municipal Engineer*, 166(4): 250-256, <http://dx.doi.org/10.1680/muen.12.00049>.
- Duarte, F., Casimiro, F., Correia, D., Mendes, R. and Ferreira, A. (2013b). A new pavement energy harvest system. *Proceedings of the International Renewable and Sustainable Energy Conference, Ouarzazate, Morocco*. IEEE – Institute of Electrical and Electronics Engineers, New York, NY, USA (CD-ROM).
- Duarte, F., Champalimaud, J. and Ferreira, A. (2014). Waynergy Vehicles: an innovative pavement energy harvest system. *Proceedings of the 2nd International Congress on Energy Efficiency and Energy Related Materials*, Oludeniz, Turkey. Springer, London, UK (CD-ROM).
- Duarte, F., Champalimaud, J. and Ferreira, A. (2016). Waynergy Vehicles: an innovative pavement energy harvest system. *Proceedings of the Institution of Civil Engineers – Municipal Engineer*, 169(1): 13-18, <http://dx.doi.org/10.1680/muen.14.00021>.
- EIA (2014). *Levelized Cost and Levelized Avoided Cost of New Generation Resources in the Annual Energy Outlook 2014*. U.S. Energy Information Administration, Washington DC, USA. Available from: http://www.eia.gov/forecasts/aeo/pdf/electricity_generation.pdf. Accessed in September, 2015.
- Elliott, S. J. and Zilletti, M. (2014). Scaling of electromagnetic transducers for shunt damping and energy harvesting. *Journal of Sound and Vibration*, 333(8): 2185-2195.
- EnergyIntelligence (2014). <http://www.energyintel.us/>. Accessed in December, 2014.
- Galich, T. (2002). *Force stand for electrical energy producing platform*. US Patent US6376925 B1, Apr.
- Gao, Q., Huang, Y., Li, M., Liu, Y. and Yan, Y. Y. (2010). Experimental study of slab solar collection on the hydronic system of road. *Solar Energy*, 84(12): 2096-2102.

- Genziko (2014). <http://www.genziko.com/>. Accessed in December, 2014.
- Harb, A. (2011). Energy Harvesting: State-of-the-art. *Renewable Energy*, 36(10): 2641-2654.
- Hasebe, M., Kamikawa, Y. and Meiarashi, S. (2006). Thermoelectric Generators using Solar Thermal Energy in Heated Road Pavement. In *Proceedings ICT '06 – 25th International Conference on Thermoelectrics (ICT)*, Vienna, Austria. IEEE – Institute of Electrical and Electronics Engineers, New York, NY, USA, pp. 697–700.
- Hendrickson, B. (2010a). *Adaptive, Low-impact vehicle energy harvester*. US Patent US20100192561 A1, Aug.
- Hendrickson, B. (2010b). *Vehicle energy harvesting roadway*. International Patent Application PCT/US2010/020676, Patent WO2010081113 A1, Jul.
- HES (Highway Energy Services) (2015). <http://www.hughesresearch.co.uk/>. Accessed in January, 2015.
- Hill, D., Agarwal, A. and Tong, N. (2014). *Assessment of piezoelectric materials for roadway energy harvesting*. DNV KEMA Energy and Sustainability, Sacramento, FL, USA. Available from: <http://www.energy.ca.gov/2013publications/CEC-500-2013-007/CEC-500-2013-007.pdf>. Accessed in September 2015.
- Horianopoulos, D. and Horianopoulos, S. (2007). *Traffic-actuated electrical generator apparatus*. International Patent Application PCT/CA2006/001710, Patent WO 2007045087 A1, Apr.
- Houghton, L. (2011). *Hydraulic powermat*. UK Patent Application GB 2476826 A, Intellectual Property Office, UK, Jul.
- Hughes, P., Hughes, A.M., Hughes, R. and Hughes, A.P. (2004). *Apparatus for converting kinetic energy*. International Patent Application PCT/GB2004/000364, Patent WO2004067850 A1, Aug.
- Hughes, P., Hughes, A.M., Hughes, R. and Hughes, A.P. (2009). *Improvements in and relating to apparatus for converting kinetic energy*. International Patent Application PCT/GB2009/050145, Patent WO2009101448 A1, Aug.

- Hunter, J. (2006). *Vehicle actuated road imbedded magneto generator*. US Patent US7102244 B2, Sep.
- ICAX (2014). <http://www.icax.co.uk>. Accessed in November, 2014.
- IEM (International Electronic Machines Corporation) (2015). <http://www.iem.net/>. Accessed in June, 2015.
- Innowattech (2014). <http://www.innowattech.co.il/>. Accessed in July, 2014.
- Jang, J. S. (2011). *Electrical generator apparatus, particularly for use on a vehicle roadway*. US Patent US20110187125 A1, Aug.
- Kang-Won, W. and Correia, A.J. (2010). *A pilot study for investigation of novel methods to harvest solar energy from asphalt pavements*. Korea Institute of Construction Technology (KICT), Goyang City, South Korea.
- Kazmierski, T. and Beeby, S. (Eds.). (2009). *Energy harvesting Systems - Principles, Modeling and Applications*. Springer, New York, NY, USA.
- Kelk (2015). <http://www.kelk.co.jp/english/index.html>. Accessed in February, 2015.
- Kenney, T. (2004). *System and method for electrical power generation utilizing vehicle traffic on roadways*. US Patent US20040130158 A1, Jul.
- Khaligh, A. and Onar, O. C. (2010). *Energy harvesting: solar, wind, and ocean energy conversion systems*. CRC Press Inc., Boca Raton, FL, USA.
- Kinergy Power (2014). <http://www.kinergypower.com/index.shtml>. Accessed in December, 2014.
- Klein, G., Tsikhotsky, E., Abramovich, H. and Milgrom, C. (2012). *Modular Piezoelectric generators with a mechanical force multiplier*. International Patent Application PCT/IL2012/050369, Patent WO2013038415 A1, Mar.
- Lin, T., Wang, J. and Zuo, L. (2014). *Energy Harvesting from Rail Track for Transportation Safety and Monitoring*. University Transportation Research Center, New York, NY, USA, UTRC-II Project Final Report, pp. 1–11.

- Loomans, M., Oversloot, H., de Bondt, A., Jansen, R. and van Rij, H. (2003). Design tool for the thermal energy potential of asphalt pavements. *Proceedings of Building Simulation '03 – the 8th International Building Performance Simulation Association International Conference, Eindhoven, the Netherlands*, pp. 745–752.
- Lund, J. W. (2000). Pavement snow melting. *Geo-Heat Center Quarterly Bulletin*, 21(2): 12-19.
- Lundgren, R. (1984). *Device for generating electricity by pedestrian and vehicular traffic*. US Patent US4434374, Feb.
- Luttrull, J. (2005). *Roadway generating electrical power by incorporating piezoelectric materials*. Patent US20050127677 A1, Jun.
- Mallick, R. B., Chen, B. L. and Bhowmick, S. (2009). Reduction of urban heat island effect through harvest of heat energy from asphalt pavements. In *Proceedings of the 2nd international conference on countermeasures to urban heat Islands effect, September. Berkeley, CA, USA*. (Melvin P (ed.)). Lawrence Berkeley National Laboratory, Berkeley, CA, USA, pp. 1–20.
- Mankins, J. C. (1995). Technology readiness levels. *White Paper, April, 6*. National Aeronautics and Space Administration (NASA), Washington, DC, USA.
- Mansfield, R., Shani, N. and Shani, D. (2012). *Method and system for energy harvesting, recapture and control*. International Patent Application PCT/US2012/000033, Patent WO2012099706 A2, Jul.
- Martinez, S. (1980). *Highway turbine*. US Patent US4238687, Dec.
- Mian, Z. (2013a). *Wireless Railroad Monitoring*. US Patent US8423240 B2, Apr.
- Mian, Z. (2013b). *Energy Harvesting*. US Patent US20130221680 A1, Aug.
- Mitcheson, P. D., Green, T. C., Yeatman, E. M. and Holmes, A. S. (2004). Architectures for vibration-driven micropower generators. *Journal of Microelectromechanical Systems*, 13(3): 429-440.

- Morita, K. and Tago, M. (2000). Operational characteristics of the Gaia snow-melting system in Ninohe, Iwate, Japan. In *Proceedings of World Geothermal Congress*. Oregon Institute of Technology, Klamath Falls, OR, USA, pp. 3511–3516.
- Morley, B, Roberts, E., Dean, L., Debenham, M. and Hammond, J. (2005). *Rollers set in road to extract energy from vehicles*. UK Patent Application GB2408074 A, May.
- Munaz, A., Lee, B. C. and Chung, G. S. (2013). A study of an electromagnetic energy harvester using multi-pole magnet. *Sensors and Actuators A: Physical*, 201(2013): 134-140.
- Nakatsu, S. (1994). *Road apparatus*. UK Patent Application GB2290115 A, Dec.
- Near, C. (2013). *Power Generator*. US Patent US20130207520 A1, Aug.
- Nelson, C., Platt, S., Farritor, S., Albrecht, D. and Kamarajugadda, V. (2007). *Regenerative Power for Track-Health Monitoring*. Federal Railroad Administration, Washington, DC, USA, RR 07-22, pp. 1–4.
- Nelson, C., Platt, S., Hansen, S. and Fateh, M. (2009). Power harvesting for railroad track safety enhancement using vertical track displacement. In *SPIE Smart Structures and Materials + Nondestructive Evaluation and Health Monitoring* (Ahmadian, M. and Ghasemi-Nejhad, M. (eds)). International Society for Optics and Photonics, Bellingham, WA, USA, vol. 7288.
- NewEnergyTechnologies (2015). <http://www.newenergytechnologiesinc.com/>. Accessed in February, 2015.
- Oxtoby, D. (2010). *Road or Rail Track Energy Generator*. UK Patent GB2469294 A, Oct.
- Parr, A. (2011). *Hydraulics and pneumatics: a technician's and engineer's guide*. Elsevier, Oxford, UK.
- Penamalli, G. (2011). *Structural Health Monitoring and Energy Harvesting for Railroad*. Stony Brook University, Stony Brook, NY, USA.
- Peralta, M., Costa-Krämer, J. L., Medina, E. and Donoso, A. (2014). Analysis and fabrication steps for a 3D-pyramidal high density coil electromagnetic micro-

- generator for energy harvesting applications. *Sensors and Actuators A: Physical*, 205(2014): 103-110.
- Phillips, K. (2011). *Simulation and Control System of a Railroad Track Power Harvesting Device*. University of Nebraska, Lincoln, NE, USA.
- Pirisi, A. (2012). *System for converting potential or kinetic energy of a body weighting upon or travelling over a support or transit plane into useful energy*. US Patent US20120248788A1, Oct.
- Pirisi, A., Grimaccia, F., Mussetta, M. and Zich, R. E. (2012a). Novel speed bumps design and optimization for vehicles' energy recovery in smart cities. *Energies*, 5(11): 4624-4642.
- Pirisi, A., Grimaccia, F., Mussetta, M. and Zich, R. E. (2012b). An evolutionary optimized device for energy harvesting from traffic. In *2012 IEEE Congress on Evolutionary Computation (CEC)*. IEEE - Institute of Electrical and Electronics Engineers, New York, NY, USA.
- Pirisi, A., Mussetta, M., Grimaccia, F. and Zich, R. E. (2013). Novel speed-bump design and optimization for energy harvesting from traffic. *IEEE Transactions on Intelligent Transportation Systems*, 14(4): 1983-1991.
- Pourghodrat, A. (2011). *Energy Harvesting Systems Design for Railroad Safety*. University of Nebraska, Lincoln, NE, USA.
- Priya, S., and Inman, D. J. (Eds.) (2009). *Energy harvesting technologies*. Springer, New York, NY, USA, vol. 21.
- RES (Road Energy Systems) (2007). *Energy from asphalt - asphalt solar collectors for heating and cooling buildings and roads*. Road Energy Systems, Avenhom, the Netherlands. Available from: http://www.ooms.nl/en/7/301/road_energy_system.aspx. Accessed in September, 2015.
- Saha, C. R. (2011). Modelling theory and applications of the electromagnetic vibrational generator. In *Sustainable Energy Harvesting Technologies - Past, Present*

- and Future* (Tan, Y.K. (ed.)). InTech, Rijeka, Croatia, pp. 55-108. Available from: <http://www.intechopen.com/books/sustainable-energy-harvestingtechnologies-past-present-and-future/modelling-theory-and-applications-of-the-electromagnetic-vibrationalgenerator>. Accessed in July, 2015.
- Schreier, M., Roschewsky, N., Dobler, E., Meyer, S., Huebl, H., Gross, R., and Goennenwein, S. (2013). Current heating induced spin Seebeck effect. *Applied Physics Letters*, 103(242404): 1-5.
- Smith, R. (1979). *Road vehicle-actuated air compressor and system therefore*. US Patent US4173431, Nov.
- SolaRoad (2014). <http://www.solaroad.nl/en/>. Accessed in November, 2014.
- SR (Solar Roadways) (2015). <http://www.solarroadways.com/main.html>. Accessed in February, 2015.
- Stephen, N. G. (2006). On energy harvesting from ambient vibration. *Journal of Sound and Vibration*, 293(1): 409-425.
- Sullivan, C., Bondt, A., Jansen, R., and Verweijmeren (2007). *Innovation in the production and commercial use of energy extracted from asphalt pavements*. Ooms International Holding bv, Chelford, Cheshire, UK. Available from: <http://www.materialedge.co.uk/docs/Energy%20from%20Asphalt%20paper%2020%2011%2006.pdf>. Accessed in September, 2015.
- TNO (2014). <https://www.tno.nl/index.cfm/>. Accessed in May, 2014.
- Tu, Y., Li, J., and Guan, C. (2010). Heat transfer analysis of asphalt concrete pavement based on snow melting. In *2010 International Conference on Electrical and Control Engineering (ICECE), Wuhan, China*. IEEE – Institute of Electrical and Electronics Engineers, New York, NY, USA, pp. 3795–3798.
- Underground Power (2014). <http://www.upgen.it/>. Accessed in December, 2014.
- Valon, F. (2007). *Highway's electrogenerators*. US Patent US 20070246940 A1, Oct.
- Waydip (2015). <http://www.waydip.com/>. Accessed in February, 2015.

- Wischke, M., Masur, M., Kroer, M. and Woias, P. (2011). Vibration harvesting in traffic tunnels to power wireless sensor nodes. *Smart Materials and Structures*, 20(8): 1-8.
- Wu, G. and Yu, X. (2012). Thermal Energy Harvesting Across Pavement Structure, *Proceedings of the Transportation Research Board (TRB) 91st Annual Meeting*. Transportation Research Board, Washington, DC, USA.
- Wu, G. and Yu, X. (2013). Computer-Aided Design of Thermal Energy Harvesting System across Pavement Structure. *International Journal of Pavement Research and Technology*, 6(2): 73-79.
- Xiang, H. J., Wang, J. J., Shi, Z. F. and Zhang, Z. W. (2013). Theoretical analysis of piezoelectric energy harvesting from traffic induced deformation of pavements. *Smart Materials and Structures*, 22(9): 095024.
- Xiong, H., Wang, L., Wang, D. and Druta, C. (2012). Piezoelectric Energy Harvesting from Traffic Induced Deformation of Pavements. *International Journal of Pavement Research and Technology*. 5(5): 333-337.
- Yildiz, F. (2009). Potential ambient energy-harvesting sources and techniques. *Journal of Technology Studies*, 35(35): 40-48.
- Zhao, H., Yu, J. and Ling, J. (2010). Finite element analysis of cymbal piezoelectric transducers for harvesting energy from asphalt pavement. *Journal of the Ceramic Society of Japan*, 118(1382): 909-915.
- Zhao, H., Qin, L., Tao, Y. and Ling, J. (2013). Study on structure of PZT piles based transducer for harvesting energy from asphalt pavement. *Proceedings of the International Journal of Pavements Conference, São Paulo, Brazil. IJP, São Paulo, Brazil (CD-ROM)*.
- Zorlu, Ö. and Külah, H. (2013). A MEMS-based energy harvester for generating energy from non-resonant environmental vibrations. *Sensors and Actuators A: Physical*, 202: 124-134.

Zuo, L. and Tang, X. (2013). Large-scale vibration energy harvesting. *Journal of Intelligent Material Systems and Structures*, 24(11): 1405–1430.

Chapter 3

Development of a Software Tool to Evaluate the Vehicle-Road Interaction

3.1 Introduction

Road vehicles consume energy to work their engines and release energy in different ways, by way of different components. Part of the energy released by vehicles goes into the road pavement; 15 to 21 per cent of the energy is transferred to the vehicle's wheels, in a free rolling situation (IEA, 2012; Hendrowati *et al.*, 2012), with the maximum energy being transferred to the road pavement when there is a braking action, or when vehicle wheels hit an elevated obstacle. From the vehicle loads, it is possible to extract energy onto the pavement, which, using specific technologies, can be transformed into electrical energy (Duarte and Ferreira, 2016; Andriopoulou, 2012).

From an energetic perspective, road vehicles represent a potential energy source. The road pavement or specific equipment applied on its surface, such as speed reducer equipment (SRE) or energy harvesting devices (EHD), becomes the energy collector that extracts energy from vehicles and delivers it to specific components, which are then

responsible for its conversion into other useful means of energy, such as electrical energy.

Because of the increasing rates of road accidents with serious injuries and fatalities, road safety measures are being implemented globally, with speed reduction being the main point of action (WHO, 2010, 2013). SRE, such as speed bumps or speed humps, are the most commonly implemented measures, as they are the solution with the best performance and effectiveness in speed reduction (Elvik *et al.*, 2009; Ewing and Brown, 2009).

These humps or bumps cause great discomfort to vehicle passengers if the vehicle goes over the obstacle above the design speed. To avoid this, drivers reduce the vehicle speed by braking, before hitting the obstacle, losing energy to the brakes and to the pavement before the obstacle. This “lost” energy can be harvested on the pavement, and then converted into other means of energy.

Road vehicles can have different motion situations, such as free rolling, braking, accelerating or turning. In each of them, they will have different forces and moment distributions, which will depend on their characteristics, such as mass, geometry, suspension and tyre characteristics, among other things. In each of these situations, as the mass distributions and, consequently, the force distributions are different at each vehicle wheel, different amounts of energy are transferred to the road pavement. To perform a precise energy transfer analysis, both the static forces that vehicles induce on the road pavement and the dynamic forces resulting from the vehicle’s oscillations must be quantified. The element which contributes most to these oscillations is the road surface, which can have different profiles and be made of different materials. This is more relevant in the case of SRE or EHD, which typically induces higher oscillations on the vehicle. The geometric profile of these elements is essential to evaluate the vehicle’s dynamic behaviour.

There are some commercially available software tools for simulating the motion of vehicles, quantifying the forces induced on the pavement, as well as the forces developed by each component of the vehicle, such as tyres, suspensions, etc. The two

main software tools available for this purpose are ADAMS[®] (MSC.Software, 2016) and AUTOSIM[®] (Carsim, 2016).

Although both software tools work well, when the goal is to perform an energetic analysis on the interaction between the vehicle and the road pavement elements, such as SRE or EHD (or any other device that is applied on the road pavement, with specific motion characteristics), these software tools have limitations, because they were not developed for this purpose.

Other studies to evaluate the vehicle dynamic performance in response to the road pavement profile were done using specific models mostly based on the quarter-car model (Borowiec *et al.*, 2010; Barbosa, 2011; Florin and Liliana, 2013; Hassaan, 2014, 2015). However, the quarter-car model does not include the vehicle pitch, which is important when considerable oscillations are induced on the vehicle body, as in the case of SRE. Farroni (2016) has also developed a software tool to evaluate the tyre–road interaction, focusing on the evaluation of steering actions on vehicle, but this tool does not perform energetic analysis or allows including specific surface profiles on the pavement.

Following the aforementioned facts, a simulation software tool that allows to study the vehicle-road interaction (VRI) from an energetic perspective, in order to quantify the amount of energy released from the vehicle to the pavement or an equipment applied in the pavement surface for different motion scenarios is considered to be extremely important to quantify with a high precision the amount of energy received by the road pavement or a specific equipment applied on its surface.

This Chapter presents the development of a simulation software tool that allows to perform such analysis, allowing the user to introduce the vehicle parameters, including its mechanical properties and geometry, motion parameters and driving conditions, as well as the road parameters and the desired element (SRE or EHD) characteristics and parameters. This software tool was named RoadVISS (Road Vehicle Interaction Simulation Software) and allows the simulation of the VRI from an energetic perspective, by calculating the energy (as well as acceleration and velocity) lost by the vehicle during the interaction with the obstacle, and the energy received by the obstacle,

considering its mechanical characteristics and properties. It also allows users to select the vehicle model (quarter-car or bicycle car model) and interaction model (Single Force Analysis (SFA) or Contact Patch Analysis (CPA)), to compare both models and conclude regarding its precision.

Based on the aforementioned, this tool intends to overcome an existing gap, by quantifying precisely the energy delivered by a road vehicle in motion onto an SRE or an EHD, both in terms of the vehicle's characteristics and the characteristics of the device, thus evaluating the energy exchange process efficiency. With this, it will be possible to determine the importance of each parameter in the extraction of the vehicle's energy and optimize the efficiency of the device.

The present Chapter also aims to simulate the VRI, using the software tool RoadVISS, to determine which is the best vehicle model and interaction model, as well as to study the effects of road pavement elements (SRE and EHD), on the energy released by the vehicle. The energy captured by the SRE or EHD is also quantified and the energy conversion efficiency is evaluated, depending on the evaluated parameters.

In this work, the vertical and horizontal dynamics of vehicles will be considered, as only forward (linear) motions will be considered, excluding turning motions, which include lateral dynamics. This assumption is due to the fact that SRE and EHD are typically installed in places where vehicles only move in a straight line. Other assumptions in this study are: only two-axle light vehicles are considered; front-wheel drive; passenger weight is included with the vehicle weight; and wind speed is neglected.

3.2 Vehicle Dynamics

3.2.1 Introduction

The loads applied by a vehicle in motion on the pavement, by each wheel, depend on several parameters, such as vehicle geometry, mass, acceleration, speed and pavement

profile, among others, and have both static and dynamic components (Gillespie, 1992; Jazar, 2008).

The road pavement induces vibrations on the vehicle, which are absorbed by the tyres and the suspension system, which can either increase or decrease the loads applied on the road surface, contributing to a dynamic component of the wheel load. To study these variations, different models can be used, and the selection of the most appropriate model should be made based on the specificities of the study being performed.

The interaction between each vehicle wheel and the road surface (or an obstacle surface) is performed by the tyre, which delivers a perpendicular force onto the pavement which is distributed by its contact patch. Most authors consider only the resultant force applied by the tyre over its contact patch (SFA), neglecting the pressure distribution across its area. For most studies, this is not incorrect, as it can represent a real situation of continuous motion over a surface.

However, to study in great detail the forces applied over a specific surface which can have an inclination angle or a vertical displacement that is a function of the applied force, or in some situations, both scenarios may exist, the analysis must be performed in terms of the force applied by each part of the contact patch, to obtain a precise quantification of the force delivered by the surface during its passage over the patch. This is defined as CPA.

This section presents the static and dynamic forces of a vehicle, taking into consideration the vehicle parameters; the vehicle models, to study the dynamic components of the vehicle forces; the formulations to determine the vehicle forces; the contact patch and pressure distribution over it, to determine the forces applied over the contact patch; and the equations to determine the energy released by a vehicle when it interacts with an obstacle on the pavement.

3.2.2 Vehicle forces distribution

The distribution of the vehicle masses and forces, for parked and moving vehicles, both on horizontal and inclined road pavements is well defined in the literature (Gillespie, 1992; Wong, 2001; Blundell and Harty, 2004; Pacejka, 2005; Jazar, 2008; Popp *et al.*, 2010; Rajamani, 2011).

Tables 3.1 and 3.2 summarize the vehicle's perpendicular force distribution on level and inclined road pavements, and the vehicle's longitudinal force distribution on level and inclined pavements, respectively. These equations were extracted from the main vehicle dynamics references (Jazar, 2008; Popp *et al.*, 2010; Rajamani, 2011). Equations to determine the lift force (F_l), drag force (F_d) and rolling resistance (R_x), are presented in these references. In this work, the indices f and r will be used for the front and rear wheels, respectively. Each symbol definition is presented in the list of notations.

Table 3.1- Vehicle perpendicular force distribution on level and inclined pavements.

Motion Type	Front Wheel	Rear Wheel	
Level pavement	Stopped	$F_{z,f} = \frac{1}{2} m_v g \frac{a_2}{l_v}$	$F_{z,r} = \frac{1}{2} m_v g \frac{a_1}{l_v}$
	Free Rolling	$F_{z,f} = \frac{1}{2} m_v g \frac{a_2}{l_v} - \frac{F_{l,f}}{2}$	$F_{z,r} = \frac{1}{2} m_v g \frac{a_1}{l_v} - \frac{F_{l,r}}{2}$
	Accelerating	$F_{z,f} = \frac{1}{2} m_v g \frac{a_2}{l_v} - \frac{1}{2} m_v g \frac{h_{CG} a}{l_v g} - \frac{F_{l,f}}{2}$	$F_{z,r} = \frac{1}{2} m_v g \frac{a_1}{l_v} + \frac{1}{2} m_v g \frac{h_{CG} a}{l_v g} - \frac{F_{l,r}}{2}$
	Braking	$F_{z,f} = \frac{1}{2} m_v g \frac{a_2}{l_v} + \frac{1}{2} m_v g \frac{h_{CG} a}{l_v g} - \frac{F_{l,f}}{2}$	$F_{z,r} = \frac{1}{2} m_v g \frac{a_1}{l_v} - \frac{1}{2} m_v g \frac{h_{CG} a}{l_v g} - \frac{F_{l,r}}{2}$
Inclined pavement	Stopped	$F_{z,f} = \frac{1}{2} m_v g \left(\frac{a_2}{l_v} \cos \phi + \frac{h_{CG}}{l_v} \sin \phi \right)$	$F_{z,r} = \frac{1}{2} m_v g \left(\frac{a_1}{l_v} \cos \phi - \frac{h_{CG}}{l_v} \sin \phi \right)$
	Free Rolling	$F_{z,f} = \frac{1}{2} m_v g \left(\frac{a_2}{l_v} \cos \phi + \frac{h_{CG}}{l_v} \sin \phi \right) - \frac{F_{l,f}}{2}$	$F_{z,r} = \frac{1}{2} m_v g \left(\frac{a_1}{l_v} \cos \phi - \frac{h_{CG}}{l_v} \sin \phi \right) - \frac{F_{l,r}}{2}$
	Accelerating	$F_{z,f} = \frac{1}{2} m_v g \left(\frac{a_2}{l_v} \cos \phi + \frac{h_{CG}}{l_v} \sin \phi \right) - \frac{1}{2} m_v a \frac{h_{CG}}{l_v} - \frac{F_{l,f}}{2}$	$F_{z,r} = \frac{1}{2} m_v g \left(\frac{a_1}{l_v} \cos \phi + \frac{h_{CG}}{l_v} \sin \phi \right) + \frac{1}{2} m_v a \frac{h_{CG}}{l_v} - \frac{F_{l,r}}{2}$
	Braking	$F_{z,f} = \frac{1}{2} m_v g \left(\frac{a_2}{l_v} \cos \phi + \frac{h_{CG}}{l_v} \sin \phi \right) + \frac{1}{2} m_v a \frac{h_{CG}}{l_v} - \frac{F_{l,f}}{2}$	$F_{z,r} = \frac{1}{2} m_v g \left(\frac{a_1}{l_v} \cos \phi - \frac{h_{CG}}{l_v} \sin \phi \right) - \frac{1}{2} m_v a \frac{h_{CG}}{l_v} - \frac{F_{l,r}}{2}$

Table 3.2- Vehicle longitudinal force distribution on level and inclined pavements.

	Front Wheel	Rear Wheel	
Level pavement	Stopped	$F_{x,f} = 0$	$F_{x,r} = 0$
	Free Rolling	$F_{x,f} = -R_{x,f} - \frac{1}{2}F_d$	$F_{x,r} = -R_{x,r}$
	Accelerating	$F_{x,f} = \frac{1}{2}m_v a - R_{x,f} - \frac{1}{2}F_d$	$F_{x,r} = -R_{x,r}$
	Braking	$F_{x,f} = -\frac{1}{2}m_v a - R_{x,f} - \frac{1}{2}F_d$	$F_{x,r} = -R_{x,r}$
Inclined pavement	Stopped	$F_{x,f} = 0$	$F_{x,r} = \frac{1}{2}m_v g \sin\phi$
	Free Rolling	$F_{x,f} = \frac{1}{2}m_v(g \sin\phi) - R_{x,f} - \frac{F_d}{2}$	$F_{x,r} = -R_{x,r}$
	Accelerating	$F_{x,f} = \frac{1}{2}m_v(a + g \sin\phi) - R_{x,f} - \frac{F_d}{2}$	$F_{x,r} = -R_{x,r}$
	Braking	$F_{x,f} = \frac{1}{2}m_v(-a + g \sin\phi) - R_{x,f} - \frac{F_d}{2}$	$F_{x,r} = -R_{x,r}$

As can be seen from these equations, there is a static component of the force, which depends mainly of the vehicle's mass and geometry, and a dynamic component, which depends, apart from these two parameters, on the vehicle acceleration and speed. Also, the pavement inclination has an influence on the vehicle forces.

3.2.3 Vehicle dynamics models

Modelling of four-wheeled vehicles has been studied for the past 50 years. The dynamics and characteristics are well understood, and validated models have been developed for many applications, including the study of vehicle vibrations (Wong, 2001; Blundell and Harty, 2004; Jazar, 2008; Popp *et al.*, 2010; Rajamani, 2011).

The most simple model is the quarter-car model, which is the most commonly used and most useful model of a vehicle's suspension system (Blundell and Harty, 2004; Jazar, 2008; Popp *et al.*, 2010; Rajamani, 2011). This model only represents the sprung mass of the vehicle, the unsprung mass, the suspension system and the tyre, as presented in Figure 3.1(a). For more complex and detailed studies, regarding only forward linear

motion, the most suitable model is the bicycle car model, which is represented in Figure 3.1(b), and includes the vehicle sprung mass (equal to half the vehicle), the (moment of) inertia, the front unsprung mass, rear unsprung mass, front and rear suspension systems and front and rear tyres. The motion equations of both quarter-car and bicycle car models are well defined in the literature (Blundell and Harty, 2004; Jazar, 2008; Rajamani, 2011).

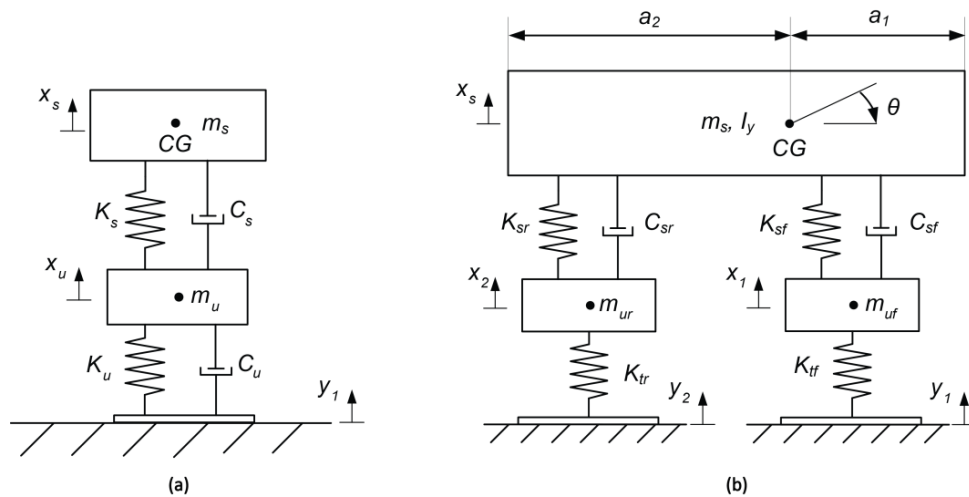


Figure 3.1- (a) Quarter car model and (b) bicycle car model (adapted from Jazar, 2008).

These models are validated for pavements without deflection or vertical motion. However, most EHDs have a vertical motion owing to the actuation of the vehicle, which has an impact on the previous models. The inclusion of a surface with vertical displacement on the pavement is represented in Figure 3.2, both for the quarter-car model - Figure 3.2(a) -, and the bicycle car model - Figure 3.2(b). In these models, there is a degree of freedom with a movable surface under the equipment, with a displacement x_h , a mass m_h and a spring with stiffness K_h .

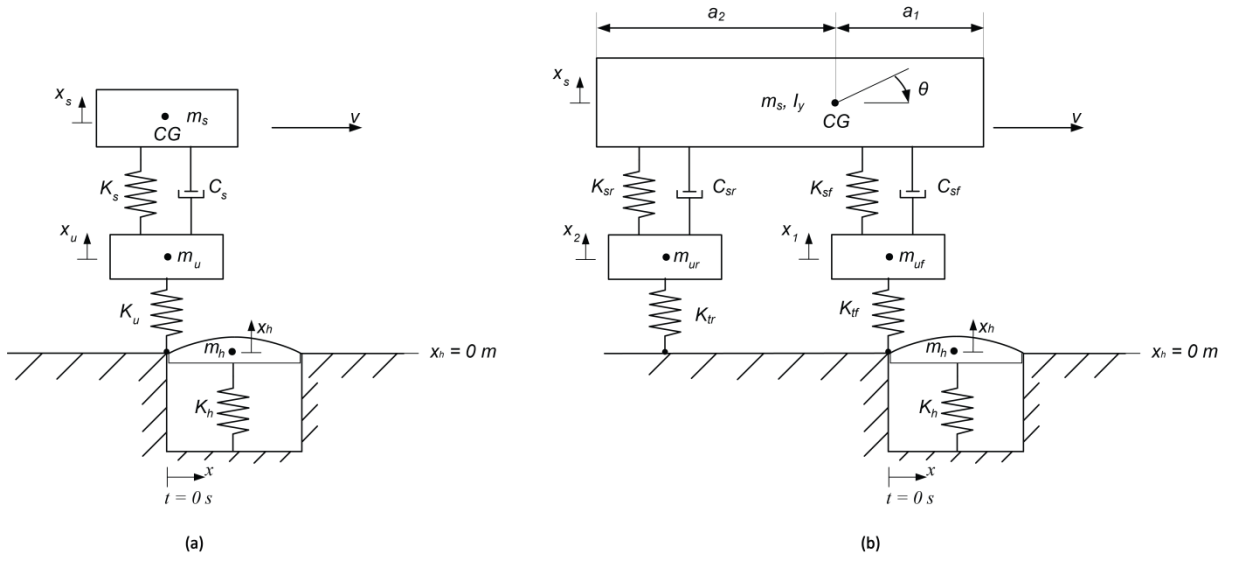


Figure 3.2- (a) Quarter car model with a harvester surface on the pavement; and (b) bicycle car model with a harvester surface on the pavement.

The governing differential equations of motion for the quarter-car model with a movable harvester surface, shown in Figure 3.2(a), are represented by Equations (3.1-3.3), whereas the governing differential equations of motion for the bicycle car model with a movable harvester surface, shown in Figure 3.2(b), are represented by Equations (3.4-3.8).

$$m_s \ddot{x}_s + C_s(\dot{x}_s - \dot{x}_u) + K_s(x_s - x_u) = 0 \quad (3.1)$$

$$m_u \ddot{x}_u + C_s(\dot{x}_u - \dot{x}_s) + K_s(x_u - x_s) - K_u(x_h - x_u) = 0 \quad (3.2)$$

$$m_h \ddot{x}_h + K_u(x_h - x_u) + K_h x_h = 0 \quad (3.3)$$

$$m_s \ddot{x}_s + C_{sf}(\dot{x}_s - \dot{x}_1 - a_1 \dot{\theta}) + C_{sr}(\dot{x}_s - \dot{x}_2 + a_2 \dot{\theta}) + K_{sf}(x_s - x_1 - a_1 \theta) + K_{sr}(x_s - x_2 + a_2 \theta) = 0 \quad (3.4)$$

$$I_y \ddot{\theta} - a_1 C_{sf}(\dot{x}_s - \dot{x}_1 - a_1 \dot{\theta}) + a_2 C_{sr}(\dot{x}_s - \dot{x}_2 + a_2 \dot{\theta}) + a_1 K_{sf}(x_s - x_1 - a_1 \theta) + a_2 K_{sr}(x_s - x_2 + a_2 \theta) = 0 \quad (3.5)$$

$$m_{uf} \ddot{x}_1 - C_{sf}(\dot{x}_s - \dot{x}_1 - a_1 \dot{\theta}) + K_{tf}(x_1 - x_h) - K_{sf}(x_s - x_1 - a_1 \theta) = 0 \quad (3.6)$$

$$m_{ur} \ddot{x}_2 - C_{sr}(\dot{x}_s - \dot{x}_2 + a_2 \dot{\theta}) + K_{tr}(x_2 - x_h) - K_{sr}(x_s - x_2 + a_2 \theta) = 0 \quad (3.7)$$

$$m_h \ddot{x}_h - K_{tf}(x_1 - x_h) - K_{tr}(x_2 - x_h) + K_h x_h = 0 \quad (3.8)$$

3.2.4 Vehicle-road interaction models

The VRI analysis can be performed considering a resultant force from the tyres over the pavement, or considering the force distributed over the tyre's contact patch, as a pressure distribution.

An analysis considering only the resultant force applied over the contact patch, which has both a perpendicular (with static and dynamic parts) and a longitudinal component, is defined as SFA.

Figure 3.3 represents the perpendicular [Figure 3.3(a)] and longitudinal [Figure 3.3(b)] force distributions for the front wheel of the vehicle when it passes on an inclined surface with an inclination angle ϕ . Based on the literature (Blundell and Harty, 2004; Jazar, 2008), the values for each force are presented in Table 3.3. The front wheel perpendicular force is represented by F_{zf} , with F_{zf_x} representing the horizontal component of this force, F_{zf_z} representing the vertical component and F_{zf_r} representing the resultant component. The same approach is used to quantify the different components of the longitudinal forces, both the acceleration force (F_a) and the tyre rolling resistance force (R_x).

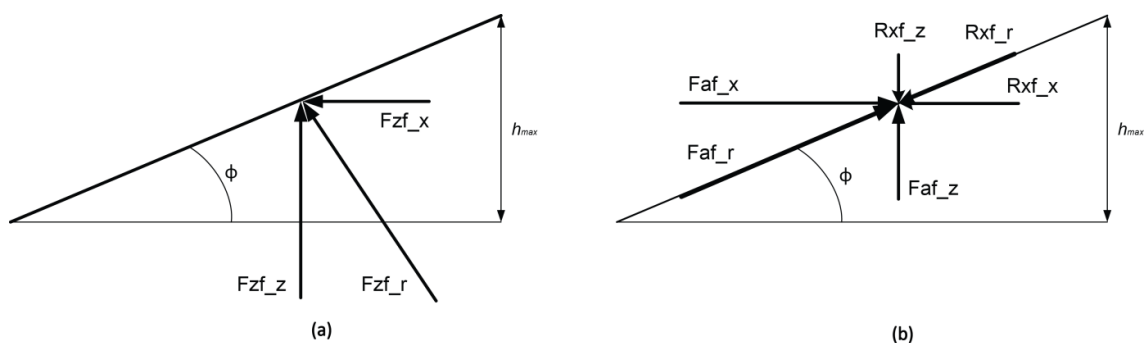


Figure 3.3- (a) Perpendicular force distribution; and (b) longitudinal force distribution.

An analysis considering the contact patch force and pressure distribution is defined as CPA. To perform such analysis, first, the contact patch geometry must be defined, and then the pressure distribution along the contact patch surface.

Equations for defining the contact patch geometry are well defined in the literature (Pacejka, 2005; Jazar, 2008; Rajamani, 2011). Based on the tyre stiffness, or on tyre pressure, and knowing the resultant force applied by the tyre, these equations allow us to determine the tyre's deflection and the geometry of the contact patch (the tyre's area in contact with the road surface).

Table 3.3- Perpendicular and longitudinal wheel forces on an inclined surface.

Component	Front wheel	Rear wheel	
Perpendicular forces	Vertical (z)	$Fzf_z = \left[\frac{1}{2} m_v g \frac{a_2}{l_v} + m_{u,f} g \right. \\ \left. - \frac{1}{2} m_v a \frac{h_{CG}}{l_v} - \frac{F_{l,f}}{2} \right] \\ + K_{t,f}(x_1 - x_h)$	$Fzr_z = - \left[\frac{1}{2} m_v g \frac{a_1}{l_v} + m_{u,r} g \right. \\ \left. + \frac{1}{2} m_v a \frac{h_{CG}}{l_v} - \frac{F_{l,r}}{2} \right] \\ + K_{t,r}(x_2 - x_h)$
	Resultant (r)	$Fzf_r = Fzf_z / \cos \phi$	$Fzr_r = Fzr_z / \cos \phi$
	Horizontal (x)	$Fzf_x = Fzf_r \sin \phi$	$Fzr_x = Fzr_r \sin \phi$
Longitudinal forces	Horizontal (x)	$Fxf_x = \left[\frac{1}{2} m_v (a + g \sin \phi) \right. \\ \left. - Rxf_r \right] \cos \phi - \frac{1}{2} F_d \\ - Fzf_x$	$Fxr_x = -Rxr_x - Fzr_x$
	Resultant (r)	$Fxf_r = Fxf_x / \cos \phi$	$Fxr_r = Fxr_x / \cos \phi$
	Vertical (z)	$Fxf_z = Fxf_r \sin \phi$	$Fxr_z = Fxr_r \sin \phi$

To determine the contact patch pressure distribution ($q(x)$), considering only the variation on the longitudinal axis, Equation (3.9) can be used (Jazar, 2008), with the maximum normal pressure ($q0$) defined by Equation (3.10). In these equations, x_{cp} represent the contact patch position, cp_a the contact patch half-length and CP_A the contact patch area.

$$q(x_{CP}) = q0 \left(1 - \frac{(x_{CP} - cp_a)^6}{cp_a^6} - \frac{(x_{CP} - cp_a)}{4 cp_a} \right) \quad (3.9)$$

$$q0 = \frac{7 F_z}{6 CP_A} \quad (3.10)$$

To convert the pressure distribution into an applied force on the surface, in a dynamic analysis, Equation (3.11) should be used, with i representing the number of the iteration, $i-1$ the number of the previous iteration, Fz_i the force of the present iteration and ΔCP_A the variation of the contact patch area that is in contact with the surface.

$$Fz_i = q(x_{CP})_i \Delta CP_{A-i} + Fz_{i-1} \quad (3.11)$$

Figure 3.4 presents the situation where the tyre's contact patch is divided in two areas: one in contact with an inclined surface, the other in contact with the road (a flat surface). The overall pressure distribution, represented by Equation (3.11), is divided in two different pressure distributions, with two different resultant forces: CP_FZR_sup , the resultant force applied on the surface; CP_FZR_pav1 , the resultant force applied on the pavement before the surface.

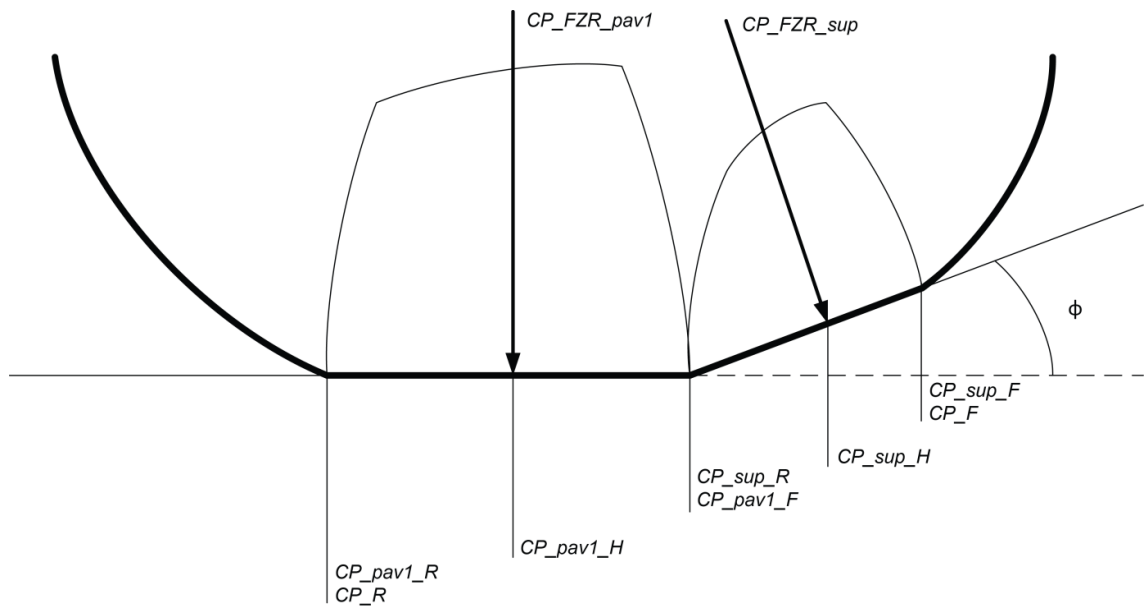


Figure 3.4- Contact patch pressure and resultant distribution of forces.

Equation (3.11) is then divided in two, one for the area in contact with the surface of the device and another for the area in contact with the road surface. The force on the area in contact with the device has two components owing to the inclination of the surface, which are represented by Equations (3.12) and (3.13), with $CP_FZR_sup_Z$ being the perpendicular component of the force applied on the surface and $CP_FZR_sup_X$ its longitudinal component.

$$CP_FZR_sup_Z = CP_FZR_sup \times \cos \phi \quad (3.12)$$

$$CP_FZR_sup_X = CP_FZR_sup \times \sin \phi \quad (3.13)$$

3.2.5 Energetic analysis

Vehicle acceleration (a) is directly proportional to the longitudinal component of the force (Equation 3.14). So, the variation of the vehicle's acceleration is given by Equation (3.15) and the vehicle's speed (v) is calculated by Equation (3.16). Knowing the longitudinal forces, it is possible to determine the vehicle's acceleration, and later, the vehicle's speed at each iteration. The same happens for vehicle position, which is given by Equation (3.17). The energy released from the vehicle (E_v) can be determined using the vehicle speed reduction, which is associated with the loss of kinetic energy, using Equation (3.18), with m_v representing the vehicle total mass and v the vehicle speed.

$$\sum F_x = m_v a \quad (3.14)$$

$$\partial a = \frac{\partial \sum F_x}{m_v} \quad (3.15)$$

$$v_i = v_{i-1} + a_i \Delta t \quad (3.16)$$

$$x_i = x_{i-1} + v_i \Delta t + \frac{1}{2} a_i \Delta t^2 \quad (3.17)$$

$$\partial E_v = \frac{1}{2} m_v (\partial v^2) \quad (3.18)$$

3.3 Road Pavement Devices

3.3.1 Introduction

Speed reducers consist of a specific type of traffic calming solution, involving vertical alignment changes in the pavement, with the goal of reducing vehicle speed by causing discomfort when vehicles go over them at high speeds (Elvik *et al.*, 2009; Ewing and Brown, 2009). EHDs are instruments actuated by vehicle tyre forces. They receive mechanical energy from the vehicle and convert it into electrical energy.

To quantify the impact that SRE and EHD induce in vehicles, it is important to study the geometric shape and dimensions of their surface.

In this section, the main characteristics of SRE and EHD will be presented, with special emphasis on their surface geometry, material and displacements, when applicable. Also, the quantification of the energy captured by the equipment will be presented and compared with the energy lost from the vehicle, allowing us to evaluate the energy extraction performance.

3.3.2 Speed reducers

To improve traffic safety, vehicle speed needs to be reduced in various places, both in- and outside urban areas. Three types of measures can be adopted for this purpose: horizontal alignment changes (chicanes, narrows, roundabouts, etc.); vertical alignment changes (humps, platforms, raised crosswalks, etc.); or complementary measures, such as illumination and urban features, among others (Elvik *et al.*, 2009; Ewing and Brown, 2009). The most effective measures to control vehicle speeds are the vertical alignment changes, as these usually affect the vehicle and their occupants if speed limits are not respected. However, there are some design rules to guarantee softness and, therefore, the design speed.

So, speed reducers should have an impact on vehicles, when they travel above the design speed, which causes discomfort for the occupants and, at the same time, should have a minimum impact on the vehicles if they travel under the design speed. This is achieved through their geometry.

In this study, different geometries for the speed reducer surface (also applied to the EHDs) were considered. There is no international uniformity for the geometric aspects of speed reducers regarding their shape, height, length or width, or for materials or applicable areas. Considering other research work (Johnson and Nedzesky, 2004; Szurgott *et al.*, 2009) and individual countries' recommendations (DGV, 2004; Ewing and Brown, 2009), nine surface profiles (SP) were considered for the speed reducers, which are presented in Figure 3.5. A set of governing equations for each SP were defined to characterize its height in function of its length. These equations are presented in Table 3.4, with y representing the surface vertical position, x representing the surface longitudinal position, ϕ representing the surface angle, L_{max} representing the maximum length of the surface and h_{max} representing the maximum height of the SP. The first profile (S0) is not considered a speed reducer itself, as it represents a flat surface, which is applicable when considered for a flat surface displacement.

In terms of materials, there are two main solutions: concrete or bituminous mixtures, if speed reducers are implemented together with the pavement, and plastic or vulcanized rubber mixtures, when commercial equipment is implemented.

3.3.3 Energy harvesting devices

Energy harvesting is described as a concept by which energy is captured, converted, stored and utilized by means of various sources, using interfaces, storage devices and other units (Priya and Inman, 2009; Khaligh and Onar, 2010). Put simply, energy harvesting is the conversion of ambient energy present in the environment into other useful means of energy; for example, electrical energy (Kazmierski and Beeby, 2009).

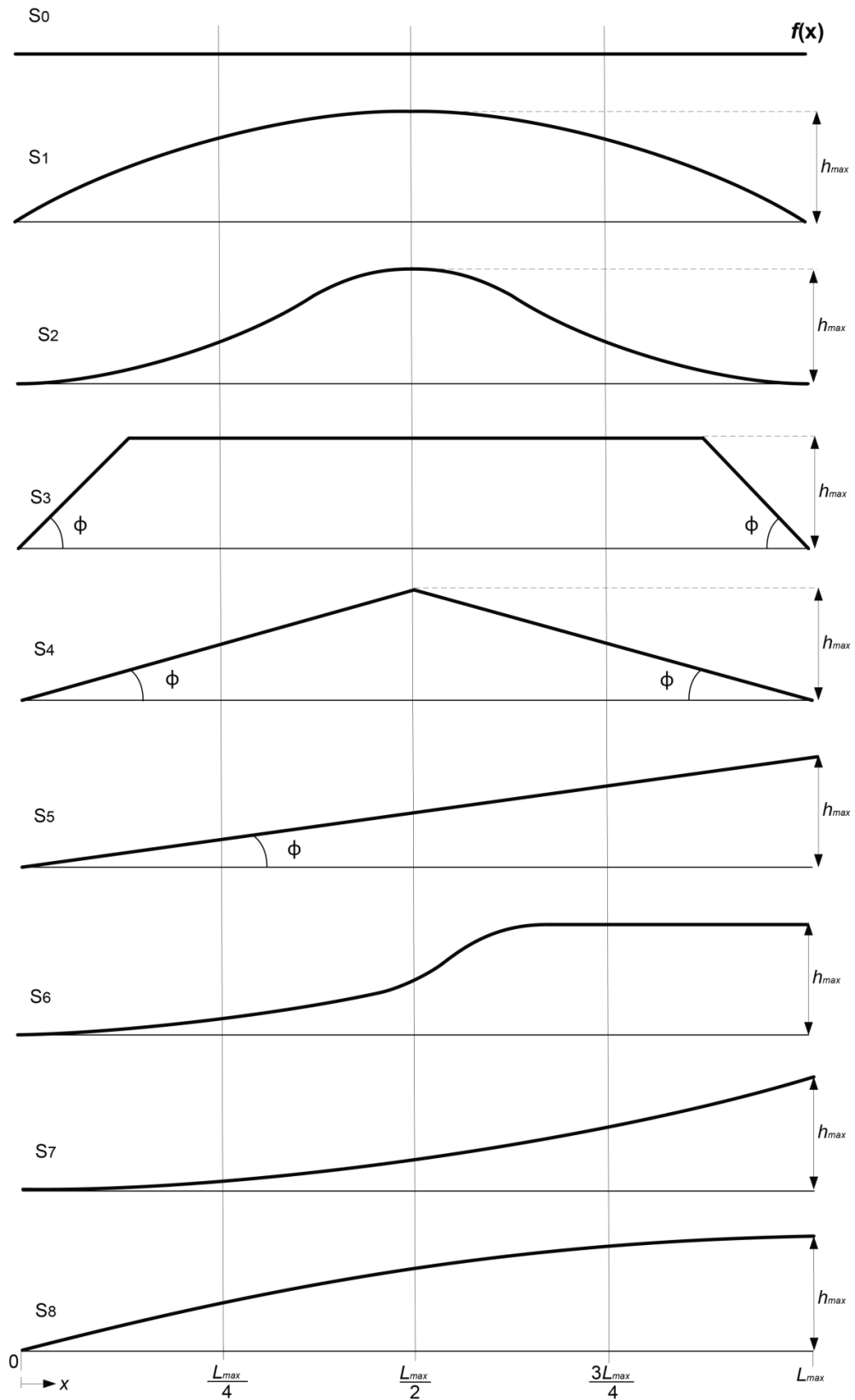


Figure 3.5- Speed reducer or EHD surface profiles.

Table 3.4- Speed reducer or EHD surface profile's equations.

ID	SP definition	Equation(s)
S0	Plane	$y(x) = 0$
S1	Convex bump	$y(x) = \sqrt{h_{max}^2 + \left[1 - \frac{(x - (L_{max}/2))^2}{(L_{max}/2)^2}\right]}$
		If $0 < x < (L_{max}/4)$
		$y(x) = \sqrt{\left[1 - \frac{x^2}{(L_{max}/4)^2}\right] \times \left(\frac{h_{max}}{2}\right)^2 + \left(\frac{h_{max}}{2}\right)}$
		If $(L_{max}/4) < x < (3L_{max}/4)$
S2	Sinusoidal bump	$y(x) = \sqrt{\left[1 - \frac{(x - (L_{max}/2))^2}{(L_{max}/4)^2}\right] \times \left(\frac{h_{max}}{2}\right)^2 + \left(\frac{h_{max}}{2}\right)}$
		If $x > (3L_{max}/4)$
		$y(x) = \sqrt{\left[1 - \frac{(x - L_{max})^2}{(L_{max}/4)^2}\right] \times \left(\frac{h_{max}}{2}\right)^2 + \left(\frac{h_{max}}{2}\right)}$
S3	Hump	If $0 < x < (L_{max}/2)$ and $y(x) < h_{max}$ $y(x) = x \sin(\phi)$ If $[0 < x < (L_{max}/2)$ and $y(x) > h_{max}]$ OR $[(L_{max}/2) < x < L_{max}$ and $y(x) > h_{max}]$ $y(x) = h_{max}$ If $(L_{max}/2) < x < L_{max}$ and $y(x) < h_{max}$ $y(x) = (L_{max} - x) \sin \phi$
S4	Triangle	If $0 < x < (L_{max}/2)$ $y(x) = x \sin(\phi)$ If $x = (L_{max}/2)$ $y(x) = h_{max}$ If $x > (L_{max}/2)$ $y(x) = (L_{max} - x) \sin(\phi)$ With $\phi = \arctan\left(\frac{h_{max}}{L_{max}/2}\right)$
S5	Ramp	With $\phi = \arctan\left(\frac{h_{max}}{L_{max}}\right)$
S6	S profile	If $0 < x < (L_{max}/2)$ $y(x) = -\sqrt{\left[1 - \frac{(x)^2}{(L_{max}/2)^2}\right] \left(\frac{h_{max}}{2}\right)^2 + \frac{h_{max}}{2}}$ If $x > (L_{max}/2)$ $y(x) = \sqrt{\left[1 - \frac{(x - L_{max})^2}{(L_{max}/2)^2}\right] \left(\frac{L_{max}}{2}\right)^2 + \frac{h_{max}}{2}}$
S7	Scale up	$y(x) = -\sqrt{\left[1 - \frac{(x)^2}{(L_{max})^2}\right] (h_{max})^2 + h_{max}}$
S8	Crest	$y(x) = \sqrt{\left[1 - \frac{(x - L_{max})^2}{(L_{max})^2}\right] (h_{max})^2}$

Road surfaces are continuously exposed to vehicle loads, making it possible to extract energy from this which, using specific technologies, can be transformed into electrical energy (Duarte and Ferreira, 2016; Andriopoulou, 2012).

Regarding the working principle of these devices, as presented with more detail in the previous Chapter, the mechanical energy transmitted by vehicle wheels to the road surface can induce two types of actions on the road pavement: vibrations or surface displacement. Vibrations are mainly harvested by piezoelectric transducers, which have a very low level of efficiency, so only small amounts of electrical energy are produced. However, these are less “invasive” to the vehicle. Most road pavement EHDs have a vertical displacement to actuate a mechanical system (electromechanical, hydraulic or pneumatic) or directly actuate an electromagnetic generator. The harvested energy is proportional to the maximum displacement of the surface, as well as its actuation speed and acceleration. However, this displacement should be as small as possible, to avoid interferences with the driving performance of the vehicle, creating pavement holes or other such things.

Also, an EHD presents stiffness and, in some cases, a damping effect due to its components (both mechanical and electrical), which should be considered in the VRI study. In this study, only the mechanical stiffness was considered.

Its surface materials and profile can be similar to SREs, as usually these devices have similar functions in terms of reducing vehicles speed.

3.3.4 Energy captured

The energy absorbed by the road surface material (E_{Su}) can be determined using Equation (3.19), where F_z is the force applied by the vehicle wheel, Δl being the deflection of the material. This can be calculated in relation to the applied load (F_z), elasticity modulus of the material (E') and the thickness (l_0) and area (A_{ha}) of the surface under study, using Equation (3.20).

$$E_{Su} = \frac{1}{2} F_z \Delta l \quad (3.19)$$

$$E' = \frac{F_z l_0}{A_{ha} \Delta l} \Leftrightarrow \Delta l = \frac{F_z l_0}{A_{ha} E'} \quad (3.20)$$

For a movable surface, applicable both for SRE and EHD, the energy associated with the surface motion (E_{Ha}) is calculated using the total force applied on the surface (F_z) and the surface displacement (x_h), using Equation (3.21). Equation (3.22) allows us to evaluate the efficiency of the process, between the energy lost by the vehicle and the energy captured by the surface of the equipment.

$$E_{Ha} = F_z x_h \quad (3.21)$$

$$\eta_{Ha} = \frac{E_{Ha}}{E_v + E_{Su}} \quad (3.22)$$

3.4 Simulation Software Tool

3.4.1 Introduction

Based on the study presented in previous sections, a simulation software tool was developed, using MATLAB[®] software, to study the VRI from an energetic perspective, named RoadVISS – Road Vehicle Interaction Simulation Software.

The purpose of the simulation software tool is to study this interaction in great detail, with the possibility of fully characterizing the vehicle under study, by defining its class, weight, axles, wheels, geometry, speed, acceleration, suspensions and tyres; defining all the mechanical parameters, such as damping and stiffness for each suspension and tyre; and fully characterizing the pavement or SRE/EHD surface, by defining its material, shape, geometry and, for a surface with displacement, its maximum displacement, mass, stiffness and damping properties. It also allows the user to select the vehicle model

(quarter-car or bicycle car model) and whether the analysis is to consider the contact patch or not.

RoadVISS calculates all the displacements, both for the vehicle and the pavement/equipment surface, the applied and received forces and the power and energy transferred, released from vehicle and received on the pavement/equipment surface, and presents the results both graphically and numerically.

3.4.2 Inputs and outputs

To select the model inputs, a graphical user interface (GUI) platform was developed (Figure 3.6).

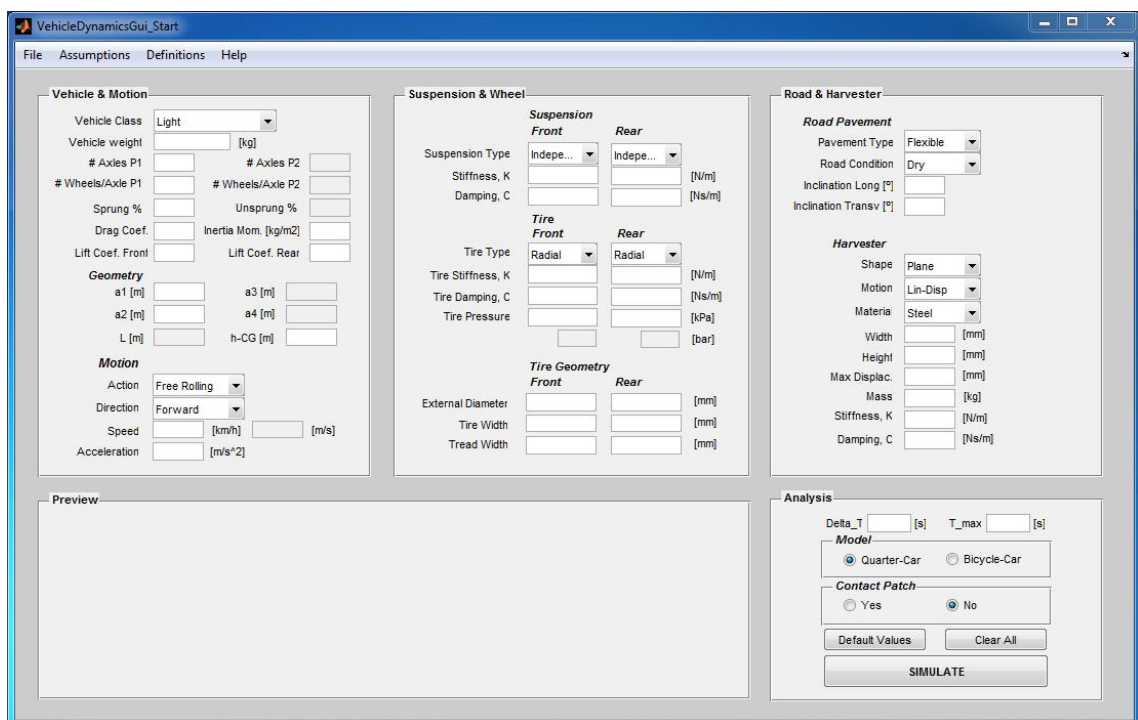


Figure 3.6- GUI to select the inputs for the computational model.

This GUI has five distinct panels: three for parameter selection; one for the preview of the selected features for the vehicle, the pavement and the harvester surface; and one for the selection of analysis features.

The first panel allows the user to select the vehicle and motion properties. In terms of the vehicle, it allows the vehicle class, weight, number of axles, wheels per axle, percentage of sprung and unsprung mass, drag and lift coefficients, and inertia moment of the vehicle to be selected. It also allows users to define the vehicle geometry in terms of distances from each axle to the centre of gravity (CG), as well as the height of the CG. In terms of vehicle motion, it allows to the selection of the action (free rolling, accelerating, braking, or stopped), the motion direction, the vehicle speed and acceleration (when the action is accelerating or braking).

The second panel allows the user to select the suspension and wheel properties. In terms of suspension, it allows users to select the suspension type and to define the suspension stiffness and damping values, for both the front and rear suspension. In terms of tyre, it allows the user to select the tyre type and to define the tyre stiffness, damping and pressure, for both the front and rear tyre. The tyre geometry in terms of external diameter, tyre width and tread width can also be defined, for both front and rear tyres.

The third panel allows the road and harvester properties to be selected. In terms of road pavement, the user can select the pavement type, the road condition, the longitudinal and transversal inclination of the pavement. For the SRE/EHD surface, users can select the shape (according to Figure 3.5), the motion type, the material of the surface, the width and height and, when the user selects a surface motion, the maximum displacement, the mass of the surface, its stiffness and damping can be defined.

The fourth panel presents a summary of the selection, showing an image of the selected vehicle, an image of the selected pavement and an image of the harvester surface, by shape. With this information, the user can confirm the selection visually.

The fifth panel allows the user to define the simulation time and each iteration interval, the vehicle model to be simulated (quarter-car or bicycle car model), and *contact patch* interaction model, selecting *Yes* for CPA, or *No* for a SFA. In this panel, the user can

clean all the fields to select new values, and can press the *Simulate* button to start the simulation.

To present the software outputs graphically, a GUI platform was developed (Figure 3.7). This GUI has two distinct panels, one which presents the outputs and another for selecting new values for the main variables of the system, as well as choosing an action (new simulation, print plots or exit).

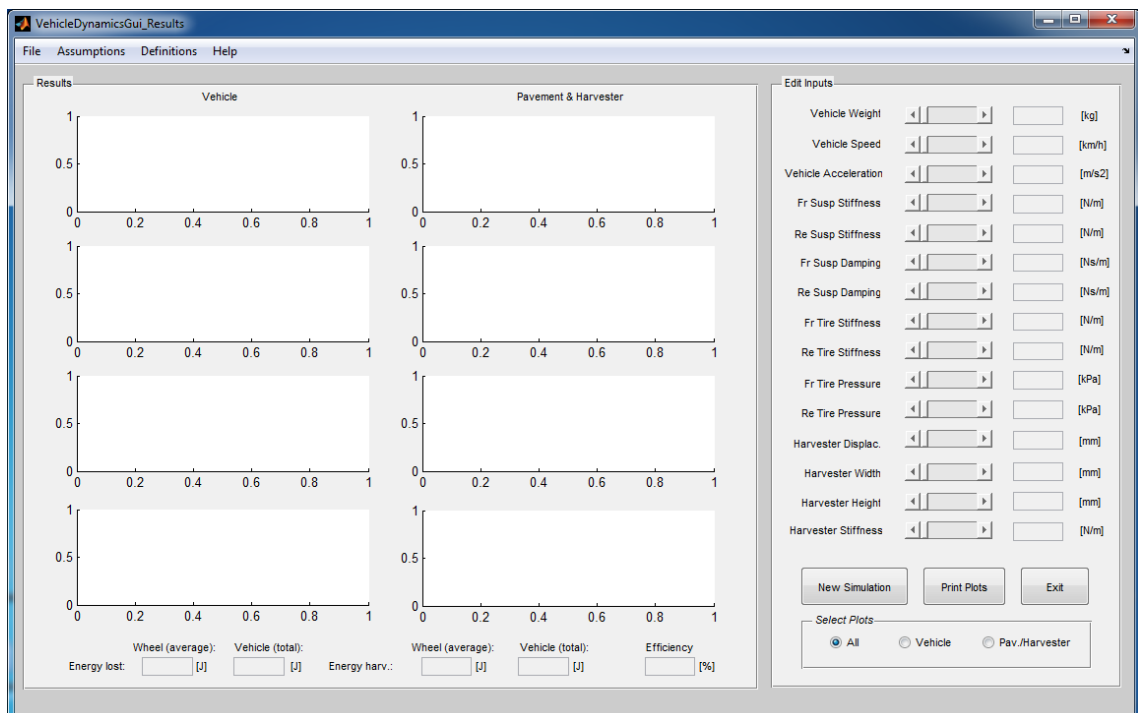


Figure 3.7- GUI to present the outputs for the computational model.

The first panel presents the outputs of the system graphically and numerically in eight graphics and five values. Graphically, the main vehicle results are presented for the vehicle (sprung mass, front unsprung mass and rear unsprung mass displacements; the forces induced by the front and rear tyres on the pavement; the power and energy lost by the vehicle in the interaction with the pavement equipment) and for the SRE or EHD (the higher and lower positions of the equipment surface, which depends on the surface profile and surface displacement; the forces received by the surface, from each wheel of

the vehicle; and the power and energy received by the surface). Numerically, the values of the energy lost by each wheel of the vehicle and by the entire vehicle are presented; the energy harvested by each wheel actuation and by the actuation of the entire vehicle; and the efficiency of the energy transfer process.

The second panel allows users to define new values for the main variables of the simulation to re-simulate the model with changes, without having to leave the results' GUI and restart the process from the first GUI. The variables that can be changed are the vehicle weight, vehicle speed, vehicle acceleration, front and rear suspension stiffness and damping, front and rear tyre stiffness and pressure, the harvester displacement, width, height and stiffness. The values are selected using a slider bar, with the user simply having to press the *New Simulation* button to start a new simulation. The graphics are updated after the new simulation is completed. This panel also offers users the possibility to print the plots, allowing them to select the desired plots to be printed and pressing the *Print Plots* button. Finally, it contains an *Exit* button to close the results GUI and return to the initial GUI.

3.4.3 Models

Four computational models were developed, using the SIMULINK[®] tool, to perform the dynamic analysis depending on the selected inputs:

- 1) quarter-car model and SFA;
- 2) bicycle car model and SFA;
- 3) quarter-car model and CPA;
- 4) bicycle car model and CPA.

Models 1 and 2 do not consider the contact patch, so they perform an SFA, while Models 3 and 4 perform a CPA.

Each model uses the equations defined in the literature (Gillespie, 1992; Wong, 2001; Blundell and Harty, 2004; Pacejka, 2005; Jazar, 2008; Popp *et al.*, 2010; Rajamani,

2011) plus the equations previously defined for movable surfaces, with Equations (3.1-3.3) being used in Models 1 and 3 and Equations (3.4-3.8) used in Models 2 and 4, with Equations (3.9-3.13) being used in Models 3 and 4. Equations (3.14-3.21) were used in all the models to quantify the energy lost by the vehicle and harvested by the surface, as well as to determine the efficiency of the process.

3.4.4 Flowchart

The simulation software flowchart is presented in Figure 3.8.

After all the data are defined by the user on the *Inputs* window and the *Simulation* button is pressed, all the data are collected and a validation is done to confirm if the data are correctly defined. If not, an error message is presented. If it is, all the variables are defined and the computational model ID is set in function of the selected *Vehicle Model* (quarter-car or bicycle car) and *contact patch* interaction model (*Yes* or *No*).

The selected model is then opened and used to determine all the software outputs. After the simulation is completed, the results are obtained and validated. If there are simulation errors, a message is presented. If not, the outputs window is opened, and the results are presented, both graphically and numerically, as explained previously.

3.5 Technical Analysis

3.5.1 Introduction

To study and quantify the energy delivered by a road vehicle in motion into an SRE or an EHD depending on the equipment characteristics and evaluate the energy exchanging process efficiency, the RoadVISS software tool is used.

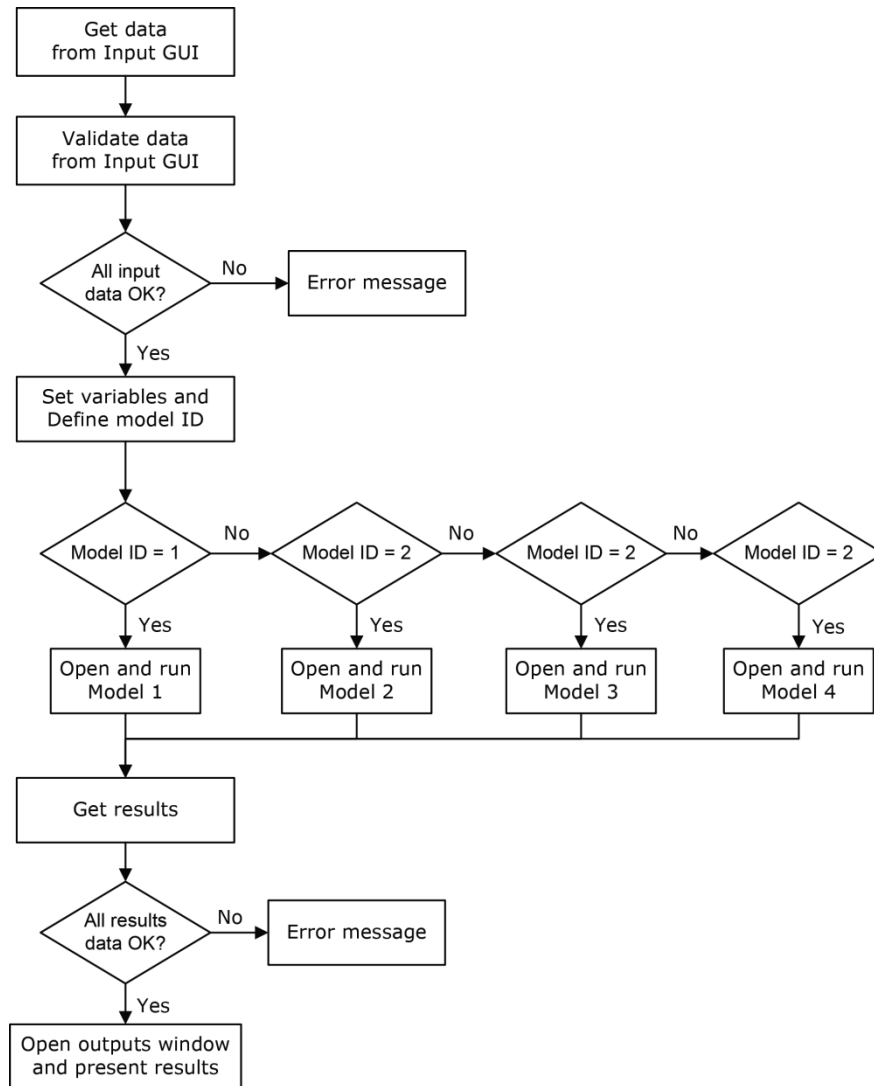


Figure 3.8- Simulation software flowchart.

First, simulations will be performed for different vehicle models (quarter-car and bicycle car models) and different VRI analysis modes (SFA and CPA), to determine the precision of each model and select the most appropriate for the remaining simulations.

Then, simulations will be performed by changing the equipment surface profile and geometry, as well as its maximum displacement, to evaluate the importance of these variables in the energy extraction process.

3.5.2 Simulations and results analysis

Using RoadVISS, a set of simulations were performed, initially with fixed values defined for the fixed variables, while the key variables vary in each simulation scenario to evaluate the impact of each key variable in the results.

The selected key variables for this study are surface profile and surface displacement. Also, the vehicle model (quarter-car/bicycle car model) and VRI interaction model (SFA or CPA) are compared.

The values defined for the fixed variables are presented in Table 3.5, as well as the initial values for the key variables (when the key variable is not changed in a scenario). The GUI with all fields filled with these values is presented in Figure 3.9. The vehicle, suspension and wheel data necessary to run the simulations are available in vehicle manufacturer's websites and vehicle datasheets.

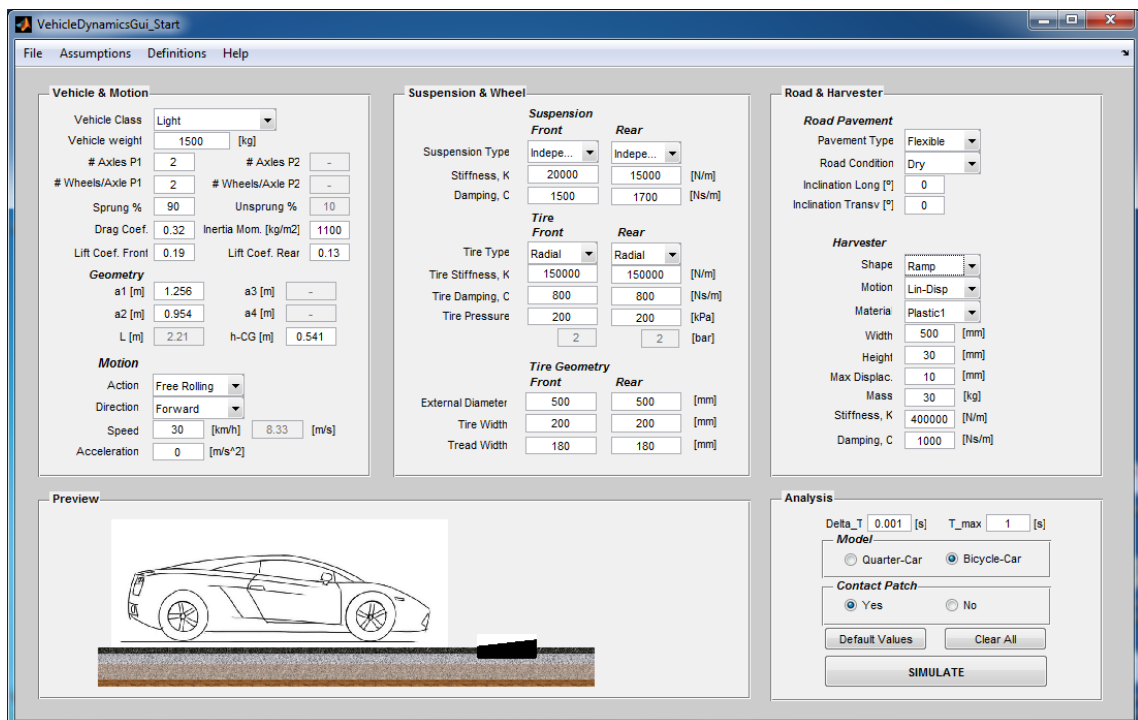


Figure 3.9- Graphical user interface with the standard inputs.

Table 3.5- Fixed and initial values for the simulation variables.

	Variable name	Value	Unit
Vehicle & Motion	Vehicle class	Light	-
	Vehicle weight	1,500	(kg)
	Number of axles P1	2	-
	Number of wheels per axle	2	-
	Sprung-Unsprung %	90%-10%	-
	Drag coefficient	0.32	-
	Inertia moment	1,100	(kg/m ²)
	Lift coefficients (Front Rear)	0.19 0.13	-
	Motion Direction	Free rolling Forward	-
	Vehicle speed	30	(km/h)
	Vehicle acceleration	0	(m/s ²)
	Suspension & Wheel	Suspension type (Front Rear)	Independent Independent
Suspension stiffness (Front Rear)		20,000 15,000	(N/m)
Suspension damping (Front Rear)		1,500 1,700	(Ns/m)
Tyre type (Front Rear)		Radial Radial	-
Tyre stiffness (Front Rear)		150,000 150,000	(N/m)
Tyre damping (Front Rear)		800 800	(Ns/m)
Tyre pressure (Front Rear)		200 200	(kPa)
Tyre external diameter (Front Rear)		500 500	(mm)
Tyre width (Front Rear)		200 200	(mm)
Tyre tread width (Front Rear)	180 180	(mm)	
Road pavement & SRE/EHD	Pavement type	Flexible	-
	Road condition	Dry	-
	Inclination longitudinal transversal	0 0	(°)
	Harvester shape	Ramp	-
	Motion	Linear displacement	-
	Equipment material	Rubber	-
	Equipment width height	500 30	(mm)
	Equipment maximum displacement	10	(mm)
	Equipment mass	30	(kg)
	Equipment stiffness	400,000	(N/m)
Equipment damping	1,000	(Ns/m)	
Analysis	Simulation time	1	(s)
	Iteration time	0.001	(s)
	Vehicle model	Bicycle car	-
	Contact Patch Analysis	Yes	-

3.5.2.1 Scenario 1 - Different vehicle models

In the first scenario, three different SPs (*Ramp*, *S profile* and *Bump*) were considered to be simulated with the two vehicle models, quarter-car and bicycle car model. All the remaining values for the simulations are presented in Table 3.5. The goal is to evaluate the differences in the total energy released by the vehicle and harvested by a surface, when different vehicle models are considered.

The simulation results are presented in Table 3.6. The value of the total energy released by the vehicle using the quarter-car model is achieved by multiplying the calculated vehicle released energy by the number of vehicle wheels. With the bicycle car model, the value is achieved by multiplying the calculated vehicle released energy by two, in other words by the number of vehicle sides.

Table 3.6- Scenario 1 results.

Vehicle model	SP	F_z max (N)	E_v (J)	E_{Ha} (J)	η (%)
Quarter car	Ramp	4,622.86	428.00	116.00	27.10
Quarter car	S profile	6,185.52	412.00	100.00	24.27
Quarter car	Bump	4,003.90	1,064.00	144.00	13.53
Bicycle car	Ramp	5,432.91	672.00	118.00	17.55
Bicycle car	S profile	6,834.69	682.00	108.00	15.83
Bicycle car	Bump	4,724.81	808.00	138.00	17.08

From the results presented in Table 3.6, it is possible to compare the differences between the usage of the quarter-car model and the bicycle car model. Some conclusions can be stated from the results analysis:

- The maximum force is always higher when considered the bicycle car model, due to the fact that it considers two different wheels, and for the considered vehicle geometry, the rear wheel induces higher forces than the front wheel. For the same conditions, the results' difference can reach almost 20 per cent.

- For surface profiles with smaller inclination angles, as the Ramp or S profile, the vehicle released energy is higher for the bicycle car model, mainly because of the fact that, when considered two different actuations, and as the rear wheel has a higher impact, the total losses are higher than when a single wheel is considered. For these surfaces, the received energy on the SRE/EHD does not change too much between vehicle models. So, the energy extraction efficiency is lower when considered the bicycle car model. For the same conditions, the results difference can reach almost 65 per cent.
- For surface profiles with high inclination angles, as the Bump profile, the vehicle released energy is much higher for the quarter-car model. This difference can be explained due to the inclusion of the pitch angle on the bicycle car model, which allows to distribute the chassis oscillation between front and rear wheel, leading to lower energy losses. Again, the value of the harvested energy does not change significantly, leading to a higher energy extraction efficiency for the bicycle car model. For the same conditions, the efficiency results' difference can reach almost 60 per cent.

When the bicycle car model is considered, the inclusion of the pitch angle and the different mass distribution according with the vehicle geometry increases the precision of the calculations and gives more realism to the results. So, the results for the bicycle car model are more precise and closer to the reality than the quarter-car model results, and the difference between them is considerable, reaching almost 60 per cent in the process efficiency. Bicycle car model should be used in VRI analysis.

3.5.2.2 Scenario 2 - Different interaction models

In the second scenario, two different surface displacements (0 and 10 mm) for a Ramp surface profile were considered to be simulated with the two vehicle models, quarter-car and bicycle car model, both for SFA and CPA. All the remaining values for the simulations are presented in Table 3.5. The goal is to evaluate the differences in the

total energy released by the vehicle and harvested by a surface, when different interaction models are considered. The simulation results are presented in Table 3.7.

Table 3.7- Scenario 2 results.

Interaction model	Vehicle model	x_h max (mm)	F_z max (N)	E_v (J)	E_{Ha} (J)	η (%)
SFA	Quarter car	0	4,615.70	516.00	0.00	0.00
	Quarter car	10	4,502.81	468.00	156.00	33.33
	Bicycle car	0	5,608.96	544.00	0.00	0.00
	Bicycle car	10	5,653.84	512.00	150.00	29.30
CPA	Quarter car	0	4,472.12	460.00	0.00	0.00
	Quarter car	10	4,422.86	428.00	116.00	27.10
	Bicycle car	0	5,398.68	734.00	0.00	0.00
	Bicycle car	10	5,432.92	672.00	118.00	17.56

From the results presented in Table 3.7, it is possible to compare the differences between the usage of the SFA and CPA models. Some conclusions can be drawn from the analysis of the results:

- The maximum force is always higher with the SFA model, due to the fact that it measures the tyre's resultant force as being constantly applied to the surface of the device, while the CPA considers the force correspondent to the tyre area in contact with the surface of the device, leading to a progressive force being applied to it, and, consequently, a peak value lower than that for the SFA. For the same conditions, the difference in results for the maximum force is 4 per cent.
- When the SFA is combined with the quarter-car model, the energy released by the vehicle in the interaction is similar to the CPA combined with the quarter-car model, but the energy harvested by the device is much higher, leading to a higher conversion efficiency (in this case, 23 per cent higher). This is due to the fact that a higher resultant force is considered during the whole interaction,

while on the CPA, a progressive force is applied, leading to a lower surface speed and a smaller force during the surface downward motion, and consequently, a smaller amount of energy is harvested.

- When the SFA is combined with the bicycle car model, the energy released by the vehicle in the interaction is lower than when the CPA is combined with the quarter-car model, but the energy harvested by the device is much higher, leading to a higher conversion efficiency (in this case, 67 per cent higher). The explanation is similar to that previously given for the quarter-car model.

These are accepted and expected results, as for the CPA analysis, the force induced by the vehicle wheel increases progressively over the surface, leading to a progressive increase in the surface displacement and consequently in its velocity. As for SFA, the resultant force is permanently applied on the surface from the moment the wheel makes contact, so the values for the energy received are higher than for CPA. However, CPA is more realistic and precise, as it is closer to reality than SFA. Considering the conversion efficiency results, the difference between these two models can reach 67 per cent.

Regarding the results comparing the surface displacement, it can be seen that in most scenarios, the energy lost by a vehicle decreases when the surface has motion, which may be an important conclusion, justifying that equipment with motion can be less invasive for vehicles than equipment without surface motion, and at the same time, they are more efficient, as they are able to convert a part of the vehicle's mechanical energy into other means of energy, while static equipment does not make use of vehicle released energy.

3.5.2.3 Scenario 3 - Different surface profile and displacement

In the third scenario, three different surface displacements (5, 10 and 20 mm) for seven different surface profiles (only surface S1 was not considered) were simulated using the

bicycle car model and CPA. All the remaining values for the simulations are presented in Table 3.5. The goal is to evaluate the differences in the total energy released by the vehicle and harvested by a surface, when different surface profiles and displacements are considered. The simulation results are presented in Table 3.8.

Table 3.8- Scenario 3 results.

SP	x_h max (mm)	F_z max (N)	E_v (J)	E_{Ha} (J)	η (%)
Convex bump	5	5,138.27	896.00	60.00	6.70
	10	4,724.80	808.00	138.00	17.08
	20	4,771.38	802.00	268.00	33.41
Ramp	5	5,472.96	690.00	46.00	6.67
	10	5,432.92	672.00	118.00	17.56
	20	5,779.61	668.00	182.00	27.24
Hump	5	5,026.87	1,508.00	72.00	4.77
	10	4,549.53	1,980.00	168.00	8.48
	20	4,981.83	2,080.00	356.00	17.12
Triangle	5	5,893.54	674.00	56.00	8.31
	10	5,432.56	550.00	130.00	23.64
	20	5,287.62	588.00	224.00	38.10
S profile	5	6,914.31	840.00	42.00	5.00
	10	6,834.69	682.00	108.00	15.84
	20	6,927.92	546.00	250.00	45.78
Scale up	5	5,100.01	266.00	40.00	15.04
	10	5,204.35	344.00	124.00	36.05
	20	5,458.93	356.00	168.00	47.19
Crest	5	5,015.76	856.00	56.00	6.54
	10	4,616.98	806.00	130.00	16.13
	20	5,403.82	760.00	252.00	33.16

From the results presented in Table 3.8, it is possible to compare the differences between the usage of different surface profiles and different maximum displacement of the surface. Some conclusions can be drawn from the results:

- For the same surface displacement, the surface profile has a great influence on the energy released by the vehicle and harvested from the surface. It can vary from only 266.00 J of lost energy with a Scale up profile, with 5-mm maximum

displacement, to 1,508.00 J with a Hump surface profile, for the same displacement, leading to completely different values of harvested energy and conversion efficiency.

- With an increase in the surface maximum displacement, for most surfaces, the vehicles' released energy decreases, and for all surfaces, the harvested energy increases, increasing the efficiency of the process. It can therefore be concluded that the surface maximum displacement is an essential feature for controlling the extraction of energy from a vehicle, as well as the harvested energy from a SRE or EHD. However, this displacement should be limited to take into account the oscillation induced on the vehicle, which should respect specific limits of ride comfort.

Analysing the results, it can be seen that there is no perfect combination, as this is dependent on the goal of each application. If the goal is to minimize the impact on the vehicle, minimizing its lost energy, the Scale-up profile presents better results. If the goal is to maximize the harvested energy, Bump and Hump profiles present better results. If process efficiency is the goal, Scale-up and S profile are the most appropriate surface profiles.

3.6 Summary and Conclusions

In this Chapter it was presented the development of a simulation software tool - RoadVISS - that allowed users to study the forces induced by a vehicle in motion into the road pavement, a SRE or an EHD, as well as the energy lost by the vehicle, associated to the contact with the referred surface, and the energy received by that surface. Based on this tool it is possible to determine which is the best vehicle model and VRI model, as well as to study the effects of road pavement elements, both SRE and EHD, on vehicle energy extraction. It also enables to study the effect of the characteristics of the equipment on the vehicle energy extraction process.

The software was developed in MATLAB[®] environment, including a GUI where the user can select and define all the variables associated to the simulation, and another GUI where the results are presented. The software has an extensive database of considered variables, allowing a huge amount of different combinations of values to be simulated, leading to the possibility of performing a great number of studies. The outputs of the system are focused on the forces and energy released by the vehicle and received by the pavement or by an energy harvest surface, but the computational model allows users to define new outputs and study other variables.

From the simulations performed, several conclusions have been presented in the analysis of the results. The first, and one of the most important conclusions, is related to the precision of the vehicle models. The simulations performed showed that bicycle car model results are more precise than the quarter-car model results, differing by up to 60 per cent. As most VRI studies use the quarter-car model (Borowiec *et al.*, 2010; Barbosa, 2011; Florin and Liliana, 2013; Hassaan, 2014, 2015), which is less precise than the bicycle car model, this is an important conclusion, meaning that future VRI research should adopt the bicycle car model to improve the precision of results.

Also, most studies consider that a resultant force is applied on the pavement, corresponding to the SFA model, as well as the existing software (Carsim, 2016; MSC. Software, 2016). In this study, the application of SFA was compared with that of CPA, and it was found that, especially for the cases when the surface has motion, the difference in results can reach 67 per cent, with the CPA model being more precise than SFA. Again, future VRI studies must adopt the CPA model to maximize the precision of results.

Regarding variations in the surface parameters (shape and displacement), it can be concluded that these variables have a great influence on the energy released by the vehicle, as well as on the energy harvested by the equipment surface. The surface shape and its maximum displacement are variables that contribute the most to the interaction results, both in terms of the vehicle's released energy and the surface harvested energy. Other variables can be changed during the simulations, such as the vehicle or harvester geometry, which will impact the amount of energy released and harvested. The

selection of the surface parameters should be done according to the goals of each application and the most appropriate solution for all scenarios was identified.

In conclusion, to design an SRE or EHD, a huge amount of simulations should be performed, relating the different key variables and optimizing its design for the place of application, design speeds, average traffic weights and available space for the equipment, among other features. RoadVISS software allows us to perform these simulations and it is an appropriate tool to support the design of an SRE or an EHD, in a way that any of the existing software allows to do.

The developed software tool can have multiple applications, from the study of vehicle suspensions and tyres, regarding their interaction with speed reducers, to the design of SRE themselves, but one of the main applications can be the design of EHD to implement on road pavements, which make use of vehicles' released energy to convert it into electrical energy. The developed models are validated for two-axle light vehicles. Additional developments will be performed to include multiple-axle light vehicles and heavy vehicles on the models.

3.7 References

- Andriopoulou, S. (2012). *A review on energy harvesting from roads*. KTH, Stockholm, Sweden.
- Barbosa, R.S. (2011). Vehicle dynamic response due to pavement roughness. *Journal of the Brazilian Society of Mechanical Sciences and Engineering*, 33(3): 302-307.
- Borowiec, M., Sen, A.K., Litak, G., Hunicz, J., Koszalka, G. and Niewczas, A. (2010). Vibrations of a vehicle excited by real road profiles, *Forschung im Ingenieurwesen*, 74(2): 99-109.
- Blundell, M. and Harty, D. (2004). *Multibody Systems Approach to Vehicle Dynamics*. Elsevier Butterworth-Heinemann, Oxford, UK.

- Carsim (Mechanical Simulation Corporation) (2016). <http://www.carsim.com>. Accessed in July, 2016.
- DGV (2004). *Technical Paper – Installation and Signalization of Speed reducer bumps (In Portuguese)*, pp. 1-18.
- Duarte, F. and Ferreira, A. (2016). Energy harvesting on road pavements: state of the art, *Proceedings of Institution of Civil Engineers: Energy*, 169(2): 79-90.
- Duarte, F., Ferreira, A. and Fael, P. (2016). Software for simulation of vehicle-road interaction. *New Advances in Information Systems and Technologies*, Vol. 444 of the *Series Advances in Intelligent Systems and Computing*, Springer International Publishing, pp. 681-690.
- Elvik, R., Vaa, T., Erke, A. and Sorensen, M. (2009). *The Handbook of Road Safety Measures*. Emerald, Bingley, UK.
- Ewing, R. and Brown, S. (2009). *US Traffic Calming Manual*. American Planning Association. Chicago, IL, USA.
- Farroni, F. (2016). TRICK-tire/road interaction characterization & knowledge-a tool for the evaluation of tire and vehicle performances in outdoor test sessions. *Mechanical Systems and Signal Processing*, 72(2016): 808-831.
- Florin, A. and Liliana, P. (2013). Passive suspension modeling using MATLAB, quarter-car model, input signal step type. *New Technologies and Products in Machine Manufacturing Technologies*, pp. 258-263.
- Gillespie, T. (1992). *Fundamentals of Vehicle Dynamics*. Society of Automotive Engineers, Warrendale, PA, USA.
- Hassaan, G.A. (2014). Car dynamics using quarter model and passive suspension, Part I: effect of suspension damping and car speed. *International Journal of Computer Techniques*, 1(2): 1-9.
- Hassaan, G.A. (2015). Car dynamics using quarter model and passive suspension, Part II: a novel simple harmonic hump. *Journal of Mechanical and Civil Engineering*, 12(1): 93-100.

- Hendrowati, W., Guntur, H. L. and Sutantra, I. N. (2012). Design, modelling and analysis of implementing a multilayer piezoelectric vibration energy harvesting mechanism in the vehicle suspension. *Engineering*, 4(11): 728-738.
- IEA. (2012). *Technology Roadmap: Fuel Economy of Road Vehicles*. International Energy Agency, Paris, France. Available from http://www.iea.org/publications/freepublications/publication/Fuel_Economy_2012_WEB.pdf. Accessed in September, 2015.
- Jazar, R. (2008). *Vehicle Dynamics: Theory and Application*. Springer, New York, NY, USA.
- Johnson, L. and Nedzesky, A. (2004). A Comparative Study of Speed Humps, Speed Slots and Speed Cushions. *Annual Meeting Compendium*, Institute of Transportation Engineers (ITE), Washington, DC, USA.
- Kazmierski, T., and Beeby, S. (Eds.). (2009). *Energy harvesting Systems - Principles, Modeling and Applications*. Springer, New York, NY, USA.
- Khaligh, A. and Onar, O. C. (2010). *Energy harvesting: solar, wind, and ocean energy conversion systems*. CRC Press Inc., Boca Raton, FL, USA.
- MSC.Software (Adams) (2016). <http://www.mscsoftware.com/product/adams>. Accessed in July, 2016.
- Pacejka, H. (2005). *Tire and Vehicle Dynamics*. Elsevier, Butterworth-Heinemann, Oxford, UK.
- Popp, K., Schiehlen, W., Kroger, M. and Panning, L. (2010). *Ground Vehicle Dynamics*. Springer, Berlin, Germany.
- Priya, S. and Inman, D. J. (Eds.) (2009). *Energy harvesting technologies*. Springer, New York, NY, USA, vol. 21.
- Rajamani, R. (2011). *Vehicle Dynamics and Control*. Springer, New York, NY, USA.
- Szurgott, P., Kwasniewski, L. and Wekezer, J. (2009). Dynamic interaction between heavy vehicles and speed bumps. In *ECMS: Proceedings 23rd European Conference on Modelling and Simulation*, pp. 585-591.

Wong, J. (2001). *Theory of Ground Vehicles, 3rd Ed.* Wiley, New York, NY, USA.

WHO (2010). *European Status Report on Road Safety: Towards Safer Roads and Healthier Transport Choices.* World Health Organization, Geneva, Switzerland. Available from: http://www.euro.who.int/__data/assets/pdf_file/0015/43314/E92789.pdf?ua=1. Accessed in May, 2016.

WHO (2013). *Global Status Report on Road Safety 2013: Supporting A Decade of Action.* World Health Organization, Geneva, Switzerland. Available from: http://www.who.int/violence_injury_prevention/road_safety_status/2013/en/. Accessed in May, 2016.

Chapter 4

Road Pavement Energy Harvesting: Optimizing the Energy Extraction from Vehicles to Promote Road Safety

4.1 Introduction

Road accidents are considered by the World Health Organization (WHO) to be one of the main problems affecting public health in the WHO European Region, and are responsible for causing the death of about 120,000 people per year. Road accidents are the leading cause of death in children and young adults aged 5 to 29 years old (WHO, 2010). Additionally, the WHO estimates that each year about 2.4 million people are seriously injured as a result of road accidents in the WHO European Region alone. Worldwide, the WHO estimates that there are about 1.24 million deaths due to road accidents (WHO, 2013).

All this has a massive social impact directly and indirectly because besides the decrease in productivity caused by death or serious injury to people of a working age, a great

strain is caused on health system resources. In addition to the pain and suffering caused to the families of victims, road accidents cause substantial economic loss for society, estimated by the WHO to be as high as 3% of gross domestic product in many of the countries studied (WHO, 2010, 2013).

Analyzing road accidents and their fatality rate, the WHO concludes that, globally, 22% of deaths due to road accidents are pedestrians, 5% are cyclists, 23% are motorcyclists, 50% are so-called vulnerable road users (WHO, 2013). In the European region, this figure is slightly lower, standing at 43%, with 27% of deaths involving pedestrians.

One of the main causes of accidents with vulnerable road users is excess of speed, especially within urban areas. Most accidents with pedestrians (70%) occur on pedestrian crossings or permitted crossing areas and in 80% of cases, with the pedestrian in movement (Holzmann, 2008).

The WHO (2013) recommends six strategic points for action in order to reduce the number of accidents effectively and rapidly, especially among vulnerable road users, with the first and most relevant being speed reduction.

This issue is of great importance on several levels. Firstly, because the need to reduce speed is properly studied and based on traffic engineering and road safety manuals (Seco *et al.*, 2008; Elvik *et al.*, 2009) - the higher the speed, the greater the time and distance for braking and stopping and, consequently, the greater the severity of accidents. The state of the pavement (dry or wet) also has an influence on braking and stopping distances, but the main factor is the vehicle speed at the moment that it begins to brake (Seco *et al.*, 2008). Similarly, studies show that the probability of an accident involving a pedestrian being fatal is greatly reduced by the reduction of impact speed. The probability of death is 80% if the speed is 65 km/h, 45% if the speed is 50 km/h and lower than 10% if the speed is 30 km/h. These numbers highlight the importance of controlling speed to keep it below 50 km/h in urban areas and below 30 km/h in residential areas or pedestrian crossings.

Traffic calming measures have emerged as a way to minimize negative impacts of traffic in places where vehicles move by moderating their speed, with the main

objective of reducing motorized vehicle speed to that of non-motorized vehicles and/or pedestrians moving in the same space. One of the most effective measures is to change vertical alignments, in particular with the implementation of speed reduction equipment (SRE), such as speed bumps or speed humps. SREs are the most commonly used traffic calming measure globally because they ensure a significant reduction in vehicle speed (Seco *et al.*, 2008; Elvik *et al.*, 2009).

This equipment has the advantage of reducing the vehicle speed indirectly, rather than directly by way of the impact on the vehicle, as it forces drivers to reduce vehicle speed before hitting the equipment to avoid impact (Silva, 2010). SREs increase the respect between vehicles and pedestrians on pedestrian crossings and are able to reduce the number of road accidents by 41% (Silva, 2010), although many authorities indicate substantially lower values, such as ITE, who suggest a reduction of 13% (Ewing and Brown, 2009). According to Gifford (2004), accidents can be reduced in 20 mph zones (32 km/h) by as much as 60%.

Due to the impact of these devices on vehicles and their occupants, overcoming the admitted discomfort levels defined by *ISO 2631-1* (ISO, 1997), such solutions are not suitable for application in locations on roads where the design speed is usually between 40 and 50 km/h (Seco *et al.*, 2008), which limits their range of application. Another major drawback of SREs is the noise generated by the impact of the vehicle on the equipment, which is considered a nuisance in residential areas, especially at night (Silva, 2010; Freitas *et al.*, 2013).

From the analysis performed, it can be concluded that traffic calming measures are effective to some extent, yet there is plenty of margin for improvement and development. In the particular case of SREs, they are seen as the most effective measure in speed reduction, though possible locations for implementation are limited. If solutions were optimized and less invasive in terms of the impact on vehicle occupants, while remaining effective in terms of speed reduction, the potential application of these devices would be greater and their contribution to an effective speed reduction would be better, producing a significant decrease in the rate of road accidents.

Energy harvesting devices (EHD), when implemented in the road pavement, extracts energy from vehicles which, in most cases, decrease the kinetic energy of vehicles, meaning that it will decrease its speed. If this process is done without affecting the ride comfort, it enables the vehicle speed to be reduced without any driver action. The speed reduction is directly proportional to the extracted energy. In the same manner, a road pavement EHD is able to produce more electrical energy according to the amount of energy harvested from vehicles. So, in order to improve a road pavement EHD performance, it should be studied the most appropriate techniques to maximize the amount of energy harvested from the vehicle without affecting the ride comfort and, at the same time, this study will lead to a solution to reduce the vehicle speed without any driver action, promoting road safety with a new approach. If successful, it will be possible to implement these devices in places where vehicles move at speeds higher than 40 km/h and reduce their speed without causing discomfort to occupants.

In this Chapter the study of typical SRE is presented, to understand its common characteristics. After that, a new approach to harvest mechanical energy from vehicles minimizing the impact to the vehicle is presented. The proposed system is modelled, computationally simulated and experimentally validated, so that conclusions of its performance can be drawn.

4.2 Speed Reduction Equipment

4.2.1 Introduction

SRE consists of a specific type of traffic calming solution, involving vertical alignment changes in the pavement, with the goal of reducing vehicle speed by causing discomfort to their occupants when vehicles travel above the design speed (Elvik *et al.*, 2009; Ewing and Brown, 2010). To quantify the impact that a SRE induces on a moving vehicle, it is important to study the geometric shape and dimensions of its surface, as well as the vehicle-road interaction.

In this section, the main characteristics of existing SRE will be presented, with special emphasis on their surface geometry and working principles. Based on this information, the models defined in Chapter 3 for SRE can be tested later in this work.

4.2.2 Existing equipment analysis

SREs should have an impact on vehicles when they travel above the design speed, by causing discomfort for the occupants and, at the same time, they should have minimum impact on the vehicles if they travel under the design speed. This is achieved through their geometry and surface profile.

Considering the existing products on the market, most of them are speed humps and speed bumps, manufactured using a high-strength rubber (usually vulcanized) with convex or sinusoidal surface profiles, the most widely used products being a maximum of 3 or 5 cm high at the centre and 50 or 90 cm wide, respectively (3M, 2016). The 3 cm speed bumps are used in places with a speed limit not exceeding 35 km/h, while the 5 cm height are used in places with a speed limit not exceeding 20 km/h. To fix these devices to the pavement, screws are fastened in plastic expansion anchors applied in holes made in the upper layers of the pavement.

Some manufacturers have different surface profiles, such as triangular or trapezoidal shapes, using the high strength rubber as the predominant material, or using recycled plastic as the main alternative (TSS, 2016; Hongqiao Traffic, 2016).

There is no international uniformity to the geometric aspects of SRE regarding their shape, height, length or width. Considering other research (Johnson and Nedzesky, 2004; Szurgott *et al.*, 2009), individual countries recommendations (DGV, 2004; Ewing and Brown, 2010), and the previously mentioned products, it can be concluded that the mostly commonly used surface profiles on SREs are, respectively, *convex bump* (S1), *sinusoidal bump* (S2), *trapezoidal* (S3) and *triangular* (S4), as presented in Figure 4.1, with L_{max} being the maximum width and h_{max} the maximum height of the SRE surface. The equations that characterize each surface profile were presented in Table 3.4.

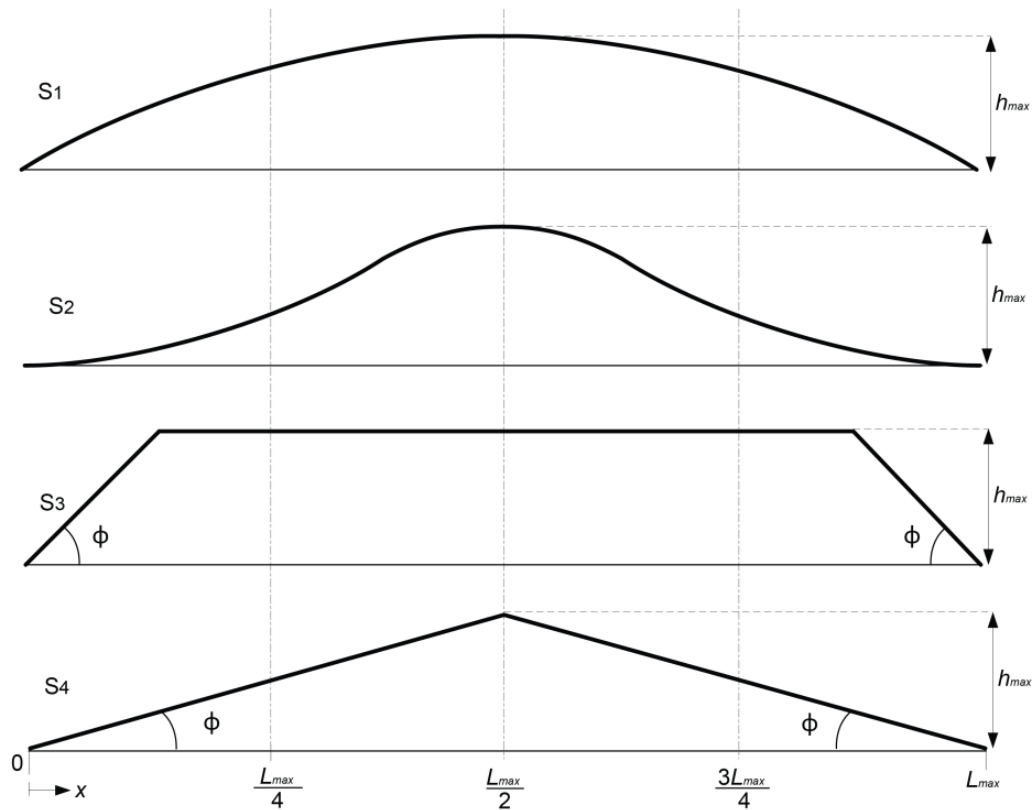


Figure 4.1- Typical SRE surface profiles.

In terms of materials, there are two main solutions: concrete or bituminous mixtures, if speed reducers are implemented together with the pavement; plastic or vulcanized rubber mixtures, when commercial equipment is implemented. Speed bumps and speed humps built directly in the pavement (in concrete or bituminous mixture) are not considered in this work, as they are built by the infrastructure manager in accordance with local standards.

Regarding the SRE patented devices, the majority are based on the same basic principle: application of a device in the road surface that acts as a barrier to vehicle motion, promoting the impact of the vehicle's tyres with the equipment and thus creating an oscillation in the vehicle, imposing discomfort to their occupants and reduce the linear velocity of the vehicle.

One of the first patents related to a SRE goes back to 1982 was registered by Lecompte (1982), in Canada, and consisted of a device which is very similar to the existing speed bumps: convex surface, prefabricated high strength rubber, applied on the road surface and fixed by screws.

In the USA, several patents were registered in the 90's, where, in addition to the speed bump registered by Lecompte (1982), mechanisms were added below the surface of the equipment, allowing its displacement, as in the case of patents US4974991 (Mandavi, 1990), US5267808 (Welford, 1993) and US5509753 (Thompson, 1996). However, all these devices had the same principle of typical speed bumps, with the disadvantage of requiring a major adjustment in the pavement, in order to install the respective mechanisms under the SRE. Sinclair (1997) registered a design patent, USD387181, for a modular speed bump with reflective elements, similar to most SRE currently available on the market.

In the 2000s, new patents were registered, in order to give greater dynamism to the speed bumps and minimize the impact of the vehicle interacting with it. One example is the system developed by Kamienschick (2000), where it is intended that the equipment surface has a deflection effect when vehicle wheels pass over it. However, this keeps the typical shape of a speed bump, installed above the pavement, containing air, oil or another fluid inside it. In the case of equipment failure, the fluid will be spilled to the pavement, which can have disastrous effects. A new product with this working principle is being developed by Bandennova (2016), without any technical data available so far.

4.2.3 Energetic analysis

The interaction of a vehicle with a typical SRE can be characterized by typical VRI equations, as defined in Chapter 3 by the equations in Tables 3.1 and 3.2, as well as the models defined in the vehicle dynamics literature (Gillespie, 1992; Wong, 2001; Blundell and Harty, 2004; Pacejka, 2005; Jazar, 2008; Popp *et al.*, 2010; Rajamani, 2011).

The energetic analysis from this interaction can also be performed based in Chapter 3 models, with Equation (3.18) quantifying the energy lost by the vehicle in the interaction and Equation (3.19) the energy harvested by the SRE surface.

4.3 Road Pavement Energy Harvesting Device for Speed Reduction Purposes

4.3.1 Introduction

A new solution is proposed to promote a more effective speed reduction, based on the RPEH device's working principles. This approach consists of a device to be implemented on the road pavement with a movable surface which has a degree of freedom in the vertical axis and is actuated by the passage of a vehicle wheel over it. The device is connected to a mechanical system below it, which receives and temporarily stores the surface harvested mechanical energy delivered from the vehicle during the interaction with the equipment surface. After the vehicle wheel leaves the contact with the equipment surface, the accumulated energy is used to restore the surface to its initial position.

The new SRE design has two main components: its surface profile and displacement, and the mechanical system responsible for energy storage and surface position control. Both components will be studied in this section.

4.3.2 Surface profile

The surface profiles presented in Figure 4.1, typical for standard SRE without surface displacement, have a common feature: the initial and final height is the same at the road pavement level so that the vehicle wheel starts and finishes the contact with the equipment at pavement level.

When the SRE surface has vertical motion, moving downwards with the force exerted by the moving vehicle wheel, its final height should not be the same as its initial height, so that the vehicle tyre can reach the pavement level immediately after it leaves contact with the SRE surface. So, at the surface maximum length, the surface profile height should be the same as the surface maximum displacement. To accomplish this important feature, four different surface profiles are presented in Figure 4.2. Each surface profile (SP) has the following denomination: *Ramp* (S5); *S profile* (S6); *Scale up* (S7); and *Crest* (S8). Each SP equation is presented in Table 3.4.

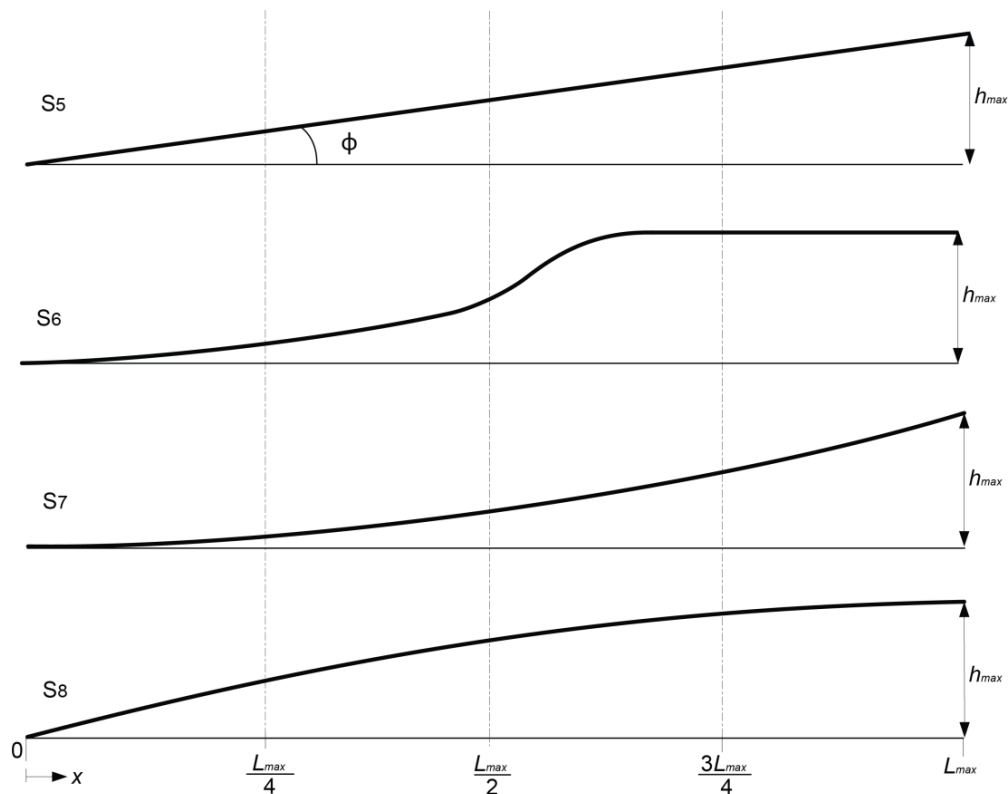


Figure 4.2- New SRE surface profiles for a one degree of freedom movable surface.

4.3.3 VRI models with movable surface

The main models for studying the VRI were presented in Chapter 3 with special emphasis on the bicycle-car model, which is the most appropriate model to study the interaction between a vehicle and a SRE in the pavement. Those models were validated for pavements without a movable surface. However, when considering equipment whose surface moves vertically due to the actuation of the vehicle, these models are incomplete.

The inclusion of a surface with vertical displacement in the pavement for the bicycle car model determines a significant change in the models. A new model to better define this interaction was proposed in Chapter 3. Considering the bicycle car model, as in Figure 3.2b, Equations (3.4-3.8) defines the model to be considered in this work, with a one degree of freedom movable system implemented under the equipment surface, which has a displacement x_h , a mass m_h , and a spring with stiffness K_h .

4.3.4 Mechanical system modelling

The main element of the mechanical system responsible for the opposition force to the surface motion, for the mechanical energy storage and for the surface position replacement is a spring. This could be directly actuated by the equipment surface, but it would limit the spring's force to its displacement and stiffness. To increase the spring displacement and, consequently, its reactive force, a mechanical system is coupled to the surface, in order to transmit the received force to the spring and multiply the displacement. This system, presented in Figure 4.3, is based on a crank of length l_{cr} connected to a surface at a fixed point, moving linearly with the linear motion of the surface (x_h), and transmitting the force from the surface to a piston, which is connected to the spring, causing a horizontal linear motion (x_{sp}). This is defined as a crank to slider (CTS) mechanical system.

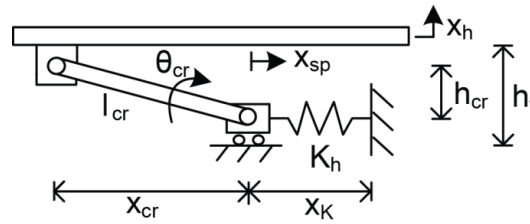


Figure 4.3- SRE mechanical system.

The kinematic relations of the system are defined by Equations (4.1-4.5), with x_{sp-in} representing the initial position of the piston and h_{cr-in} representing the initial height of the crank axis.

$$h_{cr} = l_{cr} \sin\theta_{cr} \Leftrightarrow \theta_{cr} = \sin^{-1}\left(\frac{h_{cr}}{l_{cr}}\right) \quad (4.1)$$

$$x_{cr} = l_{cr} \cos\theta_{cr} \quad (4.2)$$

$$x_{sp} = x_{sp-in} + x_{cr} \quad (4.3)$$

$$h_{cr} = h_{cr-in} + x_h \quad (4.4)$$

$$x_K = x_{sp} \quad (4.5)$$

Figure 4.4 represents the force diagrams of the system for a downward motion of the surface, with Equations (4.6-4.10) defining the force transmission. In these equations, F_{SM1} represents the force entering the mechanical system, F_{SM2} the force transmitted by the piston to the spring, and F_{SM3} the force exerted by the spring onto the piston, while F_{SM2s} and F_{SM1s} represent the reaction force on the crank's extremities connected to the piston and the surface, respectively. The opposition forces are represented by an index s , for example, the opposition force to F_{SM1} is represented by F_{SM1s} . The force exerted by the surface mass is not considered in the force analysis, due to its low expressivity.

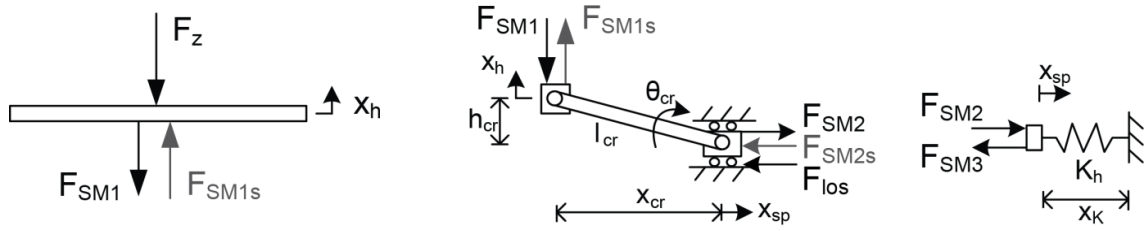


Figure 4.4- Force diagrams for the downward motion of the surface.

$$F_{SM1} = F_z \tag{4.6}$$

$$F_{SM2} = \frac{F_{SM1}}{tg\theta_{cr}} \tag{4.7}$$

$$F_{SM3} = K_h x_K \tag{4.8}$$

$$F_{SM2s} = F_{SM3} \tag{4.9}$$

$$F_{SM1s} = F_{SM2s} tg\theta_{cr} \tag{4.10}$$

Equations (4.11-4.12) represent the dynamic equations that define the motion of the system, for the surface (4.11) and for the piston (4.12), F_{los} the losses being due to mechanical friction.

$$\ddot{x}_h = \frac{1}{m_h} [F_{SM1s} - F_z] \tag{4.11}$$

$$\ddot{x}_{sp} = \frac{1}{m_{sp}} [F_{SM2} - F_{SM3} - F_{los}] \tag{4.12}$$

When the surface is stopped at the lower limit after maximum displacement is reached, the dynamic equations are equal to zero, and the force transmission equations are equal to those defined by Equations (4.6-4.10).

For an upward motion of the surface, the force transmission through the mechanical system is presented in Figure 4.5, and the forces are defined by Equations (4.13-4.15). The opposition force from the surface, F_{SM1s} , is defined by the surface mass ($m_h \cdot g$).

$$F_{SM3} = K_h x_K \tag{4.13}$$

$$F_{SM2} = F_{SM3} \tag{4.14}$$

$$F_{SM1} = F_{SM2} tg\theta_{cr} \tag{4.15}$$

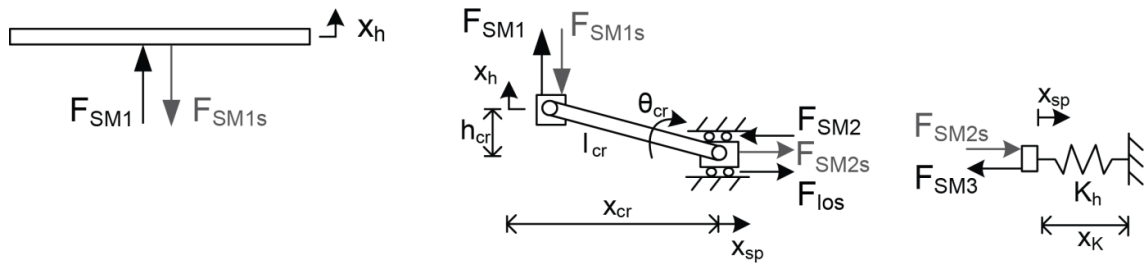


Figure 4.5- Force diagrams for the upward motion of the surface.

Equations (4.16-4.17) represent the dynamic equations that define the motion of the system for the surface (4.16) and for the piston (4.17), respectively.

$$\ddot{x}_h = \frac{1}{m_h} [F_{SM1} - F_{SM1s}] \tag{4.16}$$

$$\ddot{x}_{sp} = \frac{1}{m_{sp}} [-F_{SM3} + F_{SM2s} + F_{los}] \tag{4.17}$$

This system has the ability to multiply the force received by the surface by a higher force delivered to the spring, while reducing the displacement from the surface to the spring or the opposite, depending on the initial value of the crank angle (θ_{cr}) and the crank length (l_{cr}). Using two CTS mechanical systems connected to the surface, one on each side of the device, as shown in Figure 4.6, allow us to have more precise control over the surface displacement and distributing the loads, keeping the surface in line and balanced. Also, a linear guiding system is used, connected to the surface and to the base, so that the surface movement only occurs in the vertical axis. Considering this, F_{SM1} is divided by two, and the total spring stiffness is also divided by the two springs.



Figure 4.6- SRE with two CTS mechanical systems connected to the surface.

4.3.5 Energetic analysis

Considering a one degree of freedom movable surface, the energy harvested by the surface, associated with the surface motion is calculated using the vertical component of the force applied in the surface (F_z) and the surface displacement (x_h) using Equation (4.18). Equation (4.19) allows us to evaluate the efficiency of the process, between the energy lost by the vehicle (E_v) and the energy harvested by the surface of the equipment (E_{Ha}). The energy lost by the vehicle is determined using Equation (3.18).

$$\partial E_{Ha} = F_z \partial x_h \quad (4.18)$$

$$\eta_{Ha} = \frac{E_{Ha}}{E_v} \quad (4.19)$$

4.4 Technical Analysis

4.4.1 Introduction

Based on a software tool presented in Chapter 3, the equations of the SRE presented in the previous sections were incorporated for the different surface profiles, the vehicle dynamic models with a moving surface and the mechanical system responsible for the actuation of the surface.

The purpose of the simulation software is to study this interaction in great detail, with the possibility of fully characterizing the vehicle under study, by defining its class, weight, axles, wheels, geometry, speed, acceleration, suspensions and tyres, defining all the mechanical parameters, such as damping and stiffness for each suspension and tyre, as well as fully characterizing the pavement or SRE surface, by defining its material, shape, geometry and, for a surface with displacement, its maximum displacement, mass, and stiffness. Considering the conclusions of Chapter 3, the selected vehicle model for this analysis is the bicycle car model.

The software tool calculates all the displacements, both for the vehicle and the SRE surface, the applied and received forces, and the power and energy transferred, released

from vehicle and received on the SRE surface, and presents the results both graphically and numerically. From the vehicle's chassis displacements and from the motion equations, the software also quantifies the vertical and longitudinal accelerations, which are important to determine the discomfort induced on the vehicle's passengers.

In this section, the simulations performed with RoadVISS for two scenarios will be presented: standard speed reducers, without surface motion; and the new SRE proposed, for different surface profiles, maximum displacements and geometries, in order to identify the most effective solution, both in terms of speed reduction and ride quality.

According to Uys *et al.* (2007) and considering ISO 2631-1 (ISO, 1997), the vertical acceleration induced by the vehicle on the passengers is a key factor for measuring the ride quality. The levels of acceptability of ride quality are presented in Table 4.1. Considering these values, it is intended that the SRE do not induce vertical accelerations above 0.80 m/s^2 .

Table 4.1- Levels of acceptability of ride quality (ISO, 1997).

Vehicle chassis vertical acceleration (m/s^2)	Acceptability
<0.315	Not uncomfortable
0.315-0.630	A little uncomfortable
0.500-1.000	Fairly uncomfortable
0.800-1.600	Uncomfortable
1.250-2.500	Very uncomfortable
>2.000	Extremely uncomfortable

4.4.2 Comparison between typical SRE and the proposed solution

Using the RoadVISS software tool to perform the simulations both for standard SRE and for the new proposed device, a vehicle with the characteristics presented in Table 4.2 was defined, using the bicycle car model and the contact patch analysis. The initial speed considered was 50 km/h as this is the speed limit in urban areas.

Table 4.2- Fixed and initial values for the simulation variables.

	Variable name	Value	Unit
Vehicle & motion	Vehicle class	Light	-
	Vehicle weight	1,500	(kg)
	Number of axles P1	2	-
	Number of wheels per axle	2	-
	Sprung-Unsprung %	90%-10%	-
	Drag coefficient	0.32	-
	Inertia moment	1,100	(kg.m ²)
	Lift coefficients (Front Rear)	0.19 0.13	-
	Motion Direction	Free rolling Forward	-
	Vehicle speed	50	(km/h)
	Vehicle acceleration	0	(m/s ²)
Suspension & wheel	Suspension type (Front Rear)	Independent Independent	-
	Suspension stiffness (Front Rear)	20,000 15,000	(N/m)
	Suspension damping (Front Rear)	1,500 1,700	(Ns/m)
	Tyre type (Front Rear)	Radial Radial	-
	Tyre stiffness (Front Rear)	150,000 150,000	(N/m)
	Tyre damping (Front Rear)	800 800	(Ns/m)
	Tyre pressure (Front Rear)	200 200	(kPa)
	Tyre external diameter (Front Rear)	500 500	(mm)
	Tyre width (Front Rear)	200 200	(mm)
	Tyre tread width (Front Rear)	180 180	(mm)

4.4.2.1 Scenario 1 - Standard SRE

Considering the SRE available on the market, more specifically the commercial speed bumps, which have a convex and sinusoidal profile with different widths (400, 500, 600 and 900 mm) and different maximum heights (20, 25 and 30 mm), and also some products with triangular and trapezoidal surface profiles, as presented in Figure 4.1, simulations for a vehicle with the characteristics presented in Table 4.2 were performed in order to determine the impact of the different SRE on the vehicle, in terms of maximum induced force from vehicle to the SRE (F_z), vehicle released energy (E_v), chassis maximum vertical displacement (x_s), maximum vertical acceleration (\ddot{x}_s), maximum longitudinal acceleration (\dot{v}_x), and vehicle speed reduction (v_{red}). The simulation results are presented in Table 4.3.

Table 4.3- Standard SRE simulation results.

SP	L _{max} (mm)	h _{max} (mm)	F _{z max} (mm)	E _v (J)	x _{s max} (mm)	ẍ _{s max} (m/s ²)	ṽ _{x max} (m/s ²)	v _{red} (km/h)
S1	400	20	5,691.16	760.00	1.61	2.25	-3.24	0.13
	500	25	6,456.17	954.00	2.22	2.96	-3.40	0.16
	600	30	6,685.55	1,200.00	3.37	3.58	-3.47	0.21
	900	50	7,739.05	2,248.00	6.48	5.11	-3.82	0.39
S2	400	20	6,588.26	776.00	0.95	1.68	-2.12	0.13
	500	25	7,121.65	836.00	1.23	2.33	-2.66	0.19
	600	30	7,669.48	1,028.00	2.34	2.95	-2.95	0.21
	900	50	9,738.73	2,680.00	3.89	4.83	-4.1	0.47
S3	500	30	7,045.11	3,368.00	3.25	3.13	-6.15	0.59
	750	40	8,345.22	4,562.00	5.89	4.04	-6.99	0.79
	1000	50	10,301.18	5,782.00	8.67	4.94	-7.11	1.01
S4	400	20	6,006.95	570.00	0.98	1.54	-0.75	0.10
	600	30	7,025.51	864.00	1.79	2.47	-0.83	0.15
	800	40	7,603.11	1,040.00	2.89	3.23	-0.84	0.18

From the results presented in Table 4.3, it is possible to compare the differences between each SRE, depending on its particular characteristics. Some conclusions can be drawn from the analysis of the results:

- All the SRE analysed induce a vertical acceleration higher than 0.80 m/s^2 , which indicates, according with ISO 2631-1 (ISO, 1997), that all SRE induce an uncomfortable ride quality to the vehicle passengers, when passing over the SRE at 50 km/h; in fact, most of the SRE studied present a vertical acceleration higher than 2.50 m/s^2 , resulting in extremely uncomfortable ride quality for passengers.
- Comparing each of the SRE, one can conclude that the *Triangular* surface profile (S4) presents the lowest vertical acceleration induced on vehicle passengers, but is also the profile with the lowest energy extraction, meaning the lowest vehicle speed reduction.
- The convex *Convex bump* surface profile (S1), which is the mostly used profile on municipal roads, especially 600 mm wide by 30 mm height version, gives to

the vehicle passengers an extremely uncomfortable ride quality and only promotes a direct speed reduction of 0.21 km/h.

- The *Sinusoidal bump* surface profile (S2), when compared with the *Convex bump* surface profile (S1), induces lower vertical acceleration to the vehicle chassis so less discomfort to passengers with similar results in terms of speed reduction, meaning that this profile is more appropriate to improve ride quality.
- The *Trapezoidal* surface profile (S3) presents the highest speed reduction values; however, due to the very high vertical acceleration induced to the vehicle passengers, its use should be very limited.

From all the simulations, it can be concluded that all SRE induce very uncomfortable or extremely uncomfortable ride quality to the vehicle passengers, without resulting in high values of vehicle speed reduction. It may be concluded, therefore, that the effectiveness of these devices is due only to the discomfort caused to vehicle passengers, leading to speed reduction before the equipment due to a braking action and not by the equipment itself.

4.4.2.2 Scenario 2 - New device with movable surface

Considering the new solution proposed with a movable surface and considering the same vehicle and motion conditions as in the previous simulations for standard SRE, a set of simulations were performed for the different surface profiles presented in Figure 4.3, with different widths (200, 400 and 600 mm) and maximum heights (20, 25 and 30 mm), the maximum displacement being equivalent to the surface maximum height. The considered spring stiffness value is 200,000 N/m, and the surface material is recycled plastic with a rubber layer on top, with a total mass of 20 kg. The values for r_l and θ_{l-in} are, respectively, 0.10 m and 1.22 rad (or 70°). The simulation results are presented in Table 4.4.

From the results presented in Table 4.4, it is possible to compare the differences between each surface profile and SRE characteristics. Some conclusions may be drawn from the analysis of the results:

- Surface profiles *Ramp* (S5), *S profile* (S6) and *Scale Up* (S7) induce a vertical acceleration lower than 0.80 m/s^2 , meaning that these three profiles provide a comfortable or a little uncomfortable ride quality, while energy is being harvested from the vehicle, leading to a speed reduction.
- Surface profile *Crest* (S8) induces a vertical acceleration between 0.74 and 1.35 m/s^2 , values that are considered uncomfortable in terms of ride quality.
- In terms of speed reduction, *Crest* is the surface profile that allows the most energy to be harvested from the vehicle and, consequently, to maximize speed reduction, followed by the surface profile *Ramp*, *S Profile* and *Scale Up*, respectively.
- The surface profile that presents the best relation speed reduction versus ride quality is *Ramp* (S5), with special emphasis on the 200 mm wide by 25 mm maximum displacement equipment, which allows a vehicle speed reduction of 0.13 km/h only in 0.20 metres, meaning that with five consecutive devices applied on the pavement it would be possible to reduce the vehicle speed by 0.67 km/h and with a good level of ride quality (a little uncomfortable).

When comparing the achieved results using a movable surface and surface profiles S5-S8 with the standard SRE with surface profiles S1-S4, it may be concluded that the relationship between vehicle speed reduction and ride quality is much better with the newly proposed device with movable surface, for all the studied surfaces, both in terms of speed reduction and ride quality.

Table 4.4- New SRE with movable surface simulation results.

SP	L_{\max} (mm)	h_{\max} (mm)	$F_z \max$ (mm)	E_v (J)	$x_s \max$ (mm)	$\ddot{x}_s \max$ (m/s ²)	$\dot{v}_x \max$ (m/s ²)	v_{red} (km/h)
S5	200	20	3,524.92	580.00	0.14	0.36	-0.62	0.10
	200	25	3,968.15	724.00	0.31	0.49	-0.78	0.13
	400	20	3,494.58	396.00	0.06	0.34	-0.29	0.07
	400	25	3,501.22	500.00	0.06	0.29	-0.36	0.09
	600	25	4,853.91	462.00	0.02	0.23	-0.33	0.08
	600	30	4,507.48	534.00	0.16	0.81	-0.38	0.10
S6	200	20	4,119.11	286.00	0.18	0.38	-1.29	0.05
	200	25	4,763.49	350.00	0.33	0.61	-1.23	0.06
	400	20	4,120.48	134.00	0.04	0.39	-0.54	0.03
	400	25	4,187.17	266.00	0.04	0.32	-0.95	0.05
	600	25	5,160.44	272.00	0.13	0.92	-0.72	0.05
	600	30	4,888.78	326.00	0.14	0.92	-0.65	0.06
S7	200	20	3,478.42	88.00	0.06	0.44	-1.02	0.02
	200	25	3,497.61	110.00	0.03	0.37	-1.36	0.02
	400	20	2,862.85	104.00	0.24	0.35	-0.65	0.02
	400	25	2,939.65	142.00	0.21	0.36	-0.61	0.03
	600	25	4,216.41	222.00	0.31	0.52	-0.89	0.04
	600	30	3,619.58	224.00	0.4	0.62	-0.10	0.04
S8	200	20	3,767.39	820.00	0.64	1.02	-3.34	0.14
	200	25	4,719.91	966.00	0.88	1.35	-3.45	0.17
	400	20	3,996.51	780.00	0.57	0.74	-3.16	0.14
	400	25	3,900.17	860.00	0.84	0.88	-3.18	0.15
	600	25	4,541.08	898.00	1.13	0.87	-3.17	0.15
	600	30	4,290.05	938.00	1.18	0.86	-3.19	0.16

As the movable surface concept induces both a small vertical acceleration and chassis vertical displacement (lower than 1 mm for almost all scenarios), it allows multiple SRE to be implemented consecutively in the pavement, without or with a very small distance between each other, enabling vehicle speed reduction to be maximised in a very small distance.

4.4.3 Potential contribution to road safety

A study by Donario and Santos (2012), sponsored by the *Portuguese Authority for Road Safety*, assessed the economic and social cost of road accidents nationwide. From this study several important conclusions were drawn, in particular the following numbers:

- Average annual economic and social cost of road accidents: about 2,500 million Euros, representing 1.54% (on average) of Portuguese GDP in 2010;
- Average annual economic and social cost for each accident with victims: 60,000 Euros;
- Average annual economic and social cost for each accident with fatalities: 735,000 Euros;
- Average annual economic and social cost for each accident with serious injuries: 121,000 Euros;
- Average annual economic and social cost for each accident with minor injuries: 32,000 Euros;
- Average annual economic and social cost per victim: 44,000 Euros;
- Average annual economic and social cost per fatality: 664,000 Euros;
- Average annual economic and social cost per seriously injured victim: 96,000 Euros;
- Average annual economic and social cost per slightly injured victim: 23,000 Euros.

These numbers are in accordance with the numbers presented by the WHO (2010, 2013).

Considering the facts presented in the introduction to this work, it has been established that the most affected groups in urban areas are vulnerable road users, accounting for 43% of road fatalities in the European region, with 27% being pedestrians (WHO, 2013), and given that the WHO itself points out that speed is the main cause for accidents with vulnerable road users, reducing speed in urban areas is extremely important to directly reduce the number of fatalities in road accidents, especially involving vulnerable road users.

As studied by Seco *et al.* (2008), the probability of an accident involving a pedestrian being fatal considerably decreases with the reduction of impact speed, the probability being 80% if the speed is 65 km/h, 45% if the speed is 50 km/h and lower than 10% if the speed is 30 km/h.

Since the vast majority of pedestrian accidents occur on pedestrian crossings (Holzmann, 2008), it is of great importance to effectively reduce vehicle speed on the approach to pedestrian crossings, without the problems presented by typical SRE, as discussed in this research work.

The proposed device with movable surface, using the *Ramp* surface profile with the dimensions of 200x25 mm (width x maximum height), with a maximum displacement of 25 mm, which for the studied vehicle at a 50 km/h speed induces a vertical acceleration in the vehicle chassis of 0.49 m/s^2 , considered to be a little uncomfortable, results in a vehicle speed reduction of 0.67 km/h per metre.

Table 4.5 presents a case study for speed reduction based on the vehicle initial speed and the total length of consecutive SRE installed in the pavement, with the exit speed and the obtained speed reduction presented as outputs.

Table 4.5- Speed reduction case study.

Initial speed (km/h)	SRE total length (m)	Exit speed (km/h)	v_{red} (km/h)	Speed reduction percentage
60	20	47.0	13.0	21.7%
	30	44.4	15.6	26.0%
	40	38.7	21.3	35.5%
	50	35.9	24.1	40.2%
50	20	45.0	5.0	10.0%
	30	40.9	9.1	18.3%
	40	38.2	11.8	23.7%
	50	35.4	14.6	29.2%
40	20	34.5	5.5	13.7%
	30	31.6	8.4	21.0%
	40	28.2	11.8	29.4%
	50	24.9	15.1	37.8%

From Table 4.5 it is possible to conclude that for an entry speed of 50 km/h, with 50 metres of the proposed SRE installed consecutively in the pavement, vehicle speed can be reduced by approximately 14.6 km/h, or about 29.2% related to initial speed, slowing

down the vehicle from 50 km/h to 35.4 km/h. As studied by Holzmann (2008), a reduction from 50 km/h to 30 km/h can reduce the probability of fatality in an accident from 45% (medium-low) to 10% (very low), which is highly significant.

From this analysis, with 50 metres of the proposed SRE applied on the pavement, on each side of the road, before a pedestrian crossing, it is possible to reduce vehicle speed by almost 40% (depending on the initial speed), reducing very significantly the probability of a fatal accident.

Based on the values presented by Donario and Santos (2012), for each fatality avoided, 664,000 Euros could be saved; for each seriously injured victim avoided 96,000 Euros could be saved and for each slightly injured victim, 23,000 Euros could be saved. Considering these values, and based on WHO (2010, 2013) estimates, it may be concluded that the estimated total cost of pedestrian accidents is approximately 675 million Euros, just in Portugal. So, with a 100,000 Euro investment for each critical pedestrian crossing, for every victim avoided there would an immediate return on the investment.

4.5 Experimental Validation

4.5.1 Introduction

Following the computational simulations, a prototype of the system was designed, simulated and constructed for experimentally evaluating the results. This prototype, besides the mechanical system, also includes sensors and instrumentation components to measure different variables, a data logger to collect these data and software to receive data and generate plots. The prototype was then implemented in a controlled environment and different scenarios were tested. A new set of computational simulations was performed, for the same scenarios as those tested experimentally, so that both results could be directly compared. The analysis of the results is also presented in this section.

4.5.2 Prototype

The design of the experimental prototype was based on the CTS mechanical system presented in Figure 4.3, but using two CTS systems, as presented in Figure 4.6. Considering the usage of low weight and low cost materials, especially plastic, as the core material for the components of the prototype, a multiple crank system was adopted. The components were designed so that the prototype can support the passage of a heavy vehicle with 10 tons per axle, with a safety factor of 1.5. Also, a linear guiding system was used to guarantee a uniform displacement of the system surface, with a linear guide and a linear bearing in each corner of the prototype. The values considered for the prototype components, specially the crank length (l_{cr}), its initial position (θ_{cr-in}), the maximum displacement of the surface (x_{h-max}) and the spring stiffness (K_h), were the same as presented in previous sections.

The prototype design is presented in Figure 4.7, without sensors, instrumentation components and the surface with a specific profile. Three SPs (*Crest*, *Ramp* and *S profile*) were designed and built for the experimental tests. The external dimensions of the prototype are 0.8 x 0.3 m, having a total area of 0.24 m². Its total height is 0.11 m. The external dimensions of the surface are 0.775 x 0.275 m, giving a total area of 0.213 m².

Besides the mechanical system, sensors and instrumentation components were also included in the prototype, namely two Tedeo-Huntleigh load cells, model 1250 (Vishay, 2017), with a 1,000 kg maximum load each, to measure the force received by the surface of the prototype and transferred to the mechanical system (F_{SMI}), applied between the surface with a specific profile and the mechanical system surface; and two linear encoders Variohm - IPL Linear Position Sensor, model IPL-0025-103-3%-ST (Farnell, 2017) to measure the linear displacement of the prototype surface (x_h) and the linear displacement of the mechanical system (x_{SM}), applied in a fixed and a moving part of the systems to measure the displacements.

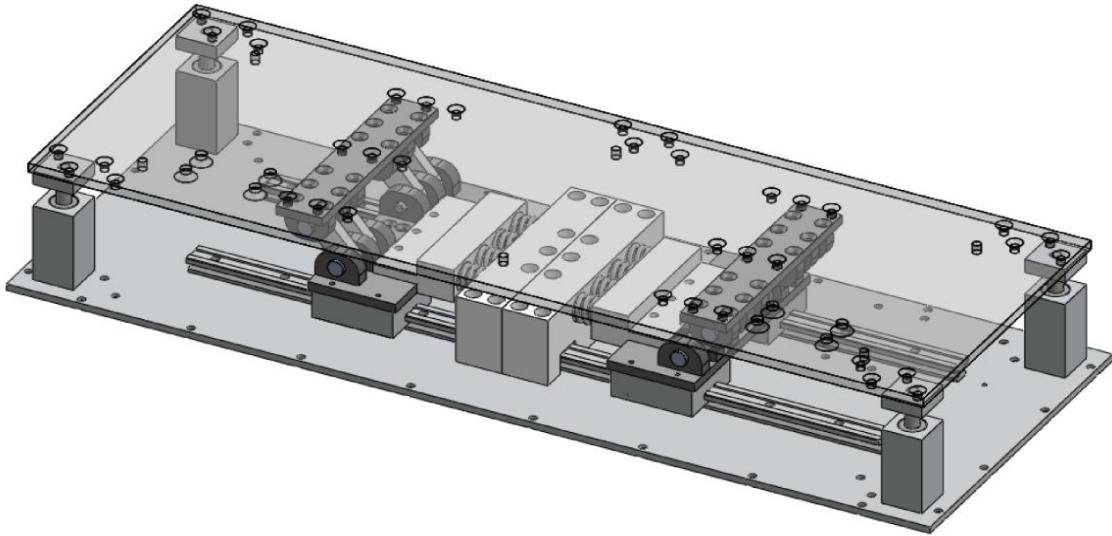


Figure 4.7- Prototype design without sensors and instrumentation components.

These sensors were connected to a *Data Logger* from National Instruments, model NI USB-6003 (National Instruments, 2017), with an intermediate instrumentation system to adapt the sensors signals to the data logger requirements. The *Data Logger* was connected to a laptop via USB, transferring the acquired data with a frequency of 100 Hz, and software was developed using LabVIEW[®] to read the received data and convert it into plots, as well as store these data in readable files.

To convert the measured loads from the load cells into a received force, the values from both load cells were added and multiplied for 9.81 m/s^2 , and to determine the load delivered by the slider to the springs, Equation (4.7) was used. In this equation, to define the angle θ_{cr} , Equations (4.1-4) were used considering the displacements x_h and x_{cr} measured by the linear encoders. With these values, the energy harvested from the surface (E_h) was measured using Equation (4.18).

In Figure 4.8a the prototype is presented with the sensors and with the *Crest* surface profile, while Figure 4.8b shows the *Data Logger* and the instrumentation circuit.

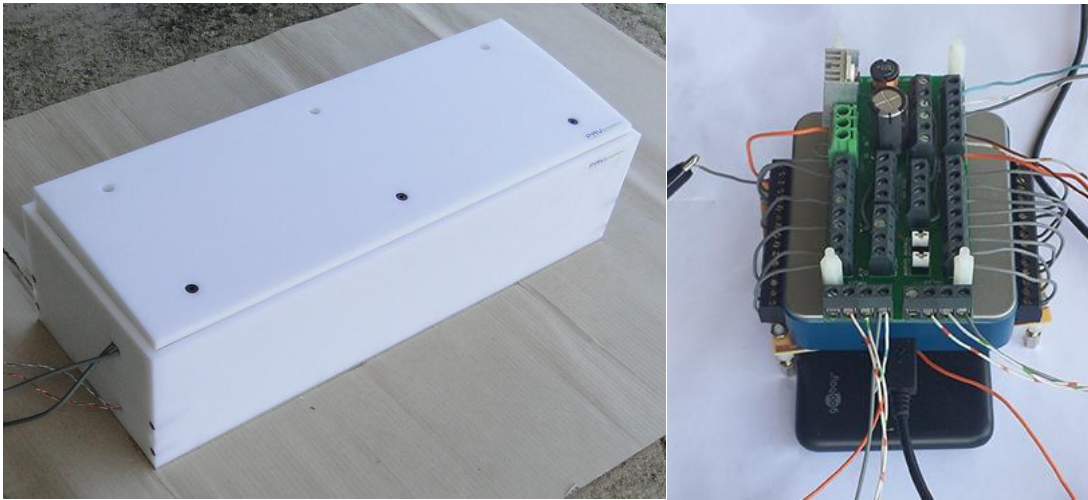


Figure 4.8- (a) Prototype system fully assembled with sensors, trimetric view; (b) data logger with instrumentation.

4.5.3 Test scenarios

The prototype was installed in a road pavement surface of a car parking space by opening a hole with the external dimensions of the prototype ($0.8 \times 0.3 \times 0.11 \text{ m}^3$), with the prototype surface at the external level of the road surface. Figure 4.9 shows the prototype implemented in the road pavement surface. Considering the working principle of the designed system, when the vehicle wheels start contact with the prototype surface, it will be at the pavement level, and when the wheel leaves the contact with the prototype surface it still continues at the road pavement level, avoiding the typical bump effect of speed bumps.

To perform multiple tests with the prototype and evaluate its performance under different conditions, different vehicles weighing 1,000 kg (VE_1) and 2,000 kg (VE_2), different prototype surface profiles as presented in previous sections (*Crest*, *Ramp* and *S profile*), different values for the spring stiffness of 200 kN/m (K_{h1}) and 400 kN/m (K_{h2}) and different vehicle speeds, of 20, 30, 40 and 50 km/h were considered. Table 4.6 presents the different scenarios for the prototype experiments.



Figure 4.9- Prototype installed in a road pavement.

Table 4.6- Test scenarios for the system prototype.

Vehicle weight (kg)	SP	Total spring stiffness (kN/m)	Vehicle speed (km/h)
VE ₁ =1,000	S8=Crest	K ₁ =200	10 20 30 40
		K ₂ =400	10 20 30 40
	S5=Ramp	K ₁ =200	10 20 30 40
		K ₂ =400	10 20 30 40
	S6=S profile	K ₁ =200	10 20 30 40
		K ₂ =400	10 20 30 40
VE ₂ =2,000	S8=Crest	K ₁ =200	10 20 30 40
		K ₂ =400	10 20 30 40
	S5=Ramp	K ₁ =200	10 20 30 40
		K ₂ =400	10 20 30 40
	S6=S profile	K ₁ =200	10 20 30 40
		K ₂ =400	10 20 30 40

4.5.4 Computational simulations

Using the RoadVISS software tool to perform the simulations for the new SRE proposed in this work and also to evaluate the impact of the vehicle characteristics in the system performance, two vehicles with the characteristics presented in Table 4.7 were considered, using the bicycle car model and the CPA. Also, different initial vehicle speeds (v_{ini}) were evaluated, from 20 km/h to 50 km/h, as this is the speed limit in urban areas.

Table 4.7- Fixed and initial values for the simulation variables.

	Variable name	Value (VE ₁)	Value (VE ₂)	Unit
Vehicle & motion	Vehicle class	Light		-
	Vehicle weight	1,000	2,000	(kg)
	Number of axles P1 wheels/axle	2 2		-
	Distance a1 a2	0.914 1.557	1.055 1.651	(m)
	Sprung-Unsprung %	90%-10%		-
	Drag coefficient	0.3	0.34	-
	Inertia moment	750	1,470	(kg.m ²)
	Lift coefficients (Front Rear)	0.17 0.12	0.21 0.15	-
	Motion Direction	Free rolling Forward		-
	Vehicle speed	20 30 40 50		(km/h)
	Vehicle acceleration	0		(m/s ²)
	Suspension & wheel	Suspension type (Front Rear)	Independent Independent	
Suspension stiffness (Front Rear)		20,000 15,000	25,000 18,000	(N/m)
Suspension damping (Front Rear)		1,500 1,700	1,700 1,900	(Ns/m)
Tyre type (Front Rear)		Radial Radial		-
Tyre stiffness (Front Rear)		140,000 140,000	160,000 160,000	(N/m)
Tyre pressure (Front Rear)		200 200	250 250	(kPa)
Tyre external diameter (Front Rear)		400 400	500 500	(mm)
Tyre width (Front Rear)		190 190	220 220	(mm)
Tyre tread width (Front Rear)	175 175	200 200	(mm)	

Considering the new solution proposed for a SRE with a movable surface, a set of simulations were performed for the different SPs presented in Figure 4.2, with a surface width (L_{max}) of 275 mm and a maximum height (h_{max}) of 20 mm, the maximum

displacement (x_{h-max}) being equivalent to the surface maximum height. The total spring stiffness was changed between simulations, with K_{h1} equal to 200,000 N/m and K_{h2} equal to 400,000 N/m, and the surface material is recycled plastic with a rubber layer on top, with a total mass of 18 kg. The values for l_{cr} and θ_{cr-in} are, respectively, 0.04 m and 0.848 rad (or 48.6°). The simulation results for VE_1 and VE_2 are presented in Tables 4.8 and 4.9, respectively, for the maximum value of the force transmitted by the surface (F_{SMI}), the energy harvested by the surface during the vehicle front wheel actuation ($E_{Ha FW}$), rear wheel actuation ($E_{Ha RW}$), and the total energy harvested by the surface (E_{Ha}).

Table 4.8- Simulation results of the new SRE with movable surface for VE_1 .

SP	K_h (kN/m)	v_{ini} (km/h)	F_{SMI} (N)	$E_{Ha FW}$ (J)	$E_{Ha RW}$ (J)	E_{Ha} (J)		
S8	200	20	3,426.3	33.8	22.4	56.2		
		30	2,640.1	46.9	30.3	77.3		
		40	3,379.1	54.9	35.1	90.0		
		50	3,956.2	57.7	36.0	93.7		
		20	3,614.8	23.6	28.9	52.5		
	400	30	3,076.4	34.8	25.8	60.5		
		40	3,527.5	46.0	30.7	76.7		
		50	3,722.4	50.0	31.5	81.5		
		S5	200	20	3,326.6	31.8	17.3	49.1
				30	2,269.9	43.1	25.8	68.9
40	2,890.1			47.8	29.6	77.4		
50	3,137.4			52.1	30.6	82.7		
400	20			3,834.0	21.2	20.9	42.1	
	30	2,134.9	27.8	17.3	45.1			
	40	3,027.5	36.7	21.2	57.9			
	50	3,327.4	40.3	23.5	63.8			
	S6	200	20	4,350.4	44.9	25.0	69.9	
30			3,398.4	48.7	32.4	81.1		
40			3,590.1	54.8	36.6	91.4		
50			3,942.8	58.1	36.7	94.8		
400			20	4,765.2	38.2	18.0	56.2	
		30	4,331.2	31.4	18.4	49.8		
		40	4,126.5	42.1	26.6	68.7		
		50	4,311.7	45.9	29.5	75.4		

Table 4.9- Simulation results of the new SRE with movable surface for VE_2 .

SP	K_h (kN/m)	v_{ini} (km/h)	F_{SM1} (N)	E_{Ha} FW (J)	E_{Ha} RW (J)	E_{Ha} (J)
S8	200	20	5,024.2	53.1	40.1	93.2
		30	4,540.2	56.9	51.5	108.4
		40	3,878.5	69.1	62.0	131.1
		50	4,492.6	81.5	66.5	148.0
		20	5,422.1	60.0	34.0	94.0
	400	30	5,049.8	42.4	37.9	80.3
		40	5,164.5	69.8	67.5	137.3
		50	5,036.1	82.8	68.4	151.2
		20	4,833.2	44.1	34.8	78.9
		30	4,133.0	53.8	46.1	99.9
S5	200	40	4,145.5	65.4	55.0	120.4
		50	4,550.5	75.4	58.7	134.1
		20	5,510.2	57.2	33.4	90.6
		30	4,978.1	39.7	30.1	69.8
		40	4,333.2	57.7	53.6	111.3
	400	50	5,153.8	71.1	61.8	132.9
		20	5,195.1	44.9	42.3	87.2
		30	4,483.7	51.7	49.2	100.9
		40	4,049.4	63.7	57.5	121.2
		50	4,504.2	68.8	63.3	132.1
S6	400	20	5,321.1	54.9	47.2	102.1
		30	4,930.2	37.0	31.2	68.2
		40	4,527.5	51.7	50.1	101.8
		50	4,607.8	63.2	59.5	122.7

Considering E_{Ha} as the most important variable to evaluate the performance of the system, Figure 4.10 presents the energy harvested for VE_1 , for the different surfaces and for different spring stiffness, while Figure 4.11 presents the results for the same scenarios but for VE_2 .

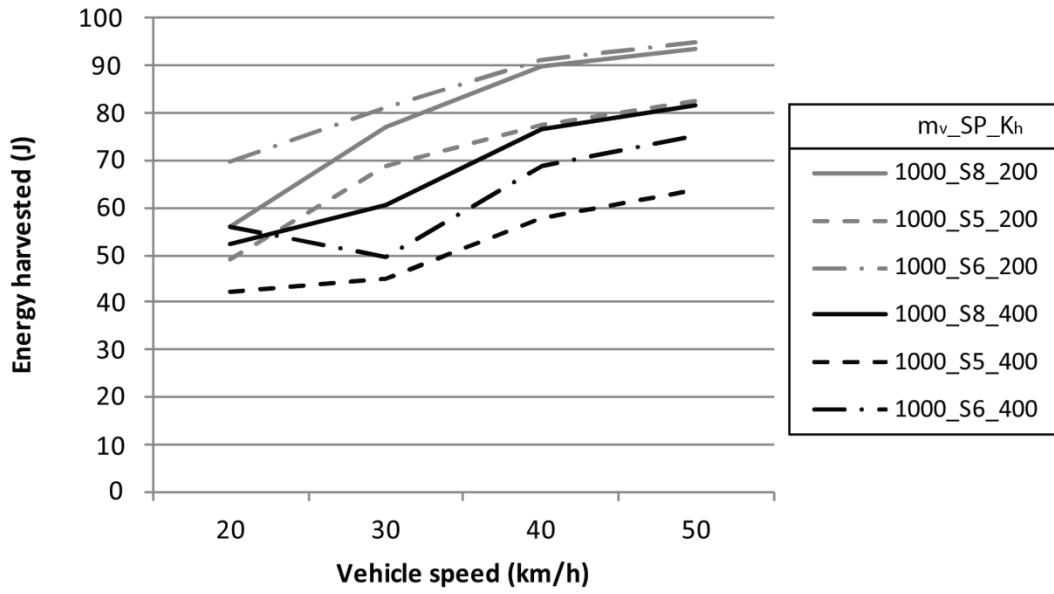


Figure 4.10- Simulation results of the total energy harvested for VE_1 .

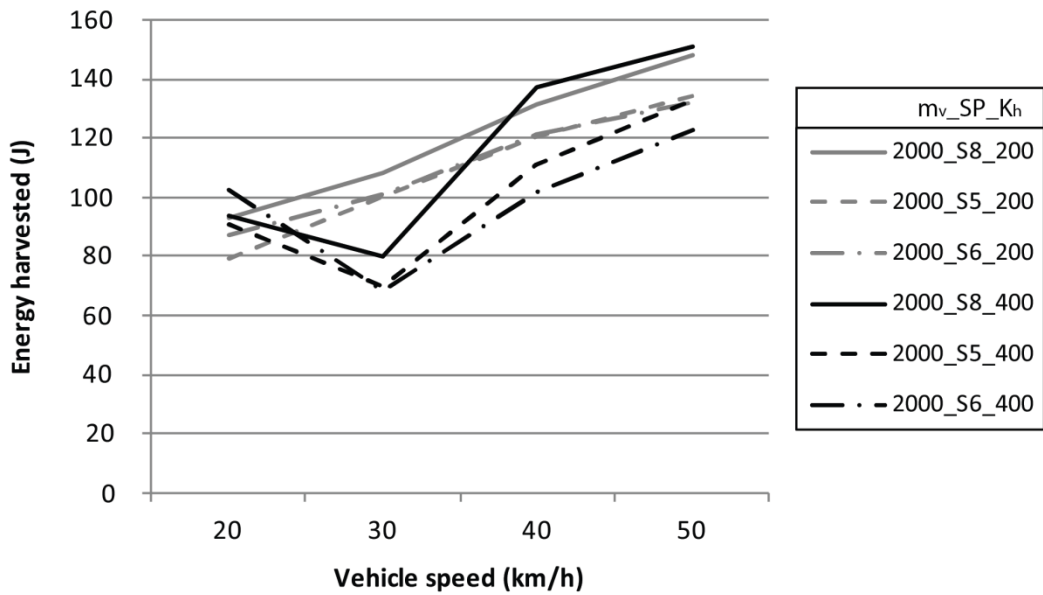


Figure 4.11- Simulation results of the total energy harvested for VE_2 .

From the results presented in Tables 4.8 and 4.9, as well as Figures 4.10 and 4.11, it is possible to compare the differences between each surface profile and SRE characteristics. Some conclusions may be drawn from the analysis of the results:

- Surface profile S8 has the best performance of energy extracted from both types of vehicles in almost all scenarios, with a few exceptions where surface profile S6 has a better performance. For all scenarios, S5 has the lowest values of energy harvested from vehicles. As the extracted energy is proportional to the vehicle speed reduction, surface profile S8 reduced the vehicle speed the most efficiently;
- In most scenarios, the energy harvested from the device's surface is higher the lower value of the spring stiffness;
- The lower value of the spring stiffness, the increase in the harvested energy is proportional to the increase in the vehicle speed for all the tested scenarios. However, for the highest spring stiffness value, the harvested energy is not proportional to the vehicle speed increase.

4.5.5 Experimental results

Both the VE_1 and VE_2 used in the experimental tests have the same characteristics as the vehicles considered in the computational simulations, as presented in Table 4.7, so that the experimental test results can be compared with the appropriate level of confidence.

Tables 4.10 and 4.11 show the results of the experimental tests with the prototype, for VE_1 and VE_2 , respectively. In these tables, the different variables presented in Table 4.6 are identified, and the values regarding the force received by the surface and transmitted to the mechanical system (F_{SMI}), the energy harvested by each vehicle wheel ($E_{Ha FW}$ and $E_{Ha RW}$), as well as the total energy harvested from both wheels from one side of the vehicle (E_{Ha}) are presented.

Considering the total E_{Ha} as the most important variable to evaluate the performance of the system, Figure 4.12 presents the energy harvested for VE_1 , for the different surfaces and the different spring stiffness, while Figure 4.13 presents the results for the same scenarios but for VE_2 .

Table 4.10- Prototype test results for VE_1 .

SP	K_h (kN/m)	v_{ini} (km/h)	F_{SM1} (N)	E_{Ha} FW (J)	E_{Ha} RW (J)	E_{Ha} (J)
S8	200	20	3,694.2	50.0	31.5	81.5
		30	3,339.1	60.1	40.8	100.9
		40	3,673.1	65.8	37.2	103.0
		50	3,791.5	69.6	38.8	108.4
	400	20	3,640.1	45.4	38.4	83.8
		30	4,012.1	53.8	30.6	84.4
		40	4,641.7	83.8	31.3	115.1
		50	4,230.2	65.4	28.5	93.9
S5	200	20	3,195.4	40.3	33.7	74.0
		30	3,350.0	48.1	32.5	80.6
		40	2,612.6	41.3	22.6	63.9
		50	2,562.9	43.7	21.7	65.4
	400	20	2,963.0	30.1	24.3	54.4
		30	3,033.1	29.1	20.9	49.9
		40	3,235.7	45.8	22.2	68.0
		50	2,938.4	45.2	32.2	77.4
S6	200	20	3,573.7	45.5	30.8	76.3
		30	2,901.5	46.3	27.0	73.3
		40	3,639.6	60.5	38.9	99.4
		50	2,699.2	36.2	17.2	53.3
	400	20	2,759.0	42.9	17.6	60.5
		30	3,137.4	38.5	24.3	62.8
		40	3,667.8	54.5	24.2	78.7
		50	3,730.5	65.2	31.9	97.2

Table 4.11- Prototype test results for VE_2 .

SP	K_h (kN/m)	v_{ini} (km/h)	F_{SM1} (N)	E_{Ha} FW (J)	E_{Ha} RW (J)	E_{Ha} (J)
S8	200	20	3,969.1	57.0	50.6	107.6
		30	3,661.5	44.9	48.3	93.1
		40	3,831.1	56.0	51.4	107.4
		50	3,791.2	58.0	43.7	101.7
	400	20	6,480.1	69.6	72.8	142.5
		30	4,539.7	77.0	84.0	161.0
		40	3,491.2	85.2	82.3	167.5
		50	5,526.0	102.5	96.9	199.4
S5	200	20	3,969.0	57.0	47.3	104.3
		30	3,909.0	52.0	47.3	99.3
		40	3,771.3	56.7	56.0	112.7
		50	3,972.9	63.5	51.8	115.3
	400	20	3,573.9	44.1	41.3	85.4
		30	3,934.1	67.2	63.8	131.0
		40	3,854.0	68.7	62.7	131.4
		50	3,470.2	50.3	50.3	100.7
S6	200	20	4,617.9	47.0	49.0	96.0
		30	3,353.3	46.3	54.0	100.3
		40	3,767.6	51.4	54.9	106.3
		50	4,410.7	71.2	61.3	132.4
	400	20	3,700.3	52.0	48.9	100.9
		30	3,559.9	59.8	56.0	115.9
		40	3,736.3	67.2	61.3	128.4
		50	3,838.8	66.5	55.5	122.0

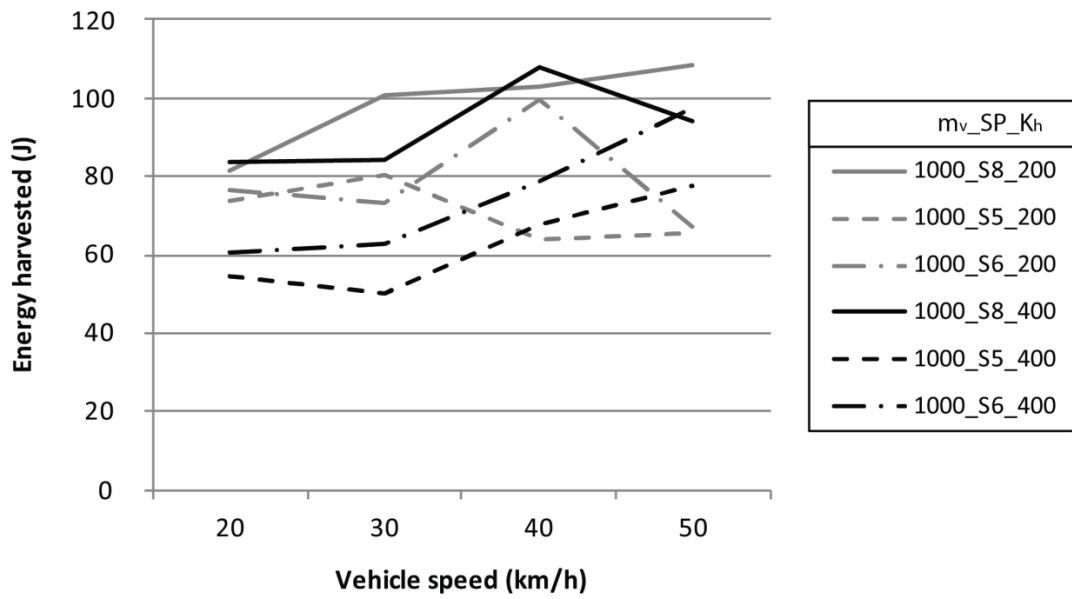


Figure 4.12- Experimental results of the total energy harvested for VE_1 .

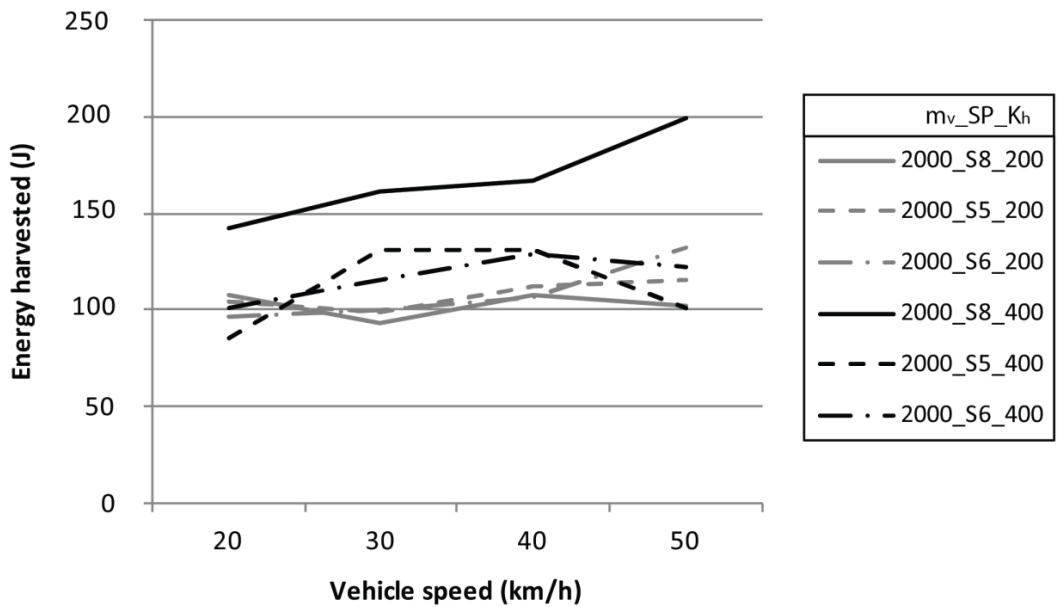


Figure 4.13- Experimental results of the total energy harvested for VE_2 .

Analyzing the results, the following conclusions can be drawn.

- For VE_1 and for the same surface profile, E_{Ha} is generally higher for a lower value of the spring stiffness, but for VE_2 the opposite happens. This allows us to conclude that for higher vehicle weights, higher values of spring stiffness must be used to optimize the energy harvested from vehicles.
- The surface profile S8 is the one which presents a higher value of E_{Ha} for most scenarios, which was also verified with the computational simulations, allowing us to conclude that this is the optimal surface profile regarding energy extraction and, consequently, speed reduction.
- An increase in the vehicle speed for VE_1 is proportional to an increase in the E_{Ha} only in half of the tested scenarios, while for VE_2 this proportionality was registered only for one scenario. This allows us to conclude that in the experimental tests the proportionality between the vehicle speed and the energy harvested was not fully validated.
- For similar surface profiles and spring stiffness, the energy harvested from the equipment increases with the vehicle weight, almost in direct proportion.

4.5.6 Discussion

Tables 4.12 and 4.13 present the difference between the simulations and the experimental results for similar tested scenarios using VE_1 and VE_2 , respectively.

Table 4.12- Difference between the simulations and experimental results for tested scenarios using VE_J .

SP	K_h (kN/m)	v_{ini} (km/h)	F_{SM1} (N)	E_{Ha} FW (J)	E_{Ha} RW (J)	E_{Ha} (J)
S8	200	20	7.8%	47.9%	40.9%	45.1%
		30	26.5%	28.1%	34.5%	30.6%
		40	8.7%	19.9%	6.0%	14.5%
		50	-4.2%	20.6%	7.8%	15.7%
	400	20	0.7%	92.4%	32.7%	59.6%
		30	30.4%	54.7%	18.6%	39.3%
		40	31.6%	82.1%	2.0%	50.0%
		50	13.6%	30.8%	-9.4%	15.3%
S5	200	20	-3.9%	26.6%	94.9%	50.7%
		30	47.6%	11.6%	26.1%	17.0%
		40	-9.6%	-13.7%	-23.7%	-17.5%
		50	-18.3%	-16.2%	-29.0%	-20.9%
	400	20	-22.7%	42.0%	16.4%	29.3%
		30	42.1%	4.5%	20.7%	10.7%
		40	6.9%	24.7%	4.7%	17.4%
		50	-11.7%	12.1%	36.8%	21.2%
S6	200	20	-17.9%	1.2%	23.2%	9.1%
		30	-14.6%	-4.9%	-16.8%	-9.6%
		40	1.4%	10.4%	6.4%	8.8%
		50	-31.5%	-37.8%	-53.2%	-43.7%
	400	20	-42.1%	12.2%	-2.2%	7.6%
		30	-27.6%	22.6%	32.0%	26.1%
		40	-11.1%	29.5%	-9.1%	14.6%
		50	-13.5%	42.1%	8.2%	28.9%
Average			-1.1%	22.0%	12.8%	17.7%

Table 4.13- Difference between the simulations and experimental results for tested scenarios using VE_2 .

SP	K_h (kN/m)	v_{ini} (km/h)	F_{SM1} (N)	E_{Ha} FW (J)	E_{Ha} RW (J)	E_{Ha} (J)
S8	200	20	-21.0%	7.3%	26.2%	15.4%
		30	-19.4%	-21.1%	-6.3%	-14.1%
		40	-1.2%	-18.9%	-17.1%	-18.1%
		50	-15.6%	-28.9%	-34.3%	-31.3%
	400	20	19.5%	16.1%	114.2%	51.6%
		30	-10.1%	81.7%	121.7%	100.5%
		40	-13.0%	22.1%	21.9%	22.0%
		50	9.7%	23.8%	41.6%	31.9%
S5	200	20	-17.9%	29.2%	36.0%	32.2%
		30	-5.4%	-3.3%	2.5%	-0.6%
		40	-9.0%	-13.3%	1.7%	-6.4%
		50	-12.7%	-15.7%	-11.8%	-14.0%
	400	20	-35.1%	-22.8%	23.6%	-5.7%
		30	-21.0%	69.2%	111.9%	87.6%
		40	-11.1%	19.0%	16.9%	18.0%
		50	-32.7%	-29.2%	-18.5%	-24.3%
S6	200	20	-11.1%	4.7%	15.8%	10.1%
		30	-25.2%	-10.5%	9.8%	-0.6%
		40	-7.0%	-19.3%	-4.5%	-12.3%
		50	-2.1%	3.4%	-3.2%	0.3%
	400	20	-30.5%	-5.3%	3.6%	-1.2%
		30	-27.8%	61.6%	79.6%	69.9%
		40	-17.5%	29.9%	22.3%	26.2%
		50	-16.7%	5.2%	-6.8%	-0.6%
Average			-13.9%	7.7%	22.8%	14.0%

From these Tables, some conclusions can be drawn.

- For VE_1 , the average difference of F_{SMI} is 1.1%, a very small value that allows us to conclude that, on average, the simulations are accurate. Analyzing individual values, the maximum difference was 42%, a considerable value, registered for lower vehicle speeds. For VE_2 , the average difference of F_{SMI} is 13.9%, a higher value than for VE_1 , but it is still a reasonable value that allows us to consider the simulations results with very positive precision.
- Regarding E_{Ha} and for VE_1 , the average difference is 17.7%, with higher values achieved experimentally when compared to the simulation results. A possible justification for this difference could be a higher vehicle tyre pressure or a higher spring stiffness from its suspension system when compared to the values considered in the simulations.
- Regarding E_{Ha} and for VE_2 , the average difference is 14.0%, which is a very positive result, allowing us to accept the simulation results. Analyzing individual simulations, there are some exceptions with a great difference between both results, but generally the precision was very good, with multiple results having a difference lower than 2%. As considered for VE_1 , a small difference in the pressure of the vehicle's tyres or a higher spring stiffness from its suspension system can justify the registered differences.

4.6 Summary and Conclusions

The social and economic costs resulting from high rates of fatalities and serious injuries due to road accidents increase every year and are currently a topic of very high relevance. It is of the utmost importance that the number of accidents on roads be reduced, so the WHO (2010, 2013), has identified six key areas for action. The first area and the one that can have the greatest impact is the effective reduction of traffic speed, especially in urban areas, where accident rates are very high, particularly affecting

vulnerable road users, especially pedestrians. There are already solutions on the market and traffic engineering techniques that contribute to this goal, but as accident rates continue to increase, more effective measures or solutions are needed.

By extracting kinetic energy from the vehicles motion it is possible to reduce its speed, with a system which is applied directly on the road pavement, making it impossible for the vehicles to avoid interacting with it. This solution is different from the existing SRE, as it has a one degree of freedom movable surface, with a specific profile and geometry that allows the impact on the vehicle to be minimised, keeping ride quality acceptable and without affecting vehicle passengers.

Different surface profiles and dimensions were evaluated through computational simulations, and the solution that presents the best relation between the energy harvested from the vehicle and the vertical acceleration induced on the vehicle chassis is the *Ramp* surface profile, which is 200 mm wide and a maximum of 25 mm height and has a maximum displacement of 25 mm. When compared to standard speed bumps, this solution can extract 81% more energy for the same width, with 87% lower impact on the vehicle, for the same device height.

Different surface profiles and spring stiffness were evaluated through experimental tests, and the solution that presents the best results for the energy harvested from the vehicle is the *Crest* surface profile, using a 200 kN/m spring stiffness for a 1,000 kg vehicle and a 400 kN/m spring stiffness for a 2,000 kg vehicle. The energy harvested from the equipment's surface is proportional to the energy lost by the vehicle, which is proportional to its speed reduction. So, the more energy the equipment is able to extract, the greater the reduction of vehicle speed.

From the analysis of results and the comparison between computational simulations and experimental results, it was possible to conclude that there is a small difference between the experimental results and the simulation results. On average, this is lower than 20% and can be explained due to differences in the pressure of the vehicles' tyres or in the stiffness of their suspension systems, when compared to the considered values in the simulations. So, one can conclude that the difference between the computational

simulations and the achieved results is acceptable, allowing to validate the software tool presented in Chapter 3.

The values presented are from half a vehicle, meaning that the total amount of energy extracted from a vehicle, if two prototypes are used side-by-side, would be twice the value presented here. Also, the prototype surface has a total width of 0.275 m, meaning that multiple devices can be implemented consecutively in the pavement, maximizing the energy extraction in a small amount of space.

For the conditions simulated, where a 50-metre section of pavement has the proposed SRE applied on its surface, it would be possible to reduce vehicle speed from 50 km/h to 35.4 km/h, from 60 km/h to 35.9 km/h, or from 40 km/h to 24.9 km/h, without any breaking action from the vehicle driver, and induce a very low vertical acceleration on vehicle chassis, keeping the ride quality at an acceptable level (a little uncomfortable). When compared to a typical speed bump, which induced an extremely uncomfortable ride quality on the vehicle passengers and has a smaller impact on direct speed reduction, it can be concluded that the proposed solution presents a better performance and effectiveness.

The main difference of the proposed solution when compared to existing equipment is that speed reduction is performed by harvesting energy from the vehicle without any action by its driver, instead of inducing a great discomfort on the vehicle occupants, forcing the vehicle driver to break.

4.7 References

Badennova (2016). <http://www.badennova.com/>. Accessed in July, 2016.

Blundell, M. and Harty, D. (2004). *Multibody Systems Approach to Vehicle Dynamics*. Elsevier Butterworth-Heinemann, Oxford, UK.

DGV (2004). *Technical Paper – Installation and Signalization of Speed reducer bumps (In Portuguese)*, pp. 1-18.

- Donario, A. and Santos, R. (2012). *Custo Económico e Social dos Acidentes de Viação em Portugal (In Portuguese)*. Ediuial. Lisboa, Portugal.
- Elvik, R., Vaa, T., Erke, A. and Sorensen, M. (2009). *The Handbook of Road Safety Measures*. Emerald, Bingley, UK.
- Ewing, R. and Brown, S. (2009). *US Traffic Calming Manual*. American Planning Association, Chicago, IL, USA.
- Farnell (2017). IPL Linear Position Sensor data sheet. <http://www.farnell.com/datasheets/1833199.pdf>. Accessed in January, 2017.
- Freitas, E., Machado, P., Santos, J. and Pereira, P. (2013). Planos de ação de redução do ruído: consideração do custo benefício de superfícies de baixo ruído e do impacto de medidas de gestão da velocidade (*In Portuguese*). In: *XVII Congreso Ibero-Latinoamericano del Asfalto-CILA*.
- Gifford, R. (2004). *Road Humps should be dug up: The Case Against*. Parliamentary Advisory Council for Transport Safety. London, UK.
- Gillespie, T. (1992). *Fundamentals of Vehicle Dynamics*. Society of Automotive Engineers, Warrendale, PA, USA.
- Holzmann, F. (2008). *Adaptive cooperation between driver and assistant system* (pp. 11-19). Springer Berlin Heidelberg, Berlin, Germany.
- Hongqiao Traffic (2016). <http://www.hongqiao.cc/english/index.asp>. Accessed in July, 2016.
- ISO (1997). *Mechanical vibration and shock - Evaluation of human response to whole-body vibration. Part I: General requirements*. ISO 2631-1, Geneva, Switzerland.
- Jazar, R. (2008). *Vehicle Dynamics: Theory and Application*. Springer, New York, NY, USA.
- Johnson, L. and Nedzesky, A. (2004). A comparative study of speed humps, speed slots and speed cushions. In *ITE Annual Meeting Compendium, Institute of Transportation Engineers (ITE)*, Washington, DC, USA.

- Kamienchick, Y. (2000). *Device for speed restriction of vehicles*. US Patent US6024510 A, Fev.
- Lecompte, D. (1982). *Removable Speed Reducer Bump*. Canada Patent CA1185475, Apr.
- Mandavi, S. (1990). *Vehicle speed bump device*. US Patent US4974991 A, Dec.
- National Instruments (2017). *Data logger NI USB-6003 data sheet*. <http://www.ni.com/pdf/manuals/374372a.pdf>. Accessed in January, 2017.
- Popp, K., Schiehlen, W., Kroger, M. and Panning, L. (2010). *Ground Vehicle Dynamics*. Springer, Berlin, Germany.
- Rajamani, R. (2011). *Vehicle Dynamics and Control*. Springer, New York, NY, USA.
- Seco, A., Gonçalves, J. and Costa, A. (2008). *Manual do planeamento de acessibilidades e transportes (In Portuguese)*. CCDRN, Porto, Portugal.
- Silva, J. (2010). *Modelação e Avaliação do Potencial de Desempenho das Lombas Redutoras de Velocidade (In Portuguese)*. University of Coimbra, Coimbra, Portugal.
- Sinclair, D. (1997). *Speed Bump*. US Design Patent USD387181, Dec.
- Szurgott, P., Kwasniewski, L. and Wekezer, J. (2009). *Dynamic interaction between heavy vehicles and speed bumps*. In *ECMS: Proceedings 23rd European Conference on Modelling and Simulation*, pp. 585-591.
- Thompson, C. (1996). *Retractable Speed Bump*. US Patent US5509753 A, Apr.
- TSS (Traffic Safety Store) (2016). <https://www.trafficsafetystore.com/>. Accessed in July, 2016.
- Uys, P., Els, P. and Thoresson, M. (2007). *Suspension settings for optimal ride comfort of off-road vehicles travelling on roads with different roughness and speeds*. *Journal of Terramechanics*, 44(2), 163-175.
- Vishay (2017). *Load cell data sheet*. <http://www.vishay.com/docs/12017/1250.pdf>. Accessed in January, 2017.

Welford, J. (1993). *Electronically controlled speed bump device*. US Patent US5267808 A, Dec.

Wong, J. (2001). *Theory of Ground Vehicles, 3rd Ed.* Wiley, New York, NY, USA.

WHO (2010). *European Status Report on Road Safety: Towards Safer Roads and Healthier Transport Choices*. World Health Organization, Geneva, Switzerland.

Available from:
http://www.euro.who.int/__data/assets/pdf_file/0015/43314/E92789.pdf?ua=1.

Accessed in May, 2016.

WHO (2013). *Global Status Report on Road Safety 2013: Supporting A Decade of Action*. World Health Organization, Geneva, Switzerland. Available from:

http://www.who.int/violence_injury_prevention/road_safety_status/2013/en/.

Accessed in May, 2016.

3M (2016). http://www.3m.com/3M/en_US/company-us/. Accessed in July, 2016.

Chapter 5

Road Pavement Energy Harvesting: a New Electromechanical Device to Convert Vehicles Mechanical Energy into Electrical Energy

5.1 Introduction

In Chapter 2 a state-of-the-art with the main technologies used to convert vehicle mechanical energy into electrical energy, to be implemented on road pavements, and which can be both micro and macro energy harvesting was presented. In these technologies, typical systems have the following components: a surface that receives energy from vehicle tyres and delivers energy to a transmission system; a system that transmits energy from the surface to an electrical generation unit; and an electrical unit that converts the mechanical energy into electrical energy, delivering it to an electrical application.

Piezoelectric systems are the simplest, as usually they receive the mechanical energy directly from the surface and convert it into electricity. However, these work on a micro energy harvesting scale and have a very small energy conversion efficiency and output.

Electromechanical systems transmit the energy received from the surface to electromagnetic generators, adapting the surface motion, which can be linear or rotational, into a similar or different motion, depending on the generator characteristics. These systems can work both on a micro or macro scale, having higher conversion efficiencies and energy outputs than piezoelectric systems, and are the most developed group of technologies in this field.

Hydraulic and pneumatic systems use the same principle as electromechanical systems, transmitting the energy received from the surface to electromagnetic generators. Typically, these systems work on a macro scale, allowing larger amounts of energy to be transferred. However, only a very small number of systems have been developed with this principle and none of them have presented viability, mainly due to the high costs of development and implementation.

In the last few years a considerable number of systems have been developed and tested on road pavements to convert vehicle mechanical energy into electrical energy, most of which have been validated in the laboratory environment, but none of them have obtained validation in a relevant environment, such as a public road with regular traffic actuating the system for a considerable amount of time. Also, for most of the existing technologies, no system modelling or computational simulations have been published that would allow energy harvesting, transmission and conversion efficiency to be analyzed, which would make it possible to determine their global efficiency and draw conclusions about their viability.

In this Chapter, different road pavement energy harvesting devices using electromechanical systems will be studied, modelled and simulated, to study and come to conclusions about the efficiency of its different components, meaning the most efficient solutions can be known. Also, a new electromechanical system will be proposed, to transmit the energy received by the RPEH device surface into an electromagnetic generator, which will also be modelled and simulated, to come to a conclusion about its efficiency.

The software tool presented in Chapter 3 will be used as the basis for the computational simulations, and an upgrade will be performed, to include the models of the different RPEH devices. Based on this, computational simulations will be performed, allowing to conclude about each system's efficiency. A prototype of the new proposed system will be presented and tested and the experimental results will allow to conclude about its performance as well as the software tool accuracy.

5.2 RPEH Electromechanical System Development

5.2.1 Introduction

To transfer the energy received on the RPEH surface to an electric generator, different systems can be used. From Chapter 2 it can be concluded that most existing RPEH devices are electromechanical and have a mechanical system to transfer the surface motion into an electromagnetic generator. Typical solutions use a rotational electromagnetic generator for both linear and rotational surface motions.

In this section, the existing solutions will initially be analyzed and modelled. Then, a new mechanical system for converting the linear motion of a RPEH surface into a rotational motion of an inertia wheel (IW) is presented and modelled. It is connected to an electromagnetic rotational generator. Finally, the equations that quantify the transmitted and delivered energy will be defined, as well as the efficiency of each process.

5.2.2 Existing systems

In Chapter 2, Table 2.1 summarizes the most relevant electromechanical systems according to the motion conversion principle, taking patents into account. The most common RPEH devices convert the linear or rotational motion of a surface into the rotational motion of an electromagnetic generator. Besides the patents presented in

Table 2.1, other studies have been performed both by companies and academia (e.g., Pirisi *et al.*, 2013; Todaria *et al.*, 2015; Duarte *et al.*, 2016), to harvest vehicle energy on road pavements and convert it into electrical energy.

To achieve a rotational motion output, two systems are mostly used: the rack and pinion (RAP) system; and the lever system.

The most basic mechanical system for converting the linear motion of a surface into a rotational motion of a shaft is the RAP system. To apply this system in a RPEH device, the rack usually is directly connected to the surface and the pinion is in contact with the rack and connected to a shaft which, in turn, actuates the electric generator. Commonly, the generator shaft is connected to an IW, and the pinion is connected to the shaft through an unidirectional bearing, also defined as a clutch bearing. This system includes a spring, which returns the surface to its initial position. The spring stiffness should be kept to a minimum to maximize the amount of force transmitted to the mechanical system, but strong enough to replace the surface quickly, so that when the rear wheel of the vehicle passes over the surface it is already on its initial position. The RAP system typically uses an IW connected to an electric generator, as presented in Figure 5.1. The forces distribution in the device surface are presented in Figure 5.2a, when the vehicle wheel interacts with the surface. In Figure 5.2b are presented the forces distribution for the upward motion of the device surface, after the vehicle wheel leaves the contact with the surface.

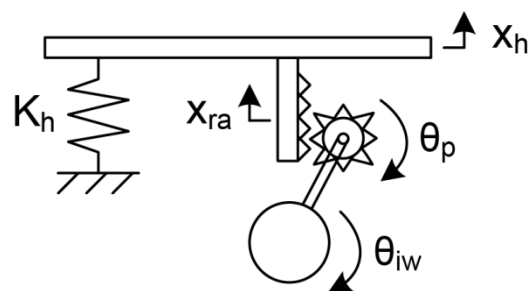


Figure 5.1- Typical RAP system connected to an IW.

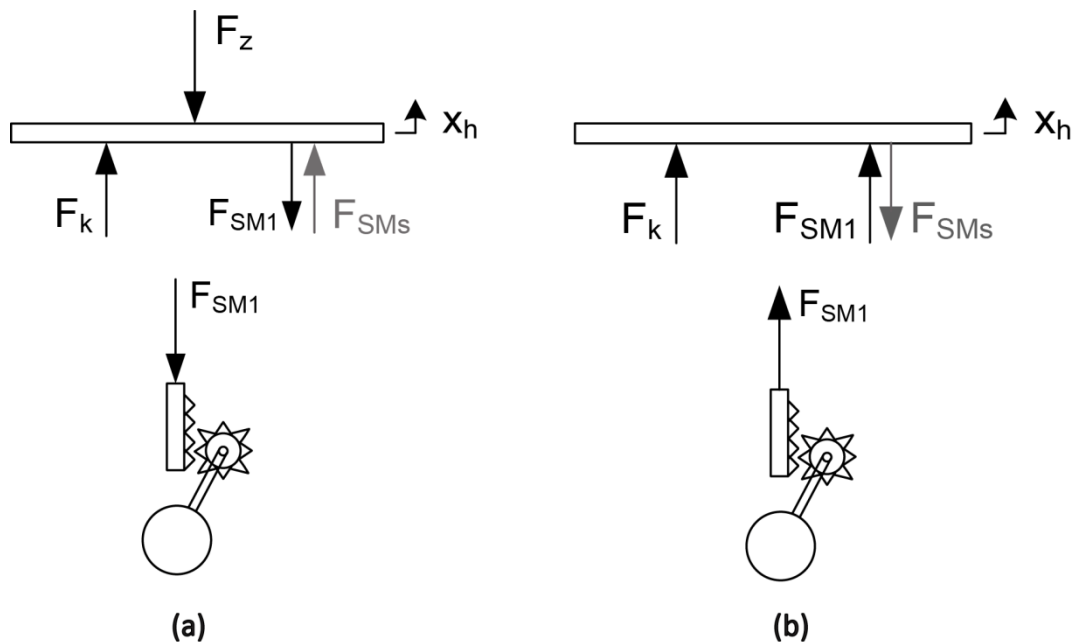


Figure 5.2- Forces distribution for the RAP system, (a) for the vehicle wheel - device surface interaction; and (b) for the upward motion of the device surface without vehicle wheel interaction.

Another mechanical system that is commonly used to convert the linear motion of a surface into a rotational motion of a shaft is the lever system. This system has the advantage of amplifying the motion of the surface, but the gain in motion represents a loss in force. So, the lever geometry must be carefully designed.

To apply this system in an energy harvesting device, a bar, directly connected to the surface, actuates a lever at a specific point, at a distance d_1 from its rotational centre. The lever has a rack connected to its extremity, at a distance d_2 from its rotational centre. The rack is in contact with a pinion, which is connected to a shaft. Commonly, the generator shaft is connected to an IW and the pinion it is connected to the shaft through a clutch bearing. This system includes a spring, which returns the surface to its initial position, similarly to the spring used in the RAP system. The lever system typically uses an IW connected to an electric generator, as presented in Figure 5.3. The forces distribution over this mechanism are presented in Figure 5.4, for the downward motion of the surface, when the vehicle wheel is interacting with the surface.

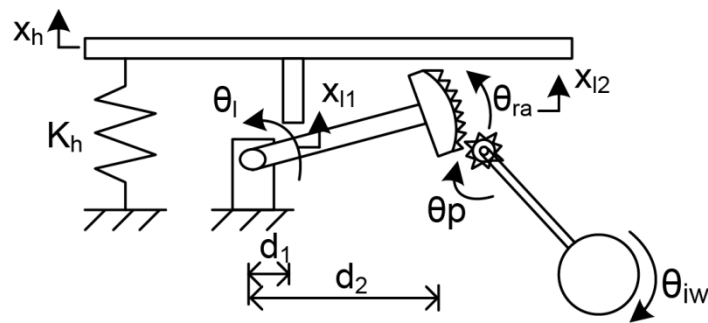


Figure 5.3- Lever system connected to an IW.

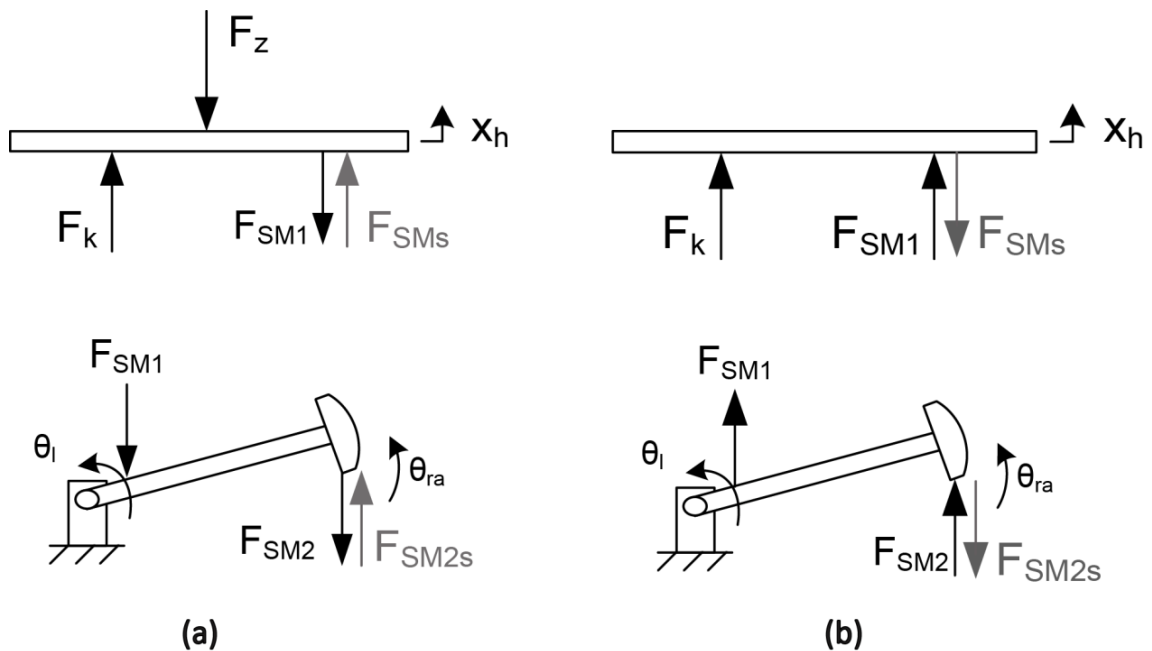


Figure 5.4- Forces distribution for the lever system, (a) for the vehicle wheel - device surface interaction; and (b) for the upward motion of the device surface without vehicle wheel interaction.

Tables 5.1 and 5.2 summarize all the equations that define both RAP systems and lever systems, respectively, in terms of kinematic, dynamic and forces analysis and for all motion scenarios: downward motion of the surface; surface stopped; and upward motion of the surface. The variable F_{SM1} is the force transmitted by the surface to the

mechanical system, while F_{SM1s} is the oppositional force of the mechanical system on the surface. The variable F_{SM2} is the force transmitted by the lever to the pinion, while F_{SM2s} is the oppositional force of the pinion on the lever.

As a clutch bearing is used, the motion equations are different for the different motion scenarios, as the IW keeps rotating after the pinion stops acting.

In some systems, gears are used to amplify the rotation of a second shaft. However, what is gained in rotation is lost in torque. To include these elements in the equations presented in Tables 5.1 and 5.2, the motion of the secondary shaft must be multiplied by the ration r_1/r_2 , with r_1 representing the radius of gear 1 and r_2 representing the radius of gear 2, but in the motion equations of the pinion and IW, both J_{iw} and J_{gen} must be multiplied by $(r_1/r_2)^2$.

Table 5.1- RAP system modelling.

Analysis	Motion		
	Downward	Stopped	Upward
Kinematic	$x_h = x_{ra}$ $x_{ra} = r_p \theta_p \Leftrightarrow \theta_p = \frac{x_{ra}}{r_p} = \frac{x_h}{r_p}$ $\theta_{iw} = \theta_p = \frac{x_h}{r_p}$	$x_h = x_{ra}$ $x_{ra} = r_p \theta_p \Leftrightarrow \theta_p = \frac{x_{ra}}{r_p} = \frac{x_h}{r_p}$	$x_h = x_{ra}$ $x_{ra} = r_p \theta_p \Leftrightarrow \theta_p = \frac{x_{ra}}{r_p} = \frac{x_h}{r_p}$
Dynamic	$\ddot{x}_h = \frac{1}{m_h} [F_{SMs} + K_h x_h - F_z]$ $\ddot{\theta}_p = \ddot{\theta}_{iw} = \frac{(F_{SM1} r_p) - ((b_{cb} + b_{gen}) \dot{\theta}_p) - ET}{J_p + J_{sh} + J_{iw} + J_{gen}}$	$\ddot{x}_h = \ddot{\theta}_p = 0$ $\ddot{\theta}_{iw} = \frac{-(b_{cb} + b_{gen}) \dot{\theta}_{iw} - ET}{J_{iw} + J_{gen}}$	$\ddot{x}_h = \frac{1}{m_h} [K_h x_h - F_{SMs}]$ $\ddot{\theta}_p = -\frac{(F_{SM1} r_p) - (b_{cb} \dot{\theta}_p)}{J_p + J_{sh}}$ $\ddot{\theta}_{iw} = \frac{-(b_{cb} + b_{gen}) \dot{\theta}_{iw} - ET}{J_{iw} + J_{gen}}$
Forces	$F_{SM1} = F_z - K_h x_h$ $F_{SMs} = \frac{(J_p + J_{sh} + J_{iw} + J_{gen}) \ddot{\theta}_p + ET}{r_p}$	$F_{SM1} = 0$ $F_{SMs} = 0$	$F_{SM1} = K_h x_h$ $F_{SMs} = \frac{(J_p + J_{sh}) \ddot{\theta}_p}{r_p}$

Table 5.2- Lever system modelling.

Analysis	Motion		
	Downward	Stopped	Upward
Kinematic	$x_h = x_{l1}$	$x_h = x_{l1}$	$x_h = x_{l1}$
	$x_{l2} = \frac{d_2}{d_1} x_{l1}$	$x_{l2} = \frac{d_2}{d_1} x_{l1}$	$x_{l2} = \frac{d_2}{d_1} x_{l1}$
	$x_{l2} = d_2 \sin(\theta_l) \Leftrightarrow \theta_l = \sin^{-1}\left(\frac{x_{l2}}{d_2}\right)$	$\theta_{ra} = \theta_l = \sin^{-1}\left(\frac{x_{l2}}{d_2}\right)$	$\theta_{ra} = \theta_l = \sin^{-1}\left(\frac{x_{l2}}{d_2}\right)$
	$\theta_r = \theta_l$	$\theta_{ra} = r_p \theta_p \Leftrightarrow \theta_p = \frac{\theta_{ra}}{r_p} \Leftrightarrow$	$\theta_{ra} = r_p \theta_p \Leftrightarrow \theta_p = \frac{\theta_{ra}}{r_p} \Leftrightarrow$
	$\theta_{iW} = \theta_p = \frac{\sin^{-1}\left(\frac{x_h}{d_1}\right)}{r_p}$	$\Leftrightarrow \theta_p = \frac{\sin^{-1}\left(\frac{x_h}{d_1}\right)}{r_p}$	$\Leftrightarrow \theta_p = \frac{\sin^{-1}\left(\frac{x_h}{d_1}\right)}{r_p}$
Dynamic	$\ddot{x}_h = \frac{1}{m_h} [F_{SM1} + K_h x_h - F_z]$	$\ddot{x}_h = \ddot{\theta}_l = \ddot{\theta}_p = 0$	$\ddot{x}_h = \frac{1}{m_h} [K_h x_h - F_{SMs}]$
	$\ddot{\theta}_l = \frac{1}{J_l + J_{ra}} [F_{SM1} d_1 - F_{SM2s} d_2]$	$\ddot{\theta}_{iW} = \frac{-(b_{cb} + b_{gen}) \dot{\theta}_{iW} - ET}{J_{iW} + J_{gen}}$	$\ddot{\theta}_l = \frac{1}{J_l + J_{ra}} [F_{SM1} d_1 - F_{SM2s} d_2]$
	$\ddot{\theta}_p = \frac{F_{SM2} r_p - (b_{cb} + b_{gen}) \dot{\theta}_p - ET}{J_p + J_{sh} + J_{iW} + J_{gen}}$		$\ddot{\theta}_p = \frac{F_{SM2} r_p - b_{cb} \dot{\theta}_p}{J_p + J_{sh}}$
	$\ddot{\theta}_{iW} = \ddot{\theta}_p$		$\ddot{\theta}_{iW} = \frac{-(b_{cb} + b_{gen}) \dot{\theta}_{iW} - ET}{J_{iW} + J_{gen}}$
Forces	$F_{SM1} = F_z - K_h x_h$	$F_{SM1} = F_{SM2} = 0$	$F_{SM1} = K_h x_h$
	$F_{SM2} = \frac{d_1}{d_2} F_{SM1}$	$F_{SM2s} = F_{SMs} = 0$	$F_{SM2} = \frac{d_1}{d_2} F_{SM1}$
	$F_{SM2s} = \frac{(J_p + J_{sh} + J_{iW} + J_{gen}) \ddot{\theta}_p + ET}{r_p}$		$F_{SM2s} = \frac{(J_p + J_{sh}) \ddot{\theta}_p}{r_p}$
	$F_{SMs} = \frac{d_2}{d_1} F_{SM2s}$		$F_{SMs} = \frac{d_2}{d_1} F_{SM2s}$

5.2.3 New mechanical system

To maximize the rotation of the generator shaft the maximum amount of force should be transmitted from the surface to the shaft, with the maximum possible displacement. In the RAP system, the force transmitted is equal to the force received on the surface, with only the force absorbed by the spring being discounted. The shaft's angular displacement is similar to the surface linear displacement, divided only by the pinion

radius. In the lever system, the surface motion is multiplied, but the force is reduced by the same proportion, considerably reducing the torque applied on the generator shaft.

A more efficient solution would combine a maximization of both the transmitted force and shaft rotation, with priority on increasing the transmitted force. To achieve this goal, a system using a crank connected from the surface to a slider is proposed, as presented in Figure 5.5. This is called a crank to slider (CTS) mechanical system.

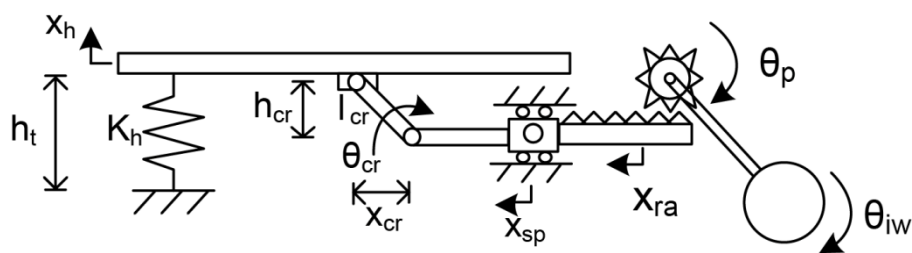


Figure 5.5- Crank to slider system connected to a RAP system and an IW.

This system has the following working principle: the surface has a linear displacement, actuating the crank with a rotational motion, which depends on its length and initial angle; the crank, in turn, will actuate the slider with a translational motion, which is directly connected to a rack; this will actuate a pinion with a rotational motion which, in turn, is connected to an IW and the electric generator shaft. The pinion is connected to the shaft through a clutch bearing. This system includes a spring, which returns the surface to its initial position and has a similar function to the spring used in the lever or RAP systems.

Table 5.3 summarizes all the equations that define this system in terms of kinematic, dynamic and forces analysis and for all motion scenarios: downward motion of the surface; surface stopped; and upward motion of the surface. F_{SM1} is the force transmitted by the surface on the mechanical system, while F_{SM1s} is the oppositional force of the mechanical system on the surface. F_{SM2} is the force transmitted by the crank to the slider piston, while F_{SM2s} is the oppositional force of the slider piston on the

crank. The forces distribution over the mechanism are presented in Figure 5.6a for the downward motion of the surface and Figure 5.6b for the upward motion of the surface.

Considering the relation between the force received in the device' surface (F_{SM1}) and the force delivered by the crank to the rack (F_{SM2}), as well as the vertical displacement of the surface (x_h) and the horizontal displacement of the rack (x_{sp}), during the surface downward motion the mechanism amplifies the force F_{SM2} (in relation to F_{SM1}) and decreases the displacement x_{sp} (in relation to x_h). The relation between the force increase and the displacement decrease is not direct and depends on the crank angle, as shown by the equations presented in Table 5.3.

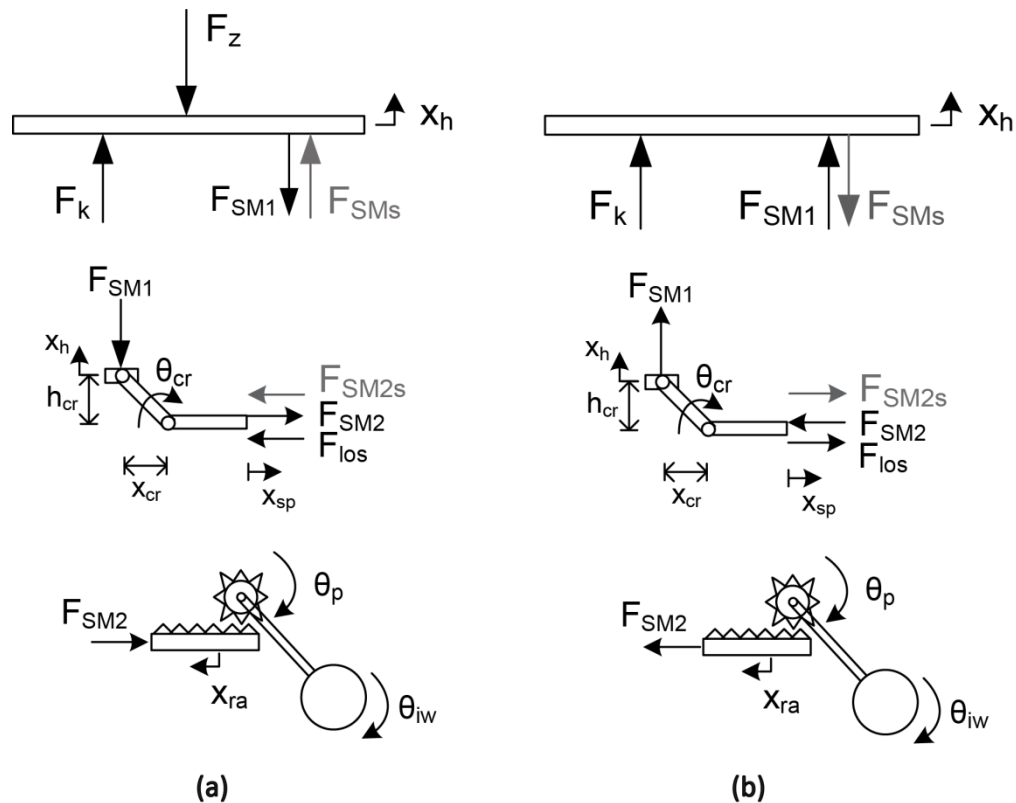


Figure 5.6- Forces distribution for the CTS system, (a) for the vehicle wheel - device surface interaction; and (b) for the upward motion of the device surface without vehicle wheel interaction.

Table 5.3- CTS system modelling using a RAP and an IW.

Analysis	Motion		
	Downward	Stopped	Upward
Kinematic	$x_{cr} = l_{cr} \cos\theta_{cr}$		
	$\theta_{cr} = \sin^{-1}\left(\frac{h_{cr}}{l_{cr}}\right)$		
	$x_{sp} = x_{sp-in} - x_{cr}$	$x_{cr} = l_{cr} \cos\theta_{cr}$	$x_{cr} = l_{cr} \cos\theta_{cr}$
	$h_{cr} = h_{cr-in} + x_h$	$\theta_{cr} = \sin^{-1}\left(\frac{h_{cr}}{l_{cr}}\right)$	$\theta_{cr} = \sin^{-1}\left(\frac{h_{cr}}{l_{cr}}\right)$
	$x_r = x_{sp}$	$x_{sp} = x_{sp-in} - x_{cr}$	$x_{sp} = x_{sp-in} - x_{cr}$
	$x_{ra} = r_p \theta_p \Leftrightarrow \theta_p = \frac{x_{ra}}{r_p}$	$h_{cr} = h_{cr-in} + x_h$	$h_{cr} = h_{cr-in} + x_h$
	$x_r = x_{sp}$	$x_r = x_{sp}$	
	$\theta_{iw} = \theta_p$		
	$\theta_{iw} = \frac{x_{sp}}{r_p} =$ $= \frac{x_{sp-in} - l_{cr} \cos\left(\sin^{-1}\left(\frac{h_{cr-in} + x_h}{l_{cr}}\right)\right)}{r_p}$	$x_{ra} = r_p \theta_p \Leftrightarrow \theta_p = \frac{x_{ra}}{r_p}$	$x_{ra} = r_p \theta_p \Leftrightarrow \theta_p = \frac{x_{ra}}{r_p}$
Dynamic	$\ddot{x}_h = \frac{1}{m_h} [F_{SMs} + K_h x_h - F_v]$		$\ddot{x}_h = \frac{1}{m_h} [K_h x_h - F_{SMs}]$
	$\ddot{x}_{sp} = \frac{1}{m_{sp}} [F_{SM2} - F_{SM2s} - F_{los}]$	$\ddot{x}_h = \ddot{x}_{sp} = \ddot{\theta}_p = 0$	$\ddot{x}_{sp} = \frac{1}{m_{sp}} [F_{SM2} - F_{SM2s} + F_{los}]$
	$\ddot{x}_r = \ddot{x}_{sp}$	$\ddot{\theta}_{iw} = \frac{-(b_{cb} + b_{gen}) \dot{\theta}_{iw} - ET}{J_{iw} + J_{gen}}$	$\ddot{\theta}_p = -\frac{F_{SM2} r_p - b_{cb} \dot{\theta}_p}{J_p + J_{sh}}$
	$\ddot{\theta}_p = \ddot{\theta}_{iw} =$ $= \frac{F_{SM2} r_p - (b_{cb} + b_{gen}) \dot{\theta}_p - ET}{J_p + J_{sh} + J_{iw} + J_{gen}}$		$\ddot{\theta}_{iw} = \frac{-(b_{cb} + b_{gen}) \dot{\theta}_{iw} - ET}{J_{iw} + J_{gen}}$
Forces	$F_{SM1} = F_v - K_h x_h$		$F_{SM1} = -K_h x_h$
	$F_{SM2} = \frac{F_{SM1}}{\tan(\theta_{cr})} - F_{los}$	$F_{SM1} = F_{SM2} = 0$	$F_{SM2} = \frac{F_{SM1}}{\tan\theta_{cr}} + F_{los}$
	$F_{SM2s} = \frac{(J_p + J_s + J_{iw} + J_{gen}) \ddot{\theta}_p + ET}{r_p}$	$F_{SMs} = F_{SM2s} = 0$	$F_{SM2s} = \frac{(J_p + J_{sh}) \ddot{\theta}_p}{r_p}$
	$F_{SMs} = F_{SM2s} \tan\theta_{cr}$		$F_{SMs} = F_{SM2s} \tan\theta_{cr}$

5.2.4 Energetic analysis

When the output motion of the mechanical system is linear, as in the CTS system, the energy transmitted by the piston is defined by Equation (5.1). When the output motion is rotational, as in the RAP or the lever system, the energy transmitted by the pinion is

defined by Equation (5.2). The energy delivered by the IW to the electric generator is defined by Equation (5.3).

$$\partial E_{Tr} = F_{SM2} \partial x_{sp} \quad (5.1)$$

$$E_{Tr} = \frac{1}{2} J_p \dot{\theta}_p^2 \quad (5.2)$$

$$E_{De} = \frac{1}{2} J_{iw} \dot{\theta}_{iw}^2 \quad (5.3)$$

The efficiency of the energy transmission system is defined by Equation (5.4), relating the transmitted energy with the energy harvested by the RPEH surface. The efficiency of the energy delivering system is defined by Equation (5.5), relating the energy delivered by the IW with the energy transmitted by the mechanical system.

$$\eta_{Tr} = \frac{E_{Tr}}{E_{Ha}} \quad (5.4)$$

$$\eta_{De} = \frac{E_{De}}{E_{Tr}} \quad (5.5)$$

5.3 Electrical System

5.3.1 Introduction

To convert the mechanical energy delivered by a mechanical system into electrical energy, RPEH devices can use both permanent-magnet direct-current (DC) electric generators or permanent-magnet alternating-current (AC) synchronous generators. Power electronics are then used to adapt the generated current to the electric load, depending on whether it consumes DC or AC power.

In order to simplify the physical modelling of the system, the computational simulations and the experimental tests for an RPEH device under development, a DC generator connected to a DC load is used.

In this section a permanent magnet DC generator will be presented and modelled, as well as a DC load. Simple power electronics are used only to adapt the generated

current to the electric load. An energetic analysis is performed to quantify both the generated and consumed energy, as well as the energy conversion and consumption efficiencies.

5.3.2 Electrical generator

The most basic electrical circuit to implement in RPEH devices is a purely DC circuit, with a DC electric generator, a DC purely resistive electric load and a diode between both, or a diode bridge in some circuits. Such a circuit is presented in Figure 5.7.

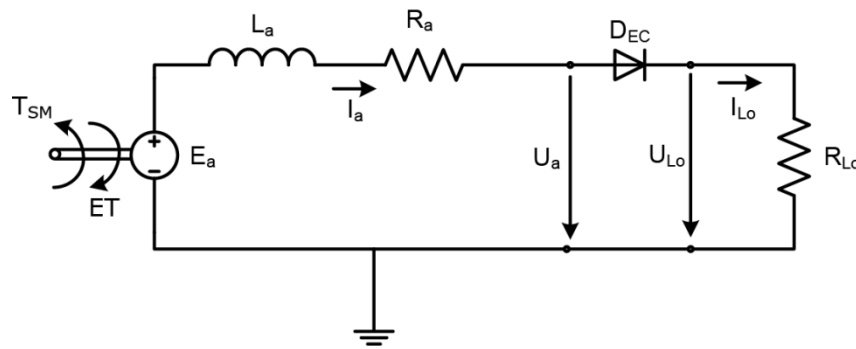


Figure 5.7- Purely DC electric circuit with a DC electric generator and a resistive load.

Both permanent-magnet DC generator and resistive load models were developed according to the main electric machine references, i.e. Chapman (2004), Murthy (2008) and Lyshevski (2008).

The mechanical system torque (T_{SM}) actuates the generator shaft, with a rotational speed, already defined by the IW speed ($\dot{\theta}_{iw}$), resulting in the development of an electromagnetic force (E_a), which represents the generator armature induced voltage.

Equation (5.6) allows E_a to be determined in relation to the generator shaft rotational speed, multiplying it by the generator constant (k_a). Equation (5.7) defines the generated voltage (U_a) in relation to the armature voltage (E_a), armature resistance (R_a) and the armature current (I_a). To determine the current produced in the armature windings,

Equation (5.8) must be used, where the armature current (I_a) is calculated in relation to the armature inductance (L_a), the armature resistance (R_a), the circuit resistive load (R_{Lo}), the generator constant (k_a), and the rotor angular speed ($\dot{\theta}_{iw}$). The electric torque (ET) produced by the generator, which opposes to the mechanical system motion, is determined by Equation (5.9).

$$E_a = k_a \dot{\theta}_{iw} \quad (5.6)$$

$$U_a = E_a - R_a I_a \quad (5.7)$$

$$\frac{dI_a}{dt} = -\left(\frac{R_a + R_{Lo}}{L_a}\right) I_a + \left(\frac{k_a}{L_a}\right) \dot{\theta}_{iw} = \left(\frac{1}{L_a}\right) [k_a \dot{\theta}_{iw} - (R_a + R_{Lo}) I_a] \quad (5.8)$$

$$ET = I_a k_a \quad (5.9)$$

5.3.3 Electric load

The diode implemented between the electric generator and the electric load establishes an electrical separation between both, protecting both elements, guaranteeing a regulated voltage to the load while avoiding reversible currents to the generator armature.

The electric load consists of a purely resistive load, using an electric resistance connected to the diode and to the electric ground. The current delivered to the resistive load (I_{Lo}) is the same as the current produced by the generator (I_a), while the voltage delivered to the resistive load is determined by Equation (5.10), limited by the voltage produced by the electric generator.

$$U_{Lo} = I_{Lo} R_{Lo} \quad (5.10)$$

5.3.4 Energetic analysis

The power and energy generated by the DC electric generator are determined by Equations (5.11) and (5.12), respectively. The power and energy consumed in a DC purely resistive load are determined by Equations (5.13) and (5.14), respectively.

$$P_{Ge} = U_a I_a \quad (5.11)$$

$$E_{Ge} = \int P_{Ge} dt \quad (5.12)$$

$$P_{Lo} = U_{Lo} I_{Lo} \quad (5.13)$$

$$E_{Lo} = \int P_{Lo} dt \quad (5.14)$$

The efficiency of the energy conversion system (electric generator) is defined by Equation (5.15), relating the generated electric energy to the mechanical energy delivered by the IW. The efficiency of the electric circuit is defined by Equation (5.16), relating the energy consumed by the electric load to the energy generated by the electric generator.

$$\eta_{Ge} = \frac{E_{Ge}}{E_{De}} \quad (5.15)$$

$$\eta_{Co} = \frac{E_{Lo}}{E_{Ge}} \quad (5.16)$$

The total efficiency of the system, from the vehicle lost energy to the electrical energy consumed by the electric load is defined by Equation (5.17). To determine the total efficiency of the mechanical system, Equation (5.18) should be applied, relating the energy received by the mechanical system to the energy delivered to the electrical circuit. To determine the total efficiency of the electrical system, Equation (5.19) should be applied, relating the energy received by the electric circuit to the energy consumed by the electric load. To determine the total efficiency of the RPEH internal device, Equation (5.20) should be applied, relating the energy received by the mechanical system to the energy consumed by the electric load.

$$\eta_{Tot} = \frac{E_{Lo}}{E_v} \quad (5.17)$$

$$\eta_{Mec} = \frac{E_{De}}{E_{Ha}} \quad (5.18)$$

$$\eta_{Ele} = \frac{E_{Lo}}{E_{De}} \quad (5.19)$$

$$\eta_{RPEH} = \frac{E_{Lo}}{E_{Ha}} \quad (5.20)$$

5.4 Technical Analysis

5.4.1 Introduction

Based on the software tool presented in Chapter 3 to simulate the VRI from an energetic perspective, the equations of the RPEH devices presented in previous sections were incorporated for the different mechanical systems and the electrical circuit.

The purpose of the simulation software is to study this interaction in great detail, with the possibility of fully characterizing the vehicle under study, as well as fully characterizing the pavement or the RPEH device, including its surface technical parameters. Additionally, the RPEH device mechanical and electrical properties were added to the model, depending on the mechanical system selected. The upgraded software tool will be briefly presented in this section. The upgraded tool calculates all the forces and displacements for both the vehicle elements and the RPEH surface, as well as for the mechanical and electrical system components. After that, it calculates the different energies transferred from each part of the system to the others and the efficiency of each energy transfer process.

The simulations performed with RoadVISS for the three mechanical systems previously presented will be presented in this section, using the same RPEH equipment surface profile, geometry and displacement, the same vehicle and the same electric generator and load. The goal is to evaluate the different mechanical systems and draw conclusions about each system's efficiency in transmitting and delivering mechanical energy.

One RPEH device connected to one mechanical system is considered, which, in turn, is connected to one electrical system, as the surface is actuated by one side of the vehicle. So, the value presented for the energy lost by the vehicle is related to half the vehicle, as only one front and one rear wheel actuates the RPEH device surface. The parameters defined for the vehicle, the RPEH device surface, the mechanical and electrical systems, common in the simulations of the three mechanical systems are presented in Table 5.4.

Table 5.4- Input data for the computational simulations of the three systems.

	Variable name	Value	Unit
Vehicle & motion	Vehicle class	Light	-
	Vehicle weight	1,500	(kg)
	Number of axles P1 wheels per axle	2 2	-
	Sprung-Unsprung %	90%-10%	-
	Drag coefficient	0.32	-
	Inertia moment	1,100	(kg.m ²)
	Lift coefficients (Front Rear)	0.19 0.13	-
	Motion Direction	Free rolling Forward	-
	Vehicle speed acceleration	40 0	(km/h) (m/s ²)
Suspension & wheel	Suspension type (Front Rear)	Independent Independent	-
	Suspension stiffness (Front Rear)	20,000 15,000	(N/m)
	Suspension damping (Front Rear)	1,500 1,700	(Ns/m)
	Tyre type (Front Rear)	Radial Radial	-
	Tyre stiffness (Front Rear)	150,000 150,000	(N/m)
	Tyre pressure (Front Rear)	200 200	(kPa)
	Tyre external diameter (Front Rear)	500 500	(mm)
	Tyre width (Front Rear)	200 200	(mm)
RPEH device	Tyre tread width (Front Rear)	180 180	(mm)
	Surface width	250	(mm)
	Surface mass	20	(kg)
	Surface max. height max. displacement	20 20	(mm)
	Spring stiffness	40,000	(N/m)
	Pinion mass friction coefficient	1 0.002	(kg) -
	Inertia wheel radius	30	(mm)
	Electric generator constant Ka	0.25	-
	Electric generator Ra La	1.1 0.0048	(Ω) (H)
Electric generator friction coef. Inertia	0.0008 0.05	- (kg.m ²)	
Electric load Power	50	(W)	

5.4.2 Simulation software tool

Based on the software tool RoadVISS, an upgrade was performed to include the models of different RPEH devices. Applying the vehicle dynamics, VRI, as well as the mechanical and electrical system modelling equations, the software calculates all the displacements, both for the vehicle and the RPEH device components, the applied and received forces, and the energy transferred by each system component, presenting the results both graphically and numerically.

Beside the electromechanical systems previously presented, the new software tool was developed already considering future developments and models, as for hydraulic systems, mechanical energy storage systems and electrical energy storage units.

5.4.2.1 Software inputs

To select the inputs, a new GUI platform was developed, as presented in Figure 5.8.

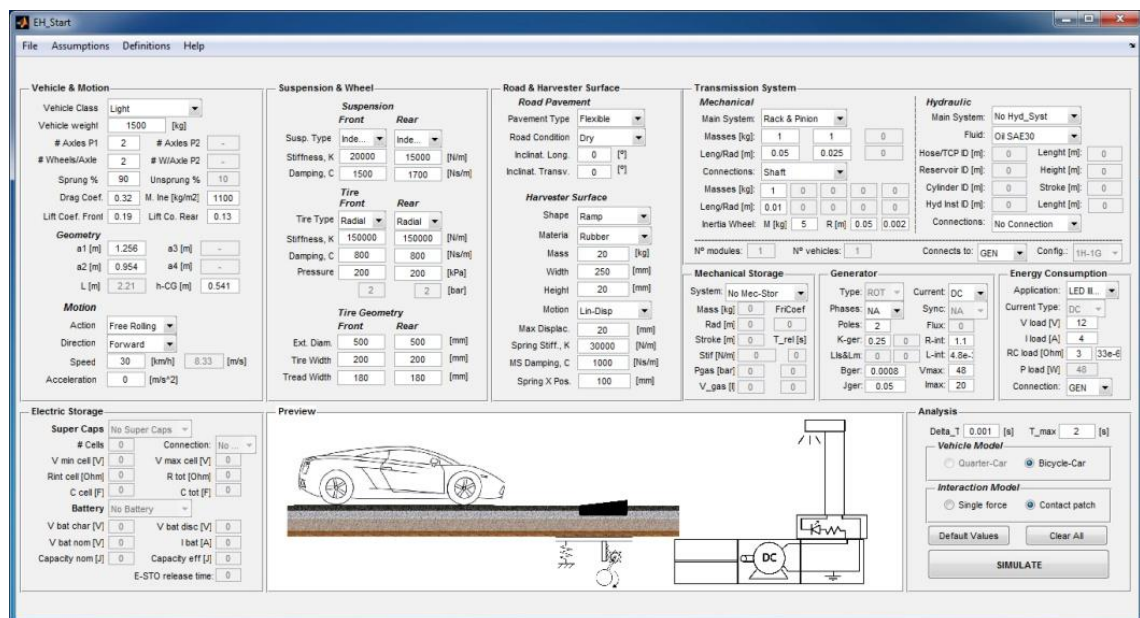


Figure 5.8- GUI to select the inputs of the upgraded software tool.

This GUI has 10 distinct panels, with eight for parameter selection, one for the preview of the selected features, regarding the vehicle, the pavement, the RPEH device (mechanical and electrical parts) and the electric load, and other for the selection of simulation features.

The first panel allows the user to select the vehicle and motion properties. In terms of the vehicle, it allows the vehicle class, weight, number of axles, wheels per axle, percentage of sprung and unsprung mass, drag and lift coefficients, and inertia moment of the vehicle to be selected. It also allows users to define the vehicle geometry in terms of distances from each axle to the centre of gravity, as well as the height of the centre of gravity. In terms of vehicle motion, it allows to the selection of the action, the motion direction, the vehicle speed and acceleration.

The second panel allows the user to select the suspension and wheel properties. In terms of suspension, it allows users to select the suspension type and to define the suspension stiffness and damping values, for both the front and rear suspension. In terms of tyre, it allows the user to select the tyre type and to define the tyre stiffness, damping and pressure, for both the front and rear tyre. The tyre geometry in terms of external diameter, tyre width and tread width can also be defined, for both front and rear tyres.

The third panel allows the road and RPEH device properties to be selected. In terms of road pavement, the user can select the pavement type, the road condition, the longitudinal and transversal inclination of the pavement. For the harvester surface, users can select the shape, the motion type, the material, the width and height, its maximum displacement, its mass, and also its stiffness and damping can be defined.

Panels four to eight allow to fully characterize the RPEH device: in panel four, its mechanical (or hydraulic, with future developments) characteristics, including the system selection and its parameters; in panel five, its mechanical storage characteristics, with future developments in this field; in panel six, its electrical generator characteristics; in panel seven, the electric load; and in panel eight, the electrical storage characteristics, with future developments in this field.

The ninth panel presents a summary of the selection, showing an image of the selected vehicle, pavement type, surface shape, RPEH device type (mechanical and electrical parts) and the electrical energy application. With this information, the user can confirm selection visually.

The tenth panel allows the user to define the simulation time and each iteration interval, as well as the vehicle model to be simulated and interaction model, in terms of the inclusion of the tyre *contact patch*. In this panel, the user can clean all the fields to select new values, and can press the *Simulate* button to start the simulation.

5.4.2.2 Software outputs

To present the software outputs graphically, a new GUI platform was developed, as presented in Figure 5.9.

This GUI has nine distinct panels, with seven for outputs graphical presentation, one for outputs numerical presentation and other for the selection of the plots to print.

The seven panels that presents the results graphically are related to each system component output: vehicle results in the first panel, both for front wheel and rear wheel forces and energy released; RPEH device surface in the second panel, both for received force and energy transferred; RPEH mechanical or hydraulic system results in the third panel, both for transmitted force and energy; RPEH mechanical storage system results in the fourth panel, both for transmitted force and stored energy; RPEH electrical generator results in the fifth panel, both for voltage, current, power and energy generated; RPEH electrical storage system results in the sixth panel, both for voltage, current, power and energy stored; and RPEH electrical load results in the seventh panel, both for voltage, current, power and energy consumed. These results are related to each vehicle side, representing half vehicle.

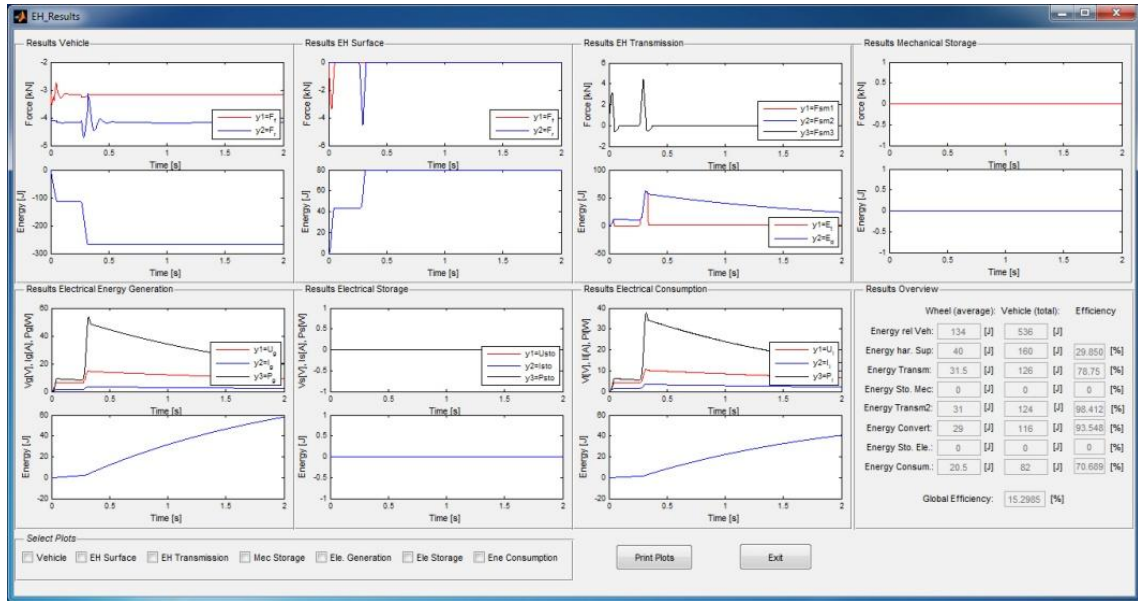


Figure 5.9- GUI to select the outputs of the upgraded software tool.

Panel eight presents the results numerically, for each component of the system, for each vehicle wheel actuation and for the entire vehicle, presenting also the efficiency of the respective component, as well as the global efficiency of the system, from the mechanical energy released by the vehicle and the electrical energy consumed by the electrical load.

Finally, panel nine offers users the possibility to print the plots, allowing them to select the desired plots to be printed and pressing the *Print Plots* button. Finally, it contains an *Exit* button to close the results GUI and return to the initial GUI.

5.4.2.3 Models

When the simulation starts, the software defines all the "static" variables, i.e., those that do not depend on the vehicle or RPEH system dynamics, such as the front and rear unsprung masses, the sprung mass, drag and lift forces, forces per axle, both vertical

and longitudinal, the contact patch geometry for each wheel, or the initial kinetic energy of the vehicle.

As considered for the RoadVISS software tool, four vehicle and interaction models were developed using the SIMULINK[®] tool:

- 1) quarter-car model and SFA;
- 2) bicycle-car model and SFA;
- 3) quarter-car model and CPA;
- 4) bicycle-car model and CPA.

The selected vehicle and interaction model is then connected to the correspondent energy harvesting mechanical (or hydraulic, with future developments) system model. Three initial models were developed using SIMULINK[®] and Simscape[®] tools:

- 1) RAP mechanical system;
- 2) Level mechanical system;
- 3) CTS mechanical system.

The selected model of the mechanical system is then connected to the electrical system model, composed by a DC electrical generator and a DC load. In the future, other models can be added to the software tool, including electrical energy storage and an AC electrical generator. This model (and future models) was developed using the SIMULINK[®] and Simscape[®] tools.

Depending on the user' selection, the software connects the vehicle and interaction selected models with the mechanical system model and with the electrical system model, defines each system parameters with the data defined in the *Input GUI*, and runs the simulation, in order to perform the dynamic analysis. The results are then presented in the *Output GUI*, both graphically and numerically.

5.4.3 Computational simulations

Considering the input data presented in Table 5.4, simulations the different mechanical systems previously presented were performed, considering two different surfaces (*Ramp* and *Crest*), presented in the Chapter 3. The electric generator and electric load characteristics were not changed, as the main goal is to study the impact of the mechanical system and its characteristics in the performance of the RPEH device.

For the RAP system, different pinion radius and IW mass values were considered to evaluate the impact of these on the global results. For the lever system, besides these two variables, two different lever geometries were also considered.

To evaluate the system performance, the vehicle released energy (E_v), RPEH surface harvested energy (E_{Ha}), mechanical system transmitted energy (E_{Tr}), mechanical system delivered energy (E_{De}), electrical system generated energy (E_{Ge}), and electrical system consumed energy (E_{Lo}) were calculated. Also, the efficiencies of the energy transferred between each part of the system were evaluated.

5.4.3.1 System 1 - RAP

Table 5.5 presents the simulation results for the energy output of each component of the RPEH device using the RAP mechanical system, considering the input data presented in Table 5.4. Table 5.6 presents the simulation results for the efficiency of each component of the system, as well as the total efficiency of the device.

5.4.3.2 System 2 - Lever

Table 5.7 presents the simulation results for the energy output of each component of the RPEH device using the lever mechanical system, considering the input data presented in Table 5.4. Table 5.8 presents the simulation results for the efficiency of each component of the system, as well as the total efficiency of the device.

Table 5.5- Simulation results for the energy outputs of the RPEH device components using the RAP mechanical system.

SP	r_p (mm)	m_{iw} (kg)	E_v (J)	E_{Ha} (J)	E_{Tr} (J)	E_{De} (J)	E_{Ge} (J)	E_{Lo} (J)
S5	15	5	263.0	83.0	19.0	19.0	17.0	13.8
		10	263.0	83.0	19.0	19.0	16.0	12.9
	20	5	265.0	82.0	37.0	37.0	33.0	27.0
		10	265.0	82.0	37.0	36.0	31.0	25.1
	25	5	266.0	81.0	59.0	59.0	53.0	43.5
		10	266.0	81.0	59.0	58.0	51.0	41.6
S8	15	5	184.0	87.0	22.0	22.0	19.9	16.1
		10	184.0	88.0	22.0	22.0	19.0	15.4
	20	5	182.0	84.0	41.0	41.0	37.0	29.9
		10	183.0	85.0	41.0	41.0	35.0	28.2
	25	5	182.0	82.0	65.0	64.0	59.0	47.9
		10	182.0	83.0	65.0	64.0	57.0	46.2

Table 5.6- Simulation results for the efficiencies of the RPEH device components using the RAP mechanical system.

SP	r_p (mm)	m_{iw} (kg)	η_{Ha} (%)	η_{Tr} (%)	η_{De} (%)	η_{Ge} (%)	η_{Co} (%)	η_{Mec} (%)	η_{Ele} (%)	η_{RPEH} (%)	η_{TOT} (%)
S5	15	5	31.6	22.9	99.7	89.7	80.9	22.8	72.6	16.6	5.2
		10	31.6	22.9	99.7	84.4	80.3	22.8	67.8	15.5	4.9
	20	5	30.9	45.1	99.9	89.3	81.8	45.1	73.1	32.9	10.2
		10	30.9	45.1	97.3	86.1	81.0	43.9	69.7	30.6	9.5
	25	5	30.5	72.8	99.9	89.9	82.1	72.8	73.8	53.7	16.4
		10	30.5	72.8	98.3	87.9	81.6	71.6	71.7	51.4	15.6
S8	15	5	47.3	25.3	99.8	90.7	80.9	25.2	73.3	18.5	8.8
		10	47.8	25.0	99.8	86.6	81.1	24.9	70.2	17.5	8.4
	20	5	46.2	48.8	99.9	90.4	80.8	48.8	73.0	35.6	16.4
		10	46.4	48.2	99.9	85.5	80.4	48.2	68.7	33.1	15.4
	25	5	45.1	79.3	98.5	92.2	81.2	78.0	74.8	58.4	26.3
		10	45.6	78.3	98.5	89.1	81.0	77.1	72.1	55.6	25.4

Table 5.7- Simulation results for the energy outputs of the RPEH device components using the lever mechanical system.

SP	d_1-d_2 (mm)	r_p (mm)	m_{iw} (kg)	E_v (J)	E_{Ha} (J)	E_{Tr} (J)	E_{De} (J)	E_{Ge} (J)	E_{Lo} (J)	
S5	40-60	20	5	262.0	84.0	15.0	15.0	12.9	10.2	
			10	262.0	84.0	15.0	15.0	12.7	10.0	
		30	5	264.0	83.0	36.0	36.0	32.0	26.1	
			10	264.0	83.0	36.0	35.9	30.9	24.9	
	40	5	266.0	82.0	66.0	65.0	59.3	48.1		
		10	266.0	82.0	66.0	65.0	58.6	47.3		
	40-80	20	5	262.0	84.0	8.0	8.0	6.5	5.1	
			10	262.0	84.0	8.0	8.0	6.4	4.9	
		30	5	263.0	84.0	19.0	19.0	16.3	12.9	
			10	263.0	84.0	19.0	18.9	16.1	12.7	
		40	5	264.0	83.0	36.0	35.0	31.2	25.2	
			10	264.0	83.0	36.0	35.0	31.0	24.9	
S8		40-60	20	5	185.0	89.0	17.0	17.0	14.6	11.6
				10	185.0	89.0	17.0	17.0	14.4	11.4
	30		5	184.0	85.0	40.0	40.0	35.6	29.0	
			10	184.0	85.0	40.0	39.9	34.3	27.7	
	40	5	182.0	82.0	73.0	72.0	65.7	53.5		
		10	182.0	82.0	73.0	72.0	64.9	52.5		
	40-80	20	5	188.0	91.0	9.0	9.0	7.4	5.8	
			10	188.0	91.0	9.0	9.0	7.3	5.8	
		30	5	186.0	88.0	22.0	22.0	18.9	15.0	
			10	186.0	88.0	22.0	22.0	18.7	14.8	
		40	5	184.0	85.0	40.0	40.0	35.6	29.0	
			10	184.0	85.0	40.0	39.9	34.3	27.7	

Table 5.8- Simulation results for the efficiencies of the RPEH device components using the lever mechanical system.

SP	d ₁ -d ₂ (mm)	r _p (mm)	m _{hw} (kg)	η _{Ha} (%)	η _{Tr} (%)	η _{De} (%)	η _{Ge} (%)	η _{Co} (%)	η _{Mec} (%)	η _{Ele} (%)	η _{RPEH} (%)	η _{TOT} (%)
S5	40-60	20	5	32.1	17.9	99.7	86.3	79.1	17.8	68.3	12.1	3.9
			10	32.1	17.9	99.7	84.9	78.8	17.8	66.9	11.9	3.8
		30	5	31.4	43.4	99.9	89.0	81.6	43.3	72.6	31.5	9.9
			10	31.4	43.4	99.7	86.0	80.6	43.3	69.3	30.0	9.4
		40	5	30.8	80.5	98.5	91.2	81.1	79.3	74.0	58.6	18.1
			10	30.8	80.5	98.5	90.1	80.8	79.3	72.8	57.7	17.8
	40-80	20	5	32.1	9.5	99.4	81.2	78.8	9.5	64.0	6.1	1.9
			10	32.1	9.5	99.4	80.1	77.7	9.5	62.2	5.9	1.9
		30	5	31.9	22.6	99.7	86.1	79.2	22.6	68.2	15.4	4.9
			10	31.9	22.6	99.5	85.1	79.0	22.5	67.2	15.1	4.8
		40	5	31.4	43.4	97.2	89.1	80.9	42.2	72.1	30.4	9.6
			10	31.4	43.4	97.1	88.8	80.2	42.1	71.2	30.0	9.4
S8	40-60	20	5	48.1	19.1	99.7	86.1	79.2	19.0	68.2	13.0	6.2
			10	48.1	19.1	99.7	85.1	79.0	19.0	67.2	12.8	6.2
		30	5	46.2	47.1	99.9	89.0	81.6	47.0	72.6	34.1	15.8
			10	46.2	47.1	99.8	86.0	80.6	46.9	69.3	32.5	15.0
		40	5	45.1	89.0	98.6	91.3	81.4	87.8	74.3	65.3	29.4
			10	45.1	89.0	98.6	90.2	80.9	87.8	73.0	64.1	28.9
	40-80	20	5	48.4	9.9	99.4	82.3	78.8	9.8	64.9	6.4	3.1
			10	48.4	9.9	99.4	82.0	78.5	9.8	64.4	6.3	3.1
		30	5	47.3	25.0	99.8	86.1	79.2	24.9	68.2	17.0	8.0
			10	47.3	25.0	99.8	85.1	79.0	24.9	67.2	16.8	7.9
		40	5	46.2	47.1	99.9	89.0	81.6	47.0	72.6	34.1	15.8
			10	46.2	47.1	99.8	86.0	80.6	46.9	69.3	32.5	15.0

5.4.3.3 System 3 - CTS

Considering the same conditions as for the RAP system and the lever system, simulations for the CTS mechanical system were also performed and the main results are presented in Tables 5.9 and 5.10 for the energy output and the efficiency of each component of the system, respectively. Besides the RPEH surface profile, pinion radius

(r_p) and IW mass (m_{iw}), the crank length (l_{cr}) was changed between simulations to evaluate the impact of this in the system's performance. The initial vertical distance between the crank axes (h_{cr-in}) was considered to be equal to 30 mm.

Table 5.9- Simulation results for the energy outputs of the RPEH device components using the CTS mechanical system.

SP	l_{cr} (mm)	r_p (mm)	m_{iw} (kg)	E_v (J)	E_{Ha} (J)	E_{Tr} (J)	E_{De} (J)	E_{Ge} (J)	E_{Lo} (J)
S5	35	15	5	261.0	85.0	21.0	20.9	18.3	14.7
			10	261.0	85.0	21.0	20.9	18.1	14.4
		20	5	262.0	85.0	39.0	38.9	34.7	28.3
			10	262.0	85.0	39.0	38.9	33.6	27.1
		25	5	263.0	85.0	64.0	63.9	57.7	47.2
			10	263.0	85.0	64.0	63.9	53.1	43.0
	40	15	5	263.0	84.0	36.0	35.9	32.0	26.0
			10	263.0	84.0	36.0	35.9	31.0	24.8
		20	5	264.0	84.0	67.0	66.9	59.7	48.7
			10	264.0	84.0	67.0	66.9	55.0	44.6
		25	5	265.0	83.0	82.0	81.9	75.3	61.7
			10	265.0	83.0	82.0	81.9	73.8	60.2
S8	35	15	5	224.0	91.0	23.0	22.9	20.0	16.0
			10	224.0	91.0	23.0	22.9	19.9	15.9
		20	5	222.0	89.0	42.0	41.9	38.0	31.0
			10	222.0	89.0	42.0	41.9	36.8	29.6
		25	5	221.0	87.0	65.0	64.9	58.6	48.0
			10	221.0	87.0	65.0	64.9	54.0	43.8
	40	15	5	222.0	88.0	38.0	37.9	33.9	27.6
			10	222.0	88.0	38.0	37.9	32.8	26.4
		20	5	219.0	85.0	67.0	66.9	60.5	49.4
			10	219.0	85.0	67.0	66.9	55.8	45.3
		25	5	218.0	83.0	82.0	81.9	75.3	61.7
			10	218.0	83.0	82.0	81.9	73.8	60.2

Table 5.10- Simulation results for the efficiencies of the RPEH device components using the CTS mechanical system.

SP	l_{cr} (mm)	r_p (mm)	m_{iw} (kg)	η_{Ha} (%)	η_{Tr} (%)	η_{De} (%)	η_{Ge} (%)	η_{Co} (%)	η_{Mec} (%)	η_{Ele} (%)	η_{RPEH} (%)	η_{TOT} (%)
S5	15	5	5	32.6	24.7	99.5	87.3	80.3	24.6	70.1	17.3	5.6
			10	32.6	24.7	99.5	86.5	79.7	24.6	68.9	17.0	5.5
	35	20	5	32.4	45.9	99.5	89.1	81.5	45.8	72.6	33.3	10.8
			10	32.4	45.9	99.5	86.2	80.7	45.8	69.6	31.9	10.3
	25	5	5	32.3	75.3	99.5	90.2	81.9	75.2	73.9	55.6	18.0
			10	32.3	75.3	99.5	83.0	81.1	75.2	67.3	50.6	16.4
	15	5	5	31.9	42.9	99.5	89.0	81.2	42.8	72.3	30.9	9.9
			10	31.9	42.9	99.5	86.2	80.1	42.8	69.0	29.6	9.4
	40	20	5	31.8	79.8	98.5	90.4	81.6	78.6	73.8	58.0	18.4
			10	31.8	79.8	98.5	83.3	81.1	78.6	67.6	53.1	16.9
	25	5	5	31.3	98.8	99.5	91.9	81.9	98.7	75.3	74.3	23.3
			10	31.3	98.8	99.5	90.1	81.5	98.7	73.4	72.5	22.7
S8	15	5	5	40.6	25.3	99.5	87.2	80.2	25.2	69.9	17.6	7.2
			10	40.6	25.3	99.5	86.6	79.8	25.2	69.1	17.4	7.1
	35	20	5	40.1	47.2	99.5	90.5	81.7	47.1	73.9	34.9	14.0
			10	40.1	47.2	99.5	87.7	80.5	47.1	70.6	33.3	13.3
	25	5	5	39.4	74.7	99.5	90.3	81.8	74.7	73.9	55.1	21.7
			10	39.4	74.7	99.5	83.1	81.2	74.7	67.5	50.4	19.8
	15	5	5	39.6	43.2	99.5	89.2	81.4	43.1	72.6	31.3	12.4
			10	39.6	43.2	99.5	86.3	80.5	43.1	69.5	30.0	11.9
	40	20	5	38.8	78.8	99.5	90.4	81.7	78.8	73.9	58.2	22.6
			10	38.8	78.8	99.5	83.3	81.2	78.8	67.6	53.3	20.7
	25	5	5	38.1	98.8	99.5	91.9	81.9	98.7	75.3	74.3	28.3
			10	38.1	98.8	99.5	90.1	81.5	98.7	73.4	72.5	27.6

5.4.4 Results analysis

Analyzing the results obtained with the computational simulations of the RPEH device, using the three different mechanical systems presented to transmit the energy received by the equipment surface and deliver it to an electrical generator, some conclusions may be drawn.

Globally, the RPEH surface harvested energy efficiency depends on the surface profile, varying significantly for each studied profile. Using the *Crest* profile (S8), the surface energy harvesting efficiency can be 30% higher than with the *Ramp* surface profile (S5), for the same conditions.

The mechanical energy delivery efficiency is close to 100% for all the studied systems and scenarios, meaning that the IW delivers almost all the energy that the pinion transmits to it. The only energy loss is due to the clutch bearing, which happens between each vehicle wheel actuation.

The DC electrical generator efficiency varies in relation to the delivered energy, as it is associated with its rotational speed. For lower rotational speeds, its efficiency is lower than 85%, while for higher rotational speeds, it can be higher than 90%. The electric energy consumption efficiency is usually around 80%, for the considered electrical load and using a diode between the electrical generator and the load.

Comparing the different mechanical systems for the same conditions, it may be concluded that:

- The lever system presents the lowest transmission efficiency, for the same pinion applied on the system; however, increasing the pinion radius and for a small relation between d_1 and d_2 , the transmission efficiency can be increased and reach very high levels of around 80%;
- The RAP system have similar transmission efficiencies when compared to the lever system, but for lower pinion radius, meaning that in the same conditions, it is more efficient;
- The CTS system is the most efficient system regarding the mechanical energy transmission, as, for the same pinion radius, it can duplicate the efficiency of the RAP system and, with its optimal characteristics, it can have a transmission efficiency of around 99%. Although this system has more mechanical parts than the other two, due to the force increase and motion decrease principle, the mechanical losses were reduced.

In all the systems studied, an increase in the pinion radius induces an increase in the energy transmission efficiency. This is understandable due to the increase in the pinion acceleration and, consequently, in its rotational speed. However, it also increases the opposition force from the IW and the electrical generator, which is why the pinion radius value cannot be higher than certain values.

For the lever system, an increase in the d_1/d_2 relation induces an increase in the energy transmission efficiency, leading to the need to increase the pinion radius. As the increase in this relation also increases the force transmitted by the lever, an increase in the pinion radius will also increase the opposition force from the IW and the electrical system. This makes this system more complex than the RAP, so it needs to be properly studied and optimized.

For the CTS mechanical system proposed, an increase in the crank length allows the system efficiency to increase as the crank initial angle decreases, leading to a higher force being transmitted by the system piston. Excluding the energy lost by the vehicle and considering the energy harvested by the surface as the system input, the efficiency of the RPEH device can be higher than 74%, including the electrical energy losses, which represents an energy conversion much higher than all the RPEH devices studied and presented in Chapter 2.

In all the performed simulations the vertical acceleration induced by the RPEH device to the vehicle body was lower than 1 m/s^2 . Considering the existing levels of acceptability of the ride quality (ISO, 1997), this indicates that the RPEH device does not cause discomfort to the vehicle driver and to its occupants.

5.5 Experimental Validation

5.5.1 Introduction

Following the computational simulations, a prototype of the CTS system was built to evaluate the results experimentally. During the prototype design, some changes were

added to the system so that it could resist to loads applied by the vehicles and keep the vertical displacement of the entire surface. These developments are presented in this section. Besides the electromechanical system, the prototype also includes sensors and instruments to measure different variables, a *Data Logger* to collect these data and software to receive data and generate plots.

The prototype was then implemented in a controlled environment and different scenarios were tested. A new set of computational simulations was performed, for the same scenarios as those tested experimentally, so that both results could be directly compared. The analysis of the results is also presented in this section.

5.5.2 Prototype

The design of the experimental prototype was based on the CTS mechanical system presented in Figure 5.5, but using two CTS systems, as presented in Figure 5.10, so that the force transmitted from the surface to the RAP system can be divided between both systems and to balance the surface so that it has purely downward motion when actuated. A linear guiding system is also used to help with this action.

Given the use of light weight and low cost materials, especially plastic, as the core material for the components of the prototype, a multiple crank system was adopted. The components were designed so that the prototype can support the passage of a heavy vehicle with 10 tons per axle, with a safety factor of 1.5. Also, a linear guiding system was used to guarantee a uniform displacement of the system's surface, with a linear guide and a linear bearing in each corner of the prototype. The values considered for the prototype components, especially the crank length (l_{cr}), its initial position (θ_{cr-in}), the maximum displacement of the surface and the spring stiffness were the same as presented in previous sections.

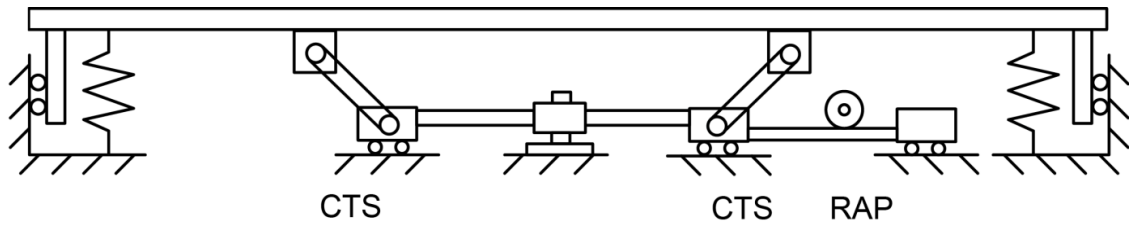


Figure 5.10- Mechanical system using two CTS systems and one RAP system.

The two sliders were mechanically connected by a vertical axis RAP system, used to cinematically unite the systems and also to transmit the forces between each other. With this approach, only one slider was connected to the RAP system that transmits the energy to the electrical generator. However, due to the lack of space for the generator in the prototype, a connection was made to an external shaft using a belt and pulley connection between the pinion shaft and the generator shaft. In the generator shaft, an IW was used to store a small amount of the mechanical energy delivered to the generator shaft, to keep it rotating between each wheel passage over the prototype. All these changes increase inertia and friction in the system but are essential to guarantee the correct operation of the system.

A DC generator was used, with the characteristics presented in Table 5.4. The electric generator was directly connected to an electric load (EL), which can be changed to test different loads - whether resistive or resistive-capacitive, as defined previously.

The prototype design is presented in Figure 5.11, without sensors, instrumentation components and the surface with a specific profile. Three surface profiles (*Crest*, *Ramp* and *S profile*) were designed and built for the experimental tests. The external dimensions of the prototype are 1.1 x 0.3 m, with a total area of 0.33 m² and a total height of 0.11 m.

Besides the mechanical system, sensors and instrumentation equipment were also included in the prototype, namely two Tedeo-Huntleigh load cells, model 1250 (Vishay, 2017), with a 1,000 kg maximum load each, to measure the force received by the surface of the prototype and transferred to the mechanical system (F_{SMI}), applied

between the surface with a specific profile and the mechanical system surface; and two linear encoders Variotm - IPL Linear Position Sensor, model IPL-0025-103-3%-ST (Farnell, 2017) to measure the linear displacement of the prototype surface (x_h) and the linear displacement of the mechanical system piston (x_{sp}), applied on a fixed and a moving part of the system to measure the displacements.

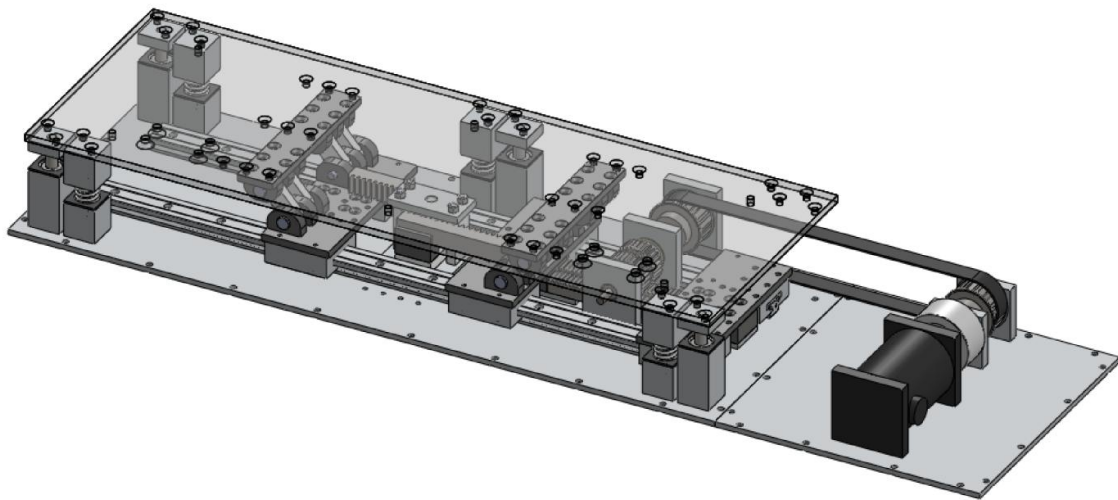


Figure 5.11- Prototype design without sensors and instrumentation components.

To monitor the electric energy that was generated, both the voltage and current were measured, using simple electric circuits. A resistive divider was used to measure the generated voltage, dividing the voltage by 10 so that the measured value is directly proportional to the measured value. To measure the generated current a INA 195 current sensor was used (Texas Instruments, 2017).

These sensors were connected to a National Instruments *Data Logger*, model NI USB-6003 (National Instruments, 2017), with an intermediate instrumentation system to adapt the sensor signals to the data logger requirements. The *Data Logger* was connected to a laptop via USB, transferring the acquired data with a frequency of 100 Hz, and software was developed using LabVIEW[®] to read the received data and convert it into plots, as well as to store these data as readable files.

To convert the measured loads from the load cells into a received force, the values from both load cells were added and multiplied by 9.81 m/s^2 , and to determine the load delivered by the slider to the crank, the equation of F_{SM2} presented in Table 5.3 was used. In this equation, to define angle θ_{cr} , the equations from the kinematic analysis presented in the same Table were used, considering the displacements x_h and x_{cr} measured by the linear encoders. With these values, the energy harvested from the surface (E_{Ha}) was measured, using Equation (4.18).

Multiplying the generated voltage by the generated current, the generated power (P_{Ge}) is measured, and integrating this value between acquisitions the electric energy generated (E_{Ge}) is calculated. As the electrical energy generated is similar to electrical energy consumed, to determine the energy conversion efficiency of the device (η_{RPEH}), Equation (5.20) was used.

In Figure 5.12 the prototype assembled with the sensors and with the *S Profile* surface is presented.

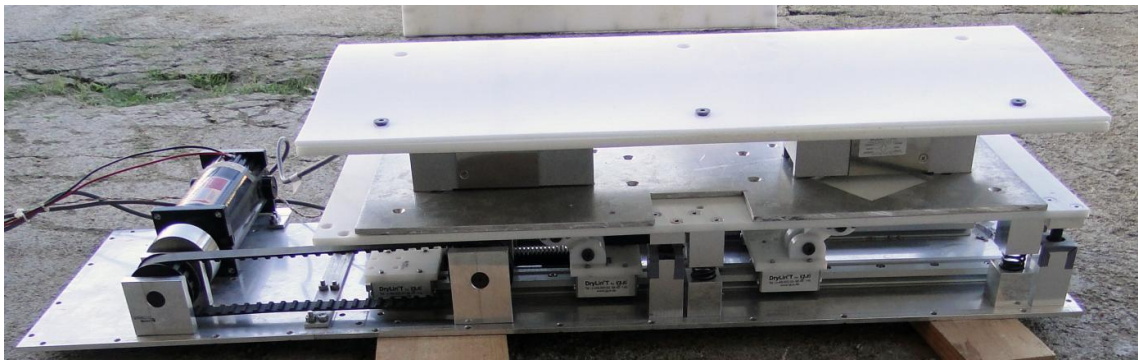


Figure 5.12- Fully assembled prototype system with sensors.

5.5.3 Test scenarios

The prototype was installed in a road pavement surface of a car parking space by opening a hole with the external dimensions of the prototype ($1.1 \times 0.3 \times 0.11 \text{ m}^3$), in

such a way that only the prototype surface was above the level of the road surface. Considering the working principle of the designed system, when the vehicle wheels starts the contact with the prototype surface, it will be at the pavement level, and when the wheel leaves the contact with the prototype surface it still continues at the road pavement level, avoiding the typical bump effect of speed bumps.

To perform multiple tests with the prototype and evaluate its performance under different conditions, different vehicles weighing 1,000 kg (VE_1) and 2,000 kg (VE_2), different prototype surface profiles (*Crest*, *Ramp* and *S profile*), different values for the EL of 10 Ohm/0 F (EL_1) and 10 Ohm/ 40 μ F (EL_2) and different vehicle speeds, of 20, 30, 40 and 50 km/h were considered. Table 5.11 presents the different scenarios for the prototype experiments.

Table 5.11- Test scenarios for the system prototype.

Vehicle type and weight (kg)	Surface profile (SP)	Electric load - Resistance / Capacitance (Ohm / μ F)	Vehicle speed (km/h)
$VE_1=1,000$	S8=Crest	$EL_1=10/0$	10 20 30 40
		$EL_2=10/40$	10 20 30 40
	S5=Ramp	$EL_1=10/0$	10 20 30 40
		$EL_2=10/40$	10 20 30 40
	S6=S profile	$EL_1=10/0$	10 20 30 40
		$EL_2=10/40$	10 20 30 40
$VE_2=2,000$	S8=Crest	$EL_1=10/0$	10 20 30 40
		$EL_2=10/40$	10 20 30 40
	S5=Ramp	$EL_1=10/0$	10 20 30 40
		$EL_2=10/40$	10 20 30 40
	S6=S profile	$EL_1=10/0$	10 20 30 40
		$EL_2=10/40$	10 20 30 40

5.5.4 Computational simulations

Using the upgraded version of the RoadVISS software tool to perform the simulations for the new RPEH system proposed in this work, two vehicles with the characteristics

presented in Table 5.12 were considered, with VE_1 representing a 1,000 kg vehicle and VE_2 representing a 2,000 kg vehicle. The bicycle-car model and the CPA were used in this study. Also, different speeds were evaluated, from 20 km/h to 50 km/h, as this is the speed limit in urban areas.

Table 5.12- Fixed and initial values for the simulation variables.

	Variable name	Value (VE_1)	Value (VE_2)	Unit
Vehicle & motion	Vehicle class	Light		-
	Vehicle weight	1,000	2,000	(kg)
	Number of axles P1 wheels/axle	2 2		-
	Distance a1 a2	0.914 1.557	1.055 1.651	(m)
	Sprung-Unsprung %	90%-10%		-
	Drag coefficient	0.3	0.34	-
	Inertia moment	750	1,470	(kg.m ²)
	Lift coefficients (Front Rear)	0.17 0.12	0.21 0.15	-
	Motion Direction	Free rolling Forward		-
	Vehicle speed	20 30 40 50		(km/h)
	Vehicle acceleration	0		(m/s ²)
Suspension & wheel	Suspension type (Front Rear)	Independent Independent		-
	Suspension stiffness (Front Rear)	20,000 15,000	25,000 18,000	(N/m)
	Suspension damping (Front Rear)	1,500 1,700	1,700 1,900	(Ns/m)
	Tyre type (Front Rear)	Radial Radial		-
	Tyre stiffness (Front Rear)	140,000 140,000	160,000 160,000	(N/m)
	Tyre pressure (Front Rear)	200 200	250 250	(kPa)
	Tyre external diameter (Front Rear)	400 400	500 500	(mm)
	Tyre width (Front Rear)	190 190	220 220	(mm)
RPEH device	Tyre tread width (Front Rear)	175 175	200 200	(mm)
	Surface width max height max displac.	275 20 20		(mm)
	Surface mass	20		(kg)
	Spring stiffness	40,000		(N/m)
	Pinion mass Pinion radius friction coef.	1 0.02 0.002		(kg) (m) -
	Inertia wheel radius	30		(mm)
	Electric generator constant Ka	0.25		-
	Electric generator Ra La	1.1 0.0048		(Ω) (H)
Electric generator friction coef. Inertia	0.0008 0.05		- (kg.m ²)	

Considering the proposed electromechanical RPEH system, a set of simulations were performed for the different surface profiles previously defined, with a surface width of

0.275 m and a maximum height of 20 mm, the maximum displacement (x_{h-max}) being equivalent to the surface maximum height. The total spring stiffness (K_h) was 40 kN/m, and the considered surface material is recycled plastic with a rubber layer on top, with a total mass of 18 kg. The values for l_{cr} and θ_{cr-in} are, respectively, 0.04 m and 0.848 rad (or 48.6°). The simulation results for VE_1 and VE_2 are presented in Tables 5.13 and 5.14, respectively, considering different vehicle speeds (20, 30, 40 and 50 km/h), and different ELs, EL_1 for a resistive load with 10 Ohm (10 W), and EL_2 for a resistive-capacitive load with 10 Ohm (10 W) and 40 μ F.

Table 5.13- Simulation results of the new RPEH system for VE_1 .

SP	EL	v_{ini} (km/h)	F_{SM1} (N)	E_{Ha} (J)	E_{Ge} (J)	η_{RPEH} (%)
S8	EL ₁	20	2.512,8	70,1	21,2	30,2%
		30	3.289,5	77,1	28,7	37,2%
		40	3.551,5	75,4	31,5	41,8%
		50	3.929,9	70,9	33,1	46,7%
	EL ₂	20	2.478,5	69,5	20,3	29,2%
		30	3.390,0	76,4	27,9	36,5%
		40	3.652,2	72,3	30,6	42,3%
		50	4.034,8	67,2	32,3	48,0%
S5	EL ₁	20	2.754,2	71,1	25,3	35,6%
		30	2.847,7	75,0	35,5	47,3%
		40	3.109,0	74,4	37,7	50,7%
		50	3.341,0	70,2	38,9	55,4%
	EL ₂	20	2.746,6	70,7	22,0	31,1%
		30	2.828,9	79,9	31,1	38,9%
		40	3.124,3	77,2	33,4	43,3%
		50	3.321,5	71,6	34,8	48,6%
S6	EL ₁	20	3.691,1	77,2	28,9	37,4%
		30	3.902,8	79,5	35,6	44,8%
		40	4.033,6	75,8	39,1	51,6%
		50	4.342,3	69,4	41,0	59,1%
	EL ₂	20	3.549,8	75,9	27,9	36,8%
		30	4.057,1	78,5	32,1	40,9%
		40	4.157,9	75,9	37,5	49,4%
		50	4.372,3	69,9	40,3	57,7%

Table 5.14- Simulation results of the new RPEH system for VE_2 .

SP	EL	v_{ini} (km/h)	F_{SM1} (N)	E_{Ha} (J)	E_{Ge} (J)	η_{RPEH} (%)
S8	EL ₁	20	4.109,8	101,2	50,9	50,3%
		30	4.671,2	129,8	65,9	50,8%
		40	5.012,8	144,2	71,5	49,6%
		50	5.548,9	135,8	70,3	51,8%
	EL ₂	20	4.012,3	100,1	43,1	43,1%
		30	4.521,8	122,9	56,2	45,7%
		40	4.982,3	142,2	64,1	45,1%
		50	5.421,1	134,4	61,1	45,5%
S5	EL ₁	20	4.578,5	97,2	53,1	54,6%
		30	4.178,5	109,9	62,1	56,5%
		40	4.891,7	125,9	70,5	56,0%
		50	5.047,5	118,5	64,8	54,7%
	EL ₂	20	4.544,1	88,1	41,1	46,7%
		30	4.071,2	107,9	53,9	50,0%
		40	4.158,9	122,9	59,9	48,7%
		50	4.912,1	116,1	56,4	48,6%
S6	EL ₁	20	4.787,5	110,8	55,9	50,5%
		30	4.688,2	129,9	65,4	50,3%
		40	4.917,8	137,1	68,8	50,2%
		50	5.272,3	120,2	65,2	54,2%
	EL ₂	20	4.653,8	98,1	42,2	43,0%
		30	3.999,4	124,0	60,1	48,5%
		40	4.421,2	136,7	66,0	48,3%
		50	5.148,2	120,4	60,4	50,2%

Considering E_{Ha} and E_{Ge} as the most important variables to evaluate the performance of the system, Figure 5.13 presents the E_{Ha} and E_{Ge} for VE_1 , for the different surfaces and for different electric loads, while Figure 5.14 presents the results for the same scenarios but for VE_2 .

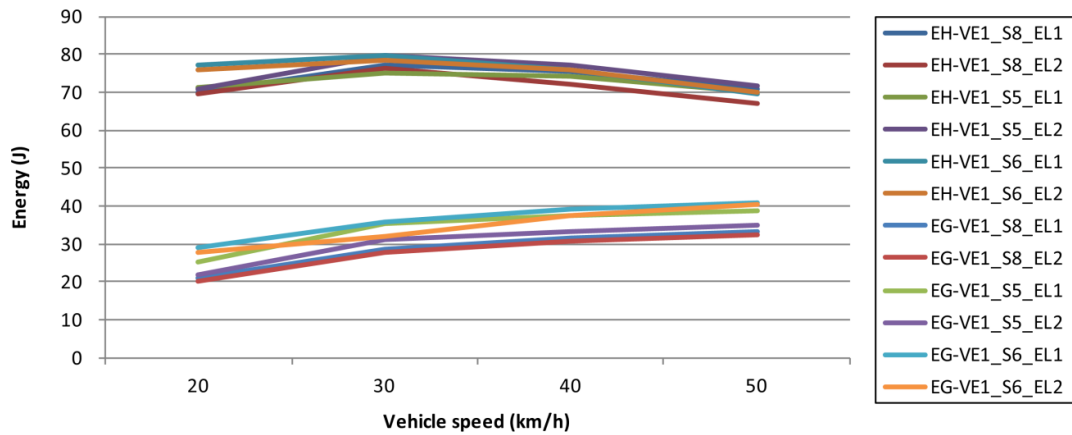


Figure 5.13- Simulation results for VE_1 .

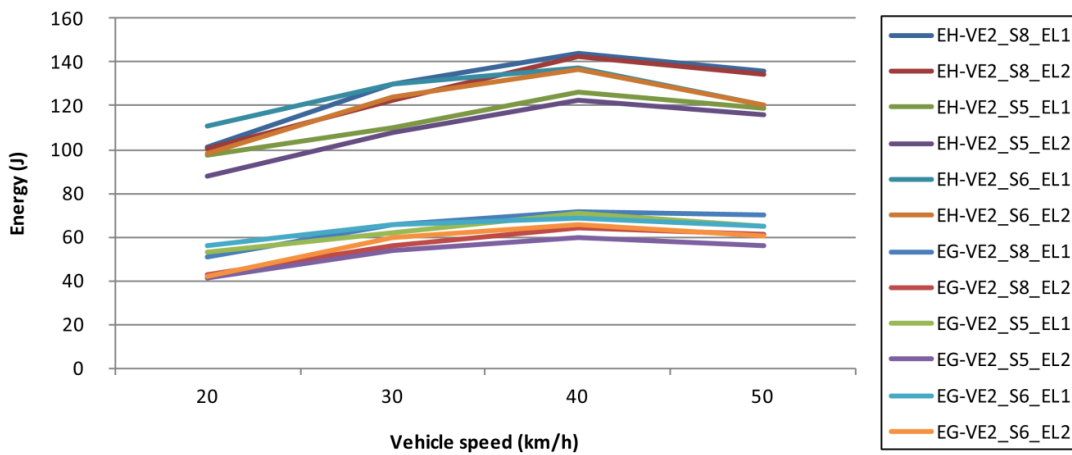


Figure 5.14- Simulation results for VE_2 .

5.5.5 Experimental results

Both the VE_1 and VE_2 used in the experimental tests have the same characteristics as the vehicles considered in the computational simulations, as presented in Table 5.12, so that the experimental test results can be compared with the appropriate level of confidence.

Tables 5.15 and 5.16 present the results of the experimental tests with the prototype, for VE_1 and VE_2 , respectively. In these tables, the different variables presented in Table 5.11 are identified, and the values regarding the force received by the surface and transmitted to the mechanical system, F_{SMI} , the energy harvested by both wheels of one side of the vehicle, E_{Ha} , the total electric energy generated, E_{Ge} , and the efficiency of the energy conversion process, η_{RPEH} , are presented.

Table 5.15- Prototype test results for VE_1 .

SP	EL	v_{ini} (km/h)	F_{SMI} (N)	E_{Ha} (J)	E_{Ge} (J)	η_{RPEH} (%)
S8	EL ₁	20	2.310,2	53,1	9,2	17,4%
		30	2.912,3	72,7	21,0	28,9%
		40	2.824,9	69,6	25,5	36,7%
		50	3.139,6	66,0	31,0	47,0%
	EL ₂	20	2.304,1	66,3	15,3	23,0%
		30	2.686,2	63,9	21,0	32,9%
		40	2.895,8	63,6	20,6	32,3%
		50	2.888,5	65,8	30,8	46,8%
S5	EL ₁	20	2.621,3	73,3	15,5	21,1%
		30	2.668,1	64,7	24,2	37,4%
		40	2.704,7	67,7	30,2	44,6%
		50	2.851,7	65,9	36,4	55,2%
	EL ₂	20	1.859,2	58,3	10,7	18,4%
		30	2.471,7	68,9	14,3	20,8%
		40	3.073,8	78,7	15,3	19,4%
		50	2.767,1	70,9	28,4	40,1%
S6	EL ₁	20	2.666,6	58,8	9,9	16,9%
		30	2.526,6	61,4	16,6	27,0%
		40	2.548,8	71,8	31,9	44,4%
		50	3.157,7	64,7	32,9	50,9%
	EL ₂	20	2.863,7	65,3	10,6	16,2%
		30	2.993,5	72,9	12,2	16,8%
		40	3.401,9	76,8	20,6	26,9%
		50	3.169,3	75,3	36,6	48,6%

Considering that the E_{Ha} and the E_{Ge} as the most important variables for evaluating the performance of the system, Figure 5.15 presents the energy harvested for VE_1 , for the different surfaces and the different electric loads, while Figure 5.16 presents the results for the same scenarios but for VE_2 .

Table 5.16- Prototype test results for VE_2 .

SP	EL	v_{ini} (km/h)	F_{SMI} (N)	E_{Ha} (J)	E_{Ge} (J)	η_{RPEH} (%)	
S8	EL ₁	20	3.282,8	86,6	30,5	35,2%	
		30	4.470,2	124,7	32,0	25,7%	
		40	3.487,6	98,8	26,4	26,7%	
		50	3.965,0	104,8	57,0	54,4%	
	EL ₂	20	3.774,3	106,4	24,6	23,1%	
		30	3.979,0	114,6	24,5	21,4%	
		40	3.650,0	107,9	33,8	31,3%	
		50	3.949,4	114,0	50,2	44,1%	
	S5	EL ₁	20	4.478,2	104,8	25,5	24,3%
			30	3.822,3	106,2	29,3	27,6%
40			4.130,1	126,0	45,1	35,8%	
50			4.131,4	122,7	58,2	47,4%	
EL ₂		20	3.934,1	71,7	15,1	21,1%	
		30	3.773,4	100,3	24,3	24,2%	
		40	3.873,2	127,7	27,0	21,1%	
		50	3.939,2	118,3	47,5	40,1%	
S6		EL ₁	20	3.582,1	88,5	20,5	23,2%
			30	4.021,2	117,9	30,6	25,9%
	40		3.923,2	106,4	33,0	31,1%	
	50		4.178,1	119,7	72,4	60,5%	
	EL ₂	20	4.312,7	107,1	14,8	13,8%	
		30	3.976,0	115,9	20,6	17,7%	
		40	3.540,3	119,7	20,4	17,0%	
		50	3.982,5	137,3	40,9	29,8%	

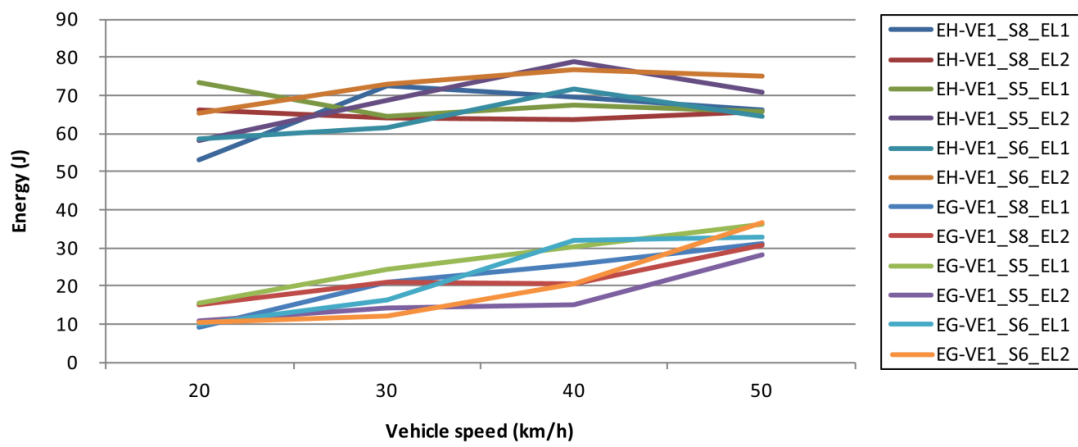


Figure 5.15- Experimental results for VE_1 .

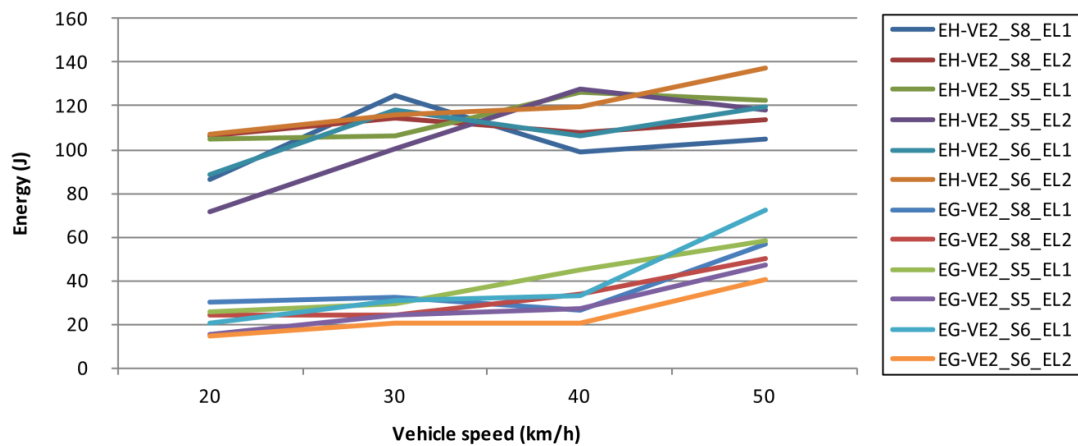


Figure 5.16- Experimental results for VE_2 .

Analyzing the experimental results, the following conclusions may be drawn.

- For all the tested scenarios, the energy generation has increased with the increase in vehicle speed, while the energy harvested does not change considerably with the vehicle speed. This means that the conversion efficiency increases considerably with the increase in vehicle speed. This increase was not

so evident in the computational simulations, mainly because the efficiency at low speeds achieved in the experimental tests was much lower than the computational simulations results.

- With the heavier vehicle, the total amount of energy harvested and generated increased, but the average energy conversion efficiency of the system was lower, with an average value of 30.1%, compared to 32.1% for VE_1 , contrary to the simulated results. A possible justification for this is the lower efficiencies achieved for lower vehicle speeds, which was more evident for VE_2 .
- The highest values of energy harvested and generated were achieved using surface profile S6, which was also verified with the computational simulations, allowing us to conclude that this is the optimal surface profile for these variables.
- Comparing the results for different electric loads, it is possible to conclude that a purely resistive load is more efficient and allows more energy to be generated than a resistive-capacitive load, as seen in the computational simulations.

5.5.6 Discussion

Tables 5.17 and 5.18 present the difference between the simulations and the experimental results for similar tested scenarios using VE_1 and VE_2 , respectively. From these, some conclusions can be drawn.

- The average difference in F_{SMI} is 19.1% and 15.7% for VE_1 and VE_2 , respectively, both lower in the experimental results. Both values are lower than 20%, which allows us to accept the computational simulation results as relatively accurate.
- Regarding E_{Ha} , the average difference between the computational simulations and experimental results is 8.6% for VE_1 and 7.2% for VE_2 , both lower for the

experimental results, but under 10%, which allows us to consider the computational simulation results as very accurate.

- For E_{Ge} , the differences between the computational simulations and the experimental results were much higher, 33.6% for VE_1 and 44.5% for VE_2 , representing very high differences that mean the computational simulations cannot be considered to be accurate. These differences can be justified by the changes made to the mechanical system to transform it into a prototype, by adding an additional CTS system, a RAP connection between both CTS systems, the inclusion of a generator shaft apart from the pinion shaft and a pulley-belt mechanical connection between these two shafts. All these connections added inertia and friction to the mechanical system, which justifies the lower values of electrical energy generation, which is dependent on the generator shaft rotation. These differences are higher for lower speeds, as the delivered forces are lower, leading to lower rotating speeds in the generator shaft and lower energy generation values.
- Consequently, the conversion efficiency was also lower in the experimental results when compared to the computational simulations, with average differences of 27.8% and 39.8% for VE_1 and VE_2 , respectively.

However, when considering the total amount of E_{Ge} for the best case scenarios, which were achieved experimentally for the 50 km/h vehicle speed and for a purely resistive electric load, it is possible to conclude that the system presented an average conversion efficiency of 52.6% for these scenarios, with a maximum of 60.5% for VE_2 and S3. This means that the system has presented a higher energy conversion efficiency than all the systems described in the literature and presented in Chapter 2 - Table 2.3, as the maximum efficiency experimentally validated was of 50.0%, a system developed by Waydip, denominated Waynergy Vehicles (Duarte *et al.*, 2016). This system has an energy generation of 92.0 J for a 2,000 kg vehicle at 50 km/h, using a surface 0.8 m wide.

Table 5.17- Difference between the simulations and experimental results for tested scenarios using VE_1 .

SP	EL	V_{ini} (km/h)	F_{SM1}	E_{Ha}	E_{Ge}	η_{RPEH}
S8	EL ₁	20	-8,1%	-24,3%	-56,4%	-42,4%
		30	-11,5%	-5,8%	-26,8%	-22,3%
		40	-20,5%	-7,7%	-19,0%	-12,1%
		50	-20,1%	-6,9%	-6,3%	0,7%
	EL ₂	20	-7,0%	-4,6%	-24,9%	-21,2%
		30	-20,8%	-16,4%	-24,7%	-10,0%
		40	-20,7%	-12,0%	-32,8%	-23,6%
		50	-28,4%	-2,2%	-4,8%	-2,7%
S5	EL ₁	20	-4,8%	3,1%	-38,8%	-40,6%
		30	-6,3%	-13,8%	-31,8%	-20,9%
		40	-13,0%	-9,1%	-20,0%	-12,0%
		50	-14,6%	-6,1%	-6,4%	-0,4%
	EL ₂	20	-32,3%	-17,5%	-51,2%	-40,8%
		30	-12,6%	-13,8%	-54,0%	-46,6%
		40	-1,6%	2,0%	-54,2%	-55,1%
		50	-16,7%	-1,0%	-18,4%	-17,5%
S6	EL ₁	20	-27,8%	-23,8%	-65,6%	-54,8%
		30	-35,3%	-22,8%	-53,4%	-39,6%
		40	-36,8%	-5,3%	-18,4%	-13,9%
		50	-27,3%	-6,8%	-19,7%	-13,9%
	EL ₂	20	-19,3%	-14,0%	-62,0%	-55,8%
		30	-26,2%	-7,1%	-61,9%	-59,0%
		40	-18,2%	1,2%	-45,0%	-45,6%
		50	-27,5%	7,7%	-9,3%	-15,8%
Average			-19,1%	-8,6%	-33,6%	-27,8%

Table 5.18- Difference between the simulations and experimental results for tested scenarios using VE_2 .

SP	EL	V_{ini} (km/h)	F_{SM1}	E_{Ha}	E_{Ge}	η_{RPEH}
S8	EL ₁	20	-20,1%	-14,5%	-40,2%	-30,1%
		30	-4,3%	-3,9%	-51,4%	-49,4%
		40	-30,4%	-31,5%	-63,1%	-46,1%
		50	-28,5%	-22,8%	-18,9%	5,2%
	EL ₂	20	-5,9%	6,3%	-43,0%	-46,4%
		30	-12,0%	-6,8%	-56,4%	-53,3%
		40	-26,7%	-24,1%	-47,3%	-30,5%
		50	-27,1%	-15,2%	-17,8%	-3,1%
S5	EL ₁	20	-2,2%	7,8%	-52,0%	-55,4%
		30	-8,5%	-3,4%	-52,9%	-51,2%
		40	-15,6%	0,1%	-36,0%	-36,0%
		50	-18,1%	3,5%	-10,2%	-13,3%
	EL ₂	20	-13,4%	-18,6%	-63,2%	-54,8%
		30	-7,3%	-7,0%	-55,0%	-51,5%
		40	-6,9%	3,9%	-54,9%	-56,6%
		50	-19,8%	1,9%	-15,8%	-17,4%
S6	EL ₁	20	-25,2%	-20,1%	-63,3%	-54,1%
		30	-14,2%	-9,2%	-53,3%	-48,5%
		40	-20,2%	-22,4%	-52,0%	-38,1%
		50	-20,8%	-0,4%	11,1%	11,6%
	EL ₂	20	-7,3%	9,1%	-64,9%	-67,8%
		30	-0,6%	-6,6%	-65,8%	-63,4%
		40	-19,9%	-12,5%	-69,2%	-64,8%
		50	-22,6%	14,0%	-32,3%	-40,7%
Average			-15,7%	-7,2%	-44,5%	-39,8%

Since the surface of the proposed system is only 0.275 m wide, it means that for the same area of Waynergy Vehicles system, three systems could be used, generating 217.2 J, a value more than twice as high. So, relating the energy generation to the area, under the same conditions, the proposed system is more efficient and generates more electrical energy.

5.6 Summary and Conclusions

Some technologies have been developed in recent years to convert vehicles' mechanical energy into electrical energy, mostly using mechanical systems to transmit the mechanical energy received by the equipment's surface to an electrical generator, which convert the mechanical energy into electrical energy. The electromechanical systems developed so far use mainly the RAP system and the lever system to perform the energy transmission, with an IW connected to the electrical generator shaft to deliver and store the mechanical energy. However, few studies present these systems modelling and calculating their efficiencies.

A new mechanical system to transmit and deliver the mechanical energy received by the RPEH surface to an electrical generator was developed in this research work. The physical models of the system were defined, as well as the physical models of the two mostly commonly used mechanical systems, as previously defined. The developed system, defined as a CTS system, aims to increase the force applied by the vehicle in the RPEH device surface, maximizing the energy delivered by the mechanical system to the electrical generator.

Based on the software tool presented in Chapter 3, an upgraded version was developed, in which the physical models of the three electromechanical systems presented in this Chapter were added. With this upgraded tool, some computational simulations were performed, to obtain the values of the energy harvested, transmitted, delivered, converted and consumed by the RPEH device.

From the analysis of the computational simulations results it can be concluded that the new mechanical system proposed, under the same conditions as the other two systems, presents a two times greater efficiency than the RAP and four times greater efficiency than the lever system for the same simulation scenario. Its main advantage is an increase in the transmitted force, leading to a higher mechanical energy transmission, meaning there is a greater acceleration of the pinion and, consequently, of the IW and the

generator shaft, leading to a higher rotation speed and a higher amount of energy transmission, delivery and conversion.

The experimental results obtained with a prototype based on the proposed system allowed most of the computational simulations results to be validated, with the exception of the electrical energy generated. The differences were understood and justified due to several parts added to the mechanical system so that it could become operational in a prototype. These changes added inertia and friction to the system, leading to lower energy generation values and lower energy conversion efficiencies, especially for lower vehicle speeds, where the forces were lower.

When comparing the experimental results with other RPEH devices, the achieved results can be considered positive, since these are better than all the existing systems, both in terms of conversion efficiency and electrical energy generated per area, with an average conversion efficiency of 52.6% for a vehicle speed of 50 km/h and a resistive electric load, and a maximum efficiency of 60.5% for VE_2 and a *S profile* surface, and a maximum energy generation of 72.4 J for the same scenario, using an area of 0.33 m².

The presented values are all for half a vehicle, meaning that the total amount of energy extracted from a vehicle, if two prototypes are used side-by-side, is twice the presented values. Also, the prototype surface has a total width of 0.275 m, meaning that multiple devices can be implemented consecutively in the pavement, maximizing the energy extraction in a small amount of space, which is another important goal of the project.

5.7 References

- Chapman, S. (2004). *Electric Machines Fundamentals, Fourth Edition*. McGraw-Hill, New York, NY, USA.
- Duarte, F., Champalimaud, J. and Ferreira, A. (2016). Waynergy Vehicles: an innovative pavement energy harvest system. *Proceedings of the Institution of Civil Engineers – Municipal Engineer*, 169(1): 13-18.

- Farnell (2017). IPL Linear Position Sensor data sheet. <http://www.farnell.com/datasheets/1833199.pdf>. Accessed in January, 2017.
- ISO (1997). *Mechanical vibration and shock - Evaluation of human response to whole-body vibration. Part I: General requirements*. ISO 2631-1, Geneva, Switzerland.
- Lyshevski, S. (2008). *Electromechanical Systems and devices*. CRC Press Inc, Boca Raton, FL, USA.
- Murthy, K. (2008). *Computer-aided design of electrical machines*. BS Publications, Hyderabad, India.
- National Instruments (2017). Data logger NI USB-6003 data sheet. <http://www.ni.com/pdf/manuals/374372a.pdf>. Accessed in January, 2017.
- Pirisi, A., Mussetta, M., Grimaccia, F. and Zich, R. E. (2013). Novel speed-bump design and optimization for energy harvesting from traffic. *IEEE Transactions on Intelligent Transportation Systems*, 14(4): 1983-1991.
- Texas Instruments (2017). INA 195 Data sheet. <http://www.ti.com/product/INA195>. Accessed in February, 2017.
- Todaria, P., Wang, L., Pandey, A., O'Connor, J., McAvoy, D., Harrigan, T. and Zuo, L. (2015). Design, modeling and test of a novel speed bump energy harvester. In *SPIE Smart Structures and Materials+ Nondestructive Evaluation and Health Monitoring* (pp. 943506-943514). International Society for Optics and Photonics.
- Vishay (2017). Load cell data sheet. <http://www.vishay.com/docs/12017/1250.pdf>. Accessed in January, 2017.

Chapter 6

Road Pavement Energy Harvesting: a New Hydraulic Device to Convert Vehicles Mechanical Energy into Electrical Energy

6.1 Introduction

A state-of-the-art study with the technologies used to convert vehicle mechanical energy into electrical energy was presented in Chapter 2. In these technologies, typical systems have the following components: a surface that receives energy from vehicle tyres and delivers energy to a transmission system; a system that transmits energy from the surface to an electrical generation unit; and an electrical unit that converts the mechanical energy into electrical energy, delivering it to an electrical application.

Piezoelectric systems are the simplest, as usually they receive the mechanical energy directly from the surface and convert it into electricity. However, these work on a micro energy harvesting scale and have a very small energy conversion efficiency and output.

Electromechanical systems transmit the energy received from the surface to electromagnetic generators, adapting the surface motion, which can be linear or rotational, into a similar or different motion, depending on the generator characteristics. These systems can work both on a micro or macro scale, having higher conversion efficiencies and energy outputs than piezoelectric systems, and are the most developed group of technologies in this field.

Hydraulic and pneumatic systems use the same principle as electromechanical systems, transmitting the energy received from the surface to electromagnetic generators. Typically, these systems work on a macro scale, allowing larger amounts of energy to be transferred. However, only a very small number of systems have been developed with this principle and none of them have presented viability, mainly due to the high costs of development and implementation.

In Chapter 5 a new electromechanical system was proposed, which revealed higher efficiency than all existing systems described in the literature. However, electromechanical systems have one limitation - for each EH unit, an energy conversion system is typically used. Beside other issues, to connect multiple EH units to a single energy conversion unit more mechanical elements and connections are needed, leading to a decrease in the system efficiency. To reduce the number of energy conversion units for multiple EH modules, an hydraulic RPEH device may present higher performance.

Considering this situation, different road pavement energy harvesting devices using hydraulic systems will be studied in this Chapter, and the most common system will be modelled and simulated, in order to study and come to conclusions about its theoretical efficiency. Also, a new hydraulic system with a mechanical actuation will be proposed, to transmit the energy received by the RPEH device surface (RPEH DS) into an electromagnetic generator, which will also be modelled and simulated, in order to come to a conclusion about its efficiency. The evaluation of each system is based on the developed systematic model and on the computations performed using the software tool presented in Chapters 3 and 5, upgraded with the hydraulic system's models.

6.2 RPEH Hydraulic System Development

6.2.1 Introduction

To transfer the energy received on the RPEH surface to an electric generator, different systems can be used. From the study presented in Chapter 2, it can be concluded that some of the existing RPEH devices have a hydraulic system to transmit the energy received on the equipment's surface into an electromagnetic rotational generator.

In this section, the hydraulic system most commonly used in RPEH devices will initially be analyzed and modelled. Then, a new hydraulic system with a mechanical actuation is presented and modelled as well. The electrical system used in this work is the same as the system presented in Chapter 5 and the same models are used. Finally, the equations that quantify the transmitted and delivered energy, as well as the efficiency of each process, will be defined.

6.2.2 Existing systems

Some companies and individual inventors have registered patents in which they use hydraulic mechanisms to harvest energy released from vehicles to the road pavement and convert it into electrical energy. These systems are designed to be implemented on roads, with the main systems presented in Chapter 2 (Angel and Gomez, 1997; Nakatsu, 1994; Galich, 2002; Kenney, 2004; Valon, 2007; Horianopoulos and Horianopoulos, 2007; Hendrickson, 2010a; Hendrickson, 2010b; Chang and Lee, 2011; Houghton, 2011).

Apart from the published patents, no technical studies are being published with experimental tests and results using these RPEH devices. From the analysis of the patents, the common working principle of these devices can be understood: the RPEH device surface, actuated by the vehicle wheels, actuates a hydraulic circuit underneath it by directly pressing a tube or a valve, which is connected to a hydraulic cylinder. This cylinder, typically a double acting cylinder (DAC), actuates a rack and pinion (RAP)

mechanical system in order to induce a rotational motion on a shaft, which is connected to an electrical generator.

Figure 6.1 presents a typical hydraulic system with a DAC connected to a RAP system. The surface of the RPEH device (RPEH DS) compresses a hydraulic fluid inside a hydraulic tube (TUB), through a contact area between both, and the fluid moves inside the DAC. If the fluid pressure is higher than the acceptable pressure, a pressure relief valve (PRV) directs the fluid back to the hydraulic reservoir (RES); if not, the fluid goes into the DAC, controlled by a hydraulic control valve (CV). The fluid exerts force onto the DAC piston, creating an oppositional force from the fluid between the DAC piston opposite side and the RES. The DAC piston is connected, by a rod, to an external RAP mechanical system which converts its linear motion into a rotational motion. The RAP system is connected to an inertia wheel (IW) which, in turn, is directly connected to an electrical generator. A spring is used under the RPEH DS to return it to its original position after the vehicle wheel leaves the contact.

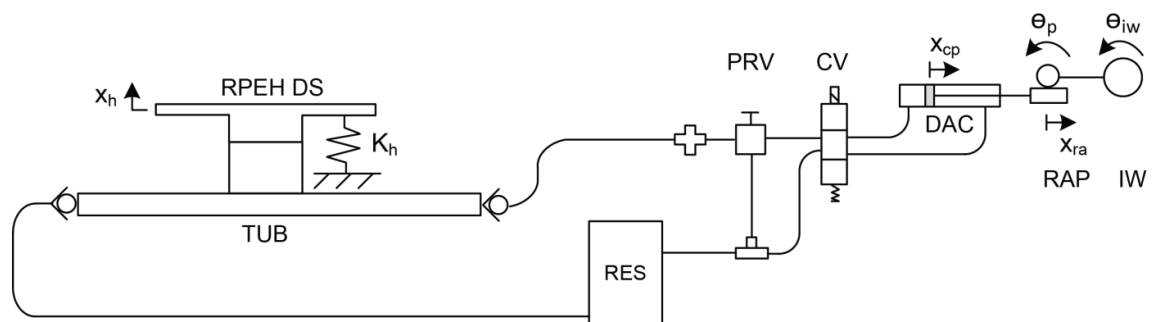
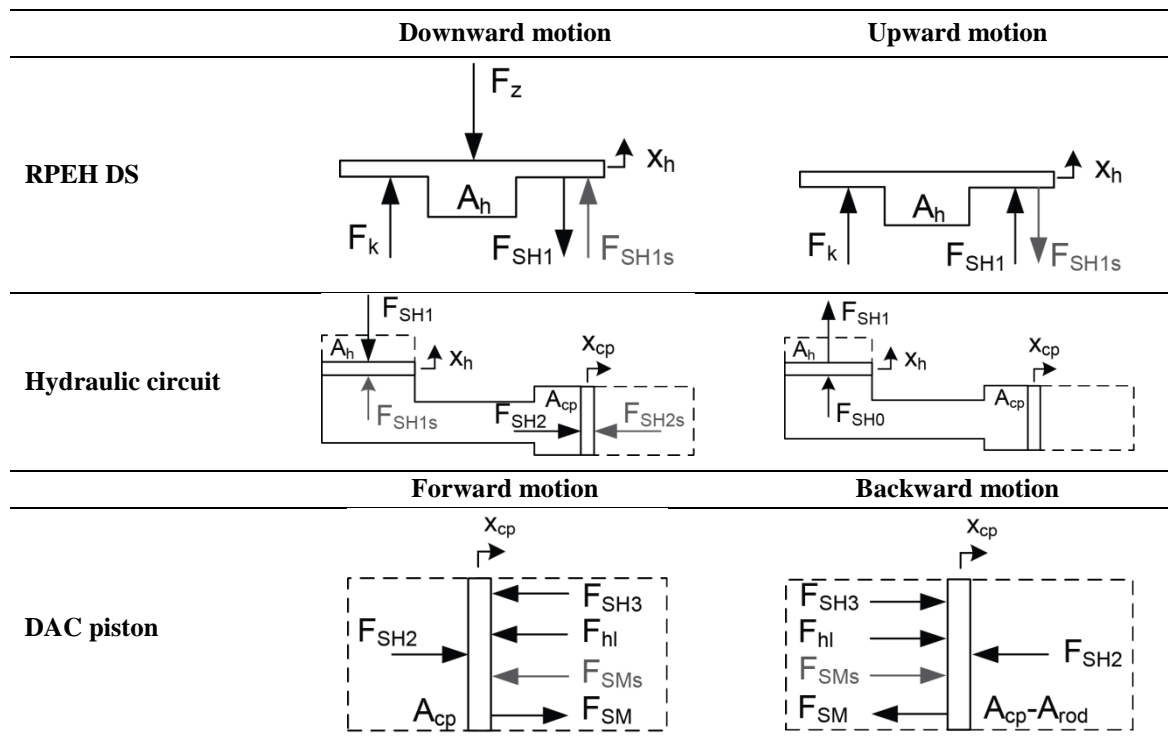


Figure 6.1- Hydraulic system with a DAC connected to a RAP mechanical system.

Table 6.1 presents the force diagrams for the different motion scenarios, both for the RPEH DS and the hydraulic installation directly connected to it and for the DAC piston of the hydraulic circuit, which is directly connected to the RAP system. The surface can have two motion scenarios, by moving downwards or upwards, while the DAC piston can have two different motion scenarios, by moving forwards or backwards. The indexes SH are related to the hydraulic circuit forces, while indexes SHs are related to

the hydraulic circuit reaction forces. The same happens for the forces in the mechanical system, using SM and SMs .

Table 6.1- Force diagrams for the RPEH DS, hydraulic circuit and DAC piston.



The working principles of hydraulic circuits and their components, as well as the main equations to model these systems are well understood and described in the literature (Rabie, 2009; Parr, 2011; and Durfee *et al.*, 2015).

Tables 6.2 and 6.3 summarize all the equations that define the RPEH hydraulic device. Table 6.2 defines the equations for the surface motion when it moves downwards, upwards, or when it is stopped, with a dynamic and forces analysis. Table 6.3 defines the equations for the DAC piston, the RAP system, and the IW, which is connected to an electrical generator, with a kinematic, dynamic, and forces analysis.

Table 6.2- RPEH DS physical modelling.

Analysis	Surface motion		
	Downward	Stopped	Upward
Dynamic	$\ddot{x}_h = \frac{1}{m_h} [F_{SH1s} + K_h x_h - F_z]$	$\dot{x}_h = 0$	$\dot{x}_h = \frac{1}{m_h} [K_h x_h]$
Forces	$F_{SH1} = F_z - K_h x_h$	$F_{SH1} = 0$	$F_{SH1} = -K_h x_h$

Table 6.3- RPEH hydraulic circuit with a DAC connected to a RAP system physical modelling.

Analysis	DAC piston motion		
	Forward	Stopped	Backward
Kinematic	$x_{cp} = \frac{A_h}{A_{cp}} x_h$		$x_{cp} = \frac{A_h}{(A_{cp} - A_{rod})} x_h$
	$x_{ra} = x_{cp}$	$x_{ra} = x_{cp}$	$x_{ra} = x_{cp}$
	$x_{cp} = r_p \theta_p \Leftrightarrow \theta_p = \frac{x_{cp}}{r_p}$	$\theta_p = \frac{x_{ra}}{r_p} = \frac{x_{cp}}{r_p}$	$x_{cp} = r_p \theta_p \Leftrightarrow \theta_p = \frac{x_{cp}}{r_p}$
	$\theta_{iw} = \theta_p = \frac{x_{cp}}{r_p}$		
Dynamic	$\ddot{x}_{cp} = \frac{1}{m_{cp}} [F_{SH2} - F_{hl} - F_{SH3} - F_{SMs}]$	$\ddot{x}_{cp} = \ddot{x}_{hf} = \ddot{\theta}_p = 0$	$\ddot{x}_{cp} = \frac{1}{m_{cp}} [F_{SH2} - F_{hl} - F_{SH3} - F_{SMs}]$
	$\ddot{x}_{hf} = \frac{A_{cp}}{A_{tub}} \ddot{x}_{cp}$	$\ddot{\theta}_{iw} = \frac{-(b_{cb} + b_{gen})\ddot{\theta}_{iw} - ET}{J_{iw} + J_{gen}}$	$\ddot{x}_{hf} = \frac{A_{cp}}{A_{tub}} \ddot{x}_{cp}$
	$\ddot{\theta}_p = \ddot{\theta}_{iw} = \frac{F_{SM} r_p - (b_{cb} + b_{gen})\ddot{\theta}_p - ET}{J_p + J_{sh} + J_{iw} + J_{gen}}$		$\ddot{\theta}_p = \frac{F_{SM} r_p - (b_{cb} + b_{gen})\ddot{\theta}_p - ET}{J_p + J_{sh}}$
Forces	$F_{SH2} = \frac{A_{cp}}{A_h} F_{SH1}$		$F_{SH2} = -\frac{A_{cp} - A_{rod}}{A_h} F_{SH1}$
	$F_{SM} = F_{SH2} - F_{hl} - F_{SH3}$		$F_{SM} = F_{SH2} + F_{hl} + F_{SH3}$
	$F_{SH3} = (p_{atm} - \Delta p_2) (A_{cp} - A_{rod}) - F_{hl2}$	$F_{SH2} = F_{SH3} = 0$	$F_{SH3} = p_{atm} A_{cp} - F_{hl2}$
	$F_{hl} = \Delta p A_{tub}$	$F_{SH1s} = F_{SH2s} = 0$	$F_{hl} = \Delta p A_{tub}$
	$F_{hl2} = \Delta p_2 A_{tub}$	$F_{hl} = F_{hl2} = 0$	$F_{hl2} = \Delta p_2 A_{tub}$
	$F_{SH1s} = \frac{A_h}{A_{cp}} F_{SH2s}$	$F_{SM} = F_{SMs} = 0$	$F_{SH1s} = \frac{A_h}{A_{cp} - A_{rod}} F_{SH2s}$
	$F_{SH2s} = F_{SH3} + F_{hl} + F_{SMs}$		$F_{SH2s} = F_{SH3} + F_{hl} + F_{SMs}$
	$F_{SMs} = \frac{(J_p + J_{sh} + J_{iw} + J_{gen})\ddot{\theta}_p + ET}{r_p}$		$F_{SMs} = \frac{(J_p + J_{sh})\ddot{\theta}_p}{r_p}$

In terms of the RPEH DS working principles, when the vehicle wheel force is higher than the spring force and the reacting force of the hydraulic circuit, the surface moves downwards, but when the vehicle wheel force is lower, it starts to decelerate, until motion is stopped. The motion of the surface is also stopped when the maximum allowable displacement is reached, with a mechanical limitation used to define the limit of the motion. When no vehicle load is applied on the surface and this is below its initial position, it will move upwards, through the spring force.

In terms of the hydraulic circuit, when it receives a force from the RPEH DS, it will increase or decrease such force depending on the relationship between the surface contact area (A_h) and the DAC piston contact area (A_{cp}), as presented in Table 6.3. The force delivered to the DAC piston is reduced by the hydraulic losses (F_{hl}), determined in relation to the pressure losses in the hydraulic circuit, which are determined through Equation (6.1), including both localized and head losses, considering laminar flow (Douglas *et al.*, 2005; Husain *et al.*, 2008).

$$\Delta p = \left(\frac{32 \mu l_{tub}}{\dot{x}_{hf} d_{tub}^2} + KH \frac{\rho}{2} + \frac{\rho}{2 C_d^2} \right) \dot{x}_{hf}^2 \quad (6.1)$$

Then, this force induces a displacement in the DAC piston in relation to the force balance between the force induced by the hydraulic circuit (F_{SH2}) and the opposition forces from the RAP mechanical system (F_{SMs}) and from a secondary hydraulic circuit between the DAC piston and the RES. A hydraulic CV controls the direction of the cylinder piston motion, allowing its direction to be inverted when it reaches its maximum displacement, by switching the fluid entrance and exit ports.

When the DAC piston moves forwards, it induces a motion with the same displacement on the rack, actuating a pinion and, by way of a shaft, actuating an IW directly connected to an electric generator. When the cylinder piston motion is stopped, the RAP motion is also stopped, but as a clutch bearing is used, the IW and the generator continue their motion while decelerating. When the DAC piston is moving backwards, for a standard RAP system with a clutch bearing, the rack will actuate the pinion in the

opposite direction, and this will not actuate the IW or, consequently, the electric generator.

6.2.3 New hydraulic system with mechanical actuation

In the hydraulic system previously presented, the force is directly transferred from the RPEH DS to the hydraulic fluid through a contact area, with the displacement of this interface being equal to the surface displacement. Analyzing the physical modulation of the system, it can be seen that the DAC piston motion is mostly determined by the hydraulic force exerted on it and the RAP motion is directly proportional to the DAC piston motion.

To maximize the force delivered to the hydraulic circuit, a new approach is proposed: the introduction of a mechanical system between the RPEH DS and the hydraulic circuit that multiplies the force received from the RPEH DS. The mechanical system is based in the crank to slider system presented in Chapter 5, and consists of a crank connected from the surface to a slider, converting the vertical motion of the surface into a longitudinal motion of the slider, decreasing the displacement and increasing the force from the surface to the slider. The slider is then connected to a single acting cylinder (SAC), through a piston with a specific area (A_{cp}). This compresses a fluid, which in turn is connected through a hydraulic circuit to a DAC. Then, a double acting RAP system is applied, which has two racks and two pinions moving in opposite directions, connected to the same shaft through clutch bearings, allowing the shaft rotation to keep going in the same direction and, consequently, delivering torque to the IW independently of the direction of the DAC piston motion. The complete system is presented in Figure 6.2.

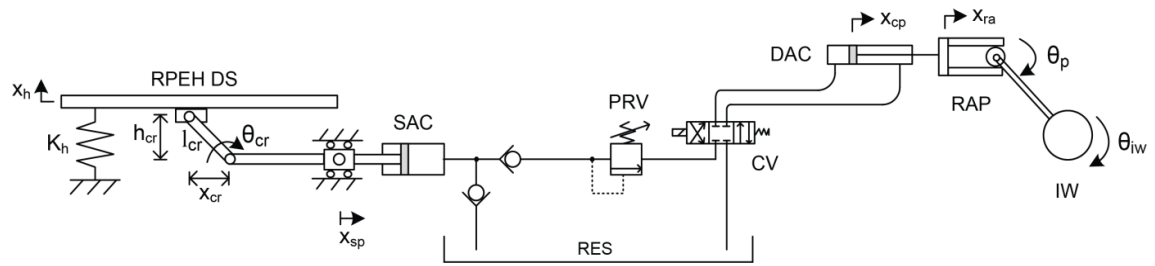


Figure 6.2- Hydraulic system with a mechanical actuation, connected to a double cylinder and a rack and pinion mechanical system.

Table 6.4- Force diagrams for the RPEH DS, mechanical system, hydraulic circuit and DAC piston.

	Downward motion	Upward motion
RPEH DS		
Mechanical system		
Hydraulic circuit		
	Forward motion	Backward motion
DAC piston		

Table 6.4 presents the force diagrams for the different motion scenarios, both for the RPEH DS, the mechanical system, and the hydraulic installation connected to it and for the DAC piston of the hydraulic circuit, which is directly connected to the double acting RAP system. The surface can have two motion scenarios, by moving downwards or upwards, while the DAC piston can have two different motion scenarios, by moving forwards or backwards.

Tables 6.5 and 6.6 summarize all the equations that define the RPEH hydraulic device with a mechanical actuation in terms of kinematic, dynamic, and forces analysis. Table 6.5 defines the equations for the RPEH DS motion when it moves downwards, upwards, or when it is stopped, as well as for the mechanical system directly connected to it. Table 6.6 defines the equations for the DAC piston, the RAP system, and the IW, which is connected to an electrical generator.

Table 6.5- RPEH DS and mechanical system physical modelling.

Analysis	Surface motion		
	Downward	Stopped	Upward
Kinematic	$h_{cr} = h_{cr-in} + x_h$		$h_{cr} = h_{cr-in} + x_h$
	$\theta_{cr} = \sin^{-1}\left(\frac{h_{cr}}{l_{cr}}\right)$	-	$\theta_{cr} = \sin^{-1}\left(\frac{h_{cr}}{l_{cr}}\right)$
	$x_{cr} = l_{cr} \cos\theta_{cr}$		$x_{cr} = l_{cr} \cos\theta_{cr}$
	$x_{sp} = x_{sp-in} + x_{cr}$		$x_{sp} = x_{sp-in} + x_{cr}$
Dynamic	$\ddot{x}_h = \frac{1}{m_h} [F_{SM1s} + K_h x_h - F_z]$	$\ddot{x}_h = \ddot{x}_{sp} = 0$	$\ddot{x}_h = \frac{1}{m_h} [K_h x_h - F_{SM1s}]$
	$\ddot{x}_{sp} = \frac{1}{m_{sp}} [F_{SM2} - F_{SM2s} - F_{los}]$		$\ddot{x}_{sp} = \frac{1}{m_{sp}} [-F_{SM2} + F_{SM2s} + F_{los}]$
Forces	$F_{SM1} = F_v - K_h x_h$		$F_{SM1} = K_h x_h$
	$F_{SH1} = F_{SM2} = \frac{F_{SM1}}{\tan\theta_{cr}} - F_{los}$	$F_{SM1} = F_{SM2} = F_{SH1} = 0$	$F_{SM2} = \frac{F_{SM1}}{\tan\theta_{cr}} - F_{los}$
	$F_{SM2s} = F_{SH1s}$	$F_{SM1s} = F_{SM2s} = 0$	$F_{SH0} = p_{atm} A_{sp}$
	$F_{SM1s} = (F_{SM2s} + F_{los}) \tan\theta_{cr}$		$F_{SM2s} = F_{SH0}$
			$F_{SM1s} = (F_{SM2s} + F_{los}) \tan\theta_{cr}$

Table 6.6- RPEH mechanically actuated hydraulic circuit with a DAC connected to a RAP system physical modelling.

Analysis	Cylinder piston motion		
	Forward	Stopped	Backward
Kinematic	$x_{cp} = \left(\frac{A_{sp}}{A_{cp}}\right) x_{sp}$		$x_{cp} = \left(\frac{A_{sp}}{A_{cp} - A_{rod}}\right) x_{sp}$
	$x_{ra} = x_{cp}$		$x_{ra} = x_{cp}$
	$x_{cp} = r_p \theta_p \Leftrightarrow \theta_p = \frac{x_{cp}}{r_p}$	-	$x_{cp} = r_p \theta_p \Leftrightarrow \theta_p = \frac{x_{cp}}{r_p}$
	$\theta_{iw} = \theta_p = \frac{x_{cp}}{r_p}$		$\theta_{iw} = -\theta_p = -\frac{x_{cp}}{r_p}$
Dynamic	$\ddot{x}_{cp} = \frac{1}{m_{cp}} [F_{SH2} - F_{hl} - F_{SH3} - F_{SMs}]$		$\ddot{x}_{cp} = \frac{1}{m_{cp}} [F_{SH2} - F_{hl} - F_{SH3} - F_{SMs}]$
	$\ddot{x}_{hf} = \left(\frac{A_{cp}}{A_{tub}}\right) \ddot{x}_{cp}$	$\ddot{x}_{cp} = \ddot{x}_{hf} = \ddot{\theta}_p = 0$	$\ddot{x}_{hf} = \left(\frac{A_{cp}}{A_{tub}}\right) \ddot{x}_{cp}$
	$\ddot{\theta}_p = \ddot{\theta}_{iw}$	$\ddot{\theta}_{iw} = \frac{-(b_{cb} + b_{gen}) \dot{\theta}_{iw} - ET}{J_{iw} + J_{gen}}$	$\ddot{\theta}_p = \frac{F_{SM3} r_p - (b_{cb} + b_{gen}) \dot{\theta}_p - ET}{J_p + J_{sh} + J_{iw} + J_{gen}}$
	$\ddot{\theta}_{iw} = \frac{F_{SM3} r_p - (b_{cb} + b_{gen}) \dot{\theta}_p - ET}{J_p + J_{sh} + J_{iw} + J_{gen}}$		$\ddot{\theta}_{iw} = -\frac{F_{SM3} r_p - (b_{cb} + b_{gen}) \dot{\theta}_p - ET}{J_p + J_{sh} + J_{iw} + J_{gen}}$
Forces	$F_{SH2} = \left(\frac{A_{cp}}{A_{sp}}\right) F_{SH1}$		$F_{SH2} = -\left(\frac{A_{cp} - A_{rod}}{A_{sp}}\right) F_{SH1}$
	$F_{SM3} = F_{SH2} - F_{hl} - F_{SH3}$		$F_{SM3} = F_{SH2} + F_{hl} + F_{SH3}$
	$F_{SH3} = (p_{atm} - \Delta p 2)(A_{cp} - A_{rod}) - F_{hl2}$	$F_{SH2} = F_{SH3} = 0$	$F_{SH3} = p_{atm} A_{cp} - F_{hl2}$
	$F_{hl} = \Delta p A_{tub}$	$F_{SH1s} = F_{SH2s} = 0$	$F_{hl} = \Delta p A_{tub}$
	$F_{hl2} = \Delta p 2 A_{tub}$	$F_{hl} = F_{hl2} = 0$	$F_{hl2} = \Delta p 2 A_{tub}$
	$F_{SH1s} = \left(\frac{A_{sp}}{A_{cp}}\right) F_{SH2s}$	$F_{SM3} = F_{SM3s} = 0$	$F_{SH1s} = \left(\frac{A_{sp}}{A_{cp} - A_{rod}}\right) F_{SH2s}$
	$F_{SH2s} = F_{SH3} + F_{hl} + F_{SM3s}$		$F_{SH2s} = F_{SH3} + F_{hl} + F_{SM3s}$
	$F_{SM3s} = \frac{(J_p + J_{sh} + J_{iw} + J_{gen}) \ddot{\theta}_p + ET}{r_p}$		$F_{SM3s} = \frac{(J_p + J_{sh} + J_{iw} + J_{gen}) \ddot{\theta}_p + ET}{r_p}$

6.2.4 Electrical system

To convert the mechanical energy delivered by the mechanical system into electrical energy, RPEH devices can use either DC or AC electric generators. Power electronics are then used to adapt the generated current to the electric load, depending on whether it consumes DC or AC power.

To simplify the physical modelling of the system and the computational simulations for the RPEH device under development, a DC generator connected to a DC load is used, as previously defined in Chapter 5. The considered circuit was presented in Figure 5.7, and the equations that fully characterize the electrical system are defined by Equations (5.6-5.10).

6.2.5 Energetic analysis

The energy lost by the vehicle during the interaction with the RPEH DS was already defined by Equation (3.18), while the energy harvested by the RPEH DS was also defined by Equation (3.21).

The energy transmitted to the cylinder piston is determined using Equation (6.2), relating the force applied in the piston to its displacement.

$$\partial E_{Tr} = F_{SH2} \partial x_{cp} \quad (6.2)$$

The energy delivered by the IW to the electric generator was already defined by Equation (5.3). The equations used to perform the energetic analysis of the electrical system were presented in Chapter 5, through Equations (5.11-5.14).

To evaluate the efficiency of the different components of the system, Equations (4.19), (5.4-5.5) and (5.15-5.16) can be used. The total efficiency of the system, from the vehicle lost energy to the electrical energy consumed by the electric load is defined by Equation (5.17). To determine the total efficiency of the mechanical and hydraulic systems, Equation (5.18) should be applied, relating the energy received by the mechanical-hydraulic system to the energy delivered to the electrical circuit. To determine the total efficiency of the electrical system, Equation (5.19) should be applied, and to determine the total efficiency of the RPEH internal device, Equation (5.20) should be applied, relating the energy received by the mechanical-hydraulic system to the energy consumed by the electric load.

6.3 Technical Analysis

6.3.1 Introduction

Based on the software tools presented in Chapters 3 and 5, the equations of the RPEH devices presented in the previous section were incorporated for the different hydraulic and mechanical-hydraulic systems.

The purpose of the simulation software is to study the complete interaction of all elements in great detail, with the possibility of fully characterizing the vehicle under study, the RPEH device surface, as well as the hydraulic, mechanical and electrical properties of the RPEH device, depending on the system selected.

The software tool calculates all the forces and displacements for both the vehicle components and the RPEH device surface, as well as for the hydraulic, mechanical, and electrical system components. After that, it calculates the different energies transferred from each part of the system to the others and the efficiency of each energy transfer process.

The simulations performed with the software tool for the two hydraulic systems presented in the previous section will be presented in this section, using the same RPEH equipment surface profile, geometry and displacement, the same vehicle, and the same electric generator and load. The goal is to evaluate the different hydraulic systems and to draw conclusions about each system's efficiency in transmitting and delivering mechanical energy.

One RPEH device connected to one hydraulic or mechanical system is considered, which, in turn, is connected to one electrical system, as the surface is actuated by one side of the vehicle. So, the value presented for the energy lost by the vehicle is in relation to half the vehicle, as only one front and one rear wheel actuates the RPEH device surface.

The parameters defined for the vehicle, the RPEH device surface, and the hydraulic, mechanical, and electrical systems, common in the simulations of both systems, are presented in Table 6.7.

Table 6.7- Input data for the computational simulations of the hydraulic systems.

	Variable name	Value	Unit
Vehicle & motion	Vehicle class	Light	-
	Vehicle weight	1,500	(kg)
	Number of axles P1 wheels per axle	2 2	-
	Sprung-Unsprung %	90%-10%	-
	Drag coefficient	0.32	-
	Inertia moment	1,100	(kg.m ²)
	Lift coefficients (Front Rear)	0.19 0.13	-
	Motion Direction	Free rolling Forward	-
	Vehicle speed acceleration	40 0	(km/h) (m/s ²)
Suspension & wheel	Suspension type (Front Rear)	Independent Independent	-
	Suspension stiffness (Front Rear)	20,000 15,000	(N/m)
	Suspension damping (Front Rear)	1,500 1,700	(Ns/m)
	Tyre type (Front Rear)	Radial Radial	-
	Tyre stiffness (Front Rear)	150,000 150,000	(N/m)
	Tyre pressure (Front Rear)	200 200	(kPa)
	Tyre external diameter (Front Rear)	500 500	(mm)
	Tyre width (Front Rear)	200 200	(mm)
	Tyre tread width (Front Rear)	180 180	(mm)
RPEH device	Surface width	250	(mm)
	Surface mass	20	(kg)
	Surface max. height max. displacement	20 20	(mm)
	Spring stiffness	30,000	(N/m)
	Hydraulic fluid	Oil SAE 30	-
	Hydraulic fluid density kinematic viscosity	865 105	(kg.m ³) (cSt)
	Hydraulic circuit CV discharge coef. KH	2.48 10.50	- -
	Hydraulic tube length	3	(m)
	Hydraulic reservoir pressure	101,325	(Pa)
	Hydraulic cylinder stroke	250	(mm)
	Pinion mass radius friction coefficient	1 20 0.002	(kg) (mm) -
	Inertia wheel mass radius	10 30	(kg) (mm)
	Electric generator constant Ka	0.25	-
	Electric generator Ra La	1.1 0.0048	(Ω) (H)
	Electric generator friction coefficient Inertia	0.0008 0.05	- (kg.m ²)
Electric load Power	50	(W)	

6.3.2 Typical hydraulic system

Considering the input data presented in Table 6.7, simulations for the standard hydraulic system were performed on two different surface profiles (*Ramp* and *Crest*), presented in Chapter 3. The RAP mechanical system, electric generator, and electric load characteristics were not changed; one of the goals is to study the impact of the hydraulic system and its characteristics in the performance of the RPEH device. For the hydraulic system, different values for the contact area between the surface and the hydraulic circuit (A_h), which defines the interaction area between the received force and the hydraulic fluid, were considered. Also, different values for the hydraulic tube area (A_{tub}) and the hydraulic cylinder area (A_{cp}) were considered. The goal is to evaluate the impact of these variables in the energy transmitted.

Table 6.8- Simulation results for the energy outputs of the RPEH device components using a standard hydraulic system.

SP	A_h (mm ²)	A_{tub} (mm ²)	A_{cp} (mm ²)	E_v (J)	E_{Ha} (J)	E_{Tr} (J)	E_{De} (J)	E_{Ge} (J)	E_{Lo} (J)
S5	20	2,5	12	257.0	92.0	73.0	9.0	7.2	5.8
			25	260.0	92.0	70.0	39.0	33.8	27.3
			50	265.0	92.0	65.0	49.5	44.6	36.2
	40	5	12	257.0	92.0	67.0	5.0	4.0	3.2
			25	257.0	96.0	71.0	27.0	22.9	18.4
			50	262.0	92.0	65.0	46.5	41.8	33.8
S8	20	2,5	12	256.0	97.0	59.0	5.5	4.4	3.4
			25	254.0	97.0	67.0	16.0	13.4	10.8
			50	256.0	96.0	64.0	28.0	23.7	19.0
	40	5	12	245.0	100.0	60.0	6.0	4.8	3.8
			25	254.0	96.0	60.0	8.0	6.6	5.3
			50	255.0	97.0	63.0	16.0	13.4	10.8
S8	20	2,5	12	183.0	102.0	77.0	9.0	7.2	5.8
			25	178.0	97.0	71.0	41.0	35.4	28.6
			50	176.0	93.0	67.0	49.0	44.1	35.8
	40	5	12	186.0	105.0	77.0	4.0	3.2	2.5
			25	180.0	100.0	72.0	26.0	22.0	17.7
			50	175.0	105.0	90.0	32.0	27.2	21.8

To evaluate the system's performance, the vehicle released energy (E_v), RPEH surface harvested energy (E_{Ha}), mechanical system transmitted energy (E_{Tr}), mechanical system delivered energy (E_{De}), electrical system generated energy (E_{Ge}), and electrical system consumed energy (E_{Lo}) were calculated. Also, the efficiencies of the energy transferred between each part of the system were evaluated.

Table 6.8 presents the simulation results for the energy output of each component of the RPEH device using the standard hydraulic system, considering the input data presented in Table 6.7. Table 6.9 presents the simulation results for the efficiency of each component of the system, as well as the total efficiency of the device.

Table 6.9- Simulation results for the efficiencies of the RPEH device components using a standard hydraulic system.

SP	A_h (mm ²)	A_{tub} (mm ²)	A_{cp} (mm ²)	η_{Ha} (%)	η_{Tr} (%)	η_{De} (%)	η_{Ge} (%)	η_{Co} (%)	η_{Mec} (%)	η_{Ele} (%)	η_{RPEH} (%)	η_{TOT} (%)
S5	20	2,5	12	35.8	79.3	12.3	80.1	79.9	9.8	64.0	6.3	2.2
			25	35.4	76.1	55.7	86.6	80.8	42.4	70.0	29.7	10.5
			50	34.7	70.7	76.2	90.1	81.1	53.8	73.1	39.3	13.6
		5	12	35.8	72.8	7.5	79.8	79.7	5.4	63.6	3.5	1.2
			25	37.4	74.0	38.0	84.7	80.3	28.1	68.0	19.1	7.1
			50	35.1	70.7	71.5	89.9	80.8	50.5	72.6	36.7	12.9
	40	2,5	12	37.9	60.8	9.3	79.5	78.9	5.7	62.7	3.6	1.3
			25	38.2	69.1	23.9	83.9	80.5	16.5	67.5	11.1	4.3
			50	37.5	66.7	43.8	84.7	80.3	29.2	68.0	19.8	7.4
		5	12	40.8	60.0	10.0	79.5	78.9	6.0	62.7	3.8	1.5
			25	37.8	62.5	13.3	82.9	79.9	8.3	66.2	5.5	2.1
			50	38.0	64.9	25.4	83.9	80.5	16.5	67.5	11.1	4.2
S8	20	2,5	12	55.7	75.5	11.7	80.1	79.9	8.8	64.0	5.6	3.1
			25	54.5	73.2	57.7	86.4	80.7	42.3	69.7	29.5	16.1
			50	52.8	72.0	73.1	90.1	81.1	52.7	73.1	38.5	20.3
		5	12	56.5	73.3	5.2	79.6	79.5	3.8	63.3	2.4	1.4
			25	55.6	72.0	36.1	84.7	80.3	26.0	68.0	17.7	9.8
			50	60.0	85.7	35.6	84.9	80.4	30.5	68.3	20.8	12.5

6.3.3 Hydraulic system with mechanical actuation

Considering the same conditions as for the standard hydraulic system, simulations for the hydraulic system with mechanical actuation were also performed and the main results are presented in Tables 6.10 and 6.11 for the energy output and the efficiency of each component of the system, respectively. The same variables were changed between simulations in order to make a direct comparison between both systems. The mechanical system parameters defined for the simulations are as follows: crank length (l_{cr}) equal to 0.04m and crank initial height between the two axes (h_{cr-in}) equal to 0.03 m.

Table 6.10- Simulation results for the energy outputs of the RPEH device components using a hydraulic system with mechanical actuation.

SP	A_{sp} (mm ²)	A_{tub} (mm ²)	A_{cp} (mm ²)	E_v (J)	E_{Ha} (J)	E_{Tr} (J)	E_{De} (J)	E_{Ge} (J)	E_{Lo} (J)
S5	20	2,5	12	261.0	91.0	81.0	63.0	57.0	46.3
			25	267.0	85.0	75.0	69.5	63.1	51.5
			50	271.0	81.0	72.0	71.3	64.8	53.0
		5	12	261.0	91.0	82.0	63.0	57.0	46.3
			25	268.0	85.0	76.0	70.0	63.6	51.9
			50	271.0	80.0	72.0	71.3	64.8	53.0
	40	2,5	12	259.0	92.0	83.0	28.0	23.7	19.0
			25	263.0	88.0	79.0	59.5	53.7	43.6
			50	270.0	81.0	73.0	66.0	60.1	49.2
		5	12	259.0	92.0	83.0	28.0	23.7	19.0
			25	264.0	88.0	79.0	59.5	53.7	43.6
			50	268.0	83.0	74.0	66.5	60.6	49.6
S8	20	2,5	12	200.0	94.0	83.0	72.0	65.6	53.7
			25	192.0	95.0	84.5	78.0	71.2	58.3
		5	50	184.0	101.0	94.5	93.5	85.6	70.2
			12	192.0	86.0	77.0	75.0	68.4	56.0
	5	2,5	25	188.0	87.0	80.0	78.0	71.4	58.5
			50	181.0	89.0	88.0	87.5	79.9	65.4

Table 6.11- Simulation results for the efficiencies of the RPEH device components using a hydraulic system with mechanical actuation.

SP	A _{sp} (mm ²)	A _{tub} (mm ²)	A _{cp} (mm ²)	η _{Ha} (%)	η _{Tr} (%)	η _{De} (%)	η _{Ge} (%)	η _{Co} (%)	η _{Mec} (%)	η _{Ele} (%)	η _{RPEH} (%)	η _{TOT} (%)
S5	20	2.5	12	34.9	89.0	77.8	90.4	81.3	69.2	73.5	50.9	17.7
			25	31.8	88.2	92.7	90.8	81.6	81.8	74.1	60.6	19.3
			50	29.9	88.9	99.0	91.0	81.7	88.0	74.3	65.4	19.5
		5	12	34.9	90.1	76.8	90.4	81.3	69.2	73.5	50.9	17.7
			25	31.7	89.4	92.1	90.9	81.6	82.4	74.2	61.1	19.4
			50	29.5	90.0	99.0	91.0	81.7	89.1	74.3	66.2	19.5
	40	2.5	12	35.5	90.2	33.7	84.7	80.3	30.4	68.0	20.7	7.4
			25	33.5	89.8	75.3	90.3	81.2	67.6	73.3	49.6	16.6
			50	30.0	90.1	90.4	91.1	81.8	81.5	74.5	60.7	18.2
		5	12	35.5	90.2	33.7	84.7	80.3	30.4	68.0	20.7	7.4
			25	33.3	89.8	75.3	90.3	81.2	67.6	73.3	49.6	16.5
			50	31.0	89.2	89.9	91.1	81.8	80.1	74.5	59.7	18.5
S8	20	2.5	12	47.0	88.3	86.7	91.1	81.8	76.6	74.5	57.1	26.8
			25	49.5	88.9	92.3	91.3	81.9	82.1	74.8	61.4	30.4
			50	54.9	93.6	98.9	91.5	82.0	92.6	75.0	69.5	38.1
		5	12	44.8	89.5	97.4	91.2	81.8	87.2	74.6	65.1	29.1
			25	46.3	92.0	97.5	91.5	82.0	89.7	75.0	67.3	31.1
	40	5	50	49.2	98.9	99.4	91.3	81.9	98.3	74.8	73.5	36.1

6.3.4 Results analysis

Analyzing the results obtained with the computational simulations of the RPEH device, for both the standard hydraulic system with a double acting cylinder directly actuated by the RPEH device surface and the same hydraulic system actuated by a mechanical system connected to the equipment's surface, some conclusions may be drawn.

Globally, the RPEH surface harvested energy efficiency depends on the surface profile, varying significantly for each studied profile. Using the *Crest* surface profile, the surface energy harvesting efficiency can be 60% higher than with the *Ramp* surface profile, under the same conditions.

For the standard hydraulic system, the average energy transmission efficiency is around 71%, which is a high value, but the average energy delivery efficiency is around 33%, which is a low value. For the hydraulic system with mechanical actuation, the average energy transmission efficiency is around 90% and the average energy delivery efficiency is around 84%, both of which are very high values, especially when compared to the standard hydraulic system.

These higher transmission and delivery efficiency values are achieved due to the inclusion of the mechanical system acting as the hydraulic system, as the force delivered to the hydraulic circuit increases, allowing the force applied in the cylinder piston to be maximized and, consequently, to have a higher acceleration of this element and a higher energy transmitted by it. With a higher force applied in the cylinder piston, a higher force is transmitted to the rack and pinion system, leading to a higher acceleration induced in the generator and inertia wheel shaft and to a higher rotational speed, leading to more mechanical energy being delivered to the electrical generator.

The DC electrical generator efficiency varies in relation to the energy delivered, as it is associated with its rotational speed. For lower rotational speeds, its efficiency is lower than 85%, while for higher rotational speeds, it is higher than 90%. The electric energy consumption efficiency is usually around 80% for the considered electrical load and using a diode between the electrical generator and the load.

Considering the variables that were changed between simulations, it may be concluded that:

- Increasing the contact area between the RPEH device surface and the hydraulic circuit, A_h , for standard hydraulic systems, or the SAC area, A_{cp} , for the new proposed system, leads to a decrease in the energy transmission efficiency (E_{Tr}) due to a decrease in the force transmitted to the DAC piston. So, A_h and A_{cp} should be as small as possible to maximize the force delivered to the cylinder piston and, consequently, the energy transmitted.
- Increasing the area of the hydraulic circuit tubes (A_{tub}) decreases the efficiency of the system, as it decreases the fluid velocity and, consequently, the fluid flow

rate transmitted to the cylinder piston. So, A_{tub} should be as small as possible to maximize the fluid velocity and, consequently, the energy transmitted to the DAC piston. However, attention should be paid to the fact that with the increase in the fluid velocity its losses will also increase.

- Increasing the area of the DAC (A_{cp}) leads to an increase in the efficiency of the system, as the force transmitted by the hydraulic circuit is amplified and the cylinder piston has a higher acceleration, leading to greater energy transmission efficiency.

Excluding the energy lost by the vehicle and considering the energy harvested by the surface as the input of the system, the global efficiency of the RPEH device using a standard hydraulic system can reach 40% for the considered and simulated values and, using a similar hydraulic system actuated by the proposed mechanical system, it can reach 74%, already including the electrical energy losses. This value represents a much higher energy conversion rate than that of all the RPEH devices presented in the literature and presented in Chapter 2, and is similar to the maximum efficiency registered in the computational simulations of the crank to slider electromechanical system presented in Chapter 5.

In all the performed simulations the vertical acceleration induced by the RPEH device to the vehicle body was lower than 1 m/s^2 . Considering the existing levels of acceptability of the ride quality (ISO, 1997), this indicates that the proposed RPEH device does not cause discomfort to the vehicle driver and to its occupants.

6.4 Summary and Conclusions

Different technologies have been developed in recent years to convert vehicles' mechanical energy into electrical energy, in places where vehicles need to release energy to the pavement to reduce their speed, some of them using hydraulic systems to transmit the mechanical energy received by the equipment's surface to an electrical

generator, which convert the mechanical energy into electrical energy. Most RPEH devices using hydraulic systems developed so far induce pressure from the equipment's surface to the fluid inside a hydraulic tube, transmitting it to a double acting cylinder. This is controlled by a hydraulic control valve and transmits the mechanical energy to a mechanical rack and pinion system, connected to an electric generator shaft with an inertia wheel. The electric generator converts the mechanical energy into electrical energy, delivering it to an electrical application. However, few studies model and calculate the efficiency of these systems.

A means of assessing the efficiency of a new hydraulic system with a mechanical actuation to transmit the mechanical energy received by the RPEH surface to the hydraulic circuit was developed in this Chapter. The physical models of the system were defined, as well as the physical models of a standard hydraulic system. The new system aims to increase the force received by the RPEH device surface and delivered to the hydraulic circuit, maximizing the energy transmitted by the hydraulic system and delivered to the electrical generator.

With both hydraulic systems modelled, as well as the rest of the RPEH device, and using a software previously developed and presented in Chapters 3 and 5, upgraded with the models developed in this Chapter, some computational simulations were performed in order to obtain the values of the energy harvested, transmitted, delivered, converted, and consumed by the RPEH device, as well as the efficiency of each process.

From the analysis of the results, it can be concluded that the proposed new system, under the same conditions as a standard hydraulic system, presents greater efficiency for the same simulation scenarios. The new system reaches mechanical energy transmission and delivery efficiency of more than 95% and global efficiency from the mechanical energy harvested by the surface to the electrical energy consumed by the electric load of 74%, almost two times higher than the best scenario for a standard hydraulic system.

Its main advantage is in the greater force transmitted from the surface to the hydraulic circuit, leading to a higher mechanical energy transmission. This particular characteristic means that higher accelerations can be induced on the cylinder piston and,

consequently, higher acceleration and rotational speed can be achieved in the inertia wheel and the generator shaft, leading to higher delivery and conversion efficiency.

The systematic model developed in this Chapter and the computations performed with this model have allowed to draw important conclusions regarding the most efficient characteristics for the proposed solution.

The proposed system should be tested experimentally, to validate the results from computational simulations and allow us to conclude about the technical viability of the system.

6.5 References

- Angel, R. and Gomez, J. (1997). *Road vehicle-actuated air compressor*. US Patent US5634774, Jun.
- Chang, H. and Lee, C. (2011). *On-road energy conversion and vibration absorber apparatus*. US Patent US20110215593 A1, Sep.
- Douglas, J., Gasiorek, J., Swaffield, J. and Jack, L. (2005). *Fluid Mechanics, Fifth Edition*. Pearson Education Limited, Essex, UK.
- Durfee, W., Sun, Z. and Van de Ven, J. (2015). *Fluid Power System Dynamics*. University of Minnesota, Minneapolis, MN, USA.
- Galich, T. (2002). *Force stand for electrical energy producing platform*. US Patent US6376925 B1, Apr.
- Hendrickson, B. (2010a). *Adaptive, Low-impact vehicle energy harvester*. US Patent US20100192561 A1, Aug.
- Hendrickson, B. (2010b). *Vehicle energy harvesting roadway*. International Patent Application PCT/US2010/020676, Patent WO2010081113 A1, Jul.

- Horianopoulos, D. and Horianopoulos, S. (2007). *Traffic-actuated electrical generator apparatus*. International Patent Application PCT/CA2006/001710, Patent WO 2007045087 A1, Apr.
- Houghton, L. (2011). *Hydraulic powermat*. UK Patent Application GB 2476826 A, Intellectual Property Office, UK, Jul.
- Husain, Z., Abdullah, Z. and Alimuddin, Z. (2008). *Basic fluid mechanics and hydraulic machines*. BS Publications, Hyderabad, India.
- ISO (1997). *Mechanical vibration and shock - Evaluation of human response to whole-body vibration. Part I: General requirements*. ISO 2631-1, Geneva, Switzerland.
- Kenney, T. (2004). *System and method for electrical power generation utilizing vehicle traffic on roadways*. US Patent US20040130158 A1, Jul.
- Nakatsu, S. (1994). *Road apparatus*. UK Patent Application GB2290115 A, Dec.
- Parr, A. (2011). *Hydraulics and pneumatics: a technician's and engineer's guide*. Elsevier, Oxford, UK.
- Rabie, M. (2009). *Fluid power engineering*. McGraw-Hill, New York, NY, USA.
- Valon, F. (2007). *Highway's electrogenerators*. US Patent US 20070246940 A1, Oct.

Chapter 7

Integration of a Mechanical Energy Storage System in a Road Pavement Energy Harvesting Hydraulic Device

7.1 Introduction

In Chapter 2, a state-of-the-art study of the technologies used to convert vehicle mechanical energy into electrical energy which can be implemented on road pavements was presented. In these technologies, most part of the systems have the following components: a surface that receives energy from vehicle tyres and delivers energy to a transmission system; a system that transmits energy from the surface to an electrical generation unit; and an electrical unit that converts the mechanical energy into electrical energy, delivering it to an electrical application. Some systems include electrical energy storage units, but almost no system includes mechanical energy storage (MES).

Analyzing some published results from RPEH device experimental tests performed in laboratory environment (Pirisi *et al.*, 2013; Todaria *et al.*, 2015; Duarte *et al.*, 2016a), it may be concluded that electric generators are actuated only when there is a vehicle passage, leading to a lower efficiency of these components when compared to their

optimal performance, as energy is spent to accelerate them, then they convert mechanical energy into electrical energy with acceptable levels of efficiency but, then, they slow down again if a vehicle actuates the RPEH device. Electrical generators of typical RPEH devices work in pulsed mode, decreasing the global efficiency of the device.

In other renewable energy source studies (Ibrahim *et al.*, 2008; Chen *et al.*, 2009; Barnes and Levine, 2011; Steinke *et al.*, 2013) the inclusion of MES devices was evaluated, so that the mechanical energy received by the energy harvesting and energy transmission elements could be stored and when mechanical energy is delivered to the electrical generator, this occurs in a continuous mode, instead of the typical intermittent mode, increasing the global efficiency of the energy conversion device. Storing water in dams for a continuous discharge over electrical generators is a classic example of this method (Huggins, 2010; Ter-Gazarian, 2011; Wood and Wollenberg, 2012). A similar process can be implemented in RPEH devices by storing the mechanical energy harvested from vehicle wheels and transmitted by a mechanical or a hydraulic system, delivering it in a continuous mode to the electrical generator of the device, increasing its efficiency.

Following the development of a RPEH device in Chapter 6, using mechanical and hydraulic systems, and using the same methodology, the application of mechanical energy storage devices will be studied, as will their integration both with typical RPEH devices based on hydraulic systems and the new RPEH device based on a hydraulic system with mechanical actuation presented in Chapter 6. Four complete systems will be modelled and simulated, in order to come to a conclusion about the variation of the device efficiencies.

7.2 Mechanical Energy Storage System for Hydraulic Devices

7.2.1 Introduction

For an RPEH device, vehicles provide the source of energy, as they induce a displacement on the device's surface, which will be transmitted to an electric generator through a mechanical or hydraulic system. Vehicle tyres interact between the vehicle and the RPEH device, inducing a force on its surface. In Chapter 3, complete models of the VRI were presented, including models that quantify the energy delivered from vehicle' tyres to a RPEH DS.

In Chapter 6, a typical RPEH device based on a hydraulic system was presented, as well its physical models. Also, a new system that combines the most common hydraulic system used in RPEH devices with a mechanical system to actuate it was presented, including the electrical system of the device. The equations that quantify the transmitted and delivered energy were defined, as well as the converted and consumed electrical energy. The efficiency of each process was also defined.

The equations regarding the energy lost by the vehicle (E_v), the energy harvested by the RPEH DS (E_{Ha}), the mechanical energy transmitted and delivered (E_{Tr} and E_{De}) and the electrical energy generated and consumed (E_{Ge} and E_{Lo}) were defined in Chapters 3, 5 and 6. In this section, different MES systems will be studied and modelled, and then incorporated into different RPEH device's models. The equations that quantify both the stored mechanical energy and the energy conversion efficiency will be defined.

7.2.2 Hydraulic pressure storage

A hydraulic accumulator is a device that stores the potential energy of an incompressible fluid held under pressure by an external source against some dynamic force, which can come from three different sources: gravity (using a weight);

mechanical spring; or a compressed gas. The potential energy stored in the accumulator becomes a quick secondary source of fluid power, capable of realizing useful work when required by the system (Mobley, 1999; Rabie, 2009; Parr, 2011; Durfee *et al.*, 2015). There are three basic types of hydraulic accumulators used in hydraulic systems: weight-loaded type; spring-loaded type; and gas-loaded type.

In the weight-loaded type, the force of gravity acting on a weight above the cylinder ram pressurizes the fluid inside the cylinder. As the force is constant and the area of the cylinder piston is also constant, the pressure inside the cylinder is kept constant during the process. This is the least commonly used type of accumulator and will not be explored in this work.

The spring-loaded type is similar to the weight loaded system, except that piston is preloaded with a spring, which is the source of energy that acts against the piston forcing the fluid into the hydraulic system. The pressure generated by this type of accumulator depends on the size and preloading of the spring. Also, the pressure exerted on the fluid is not constant.

A representation of a spring-loaded hydraulic accumulator is presented in Figure 7.1. It has a spring with stiffness K_{sto} , compressed by the accumulator piston, which moves with a displacement x_{sto} . The fluid input and output is controlled by a hydraulic accumulator control valve (ACV).

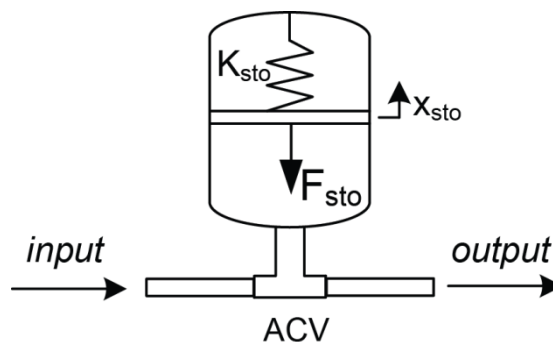


Figure 7.1- Representation of a spring-loaded hydraulic accumulator.

When the fluid enters the hydraulic accumulator with a force F_{SH} , the opposition force of the MES system is given by F_{sto} , determined by Equation (7.1). When the fluid exits the accumulator, it has a pressure defined by Equation (7.2), with A_{sto} representing the accumulator piston area. While the valve is closed, the fluid will keep the pressure p_{sto} through the energy stored by the spring, which pressurizes the fluid under the accumulator piston.

$$F_{sto} = K_{sto}x_{sto} \quad (7.1)$$

$$p_{sto} = \frac{F_{sto}}{A_{sto}} \quad (7.2)$$

Gas-loaded accumulators operate according to Boyle's law of gases which states that, for a constant temperature process, the pressure of a gas varies inversely to its volume. This means that, for example, the gas volume of the accumulator would be reduced to half if the pressure were doubled. Gas-loaded accumulators can have three different sub-types, according to the separation between the circuit fluid and the gas: piston type; diaphragm-type; and bladder-type. In this work, a piston separated system was used.

Figure 7.2 shows a representation of a gas-loaded accumulator, piston type, which has a chamber filled with gas above the piston, with a volume V_{gas} and a pressure p_{gas} , compressed by the accumulator piston, which moves with a displacement x_{sto} . The fluid input and output is controlled by a hydraulic ACV.

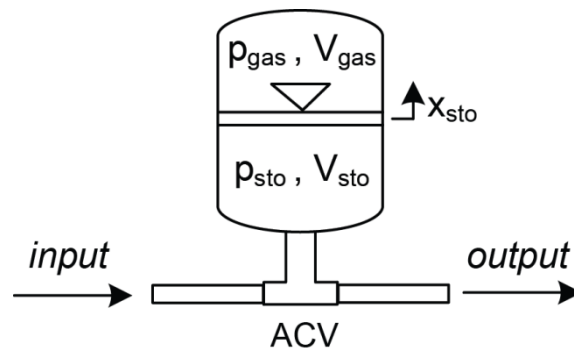


Figure 7.2- Representation of a gas-loaded hydraulic accumulator.

When the fluid enters to the hydraulic accumulator with a force F_{SH} , it will induce a displacement in the accumulator piston, compressing the gas above it and decreasing its volume (V_{gas}). Equation (7.3) defines the pressure variation of the gas depending on the variation of its volume, with the stored pressure to be equal to the gas pressure. The force exerted by the accumulator piston in the fluid is defined by Equation (7.4), which represents the force delivered to the hydraulic system when the fluid exits the accumulator.

$$p_{Gas-i} = \frac{V_{Gas_i}}{V_{Gas_{i-1}}} p_{Gas_{i-1}} \quad (7.3)$$

$$F_{sto} = p_{sto} A_{sto} \quad (7.4)$$

7.2.3 Standard RPEH device with hydraulic system with integrated mechanical energy storage

Considering a RPEH device with a typical hydraulic system transmitting the mechanical energy from the equipment's surface to a mechanical system and to an electromagnetic generator, based on standard hydraulic systems as presented in Chapter 6, two MES systems based on hydraulic pressure storage devices are presented. Figure 7.3 presents the RPEH device with a spring-loaded hydraulic accumulator working as a MES system and Figure 7.4 presents the RPEH device with a gas-loaded hydraulic accumulator, piston type, working as a MES system.

The working principle of both systems is the same, each having two storage stages: receiving energy and releasing energy. In the receiving energy stage, when the RPEH DS is moving downwards, it transmits a force onto the fluid inside the hydraulic circuit, which is transmitted to the hydraulic accumulator through the fluid pressure. The ACV lets the fluid in if the pressure is higher than the pressure inside the accumulator, inducing a displacement of the accumulator piston. If the fluid pressure is lower than the accumulator pressure, the valve remains closed.

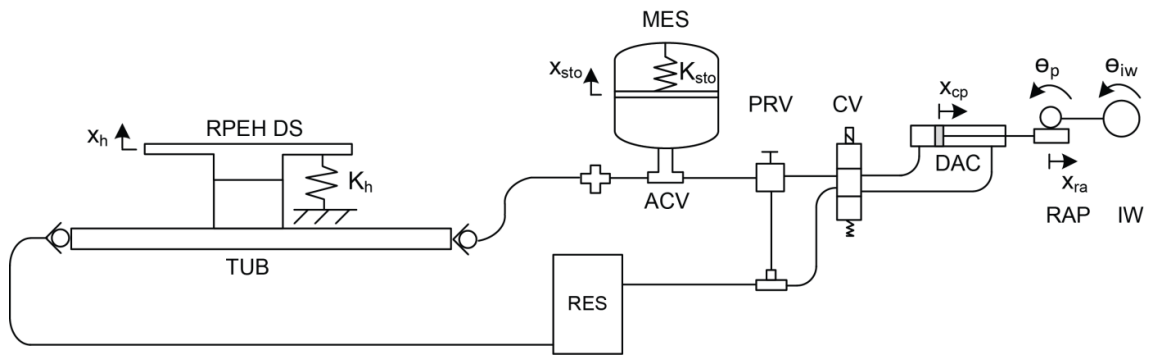


Figure 7.3- Representation of a RPEH device with a hydraulic transmission system, using a MES unit based on a hydraulic accumulator, spring-loaded type.

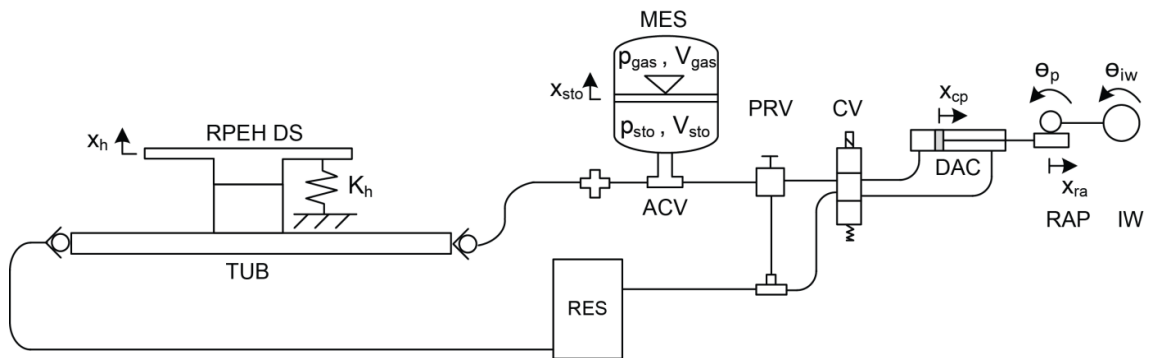


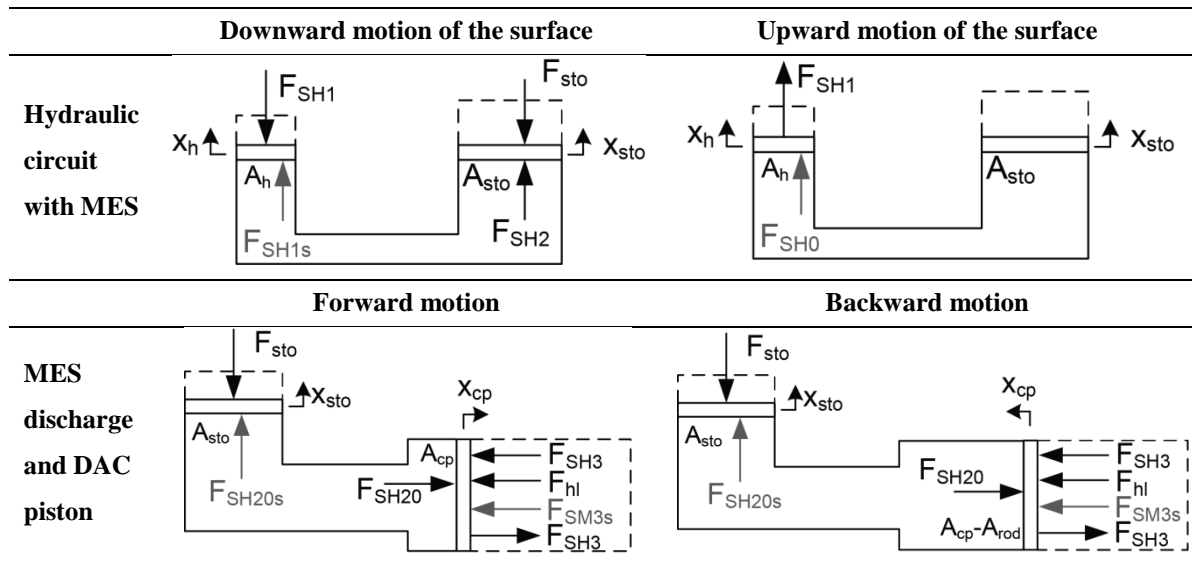
Figure 7.4- Representation of a RPEH device with a hydraulic transmission system, using a MES unit based on a hydraulic accumulator, gas-loaded type.

In the releasing energy stage, the ACV opens the circuit between the accumulator and the DAC, so that the accumulated and pressurized fluid can be released, actuating the DAC piston and, consequently, the RAP mechanical system and the electromagnetic generator.

Table 7.1 presents the force diagrams for the different motion scenarios, both for the receiving energy stage, with the RPEH DS and the hydraulic installation directly connected to the accumulator being presented, and for the releasing energy stage, with the hydraulic circuit between the accumulator and the DAC as well as the DAC piston being presented. The surface can have two motion scenarios, moving downwards or

upwards, as presented in Table 6.1, while the DAC piston can have two different motion scenarios, moving forwards or backwards.

Table 7.1- Force diagrams for the RPEH DS, MES system and DAC piston.



Tables 7.2 and 7.3 summarize all the equations that define the RPEH hydraulic device with the spring-loaded hydraulic accumulator, with a kinematic, dynamic and force analysis. Table 7.2 defines the equations for the energy charging stage when the surface moves downwards, upwards, or when it is stopped. Table 7.3 defines the equations for the energy release stage, when the accumulator piston moves downwards inducing motion on the DAC piston and, consequently, to the RAP system and the IW, which is connected to an electrical generator.

Table 7.2- System modelling for the RPEH DS charging the MES device (spring loaded).

Analysis	Surface motion		
	Downward	Stopped	Upward
Kinematic	$x_{sto} = \frac{A_h}{A_{sto}} x_h$	-	-
Dynamic	$\ddot{x}_h = \frac{1}{m_h} [F_{SH1s} + K_h x_h - F_z]$ $\ddot{x}_{hf} = \frac{A_h}{A_{tub}} \ddot{x}_h$ $\ddot{x}_{sto} = \frac{F_{SH2} - F_{sto} - F_{hl}}{m_{sto}}$	$\ddot{x}_h = \ddot{x}_{hf} = \ddot{x}_{sto} = 0$	$\ddot{x}_h = \frac{1}{m_h} [K_h x_h]$ $\ddot{x}_{hf} = \ddot{x}_{sto} = 0$
Force	$F_{SH1} = F_z - K_h x_h$ $F_{SH2} = \frac{A_{sto}}{A_h} F_{SH1}$ $F_{hl} = \Delta p A_{tub}$ $F_{sto} = K_{sto} x_{sto}$ $F_{SH2s} = F_{sto}$ $F_{SH1s} = \frac{A_h}{A_{sto}} F_{SH2s}$	$F_{SH1} = F_{SH2} = 0$ $F_{sto} = K_{sto} x_{sto}$ $F_{SH1s} = F_{SH2s} = 0$	$F_{SH1} = -K_h x_h$ $F_{SH2} = 0$ $F_{sto} = K_{sto} x_{sto}$ $F_{SH1s} = F_{SH2s} = 0$

To model the system using a gas-loaded accumulator, the equations defined in Tables 7.2 and 7.3 can be used, except the F_{sto} equation. For a gas-loaded accumulator, F_{sto} is determined using Equation (7.4), with p_{sto} to be determined using Equations (7.5-7.10), in relation to the surface displacement.

$$\Delta x_{sto} = \frac{A_h}{A_{sto}} \Delta x_h \quad (7.5)$$

$$\Delta V_{sto} = \Delta x_{sto} A_{sto} \quad (7.6)$$

$$V_{gas_i} = V_{gas_{i-1}} - \Delta V_{sto} \quad (7.7)$$

$$V_{sto_i} = V_{sto_{i-1}} + \Delta V_{sto} \quad (7.8)$$

$$p_{gas_i} = \frac{V_{gas_{i-1}}}{V_{gas_i}} p_{gas_{i-1}} \quad (7.9)$$

$$p_{sto} = p_{gas_i} \quad (7.10)$$

Table 7.3- System modelling for the MES device (spring loaded) releasing stored energy to the hydraulic and mechanical system.

Analysis	DAC piston motion		
	Forward	Stopped	Backward
Kinematic	$x_{cp} = -\left(\frac{A_{sto}}{A_{cp}}\right)x_{sto}$		$x_{cp} = \left(\frac{A_{sto}}{A_{cp} - A_{rod}}\right)x_{sto}$
	$x_{ra} = x_{cp}$		$x_{ra} = x_{cp}$
	$x_{cp} = r_p \theta_p \Leftrightarrow \theta_p = \frac{x_{cp}}{r_p}$	–	$x_{cp} = r_p \theta_p \Leftrightarrow \theta_p = \frac{x_{cp}}{r_p}$
Dynamic	$\ddot{x}_{sto} = \frac{1}{m_{sto}}[-F_{sto} + F_{SH20s}]$		$\ddot{x}_{sto} = \frac{1}{m_{sto}}[-F_{sto} + F_{SH20s}]$
	$\ddot{x}_{hf} = \left(\frac{A_{sto}}{A_{tub}}\right)\ddot{x}_{sto}$		$\ddot{x}_{hf} = \left(\frac{A_{sto}}{A_{tub}}\right)\ddot{x}_{sto}$
	$\ddot{x}_{cp} = \frac{1}{m_{cp}}[F_{SH20} - F_{hl} - F_{SH3} - F_{SMs}]$	$\ddot{x}_{sto} = \ddot{x}_{hf} = \ddot{x}_{cp} = \ddot{\theta}_p = 0$	$\ddot{x}_{cp} = \frac{1}{m_{cp}}[F_{SH20} - F_{hl} - F_{SH3} - F_{SMs}]$
Force	$\ddot{\theta}_p = \ddot{\theta}_{iw}$	$\ddot{\theta}_{iw} = \frac{-(b_{cb} + b_{gen})\dot{\theta}_{iw} - ET}{J_{iw} + J_{gen}}$	$\ddot{\theta}_p = \frac{F_{SM}r_p - (b_{cb} + b_{gen})\dot{\theta}_p - ET}{J_p + J_{sh}}$
	$\ddot{\theta}_{iw} = \frac{F_{SM}r_p - (b_{cb} + b_{gen})\dot{\theta}_p - ET}{J_p + J_{sh} + J_{iw} + J_{gen}}$		$\ddot{\theta}_{iw} = \frac{-(b_{cb} + b_{gen})\dot{\theta}_{iw} - ET}{J_{iw} + J_{gen}}$
	$F_{sto} = K_{sto}x_{sto}$		$F_{sto} = K_{sto}x_{sto}$
Force	$F_{SH20} = \left(\frac{A_{cp}}{A_{sto}}\right)F_{sto}$		$F_{SH20} = -\left(\frac{A_{cp} - A_{rod}}{A_{sto}}\right)F_{sto}$
	$F_{SM} = F_{SH20} - F_{hl} - F_{SH3}$		$F_{SM} = F_{SH20} + F_{hl} + F_{SH3}$
	$F_{SH3} = (p_{atm} - \Delta p_2)(A_{cp} - A_{rod}) - F_{hl2}$	$F_{SH20} = F_{SH3} = 0$	$F_{SH3} = p_{atm}A_{cp} - F_{hl2}$
	$F_{hl} = \Delta p A_{tub}$	$F_{sto.s} = F_{SH20s} = 0$	$F_{hl} = \Delta p A_{tub}$
	$F_{hl2} = \Delta p_2 A_{tub}$	$F_{hl} = F_{hl2} = 0$	$F_{hl2} = \Delta p_2 A_{tub}$
	$F_{sto.s} = \left(\frac{A_{sto}}{A_{cp}}\right)F_{SH20s}$	$F_{SM} = F_{SMs} = 0$	$F_{sto.s} = \left(\frac{A_{sto}}{A_{cp} - A_{rod}}\right)F_{SH20s}$
	$F_{SH20s} = F_{SH3} + F_{hl} + F_{SMs}$		$F_{SH20s} = F_{SH3} + F_{hl} + F_{SMs}$
	$F_{SMs} = \frac{(J_p + J_{sh} + J_{iw} + J_{gen})\ddot{\theta}_p + ET}{r_p}$		$F_{SMs} = \frac{(J_p + J_{sh})\ddot{\theta}_p}{r_p}$

7.2.4 New RPEH device with hydraulic system with integrated mechanical energy storage

Considering the RPEH device with a mechanically actuated hydraulic system transmitting the mechanical energy from the equipment’s surface to a mechanical system and to an electromagnetic generator, presented in Chapter 6, two MES systems based on hydraulic pressure storage are presented. Figure 7.5 presents the RPEH device with a spring-loaded hydraulic accumulator working as a MES system and Figure 7.6 presents the RPEH device with a gas-loaded hydraulic accumulator, piston type, working as a MES system.

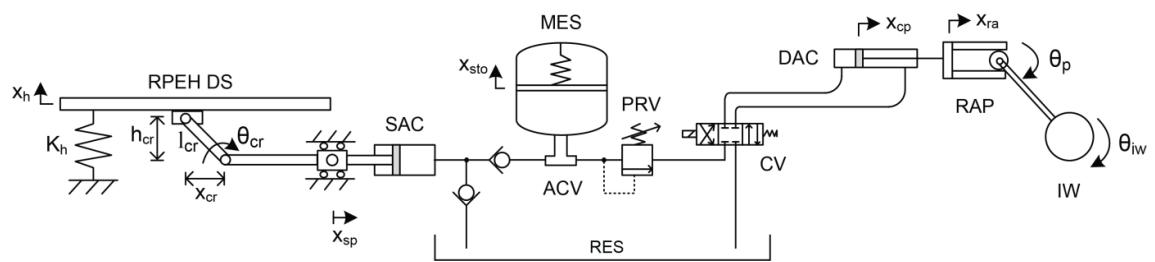


Figure 7.5- Representation of a RPEH device with a mechanically actuated hydraulic transmission system, using a MES unit based on a hydraulic accumulator, spring-loaded type.

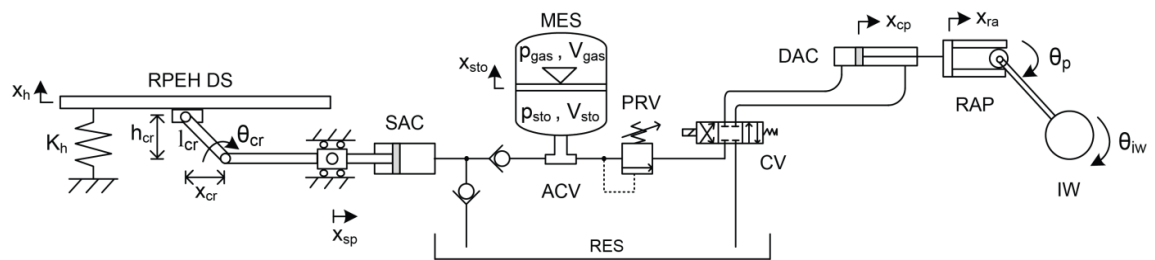


Figure 7.6- Representation of a RPEH device with a mechanically actuated hydraulic transmission system, using a MES unit based on a hydraulic accumulator, gas-loaded type.

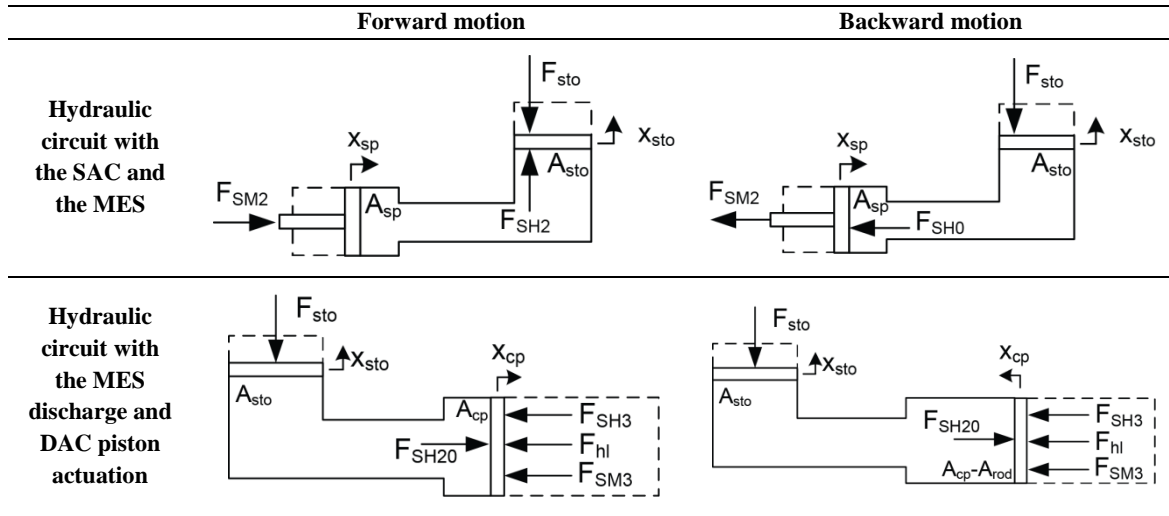
The working principle of both systems is the same, each having two storage stages: receiving energy and releasing energy. In the receiving energy stage, when the RPEH DS is moving downwards, it transmits a force onto the fluid inside the SAC through the mechanical system, which is transmitted to the hydraulic accumulator through the fluid pressure. The ACV lets the fluid in if the pressure is higher than the pressure inside the accumulator, inducing a displacement of the accumulator piston. If the fluid pressure is lower than the accumulator pressure, the valve remains closed.

In the releasing energy stage, the ACV opens the circuit between the accumulator and the DAC, so that the accumulated and pressurized fluid can be released, actuating the DAC piston and, consequently, the RAP mechanical system and the electromagnetic generator.

Table 7.4 presents the force diagrams for the different motion scenarios, both for the receiving energy stage, with the hydraulic installation directly connected to the accumulator being presented, and for the releasing energy stage, with the hydraulic circuit between the accumulator and the DAC as well as the DAC piston being presented. The RPEH DS and mechanical system diagrams are not presented, once these are similar to the diagrams presented in Table 6.4. Both the SAC and the DAC pistons can have two different motion scenarios, moving forwards or backwards.

Tables 7.5 and 7.6 summarize all the equations that define the RPEH hydraulic device with a mechanical actuation using a spring-loaded hydraulic accumulator, with a kinematic, dynamic and force analysis. Table 7.5 defines the equations for the energy charging stage when the surface moves downwards, upwards, or when it is stopped. Table 7.6 defines the equations for the energy release stage, when the accumulator piston moves downwards inducing motion on the DAC piston and, consequently, to the RAP system and the IW, which is connected to an electrical generator.

Table 7.4- Force diagrams for the RPEH DS, mechanical system, MES system and DAC piston.



To model the system using a gas-loaded accumulator, the equations defined in Tables 7.5 and 7.6 can be used, except the F_{sto} equation. For a gas-loaded accumulator, F_{sto} is determined using Equation (7.4), with p_{sto} to be determined using Equations (7.6-7.10), in relation to the surface displacement. Equation (7.11) is used to determine Δx_{sto} , in substitution of Equation (7.5).

$$\Delta x_{sto} = \frac{A_{sp}}{A_{sto}} \Delta x_{sp} \tag{7.11}$$

7.2.5 Energetic analysis

The equations regarding the energy lost by the vehicle (E_v), the energy harvested by the RPEH DS (E_{Ha}), the mechanical energy transmitted and delivered (E_{Tr} and E_{De}) and the electrical energy generated and consumed (E_{Ge} and E_{Lo}) were defined in Chapters 3, 5 and 6.

Table 7.5- System modelling for the RPEH hydraulic circuit with a mechanical actuation charging the MES device (spring-loaded).

Analysis	Surface motion		
	Downward	Stopped	Upward
Kinematic	$h_{cr} = h_{cr-in} + x_h$		$h_{cr} = h_{cr-in} + x_h$
	$\theta_{cr} = \sin^{-1}\left(\frac{h_{cr}}{l_{cr}}\right)$		$\theta_{cr} = \sin^{-1}\left(\frac{h_{cr}}{l_{cr}}\right)$
	$x_{cr} = l_{cr}\cos\theta_{cr}$	-	$x_{cr} = l_{cr}\cos\theta_{cr}$
	$x_{sp} = x_{sp-in} + x_{cr}$		$x_{sp} = x_{sp-in} + x_{cr}$
	$x_{sto} = \left(\frac{A_{sp}}{A_{sto}}\right)x_{sp}$		
Dynamic	$\ddot{x}_h = \frac{1}{m_h}[F_{SM1s} + K_h x_h - F_z]$		$\ddot{x}_h = \frac{1}{m_h}[K_h x_h - F_{SM1s}]$
	$\ddot{x}_{sp} = \frac{1}{m_{sp}}[F_{SM2} - F_{SM2s} - F_{los}]$	$\ddot{x}_h = \ddot{x}_{sp} = 0$	$\ddot{x}_{sp} = \frac{1}{m_{sp}}[-F_{SM2} + F_{SM2s} + F_{los}]$
	$\ddot{x}_{hf} = \left(\frac{A_{sp}}{A_{tub}}\right)\ddot{x}_{sp}$	$\ddot{x}_{hf} = \ddot{x}_{sto} = 0$	$\ddot{x}_{hf} = \ddot{x}_{sto} = 0$
	$\ddot{x}_{sto} = \frac{F_{SH1} - F_{sto} - F_{hl}}{m_{sto}}$		
Force	$F_{SM1} = F_z - K_h x_h$		$F_{SM1} = K_h x_h$
	$F_{SH1} = F_{SM2} = \frac{F_{SM1}}{\tan\theta_{cr}} - F_{los}$		$F_{SM2} = \frac{F_{SM1}}{\tan\theta_{cr}} - F_{los}$
	$F_{SH2} = \left(\frac{A_{sto}}{A_{sp}}\right)F_{SH1}$	$F_{SM1} = F_{SM2} = 0$	$F_{SH0} = p_{atm}A_{sp}$
	$F_{hl} = \Delta p A_{tub}$	$F_{SH1} = F_{SH2} = 0$	$F_{SM2s} = F_{SH0}$
	$F_{sto} = K_{sto}x_{sto}$	$F_{sto} = K_{sto}x_{sto}$	$F_{SM1s} = (F_{SM2s} + F_{ml})\tan\theta_{cr}$
	$F_{SH2s} = F_{sto}$	$F_{SH1s} = F_{SH2s} = 0$	$F_{sto} = K_{sto}x_{sto}$
	$F_{SM2s} = F_{SH1s} = \left(\frac{A_{sp}}{A_{sto}}\right)F_{SH2s}$	$F_{SM1s} = F_{SM2s} = 0$	$F_{SH1s} = F_{SH2s} = 0$
	$F_{SM1s} = (F_{SM2s} + F_{ml})\tan\theta_{cr}$		

The energy and power stored by a spring loaded hydraulic accumulator are determined by Equations (7.12) and (7.13), respectively. The energy stored by a gas loaded hydraulic accumulator is determined by Equation (7.14), while the stored power is determined by Equation (7.13).

$$\partial E_{sto} = F_{sto} \partial x_{sto} \quad (7.12)$$

$$p_{sto} = \frac{\partial E_{sto}}{\partial t} \quad (7.13)$$

$$E_{sto} = p_{sto} V_{sto} \quad (7.14)$$

Table 7.6- System modelling for the MES device (spring-loaded) releasing the stored energy for the hydraulic and mechanical system.

Analysis	DAC piston motion		
	Forward	Stopped	Backward
Kinematic	$x_{cp} = -\left(\frac{A_{sto}}{A_{cp}}\right) x_{sto}$		$x_{cp} = \left(\frac{A_{sto}}{A_{cp} - A_{rod}}\right) x_{sto}$
	$x_{ra} = x_{cp}$		$x_{ra} = x_{cp}$
	$x_{cp} = r_p \theta_p \Leftrightarrow \theta_p = \frac{x_{cp}}{r_p}$	-	$x_{cp} = r_p \theta_p \Leftrightarrow \theta_p = \frac{x_{cp}}{r_p}$
	$\theta_{iw} = \theta_p = \frac{x_{cp}}{r_p}$		$\theta_{iw} = -\theta_p = -\frac{x_{cp}}{r_p}$
Dynamic	$\ddot{x}_{sto} = \frac{1}{m_{sto}} [-F_{sto} + F_{SH20s}]$		$\ddot{x}_{sto} = \frac{1}{m_{sto}} [-F_{sto} + F_{SH20s}]$
	$\ddot{x}_{hf} = \left(\frac{A_{sto}}{A_{tub}}\right) \ddot{x}_{sto}$		$\ddot{x}_{hf} = \left(\frac{A_{sto}}{A_{tub}}\right) \ddot{x}_{sto}$
	$\ddot{x}_{cp} = \frac{1}{m_{cp}} [F_{SH20} - F_{hl} - F_{SH3} - F_{SMs}]$	$\ddot{x}_{sto} = \ddot{x}_{hf} = \ddot{x}_{cp} = \ddot{\theta}_p = 0$	$\ddot{x}_{cp} = \frac{1}{m_{cp}} [F_{SH20} - F_{hl} - F_{SH3} - F_{SMs}]$
	$\ddot{\theta}_p = \ddot{\theta}_{iw}$	$\ddot{\theta}_{iw} = \frac{-(b_{cb} + b_{gen})\dot{\theta}_{iw} - ET}{J_{iw} + J_{gen}}$	$\ddot{\theta}_p = \frac{F_{SM3} r_p - (b_{cb} + b_{gen})\dot{\theta}_p - ET}{J_p + J_{sh} + J_{iw} + J_{gen}}$
	$\ddot{\theta}_{iw} = \frac{F_{SM3} r_p - (b_{cb} + b_{gen})\dot{\theta}_p - ET}{J_p + J_{sh} + J_{iw} + J_{gen}}$		$\ddot{\theta}_{iw} = -\ddot{\theta}_p = -\frac{F_{SM3} r_p - (b_{cb} + b_{gen})\dot{\theta}_p - ET}{J_p + J_{sh} + J_{iw} + J_{gen}}$
Force	$F_{sto} = K_{sto} x_{sto}$		$F_{sto} = K_{sto} x_{sto}$
	$F_{SH20} = \left(\frac{A_{cp}}{A_{sto}}\right) F_{sto}$		$F_{SH20} = -\left(\frac{A_{cp} - A_{rod}}{A_{sto}}\right) F_{sto}$
	$F_{SM3} = F_{SH20} - F_{hl} - F_{SH3}$		$F_{SM3} = -F_{SH20} + F_{hl} + F_{SH3}$
	$F_{SH3} = (p_{atm} - \Delta p_2)(A_{cp} - A_{rod}) - F_{hl2}$	$F_{SH20} = F_{SH3} = 0$	$F_{SH3} = p_{atm} A_{cp} - F_{hl2}$
	$F_{hl} = \Delta p A_{tub}$	$F_{sto.s} = F_{SH20s} = 0$	$F_{hl} = \Delta p A_{tub}$
	$F_{hl2} = \Delta p_2 A_{tub}$	$F_{hl} = F_{hl2} = 0$	$F_{hl2} = \Delta p_2 A_{tub}$
	$F_{sto.s} = \left(\frac{A_{sto}}{A_{cp}}\right) F_{SH20s}$	$F_{SM3} = F_{SM3s} = 0$	$F_{sto.s} = \left(\frac{A_{sto}}{A_{cp} - A_{rod}}\right) F_{SH20s}$
	$F_{SH20s} = F_{SH3} + F_{hl} + F_{SM3s}$		$F_{SH20s} = F_{SH3} + F_{hl} + F_{SM3s}$
	$F_{SM3s} = \frac{(J_p + J_{sh} + J_{iw} + J_{gen})\ddot{\theta}_p + ET}{r_p}$		$F_{SM3s} = \frac{(J_p + J_{sh})\ddot{\theta}_p}{r_p}$

The efficiency of the MES system is defined by Equation (7.15), relating the stored mechanical energy to the mechanical energy transmitted by the hydraulic system. When a MES system is applied in the hydraulic system, the equation that defines the energy delivered is defined by Equation (7.16), relating the energy delivered by the mechanical system to the electric generator with the energy stored in the MES system.

$$\eta_{sto} = \frac{E_{sto}}{E_{Tr}} \quad (7.15)$$

$$\eta_{De} = \frac{E_{De}}{E_{sto}} \quad (7.16)$$

7.3 Technical Analysis

7.3.1 Introduction

In Chapter 3, a software tool that allows quantifying the energy transferred from vehicles to an energy harvesting device was presented. In Chapter 5, an upgraded version of the software tool was presented, to include different RPEH models, so that a complete simulation from the energy released by the vehicle to the electrical energy generated and consumed could be performed. In Chapter 6, the models for RPEH devices based on typical hydraulic systems and a new proposed hydraulic system with a mechanical actuation were presented, and both models were added to the software tool. The models presented in this Chapter for the hydraulic systems with MES were also incorporated in the software tool. This upgraded tool allows users to perform a complete analysis, from the energy release from the vehicle to the device surface to the electrical energy generated and delivered to an electrical load.

The software tool calculates all the forces and displacements for both the vehicle components and the RPEH device surface, as well as for the hydraulic, mechanical and electrical system components, including storage. After that, it calculates the different energies transferred from each part of the system to the others and the efficiency of each energy transfer process.

The simulations performed with the software tool for the RPEH hydraulic systems without storage, both typical and mechanically actuated, and for the same systems with two different MES systems, will be presented in this section. The same RPEH equipment surface profile, geometry and displacement, as well as the same vehicle and the same electric generator and load will be used. The goal is to evaluate the different MES systems and reach conclusions about their mechanical energy storage efficiency, and to compare the efficiency of the RPEH systems with and without mechanical energy storage.

As the goal is to evaluate the system's performance with and without MES and as the effectiveness of the MES can only be evaluated with multiple vehicle actuations due to the increase of the energy stored and, consequently, a higher amount of energy being delivered to the electrical generator, the simulations will be performed for 10 vehicles actuating the system. So, the results presented for all systems are related to 10 vehicle actuations.

However, one RPEH device connected to one hydraulic system is used, which, in turn, is connected to one MES system, one mechanical system and one electrical system, as the surface is actuated by one side of the vehicle. So, the value presented for the energy lost by the vehicles is for only half of each vehicle, as only one front and one rear wheel of a vehicle will actuate the RPEH device surface.

The parameters defined for the vehicle, the RPEH device surface, the hydraulic, mechanical and electrical systems, as well as the hydraulic accumulator, common to the simulations of all systems, are presented in Table 7.7.

7.3.2 Standard hydraulic system

Considering the input data presented in Table 7.7, simulations for the standard hydraulic system were performed using the *Crest* surface profile, without any MES device. The RAP mechanical system, the electric generator and the electric load parameters were not changed between simulations.

Table 7.7- Input data for the computational simulations of the three systems.

	Variable name	Value	Unit
Vehicle & motion	Vehicle class	Light	-
	Vehicle weight	1,500	(kg)
	Number of axles P1 wheels per axle	2 2	-
	Sprung-Unsprung %	90%-10%	-
	Drag coefficient	0.32	-
	Inertia moment	1,100	(kg.m ²)
	Lift coefficients (Front Rear)	0.19 0.13	-
	Motion Direction	Free rolling Forward	-
	Vehicle speed acceleration	40 0	(km/h) (m/s ²)
	Suspension & wheel	Suspension type (Front Rear)	Independent Independent
Suspension stiffness (Front Rear)		20,000 15,000	(N/m)
Suspension damping (Front Rear)		1,500 1,700	(Ns/m)
Tyre type (Front Rear)		Radial Radial	-
Tyre stiffness (Front Rear)		150,000 150,000	(N/m)
Tyre pressure (Front Rear)		200 200	(kPa)
Tyre external diameter (Front Rear)		500 500	(mm)
Tyre width (Front Rear)		200 200	(mm)
Tyre tread width (Front Rear)		180 180	(mm)
RPEH device	Surface width mass	250 20	(mm) (kg)
	Surface max. height max. displacement	20 20	(mm)
	Mech. system crank length initial height	40 30	(mm) (mm)
	Spring stiffness	30,000	(N/m)
	Hydraulic fluid	Oil SAE 30	-
	Hydraulic fluid density kinematic viscosity	865 105	(kg.m ³) (cSt)
	Hydraulic circuit CV discharge coef. KH	2.48 10.50	- -
	Hydraulic tube length	3	(m)
	Hydraulic reservoir pressure	101,325	(Pa)
	Hydraulic cylinder stroke	250	(mm)
	Pinion mass radius friction coefficient	1 20 0.002	(kg) (mm) -
	Inertia wheel mass radius	10 30	(kg) (mm)
	Electric generator constant Ka	0.25	-
	Electric generator Ra La	1.1 0.0048	(Ω) (H)
	Electric generator friction coef. Inertia	0.0008 0.05	- (kg.m ²)
Electric load Power	50	(W)	
MES	Accumulator height external diameter	1 0.25	(m) (m)
	Accumulator piston mass	2	(kg)
	Accumulator stroke	0.8	(m)

For the hydraulic system, different values of the contact area between the surface and the hydraulic circuit (A_h), which defines the interaction area between the received force and the hydraulic fluid, were simulated. Also, different values for the hydraulic cylinder area (A_{cp}) were used. The goal is to evaluate the impact of these variables on the energy transmitted.

To evaluate the system's performance, the vehicle released energy (E_v), RPEH surface harvested energy (E_{Ha}), mechanical system transmitted energy (E_{Tr}), mechanical system delivered energy (E_{De}), electrical system generated energy (E_{Ge}) and electrical system consumed energy (E_{Lo}) were calculated. Also, the efficiencies of the energy transferred between each part of the system were evaluated.

Table 7.8 presents the simulation results for the energy output of each component of the RPEH device using the standard hydraulic system without energy storage, considering the input data presented in Table 7.7. Table 7.9 presents the simulation results for the efficiency of each component of the system, as well as the total efficiency of the device.

Table 7.8- Simulation results for the energy outputs of the RPEH device components using a standard hydraulic system, without MES.

A_h (mm ²)	A_{cp} (mm ²)	E_v (J)	E_{Ha} (J)	E_{Tr} (J)	E_{De} (J)	E_{Ge} (J)	E_{Lo} (J)
20	12	1,780.0	1,170.0	1,080.0	100.0	80.1	64.0
	25	1,780.0	970.0	690.0	460.0	397.4	320.7
	50	1,740.0	980.0	770.0	490.0	441.5	358.0
40	12	1,970.0	1,040.0	580.0	70.0	55.7	43.9
	25	1,850.0	1,030.0	680.0	180.0	149.2	119.2
	50	1,800.0	990.0	630.0	270.0	226.5	182.4

Table 7.9- Simulation results for the efficiencies of the RPEH device components using a standard hydraulic system, without MES.

A_h (mm ²)	A_{cp} (mm ²)	η_{Ha} (%)	η_{Tr} (%)	η_{De} (%)	η_{Ge} (%)	η_{Co} (%)	η_{Mec} (%)	η_{Ele} (%)	η_{RPEH} (%)	η_{Tot} (%)
20	12	65.7	92.3	9.3	80.1	79.9	8.5	64.00	5.5	3.6
	25	54.5	71.1	66.7	86.4	80.7	47.4	69.72	33.1	18.0
	50	56.3	78.6	63.6	90.1	81.1	50.0	73.07	36.5	20.6
40	12	52.8	55.8	12.1	79.5	78.9	6.7	62.73	4.2	2.2
	25	55.7	66.0	26.5	82.9	79.9	17.5	66.24	11.6	6.4
	50	55.0	63.6	42.9	83.9	80.5	27.3	67.54	18.4	10.1

Considering the same conditions as for the standard hydraulic system, simulations for the hydraulic system with a MES system, based on a spring-loaded hydraulic accumulator, were also performed. Beside A_h and A_{cp} , the spring stiffness of the hydraulic accumulator (K_{sto}) and the hydraulic cylinder piston area (A_{sto}) were also changed between simulations to evaluate the impact of these variables.

Table 7.10 presents the simulation results for the energy output of each component of the system, while Table 7.11 presents the simulation results for the efficiency of each component of the system, as well as the total efficiency of the device.

Using the same conditions as for the standard hydraulic system, simulations for the hydraulic system with a MES system, based on a gas-loaded hydraulic accumulator, were performed. Beside A_h and A_{cp} , the initial pressure of the hydraulic accumulator gas (p_{gas}) and the hydraulic cylinder piston area (A_{sto}) were also changed between simulations to evaluate the impact of these variables.

Table 7.12 presents the simulation results for the energy output of each component of the system, and Table 7.13 presents the simulation results for the efficiency of each component of the system, as well as the total efficiency of the device.

Table 7.10- Simulation results for the energy outputs of the RPEH device components using a spring-loaded hydraulic accumulator connected to a standard hydraulic system.

K_{sto} (kN/m)	A_h (mm ²)	A_{sto} (mm ²)	A_{cp} (mm ²)	E_v (J)	E_{Ha} (J)	E_{Tr} (J)	E_{sto} (J)	E_{De} (J)	E_{Ge} (J)	E_{Lo} (J)	
15	20	100	25	2,150.0	1,020.0	890.0	170.0	118.8	108.3	89.0	
			50	2,150.0	1,020.0	890.0	170.0	119.9	109.2	89.7	
		200	25	2,240.0	1,010.0	878.0	85.0	49.6	42.3	33.8	
			50	2,240.0	1,010.0	878.0	85.0	50.0	42.7	34.1	
		40	100	25	2,060.0	1,020.0	790.0	190.0	137.0	125.5	103.4
				50	2,060.0	1,020.0	790.0	190.0	138.5	126.9	104.5
	200		25	2,220.0	985.0	860.0	130.0	89.8	78.6	62.9	
			50	2,220.0	985.0	860.0	130.0	90.9	79.8	63.9	
	20	20	100	25	2,060.0	960.0	840.0	220.0	164.3	151.4	125.3
				50	2,060.0	960.0	840.0	220.0	165.2	152.2	126.0
			200	25	2,160.0	990.0	850.0	140.0	98.3	86.6	69.4
				50	2,160.0	990.0	850.0	140.0	99.3	87.5	70.1
40			100	25	2,070.0	1,050.0	810.0	290.0	219.0	204.1	172.0
				50	2,070.0	1,050.0	810.0	290.0	220.7	205.9	173.8
		200	25	2,180.0	940.0	800.0	240.0	179.3	165.1	137.0	
			50	2,180.0	940.0	800.0	240.0	180.2	166.0	137.8	

Table 7.11- Simulation results for the efficiencies of the RPEH device components using a spring-loaded hydraulic accumulator connected to a standard hydraulic system.

K_{sto} (kN/m)	A_h (mm ²)	A_{sto} (mm ²)	A_{cp} (mm ²)	η_{Ha} (%)	η_{Tr} (%)	η_{sto} (%)	η_{De} (%)	η_{Ge} (%)	η_{Co} (%)	η_{Mec} (%)	η_{Ele} (%)	η_{RPEH} (%)	η_{Tot} (%)	
15	20	100	25	47.4	87.3	19.1	69.9	91.1	82.2	11.7	74.9	8.7	4.1	
			50	47.4	87.3	19.1	70.5	91.1	82.2	11.8	74.9	8.8	4.2	
		200	25	45.1	86.9	9.7	58.3	85.4	79.8	4.9	68.1	3.3	1.5	
			50	45.1	86.9	9.7	58.8	85.5	79.8	4.9	68.2	3.4	1.5	
	40	100	25	49.5	77.5	24.1	72.1	91.6	82.4	13.4	75.5	10.1	5.0	
			50	49.5	77.5	24.1	72.9	91.6	82.4	13.6	75.5	10.2	5.1	
		200	25	44.4	87.3	15.1	69.1	87.5	80.0	9.1	70.0	6.4	2.8	
			50	44.4	87.3	15.1	69.9	87.8	80.1	9.2	70.3	6.5	2.9	
	20	20	100	25	46.6	87.5	26.2	74.7	92.1	82.8	17.1	76.3	13.1	6.1
				50	46.6	87.5	26.2	75.1	92.1	82.8	17.2	76.3	13.1	6.1
			200	25	45.8	85.9	16.5	70.2	88.1	80.1	9.9	70.6	7.0	3.2
				50	45.8	85.9	16.5	70.9	88.2	80.1	10.0	70.6	7.1	3.2
40		100	25	50.7	77.1	35.8	75.5	93.2	84.3	20.9	78.6	16.4	8.3	
			50	50.7	77.1	35.8	76.1	93.3	84.4	21.0	78.7	16.6	8.4	
		200	25	43.1	85.1	30.0	74.7	92.1	83.0	19.1	76.4	14.6	6.3	
			50	43.1	85.1	30.0	75.1	92.1	83.0	19.2	76.4	14.7	6.3	

Table 7.12- Simulation results for the energy outputs of the RPEH device components using a gas-loaded hydraulic accumulator connected to a standard hydraulic system.

P_{gas} (bar)	A_h (mm ²)	A_{sto} (mm ²)	A_{cp} (mm ²)	E_v (J)	E_{Ha} (J)	E_{Tr} (J)	E_{sto} (J)	E_{De} (J)	E_{Ge} (J)	E_{Lo} (J)	
2	20	100	25	2,160.0	1,020.0	870.0	505.0	439.9	415.7	355.4	
			50	2,160.0	1,020.0	870.0	505.0	445.4	420.9	359.9	
		200	25	2,220.0	1,020.0	870.0	505.0	439.9	415.7	355.4	
			50	2,220.0	1,020.0	870.0	505.0	445.4	420.9	359.9	
	10	100	25	2,390.0	940.0	770.0	245.0	176.6	162.3	132.1	
			50	2,390.0	940.0	770.0	245.0	179.3	165.0	134.5	
		200	25	2,150.0	1,020.0	850.0	570.0	502.7	475.1	407.2	
			50	2,150.0	1,020.0	850.0	570.0	503.9	476.2	408.1	
	4	20	100	25	2,180.0	1,030.0	860.0	545.0	470.3	444.5	380.5
				50	2,180.0	1,030.0	860.0	560.0	483.8	457.2	391.4
			200	25	2,170.0	1,040.0	880.0	560.0	483.8	457.2	391.4
				50	2,170.0	1,040.0	880.0	560.0	485.0	458.3	392.3
10		100	25	2,200.0	990.0	820.0	285.0	208.6	193.6	159.1	
			50	2,200.0	990.0	820.0	285.0	209.5	194.4	159.8	
		200	25	2,070.0	1,060.0	900.0	620.0	557.4	528.4	453.4	
			50	2,070.0	1,060.0	900.0	620.0	560.5	531.3	455.9	

Table 7.13- Simulation results for the efficiencies of the RPEH device components using a gas-loaded hydraulic accumulator connected to a standard hydraulic system.

P_{gas} (bar)	A_h (mm ²)	A_{sto} (mm ²)	A_{cp} (mm ²)	η_{Ha} (%)	η_{Tr} (%)	η_{sto} (%)	η_{De} (%)	η_{Ge} (%)	η_{Co} (%)	η_{Mec} (%)	η_{Ele} (%)	η_{RPEH} (%)	η_{Tot} (%)	
2	20	100	25	47.2	85.3	58.0	87.1	94.5	85.5	43.1	80.8	34.8	16.5	
			50	47.2	85.3	58.0	88.2	94.5	85.5	43.7	80.8	35.3	16.7	
		200	25	45.9	85.3	58.0	87.1	94.5	85.5	43.1	80.8	34.8	16.0	
			50	45.9	85.3	58.0	88.2	94.5	85.5	43.7	80.8	35.3	16.2	
	10	100	25	39.3	81.9	31.8	72.1	91.9	81.4	18.8	74.8	14.1	5.5	
			50	39.3	81.9	31.8	73.2	92.0	81.5	19.1	75.0	14.3	5.6	
		200	25	47.4	83.3	67.1	88.2	94.5	85.7	49.3	81.0	39.9	18.9	
			50	47.4	83.3	67.1	88.4	94.5	85.7	49.4	81.0	40.0	19.0	
	4	20	100	25	47.2	83.5	63.4	86.3	94.5	85.6	45.7	80.9	36.9	17.5
				50	47.2	83.5	65.1	86.4	94.5	85.6	47.0	80.9	38.0	18.0
			200	25	47.9	84.6	63.6	86.4	94.5	85.6	46.5	80.9	37.6	18.0
				50	47.9	84.6	63.6	86.6	94.5	85.6	46.6	80.9	37.7	18.1
10		100	25	45.0	82.8	34.8	73.2	92.8	82.2	21.1	76.3	16.1	7.2	
			50	45.0	82.8	34.8	73.5	92.8	82.2	21.2	76.3	16.1	7.3	
		200	25	51.2	84.9	68.9	89.9	94.8	85.8	52.6	81.3	42.8	21.9	
			50	51.2	84.9	68.9	90.4	94.8	85.8	52.9	81.3	43.0	22.0	

7.3.3 Hydraulic system with mechanical actuation

Considering the input data presented in Table 7.7, simulations for the RPEH device with a mechanically actuated hydraulic system were performed using the *Crest* surface profile and without any MES device. The rack and pinion mechanical system, the electric generator and the electric load parameters were not changed between simulations.

For the mechanically actuated hydraulic system, different values of the contact area between the slider and the hydraulic circuit (A_{sp}), which defines the interaction area between the received force and the hydraulic fluid, were simulated. Also, different values for the hydraulic cylinder area (A_{cp}) were used. The goal is to evaluate the impact of these variables on the energy transmitted.

To evaluate the system's performance, the vehicle released energy (E_v), RPEH surface harvested energy (E_{Ha}), mechanical system transmitted energy (E_{Tr}), mechanical system delivered energy (E_{De}), electrical system generated energy (E_{Ge}) and electrical system consumed energy (E_{Lo}) were calculated. Also, the efficiencies of the energy transferred between each part of the system were evaluated.

Table 7.14 presents the simulation results for the energy output of each component of the RPEH device using the mechanically actuated hydraulic system without storage, considering the input data presented in Table 7.7. Table 7.15 presents the simulation results for the efficiency of each component of the system, as well as the total efficiency of the device.

Considering the same conditions as for the RPEH mechanically actuated hydraulic system, simulations for the same system with a MES system, based on a spring-loaded hydraulic accumulator, were also performed. Beside A_{sp} and A_{cp} , the spring stiffness of the hydraulic accumulator (K_{sto}) and the hydraulic cylinder piston area (A_{sto}) were also changed between simulations to evaluate the impact of these variables.

Table 7.14- Simulation results for the energy output of the RPEH device using a mechanically actuated hydraulic system without MES.

A_{sp} (mm ²)	A_{cp} (mm ²)	E_v (J)	E_{Ha} (J)	E_{Tr} (J)	E_{De} (J)	E_{Ge} (J)	E_{Lo} (J)
10	12	2,010.0	980.0	900.0	251.5	215.3	169.6
	25	2,010.0	910.0	820.0	771.0	703.2	571.7
	50	1,990.0	860.0	780.0	768.0	700.4	569.4
20	12	2,100.0	1,010.0	940.0	111.5	91.7	71.2
	25	2,040.0	980.0	890.0	290.5	250.1	197.8
	50	2,010.0	930.0	840.0	817.5	749.6	613.2

Table 7.15- Simulation results for the efficiencies of the RPEH device using a mechanically actuated hydraulic system without MES.

A_{sp} (mm ²)	A_{cp} (mm ²)	η_{Ha} (%)	η_{Tr} (%)	η_{De} (%)	η_{Ge} (%)	η_{Co} (%)	η_{Mec} (%)	η_{Ele} (%)	η_{RPEH} (%)	η_{Tot} (%)
10	12	48.8	91.8	27.9	85.6	78.8	25.7	67.45	17.3	8.4
	25	45.3	90.1	94.0	91.2	81.3	84.7	74.15	62.8	28.4
	50	43.2	90.7	98.5	91.2	81.3	89.3	74.15	66.2	28.6
20	12	48.1	93.1	11.9	82.2	77.7	11.0	63.87	7.1	3.4
	25	48.0	90.8	32.6	86.1	79.1	29.6	68.11	20.2	9.7
	50	46.3	90.3	97.3	91.7	81.8	87.9	75.01	65.9	30.5

Table 7.16 presents the simulation results for the energy output of each component of the system, while Table 7.17 presents the simulation results for the efficiency of each component of the system, as well as the total efficiency of the device.

Using the same conditions as for the RPEH mechanically actuated hydraulic system, simulations for the same system with a MES system, based on a gas-loaded hydraulic accumulator, were performed. Beside A_{sp} and A_{cp} , the initial pressure of the hydraulic accumulator gas (p_{gas}) and the hydraulic cylinder piston area (A_{sto}) were also changed between simulations to evaluate the impact of these variables.

Table 7.18 presents the simulation results for the energy output of each component of the system, and Table 7.19 presents the simulation results for the efficiency of each component of the system, as well as the total efficiency of the device.

Table 7.16- Simulation results for the energy outputs of the RPEH device components using a spring-loaded hydraulic accumulator connected to a mechanically actuated hydraulic system.

K_{sto} (kN/m)	A_{sp} (mm ²)	A_{sto} (mm ²)	A_{cp} (mm ²)	E_v (J)	E_{Ha} (J)	E_{Tr} (J)	E_{sto} (J)	E_{De} (J)	E_{Ge} (J)	E_{Lo} (J)	
100	10	100	25	2,340.0	1,010.0	990.0	330.0	276.9	255.0	211.9	
			50	2,340.0	1,010.0	990.0	330.0	279.8	258.9	215.1	
		200	25	2,400.0	990.0	970.0	311.5	259.5	238.2	197.7	
			50	2,400.0	990.0	970.0	311.5	263.5	242.7	201.4	
		20	100	25	2,330.0	1,030.0	1,010.0	450.0	379.4	356.6	302.7
				50	2,330.0	1,030.0	1,010.0	450.0	383.0	361.1	306.6
	200	10	100	25	2,340.0	1,030.0	1,000.0	410.0	344.8	321.0	271.3
				50	2,340.0	1,030.0	1,000.0	410.0	347.7	325.8	275.3
		200	25	2,400.0	1,000.0	970.0	380.0	318.4	296.1	248.5	
			50	2,400.0	1,000.0	970.0	380.0	320.7	299.2	251.1	
		20	100	25	2,380.0	1,040.0	1,020.0	490.0	403.8	381.6	323.6
				50	2,380.0	1,040.0	1,020.0	490.0	407.7	385.7	327.0
200	200	25	2,360.0	1,010.0	990.0	470.0	386.3	364.7	307.8		
		50	2,360.0	1,010.0	990.0	470.0	390.6	368.7	311.2		

Table 7.17- Simulation results for the efficiencies of the RPEH device components using a spring-loaded hydraulic accumulator connected to a mechanically actuated hydraulic system.

K_{sto} (kN/m)	A_{sp} (mm ²)	A_{sto} (mm ²)	A_{cp} (mm ²)	η_{Ha} (%)	η_{Tr} (%)	η_{sto} (%)	η_{De} (%)	η_{Ge} (%)	η_{Co} (%)	η_{Mec} (%)	η_{Ele} (%)	η_{RPEH} (%)	η_{Tot} (%)	
100	10	100	25	43.2	98.0	33.3	83.9	92.1	83.1	27.4	76.5	21.0	9.1	
			50	43.2	98.0	33.3	84.8	92.5	83.1	27.7	76.9	21.3	9.2	
		200	25	41.3	98.0	32.1	83.3	91.8	83.0	26.2	76.2	20.0	8.2	
			50	41.3	98.0	32.1	84.6	92.1	83.0	26.6	76.4	20.3	8.4	
	20	100	25	44.2	98.1	44.6	84.3	94.0	84.9	36.8	79.8	29.4	13.0	
			50	44.2	98.1	44.6	85.1	94.3	84.9	37.2	80.1	29.8	13.2	
		200	25	43.5	95.0	45.3	84.1	93.5	84.7	36.2	79.2	28.7	12.5	
			50	43.5	95.0	45.3	84.9	93.9	84.8	36.5	79.6	29.1	12.7	
	200	10	100	25	44.0	97.1	41.0	84.1	93.1	84.5	33.5	78.7	26.3	11.6
				50	44.0	97.1	41.0	84.8	93.7	84.5	33.8	79.2	26.7	11.8
			200	25	41.7	97.0	39.2	83.8	93.0	83.9	31.8	78.0	24.8	10.4
				50	41.7	97.0	39.2	84.4	93.3	83.9	32.1	78.3	25.1	10.5
20		100	25	43.7	98.1	48.0	82.4	94.5	84.8	38.8	80.1	31.1	13.6	
			50	43.7	98.1	48.0	83.2	94.6	84.8	39.2	80.2	31.4	13.7	
		200	25	42.8	98.0	47.5	82.2	94.4	84.4	38.3	79.7	30.5	13.0	
			50	42.8	98.0	47.5	83.1	94.4	84.4	38.7	79.7	30.8	13.2	

Table 7.18- Simulation results for the energy outputs of the RPEH device components using a gas-loaded hydraulic accumulator connected to a mechanically actuated hydraulic system.

P_{gas} (bar)	A_h (mm ²)	A_{sto} (mm ²)	A_{cp} (mm ²)	E_v (J)	E_{Ha} (J)	E_{Tr} (J)	E_{sto} (J)	E_{De} (J)	E_{Ge} (J)	E_{Lo} (J)	
2	20	100	25	2,440.0	1,040.0	1,000.0	340.0	299.5	276.8	230.8	
			50	2,440.0	1,040.0	1,000.0	340.0	301.9	279.0	232.7	
		200	25	2,260.0	1,080.0	1,040.0	340.0	299.5	276.8	230.8	
			50	2,260.0	1,080.0	1,040.0	340.0	301.9	279.0	232.7	
	40	100	25	2,380.0	1,040.0	920.0	460.0	414.5	390.0	331.9	
			50	2,380.0	1,040.0	920.0	460.0	419.5	394.8	335.9	
		200	25	2,420.0	1,040.0	920.0	460.0	415.8	392.1	334.5	
			50	2,420.0	1,040.0	920.0	460.0	419.5	395.6	337.5	
	4	20	100	25	2,380.0	1,080.0	1,040.0	440.0	392.0	362.2	302.1
				50	2,380.0	1,080.0	1,040.0	440.0	395.6	365.5	304.8
			200	25	2,380.0	1,080.0	1,040.0	440.0	392.0	362.2	302.1
				50	2,380.0	1,080.0	1,040.0	440.0	395.6	365.5	304.8
40		100	25	2,360.0	940.0	920.0	520.0	474.8	446.7	380.2	
			50	2,360.0	940.0	920.0	520.0	480.5	452.1	384.8	
		200	25	2,460.0	920.0	860.0	540.0	490.3	462.4	394.4	
			50	2,460.0	920.0	860.0	540.0	490.3	462.4	394.4	

Table 7.19- Simulation results for the efficiencies of the RPEH device components using a gas-loaded hydraulic accumulator connected to a mechanically actuated hydraulic system.

p_{gas} (bar)	A_h (mm ²)	A_{sto} (mm ²)	A_{cp} (mm ²)	η_{Ha} (%)	η_{Tr} (%)	η_{sto} (%)	η_{De} (%)	η_{Ge} (%)	η_{Co} (%)	η_{Mec} (%)	η_{Ele} (%)	η_{RPEH} (%)	η_{Tot} (%)		
2	20	100	25	42.6	96.2	34.0	88.1	92.4	83.4	28.8	77.1	22.2	9.5		
			50	42.6	96.2	34.0	88.8	92.4	83.4	29.0	77.1	22.4	9.5		
		200	25	47.8	96.3	32.7	88.1	92.4	83.4	27.7	77.1	21.4	10.2		
			50	47.8	96.3	32.7	88.8	92.4	83.4	28.0	77.1	21.5	10.3		
		40	100	25	43.7	88.5	50.0	90.1	94.1	85.1	39.9	80.1	31.9	13.9	
				50	43.7	88.5	50.0	91.2	94.1	85.1	40.3	80.1	32.3	14.1	
	4	20	100	25	45.4	96.3	42.3	89.1	92.4	83.4	36.3	77.1	28.0	12.7	
				50	45.4	96.3	42.3	89.9	92.4	83.4	36.6	77.1	28.2	12.8	
			200	25	45.4	96.3	42.3	89.1	92.4	83.4	36.3	77.1	28.0	12.7	
				50	45.4	96.3	42.3	89.9	92.4	83.4	36.6	77.1	28.2	12.8	
			40	100	25	39.8	97.9	56.5	91.3	94.1	85.1	50.5	80.1	40.4	16.1
					50	39.8	97.9	56.5	92.4	94.1	85.1	51.1	80.1	40.9	16.3
200	100	25	37.4	93.5	62.8	90.8	94.3	85.3	53.3	80.4	42.9	16.0			
		50	37.4	93.5	62.8	90.8	94.3	85.3	53.3	80.4	42.9	16.0			

7.3.4 Results analysis

7.3.4.1 Standard hydraulic system

Analyzing the results obtained with the computational simulations of the RPEH device, for both the standard hydraulic system without MES and with a MES system incorporated, based on a spring-loaded or a gas-loaded hydraulic accumulator, some conclusions may be drawn.

Taking the efficiency of the internal device of the RPEH to be the most important parameter to evaluate and comparing the effectiveness of the MES system, one can conclude that, for the same simulation parameters, compared to a hydraulic system the spring-loaded hydraulic accumulator does not increase the efficiency of the RPEH device, but rather decreases its efficiency, whereas the gas-loaded hydraulic accumulator improves the RPEH device efficiency.

Both MES systems were implemented between the hydraulic circuit entrance and the DAC, and are directly actuated by the fluid pressurized by the RPEH DS. The difference in the results between both systems leads us to conclude that the gas-loaded accumulator is three times more efficient than the spring-loaded accumulator, for the same conditions, which has a direct impact on the efficiency of the RPEH internal system.

As expected, the efficiency of the electrical system increases with both accumulators, as the electrical generator is actuated in a continuous mode. However, as the storage efficiency of the spring-loaded accumulator is too small, less than 36%, this does not lead to an increase in the total efficiency of the system. For the gas-loaded accumulator, as the storage efficiency is higher, reaching almost 70%, the accumulated energy means the electrical generator is actuated with its nominal speed and, consequently, works with a very high efficiency rate of almost 95%.

Analyzing individual variables, for the hydraulic system without a MES accumulator, increasing the contact area between the RPEH DS and the hydraulic circuit (A_h) reduces the harvested energy efficiency and the transmitted energy efficiency, leading to a lower

efficiency of the entire system. This is explained by the smaller displacement induced on the DAC piston. On the other hand, increasing the DAC piston area (A_{cp}) leads to an increase in the delivered energy efficiency as well as the electrical generator efficiency, as it means the force delivered on the mechanical system that actuates the electrical generator is increased.

For the hydraulic system with a spring-loaded accumulator, the increase in the spring stiffness allows the stored energy to be increased, as expected. However, the spring stiffness value cannot be increased without limit, as it works as an opposition force to the force transmitted by the hydraulic circuit and, above a certain value, the hydraulic fluid will not be able to move the accumulator piston as the opposition force is higher than the force transmitted by hydraulic fluid.

For this system, increasing the contact area between the RPEH DS and the hydraulic circuit (A_h) has a small impact on the transmitted energy efficiency, but decreases the storage energy efficiency, as the amplification of the force from the hydraulic circuit to the hydraulic accumulator is lower, leading to a smaller displacement of the accumulator piston and, consequently, a lower amount of energy is stored. Also, increasing the accumulator piston area (A_{sto}) decreases the stored energy efficiency, as its displacement is lower and, consequently, the spring force and the stored energy are lower.

For the hydraulic system with a gas-loaded accumulator, the increase in the gas pressure allows the stored energy to increase, as the stored energy is directly related to the fluid pressure, which depends on the gas pressure. However, the gas pressure value cannot be increased without limit, as it works as an opposition force to the force transmitted by the hydraulic circuit and, above a certain value, the hydraulic fluid will not be able to move the accumulator piston as the opposition force is higher than the force transmitted by hydraulic fluid, similar to the spring stiffness in the spring-loaded hydraulic accumulator.

For this system, increasing the contact area between the RPEH DS and the hydraulic circuit (A_h) has little impact on the transmitted energy efficiency, but increases the

storage energy efficiency, as the displacement induced in the hydraulic accumulator piston increases, although the amplification of the force from the hydraulic circuit on the hydraulic accumulator is decreased. By increasing the accumulator piston area (A_{sto}), there is little variation in both the transmitted energy and stored energy efficiencies.

In all the performed simulations the vertical acceleration induced by the RPEH device to the vehicle body was lower than 1 m/s^2 . Considering the existing levels of acceptability of the ride quality (ISO, 1997), this indicates that the RPEH device does not cause discomfort to the vehicle driver and to its occupants.

7.3.4.2 Hydraulic system with mechanical actuation

Analyzing the results obtained with the computational simulations of the RPEH device, both for the mechanically actuated hydraulic system with and without an incorporated MES system, based on a spring-loaded or a gas-loaded hydraulic accumulator, some conclusions may be drawn.

Taking the efficiency of the internal device of the RPEH to be the most important parameter for evaluation, and comparing the effectiveness of the MES system, one can conclude that, for the same simulation parameters, and compared to a hydraulic system with mechanical actuation, both the spring-loaded and the gas-loaded hydraulic accumulators do not increase the efficiency of the RPEH device. On the contrary, the global efficiency decreases with these accumulators.

Both MES systems were implemented between the hydraulic circuit entrance and the DAC, and are directly actuated by the fluid pressurized by the mechanical system. However, due to each system's working principles, their efficiencies are different. The storage efficiency of the gas-loaded accumulator is higher than the spring-loaded accumulator, with an average value of 46.2% for the simulated scenarios and a maximum value of 62.8%, while the spring-loaded accumulator registered an average storage efficiency value of 42.2% for the simulated scenarios and a maximum value of 48.0%. Also, the global efficiency of the entire system is higher for the gas-loaded

accumulator, compared to the spring-loaded accumulator. The best case scenario of the gas-loaded accumulator is 42.9% efficiency of the energy received in the RPEH DS and the electric energy consumed, compared to 31.4% efficiency for the spring-loaded accumulator's best case scenario.

When comparing the simulation results of the systems with and without MES, as expected, the efficiency of the electrical system increases when using both MES accumulators, as the electrical generator is actuated in a continuous mode. However, as the storage efficiency of both accumulators is not very high it represents a mechanical loss in the system, so the global efficiency of the system decreases slightly.

Analyzing individual variables for the RPEH device without a MES accumulator, increasing the contact area of the SAC piston (A_{sp}) has a small impact on the harvested energy efficiency and the transmitted energy efficiency, and both increase slightly. By increasing the DAC piston area (A_{cp}), the delivered energy efficiency increases as does the electrical generator efficiency, as there is an increase in the force delivered on the mechanical system that actuates the electrical generator.

For the hydraulic system with a spring-loaded accumulator, the increase in the spring stiffness allows the stored energy to increase, as expected. However, there is a limit to the extent the spring stiffness value can be increased, as it works as an opposition force to the force transmitted by the hydraulic circuit and, above a certain value, the hydraulic fluid will not be able to move the accumulator piston as the opposition force will be higher than the force transmitted by the hydraulic fluid.

For this system, increasing the SAC piston area (A_{sp}) has a small impact on the transmitted energy efficiency, slightly increasing the storage energy efficiency, as the amplification of the displacement from the hydraulic circuit to the hydraulic accumulator is greater, leading to a higher displacement of the accumulator piston and, consequently, more energy being stored. On the other hand, increasing the accumulator piston area (A_{sto}) decreases the stored energy efficiency, as its displacement is lower and, consequently, the spring force and the stored energy are lower.

For the RPEH device with a gas-loaded accumulator, the increase in the initial gas pressure allows the stored energy to increase, as the stored energy is directly related to the fluid pressure, which depends on the gas pressure. However, there is a limit to the extent the gas pressure value can be increased, as it works as an opposition force to the force transmitted by the hydraulic circuit and, above a certain value, the hydraulic fluid will not be able to move the accumulator piston as the opposition force will be higher than the force transmitted by the hydraulic fluid, similar to the spring stiffness in the spring-loaded hydraulic accumulator.

For this system, increasing the SAC piston area (A_{sp}) has very little impact either on the transmitted energy efficiency or on the storage energy efficiency. Also, by increasing the accumulator piston area (A_{sto}) there is a very small variation in both the transmitted energy and stored energy efficiency. By increasing the DAC piston area (A_{cp}) there is an increase in the delivered energy efficiency.

In all the performed simulations the vertical acceleration induced by the RPEH device to the vehicle body was lower than 1 m/s^2 , a value that indicates that the RPEH device does not cause discomfort to the vehicle driver and to its occupants, according to the existing levels of acceptability of the ride quality (ISO, 1997).

7.4 Summary and Conclusions

Several technologies have been developed to convert vehicles' mechanical energy into electrical energy, some of them using hydraulic systems to transmit the mechanical energy received by the surface of the equipment to an electrical generator, which converts the mechanical energy into electrical energy. Most RPEH devices using hydraulic systems developed so far induce pressure from the equipment's surface to a fluid inside a hydraulic tube, transmitting it to a double acting cylinder. This is controlled by a hydraulic control valve and transmits the mechanical energy to a mechanical RAP system, connected to an electric generator shaft with an inertia wheel. The electric generator converts the mechanical energy into electrical energy, delivering

it to an electrical application. Most part of the systems described in the literature does not include a MES unit, which can have a significant impact in the system performance, considering that other renewable energy generation systems make use of such units with successful results.

In this Chapter, different MES systems were studied and two accumulators were incorporated in RPEH devices based on hydraulic systems, both a typical system and a mechanically actuated hydraulic system, in order to study their impact on the total efficiency of the device. The goal was to increase the energy delivered to the electric generator in order to actuate this element in a continuous mode and, so, increase both the individual efficiency and the global efficiency of the device.

With the hydraulic system modelled here, as well as the rest of the RPEH device, and using a software which had been previously developed and presented in Chapters 3 and 5, computational simulations were performed in order to obtain the values of the energy harvested, transmitted, stored, delivered, converted and consumed by the RPEH device.

From the analysis of the results it can be concluded that, for the same simulation conditions of a standard hydraulic system, the spring-loaded accumulator does not increase the total system efficiency, as it has a low storage efficiency, with average values of around 18%, while the gas-loaded hydraulic accumulator has a high storage efficiency, with average values of around 60%, allowing the total system efficiency to increase by delivering a higher amount of energy to the electric generator in a continuous mode and, so, increasing its efficiency to average values of around 94%.

When MES systems are applied to the RPEH device based on a hydraulic system with mechanical actuation, presented in the previous Chapter, it can be concluded that, for the same simulation conditions as the same system without a MES unit, neither the spring-loaded nor the gas-loaded hydraulic accumulators increase the total efficiency of the device, as the storage efficiency is not very high, reaching maximum values of around 48.0% and 62.8%, respectively, and inducing losses in the mechanical system. However, both hydraulic accumulators allow mechanical energy to be stored and

delivered in a continuous mode to the electrical generator, considerably increasing its working efficiency and potential applications.

The inclusion of a MES system allows several energy harvesting and transmission devices to be connected to the same MES system, which can be connected to a single mechanical energy delivering system and to an electric system, reducing the total costs of the system and allowing electrical energy to be generated only when necessary, and not when the energy source (vehicles) is available. Harvesting and storing vehicle mechanical energy during the day to be consumed at night for road illumination or grid injection purposes, the solutions studied here become viable options, especially using the gas-loaded accumulator.

7.5 References

- Barnes, F. and Levine, J. (Eds.). (2011). *Large energy storage systems handbook*. CRC Press, Boca Raton, FL, USA.
- Chen, H., Cong, T.N., Yang, W., Tan, C., Li, Y. and Ding, Y. (2009). Progress in electrical energy storage system: A critical review. *Progress in Natural Science*, 19(3): 291-312.
- Duarte, F., Champalimaud, J. and Ferreira, A. (2016). Waynergy Vehicles: an innovative pavement energy harvest system. *Proceedings of the Institution of Civil Engineers – Municipal Engineer*, 169(1): 13-18.
- Durfee, W., Sun, Z. and Van de Ven, J. (2015). *Fluid Power System Dynamics*. University of Minnesota, Minneapolis, MN, USA.
- Huggins, R. (2010). *Energy storage, vol. 406*. Springer, New York, NY, USA.
- Ibrahim, H., Ilinca, A. and Perron, J (2008). Energy storage systems—characteristics and comparisons. *Renewable and sustainable energy reviews*, 12(5): 1221-1250.

- ISO (1997). *Mechanical vibration and shock - Evaluation of human response to whole-body vibration. Part I: General requirements*. ISO 2631-1, Geneva, Switzerland.
- Mobley, R. (1999). *Fluid power dynamics*. Butterworth-Heinemann, Woburn, MA, USA.
- Parr, A. (2011). *Hydraulics and pneumatics: a technician's and engineer's guide*. Elsevier, Oxford, UK.
- Pirisi, A., Mussetta, M., Grimaccia, F. and Zich, R. E. (2013). Novel speed-bump design and optimization for energy harvesting from traffic. *IEEE Transactions on Intelligent Transportation Systems*, 14(4): 1983-1991.
- Rabie, M. (2009). *Fluid power engineering*. McGraw-Hill, New York, NY, USA.
- Steinke, F., Wolfrum, P. and Hoffmann, C. (2013). Grid vs. storage in a 100% renewable Europe. *Renewable Energy*, 50: 826-832.
- Ter-Gazarian, A. (2011). *Energy storage for power systems, 2nd Edition*. IET, London, UK.
- Todaria, P., Wang, L., Pandey, A., O'Connor, J., McAvoy, D., Harrigan, T. and Zuo, L. (2015). Design, modeling and test of a novel speed bump energy harvester. In *SPIE Smart Structures and Materials+ Nondestructive Evaluation and Health Monitoring* (pp. 943506-943514). International Society for Optics and Photonics.
- Wood, A. and Wollenberg, B. (2012). *Power generation, operation, and control, Third Edition*. John Wiley & Sons, Hoboken, NJ, USA.

Chapter 8

A Methodology for Technical and Economic Evaluation of Road Pavement Energy Harvesting Devices

8.1 Introduction

In 2014, more than 80% of energy production came from fossil fuels (IEA, 2016), proving that, in the present energetic paradigm, most electrical energy production still makes use of fossil fuel combustion. This leads to irreversible environmental damage and means economies have a great dependency on the fuels costs (IEA, 2015). Urgent action is required to change the paradigm of electrical energy generation, which must be based on renewable resources, decentralized, located near to the point of consumption and, preferably, available when it is needed.

In the energy generation field, not only the technical aspects are critical for a new technology to be accepted and used, but to be implemented in a considerable scale the most important aspect is economic viability, and this represents the most significant challenge with renewable energy sources, when compared with non-renewable sources.

Several technologies have been developed and validated, but they are not yet economically viable to promote an adoption en masse. In the last decade, renewable energy sources such as solar and wind have been adopted increasingly, mainly through governmental incentives in an initial phase, which has led to an industrial development that allowed providers reduce production costs, so making these technologies more viable from an economic perspective, even with progressively reduced governmental incentives (Lewis and Wiser, 2007; Carley, 2009; KPMG, 2015). This proved that with the appropriate strategies and governmental incentives, other technologies can also become economically attractive.

Besides solar and wind energy, other technologies such as wave energy or biomass based systems have been studied intensively as renewable energy sources with a great potential. In some literature (Priya and Inman, 2009; Khaligh and Onar, 2010), these are called macro energy harvesting technologies. Energy Harvesting is typically described as the conversion of ambient energy present in the environment into other useful means of energy, such as electrical energy (Kazmierski and Beeby, 2009). Energy harvesting technologies can be divided in two main groups, as presented in Chapter 2: macro energy harvesting sources, which are associated mainly with solar, wind, hydro and ocean energy; and micro energy harvesting, which is mostly associated with electromagnetic, electrostatic, heat, thermal variations, mechanical vibrations, acoustic and human body motion (Yidliz, 2009; Khaligh and Onar, 2010; Harb, 2010).

As studied in Chapter 2, road surfaces are continuously exposed to vehicle loads, from which it is possible to extract energy which, using specific technologies, can be transformed into electrical energy. These are called RPEH devices. As vehicles abound in most cities of developed countries, it means that a considerable amount of energy is transferred to road pavements without being used. In places where vehicles have to reduce their speed, as for example on road type transitions, crosswalk or roundabout entrances, road crossings, among others, the amount of energy released is maximized, being these places the preferable spots to harvest energy. Road pavements can make use

of that unused energy through RPEH devices that can harvest and convert vehicle mechanical energy into electrical energy.

Although technical details of these technologies have been published, no economic analysis has been presented so far to demonstrate the economic viability of these systems. In this regard, the development of models not only for a technical but, most importantly, for an economic evaluation of such technologies should be considered. Such models would allow us to determine the most critical parameters of these technologies, the importance and critical values of each parameter, so that researchers, investors and decision makers can conclude on the feasibility of such applications. This is a topic that requires attention since only economically viable technologies are usually adopted in the energy production market.

Typically, an energy production unit is evaluated based on three key parameters, namely: the capacity factor (CF), the levelized cost of electricity (LCOE) and the price per installed watt (PPW). Renewable energy production units are no exception and these are the key parameters to evaluate all technologies technically and economically, with LCOE being the most important factor in classifying the economic potential of an energy production unit (Mathew, 2006; Bradford, 2008; Sorensen, 2011; Adaramola, 2014; Narbel *et al.*, 2014).

The CF of an electric energy power plant is the ratio of its actual output over a period of time to its potential output if it were possible for it to operate at full capacity continuously over the same period of time. The LCOE is an economic assessment of the average total cost to build and operate an electric energy power plant over its lifetime divided by the total energy output of the unit over the considered lifetime. The PPW relates the amount of money one would have to spend to implement a power plant capable of producing one watt of electricity, and is calculated by dividing the total cost of the electric energy generation unit by the amount of peak power it can produce (Sorensen, 2011; Adaramola, 2014; Narbel *et al.*, 2014).

The typical CF values of other energy generation technologies are already quantified: solar energy has CF values of around 20-30% (Adaramola, 2014; Joskow, 2011) and

wind energy has CF values of around 30-40% (Mathew, 2006; Boccard, 2009). The PPW of solar PV has values of around 2 to 5 €/W (Adaramola, 2014), depending on the country and on the sector (residential, industrial, big scale), while wind energy has values of around 2 €/W (Mathew, 2006; Boccard, 2009). The LCOE for solar PV is between 107 (EU) and 125 (USA) €/MWh (Bradford, 2008; Adaramola, 2014), while for wind energy it is around 73 (USA) and 142 (EU) €/MWh (Mathew, 2006; Boccard, 2009). These values are not as interesting as for non-renewable sources, as nuclear power, coal or gas powered energy generation stations, among others, mainly due to the intermittency of the energy sources. To give an example, nuclear power has a CF of around 90% and a LCOE of around 50 to 60 €/MWh, making it the energy source with the lowest costs (Narbel *et al.*, 2014; Khatib, 2010).

For more detailed economic evaluations, a cost benefit analysis (CBA) is also performed, in order to study the impact of the project and its importance in economic terms, and to perform a monetary valuation of the solution. This type of analysis is based on the evaluation of the return of capital (ROC), or payback time, for a specific investment; the net present value (NPV) of such investment, and the internal rate return (IRR) that the investment produces (Bradford, 2008; Sorensen, 2011; Diakoulaki and Karangelis, 2007). NPV is an indicator of how much value an investment or project adds to an investor. If the NPV is positive, the investment is considered to add (financial) value to the investor, as it has the status of positive cash inflow in the considered period. On the other hand, if the NPV has a negative value, the investment would subtract value from the investor, and the project has the status of discounted cash outflow in the considered period. The IRR on an investment is the rate of return that makes the NPV of all cash flows, both positive and negative, from a particular investment equal to zero. It is also defined as the discount rate at which the present value of all future cash flow is equal to the initial investment or the rate at which an investment breaks even. This is used to measure and compare the profitability of investments. The higher a project's IRR, the most desirable it is to invest (Bradford, 2008; Sorensen, 2011; Diakoulaki and Karangelis, 2007).

The first novel point of this Chapter is the development of a complete model to evaluate the performance of a road pavement energy harvesting system technically and economically for different energy applications that will allow researchers, investors and decision makers to decide on the feasibility of such applications.

Some software does exist for performing technical and economic evaluation of different energy production technologies, for both renewable and non-renewable energy, which calculates all the previously presented parameters in relation to the inputs defined by the user (Sinha and Chandel, 2014). Solar energy is the technology with the software tools developed in recent years for this purpose (INSEL, 2017; TRNSYS, 2017; PV*SOL, 2017; Solergo, 2017; Solterm, 2017; Polysun, 2017), while specific software for wind energy is not so common (WindSim, 2017). There are several software solutions which allow a user to simulating different energy generation technologies (HOMER, 2017; HYBRID2, 2017; HOGA, 2017; RETScreen, 2017; GRHYSO, 2017), which means a direct comparison can be made between different energy sources and technologies with the same application.

For all of these software solutions, the inputs are related with: the energy source, which in the case of solar energy is the solar availability for the considered place throughout the year, while for wind energy, this is the wind availability; for both of these there is easily accessible information in most countries and the software tools already include this information for each available location; the technical characteristics of the technology and the application; the economic aspects of both the technology and the energy application. With this information, the tool is able to determine all the technical and economic parameters and allow users to come to conclusions about the viability of the application.

Despite the existence of several software tools to evaluate the performance of different energy production technologies technically and economically, there is no tool to perform this evaluation for a RPEH technology, leaving a gap that prevents investors and decision makers from rigorously evaluating this type of solution, as well as

meaning that each researcher use their own method to evaluate the technology under development.

The second novel point of this Chapter is the development of a software tool to evaluate the performance of a road pavement energy harvesting system technically and economically for different energy applications that will allow researchers, investors and decision makers to decide on the feasibility of such applications.

All the important variables, both technical and economic, are considered and the evaluation is based on the potential energy generation of the system, the monetary valuation of that energy depending on the considered energy application, which allows different stakeholders to fully classify the system performance and make decisions about the viability of an investment.

A sensitivity analysis is performed to understand about the impact of each key variable in the technical and economic performance of the system and on the investment return and profitability. These key variables are both technical (traffic data and energy conversion efficiency of the device) and economic (system cost, energy price).

These developments allow to overcome an existing gap, by providing an entire model to evaluate RPEH systems and information about the impact of each variable in the performance of the system and its viability, allowing researchers to direct their attention to optimizing critical variables, and investors and decision makers to seek the most appropriate conditions to invest in this type of solution.

8.2 Evaluation Model Description

8.2.1 Introduction

To perform the technical and economic analysis of an electric energy generation unit, a quantitative research with performance analysis is typically used, by quantifying the electrical energy that the unit is able to produce, per year of operation and for the entire

period of the study, relating it to the investment made both to implement the energy generation unit and to maintain it over time. For this purpose, the CF, LCOE and PPW are the three key parameters for quantification.

The usage of a multi-criteria decision analysis is also considered, with the usage of scenarios and case studies to identify the optimal characteristics of the electric energy generation unit. To implement these methodologies, the values of each key variable are changed between simulations and the previously mentioned parameters are evaluated. A non-monetary evaluation can also be performed considering the impact of the solution in terms of the environmental benefits it provides.

Another important methodology used to evaluate an electrical energy generation unit is the CBA, to study the impact of the project and its economic importance, and to perform a monetary valuation of the solution. This type of analysis is based on the evaluation of the ROC, or payback time, for a specific investment; the NPV of such investment, and the IRR that the investment produces.

To evaluate these parameters, different technical and economical variables are considered, taking in consideration the specificities of each technology. In this section, the equations to perform a technical and economic analysis to a RPEH system application are presented.

8.2.2 Technical and economic analysis

The energy source of a RPEH device is the mechanical energy from moving vehicles. The first and most significant input for a technical analysis of a RPEH unit performance is the traffic data. *AADT* quantifies the annual average daily traffic, measured for all the road lanes. To determine the lane under study's daily traffic (*LDT*) using a simple method, Equation (8.1) can be used dividing *AADT* by the number of road lanes. Proportionally, the lane annual traffic is determined through Equation (8.2).

However, there are different types of vehicles, which release different amounts of energy to the pavement, so it is important to quantify the energy each vehicle releases according to its category. Four different categories were defined: TD_1 for vehicles under 1 ton; TD_2 for vehicles between 1 and 2 tons; TD_3 for vehicles between 2 and 3.5 tons; and TD_4 for vehicles weighing more than 3.5 tons. The daily traffic (DT) can then be quantified for each vehicle category, using Equation (8.3).

$$LDT = \frac{AADT}{NL} \quad (8.1)$$

$$LAT = LDT \times 365 \quad (8.2)$$

$$DT_{cat} = LDT \times (TD_{cat}/100) \quad (8.3)$$

These equations are correct for the first year of the analysis only. Considering the traffic's annual evolution (ATE), the $AADT$ changes every year and, consequently, the LDT , LAT and DT_{cat} also change. So, for a multiple year analysis, from the second year forward, Equations (8.4-8.7) should be used to quantify the updated traffic.

$$AADT_y = AADT_0 \times (1 + ATE)^y \quad (8.4)$$

$$LDT_y = LDT_0 \times (1 + ATE)^y \quad (8.5)$$

$$LAT_y = LAT_0 \times (1 + ATE)^y \quad (8.6)$$

$$DT_{cat(y)} = DT_{cat_0} \times (1 + ATE)^y \quad (8.7)$$

For each vehicle category, a certain amount of energy is released to the RPEH device, depending both on the vehicle and on the RPEH characteristics. These values can be determined using the software tool presented in Chapter 3, which allows performing an energetic analysis on the interaction between a vehicle and a RPEH device. For each traffic average speed (TAS), the average amount of energy released by each vehicle category (ERV_{cat}) can be defined, as presented by Equation (8.8). Considering the conversion efficiency of the RPEH device (η), the energy generated by each vehicle category (EGV_{cat}) can be determined by Equation (8.9).

$$ERV_{cat} = fcn(TAS) \quad (8.8)$$

$$EGV_{cat} = \eta \times ERV_{cat} \quad (8.9)$$

A RPEH unit can be defined by its installed power or by the number of meters of equipment applied on the road pavement. This study considers as inputs the number of meters of RPEH devices installed on the pavement (NMP), the installed power per RPEH unit (IPM) and each device surface' width (EHW). With these, the total number of RPEH installed units (NMI) and the total installed power (TIP) are calculated, using Equations (8.10) and (8.11), respectively.

Knowing the traffic distribution, the daily traffic for each category (DT_{cat}), and the energy generated by each category (EGV_{cat}), and the number of modules installed (NMI) in a RPEH application, the total energy generated per day can be determined using Equation (8.12), for each year, while the total energy generated per year can be determined using Equation (8.13). The total amount of energy generated during the period studied (TE_{Ge}) is determined through Equation (8.14), where YRS represent the number of years considered for the study.

$$NMI = \frac{NMP}{EHW} \quad (8.10)$$

$$TIP = NMI \times IPM \quad (8.11)$$

$$DTEG_y = \sum_{cat=1}^4 \frac{NMI \times DT_{cat(y)} \times EGV_{cat}}{3,600,000} \quad (8.12)$$

$$ATEG_y = DTEG_y \times 365 \quad (8.13)$$

$$TE_{Ge} = \sum_{y=1}^{YRS} ATEG_y \quad (8.14)$$

Associated to renewable or alternative electric energy production, the amount of CO₂ emissions avoided by not using fossil fuels in the energy production can be considered. To do such an analysis, a conversion factor (CCF) from kWh to CO₂ grams can be used, allowing us to determine the CO₂ emissions avoided per year (COY) and the total emissions of CO₂ avoided during the period under study (COP), using Equations (8.15) and (8.16), respectively. Considering the CO₂ economic value per ton (CVT), the

economic value of the avoided emissions can be quantified, per year (VCY) and for the entire period under study (VCP), using Equations (8.17) and (8.18), respectively.

$$COY = \frac{AEG \times CCF}{1,000,000} \quad (8.15)$$

$$COP = \frac{TEG \times CCF}{1,000,000} \quad (8.16)$$

$$VCY = COY \times CVT \quad (8.17)$$

$$VCP = COP \times CVT \quad (8.18)$$

To evaluate the CF of the RPEH application, the total amount of energy generated during the studied period (TE_{Ge}) should be compared to the maximum possible energy generated by the RPEH unit, which can be determined considering the total installed power, producing energy during the entire period of the study. The CF is determined using Equation (8.19), where the previous parameters are considered.

$$CF = \frac{TE_{Ge}}{\left(\frac{TIP \times 24 \times 365 \times YRS}{1000} \right)} \quad (8.19)$$

To perform an economical analysis, some important parameters should be defined. The price per RPEH module (PPM) is the first and most important, as well as the installation price per RPEH module ($ICPM$), the extra equipment price (EEP), other costs involved (OCI) and yearly maintenance price per module (YMP). Annual inflation (INF) should also be considered.

The price per module defines the price that the customer pays for each RPEH module installed, excluding taxes. The $ICPM$ is the total installation price divided by the number of RPEH devices installed on the road pavement. The EEP is the sum of all the equipment external to the road pavement, such as the energy converter, the electronic and storage units, and the inverter. The item OCI represents all the additional costs involved, such as the installation design, insurance and taxes. The YMP are the costs of maintenance of the RPEH devices, per year, and these costs are updated each year, considering the annual inflation (INF), as defined by Equation (8.20).

$$YMP_y = YMP_{(y-1)} \times INF \quad (8.20)$$

With these parameters, it is possible to determine the initial investment on the RPEH application (*CAPEX*), the annual maintenance costs (*OPEX*), and the total investment for all the years considered for the project lifetime (*TINV*), using Equations (8.21-8.23).

Knowing the *CAPEX*, *OPEX* and *TINV*, it is possible to determine the *PPW* and the *LCOE*, the two most important parameters in evaluating a renewable energy application. These are determined using Equations (8.24) and (8.25), respectively.

$$CAPEX = NMI \times (PPM + ICPM) + EEP + OCI \quad (8.21)$$

$$OPEX_y = NMI \times YMP_y \quad (8.22)$$

$$TINV = CAPEX + \left(\sum_{y=2}^{YRS} OPEX_y \right) \quad (8.23)$$

$$PPW = \frac{CAPEX}{TIP} \quad (8.24)$$

$$LCOE = \frac{TINV}{TEG} \quad (8.25)$$

8.2.3 Cost benefit analysis

To perform a CBA for a renewable energy production system, two different energy applications (EA) are usually considered: the injection of the produced energy into the grid (GI), receiving a defined amount of money for each kWh injected into the grid; or the self-consumption (SC) of the generated energy, avoiding buying electricity from the grid. Both EA were considered in the present study.

In the GI application, only two variables are needed to perform the CBA: the initial price at which the electricity operator buys the produced electrical energy (*GIEP*) and the energy price yearly evolution (*GIYE*). Then, the price at which the electricity operator buys the produced electrical energy for each year (*GIAEP*) can be determined,

as expressed by Equation (8.26). Knowing this value, to determine the annual income (*GIAI*) and the total income for the studied period (*GIPI*), Equations (8.27) and (8.28) can be used, respectively. The total profits can be determined by subtracting the *TINV* from the *GIPI*.

$$GIAEP_y = GIAEP_{(y-1)} \times GIYE \quad (8.26)$$

$$GIAI_y = GIAEP_y \times AEG_y \quad (8.27)$$

$$GIPI = \sum_{y=1}^{YRS} GIAI_y \quad (8.28)$$

To determine the *ROC*, or payback time, Equation (8.29) can be used, relating the *TINV* to the average value of the *GIAI*. The annual cash flow (*CFLO*) is determined through Equation (8.30), relating the *CAPEX* to the yearly *GIAI* and *OPEX*, and the updated cash flow (*CFLOU*) is determined by Equation (8.31), considering the annual inflation (*INF*). These two variables are important to determine the *NPV* and the *IRR* of the investment, calculated through Equations (8.32) and (8.33), respectively.

$$ROC = \frac{TINV}{\left(\frac{\sum_{y=1}^{YRS} GIAI_y}{YRS} \right)} \quad (8.29)$$

$$\left. \begin{array}{l} y = 1: \quad CFLO_1 = -CAPEX + GIAI_1 \\ y > 1: \quad CFLO_y = CFLO_{(y-1)} + GIAI_y - OPEX_y \end{array} \right\} \quad (8.30)$$

$$\left. \begin{array}{l} y = 1: \quad CFLOU_1 = CFLO_1 \\ y > 1: \quad CFLOU_y = \frac{CFLO_y}{\left(1 + \frac{INF}{100}\right)^y} \end{array} \right\} \quad (8.31)$$

$$NPV = \sum_{y=1}^{YRS} CFLOU_y \quad (8.32)$$

$$NPV = \sum_{y=1}^{YRS} \frac{CFLO_y}{(1 + IRR)^y} = 0 \quad (8.33)$$

In the SC application, more variables are needed besides the initial energy price (*SCEP*) and the energy price annual inflation (*SCEI*). First, it is necessary to determine the annual energy consumption (*SCYCE*) of the electrical application and, for that, the

installed power ($SCIP$) and the average consumption hours per day ($SCAH$) are needed. With these variables, $SCYCE$ is determined through Equation (8.34). The total energy consumed during the considered period ($SCPCE$) can be determined through Equation (8.35), without considering any energy consumption variation during the period. Knowing the total energy generated by the RPEH application (TE_{Ge}), it is possible to determine the percentage of energy contribution ($SCPC$) to supply the electrical application, through Equation (8.36). Ideally, this value should be close to 100%, as for lower values the energy generated will not be enough to fully supply the electrical application, and for higher values there is more energy being generated than required - in this case, the exceeding energy could be injected into the grid.

$$SCYCE = \frac{SCIP \times SCAH \times 365}{1000} \quad (8.34)$$

$$SCPCE = SCYCE \times YRS \quad (8.35)$$

$$SCPC = \frac{TE_{Ge}}{SCPCE} \times 100 \quad (8.36)$$

As for the GI application, the energy price ($SCEPY$) should also be updated for each year, through Equation (8.37). Then, the annual savings ($SCAS$) and the total savings for the period considered ($SCECP$) can be determined by Equations (8.38) and (8.39), respectively. The total savings can be quantified by subtracting the $TINV$ from the $SCECP$.

$$\left. \begin{array}{l} y = 1: \quad SCEPY_1 = SCEP \\ y > 1: \quad SCEPY_y = SCEPY_{(y-1)} \times SCEI \end{array} \right\} \quad (8.37)$$

$$\left. \begin{array}{l} SCPC < 100: \quad SCAS_y = SCEPY_y \times TEG \\ SCPC > 100: \quad SCAS_y = SCEPY_y \times SCPCE \end{array} \right\} \quad (8.38)$$

$$SCECP = \sum_{y=1}^{YRS} SCAS_y \quad (8.39)$$

To determine the ROC for this EA, the $GIAI$ should be substituted by the $SCAS$ in Equation (8.29). Similarly, to determine the $CFLO$, the $GIAI_y$ should be substituted by

the $SCAS_y$ in Equation (8.30). Then, the $CFLOU$, NPV and IRR are determined through Equations (8.31-8.33).

8.3 Software Tool for Technical and Economical Evaluation of RPEH Applications

8.3.1 Introduction

Based on the study presented in the previous section, a simulation software tool was developed, using MATLAB[®] software, in order to study the technical and economic performance of an RPEH system, as well as to perform the cost benefit analysis of these systems for different energy applications. The software was named RETEES - Road Energy Technical and Economic Evaluation Software.

The purpose of the simulation software is to perform this analysis in great detail, with the possibility of fully characterizing the traffic of the road where the system is implemented, the technical features of the RPEH devices, as well as their economical features, and the energy applications where the electrical energy generated by the RPEH unit is used. With all these data, the software determines all the technical and economic data defined in the previous section, typically used for other renewable and non-renewable energy sources, allowing the viability of the technology application for each scenario to be determined. The results are presented both numerically and graphically. Also, the software allows a sensitivity analysis to be performed, by defining a key variable and indicating its values, recalculating the outputs for the different scenarios.

In this section, the simulation software is briefly presented in terms of the input and output graphical user interfaces and the flowcharts that illustrate its working principles. In Figure 8.1 a schematic representation of RETEES is presented.

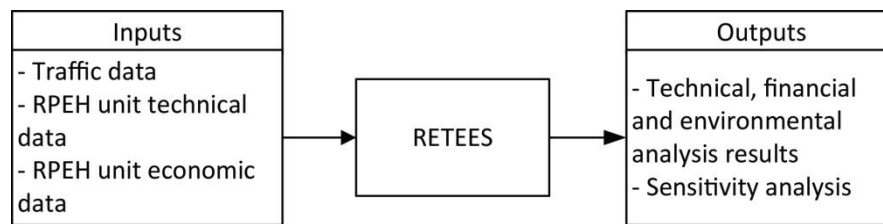


Figure 8.1- Schematic representation of RETEES.

8.3.2 Inputs and calculations

To select the model inputs, a GUI platform was developed, as presented in Figure 8.2. This GUI has 3 distinct panels for parameter selection and four buttons.

The first panel allows the user to define the traffic data, by defining the total AADT of the road under study and the number of lanes of that road; the average traffic speed, important to determine the average energy released by each vehicle type; the traffic distribution by vehicle type, as mentioned in previous section; and the duration of the analysis, in terms of years, as well as the annual traffic evolution.

The second panel allows the user to define the RPEH system and application's technical data, with the number of meters installed in the pavement, each RPEH module's width, the power installed by module and the conversion efficiency of each module - from which it is possible to determine the energy generated by the RPEH module for each vehicle type. It also allows users to define the grams of CO₂ saved for each kWh of electrical energy produced and the evaluation of each ton of CO₂. The user can accept the determined values of energy generation per vehicle type per module, or can introduce these values manually.

The screenshot shows the RETEES GUI with three main panels:

- Traffic data:** Includes fields for AADT, Number lanes, Average speed (50 km/h), Duration (Multi-year), Number years, Traffic evol (%), and Traffic distribution (TD1-TD4). It also has fields for Lane daily/monthly/yearly traffic and Daily traffic distribution (DT1-DT4).
- Energy generation application:** Includes fields for Number of meters, Module width (m), Power p/ module (W), Conv. Eff. (%), CO2 (g) per kWh, and CO2 value (€/ton). It also has Energy generation per vehicle passage (EG1-EG4) and Energy generation per vehicle type / day (EG1-EG4) sections.
- Economic analysis:** Includes fields for Price p/ module (€), Other costs (€), Installation price p/m (€), Yearly maint p/m (€), Extra equipment price (€), Annual inflation (%), Energy application (None), Self consumption (Installed power (W), Aver. hours/day (h), Energy price (€/kWh), Price ev/year (%), Energy cost (€/kWh), Energy inflation (%)), Initial investment (€), Annual maint. costs (€), Total investment period (€), CO2 valuation p/ year (€), and CO2 valuation - total (€).

Buttons at the bottom include 'Default values', 'Clear all', 'Technical & Economic Analysis', and 'Cost Benefit Analysis'.

Figure 8.2- RETEES GUI to select the inputs for the computational model.

The third panel allows the user to define both the RPEH system economic data, by introducing the price of each RPEH module, the installation price per RPEH module, the extra equipment price (e.g., the inverter costs), other costs involved (e.g., the application design costs), the yearly maintenance price per module (*YMP*) and the annual costs inflation. This panel also allows users to define the energy application data, for cost benefit analysis, by defining the energy application - grid injection or self consumption - and the specific data of each application: the energy price per kWh and the annual evolution of this price, for the grid injection energy application; and the installed power, average consumption hours per day, energy cost per kWh and energy price inflation, for the self consumption energy application.

Figure 8.3 presents the flowcharts for each action in the input GUI.

While the user inserts data in this GUI, the corresponding initial outputs of each section are automatically calculated and presented in the GUI (Figure 8.3a). For example, with *AADT* and *NL* defined, *LDT*, *LMT* and *LAT* are automatically determined and presented,

and with TD_1 - TD_4 defined, DT_1 - DT_4 are also automatically determined and presented in the GUI.

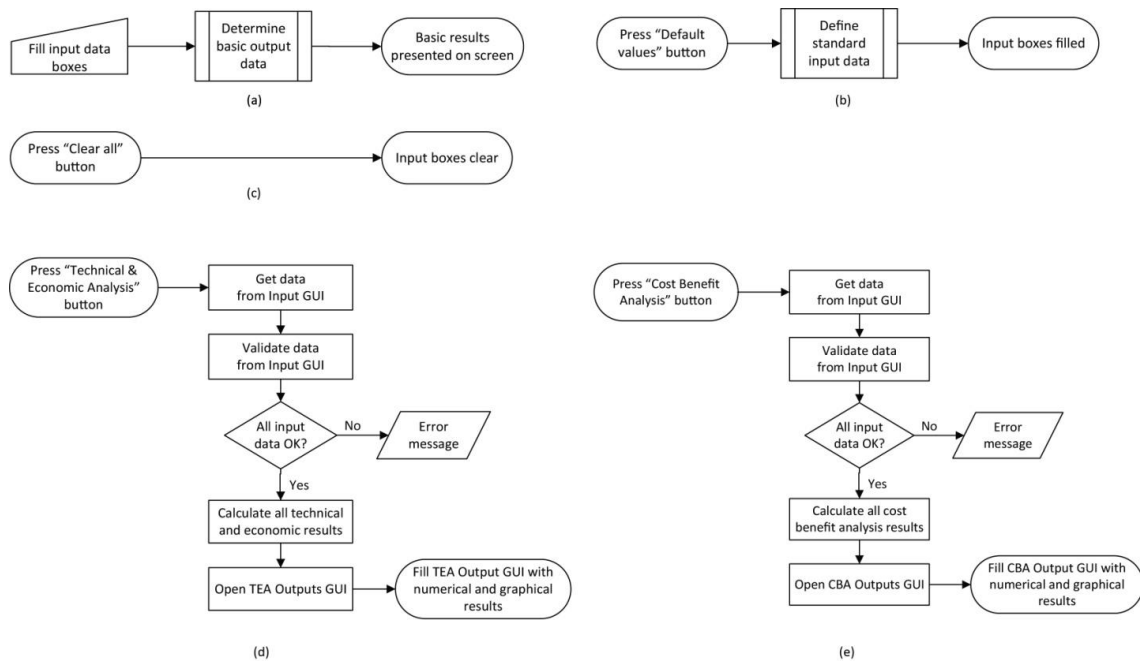


Figure 8.3- RETEES flowcharts from Inputs GUI actions and buttons: (a) fill input data action; (b) press "Default values" button; (c) press "Clear all" button; (d) press "Technical & Economic Analysis" button; (e) press "Cost Benefit Analysis" button.

When the user presses the button *Default values*, all the input boxes are automatically presented with standard scenario values (Figure 8.3b), and if the user presses the button *Clear all*, all the input boxes values are automatically cleared (Figure 8.3c).

After all the data is defined by the user in the *Inputs* GUI and the *Technical & Economic Analysis* button is pressed, all the data is collected and a validation is done to confirm if the data is correctly defined. If it is not, an error message is presented. If it is correct, all the variables are defined and the computational model computes all the technical and economic results for the selected period, based on the equations presented

in the previous section for the TEA. After the simulation is completed, the results are obtained and validated. A TEA *Output* GUI is opened and the results are presented, both graphically and numerically (Figure 8.3d). If the *Cost Benefit Analysis* button is pressed, the validation and computation processes are similar, but the CBA data is determined instead of the TEA, based on the equations presented in the previous section for the CBA, and a CBA *Output* GUI is opened where the results are presented, both graphically and numerically (Figure 8.3e).

8.3.3 Outputs and results presentation

Two different *Output* GUI's were developed, one for each type of analysis: one for the TEA outputs (Figure 8.4) and another for the CBA outputs (Figure 8.5). The layout of both GUI's is identical, with four distinct panels - one to present the numerical results and another to present the graphical results of the TEA/CBA; one to define the sensitivity analysis data and another to present the sensitivity analysis graphical results - and four buttons.

In the TEA *Output* GUI several numerical results are presented in the left panel, as shown in Figure 8.4, with special emphasis on the *Cost per installed Watt*, *Levelized Cost of Electricity* and the *Capacity Factor*, the most important parameters of the TEA. Also, three graphical intermediate results are presented in the upper panel: the annual variation of the LDT (in vehicles per day), the quantity of the annual energy generation (in kWh) and the annual OPEX (in Euros).

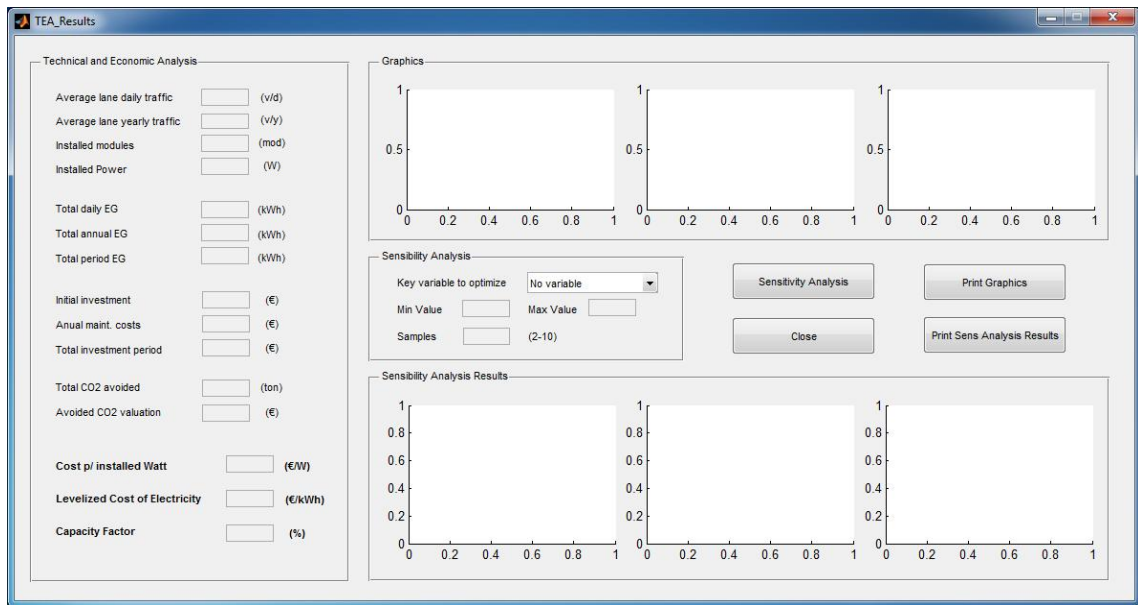


Figure 8.4- RETEES GUI to present the outputs for the TEA.

The *Sensitivity Analysis* panel allows the user to select the key variable to optimize and its values, with a more detailed explanation presented in Section 3.4. The *Sensitivity Analysis Results* panel shows the results for each scenario graphically, for the three main outputs (*PPW*, *LCOE* and *CF*).

In the *CBA Output* GUI (Figure 8.5) the numerical results presented are focused on each energy application and on the main evaluation parameters - the *ROC*, *NPV* and *IRR*, while the graphical results present the annual cash-flow (in Euros), the value of the annual energy sold/saved (in Euros) and the global financial performance (in Euros), where the total investment, total income/savings and total profits are presented.

The four buttons are similar for both GUI's and these are related to: the *Sensitivity Analysis*, *Print TEA/CBA Graphics*, *Print Sensitivity Analysis Results* and *Close* the GUI. Each button action flowchart is presented in Figure 8.6.

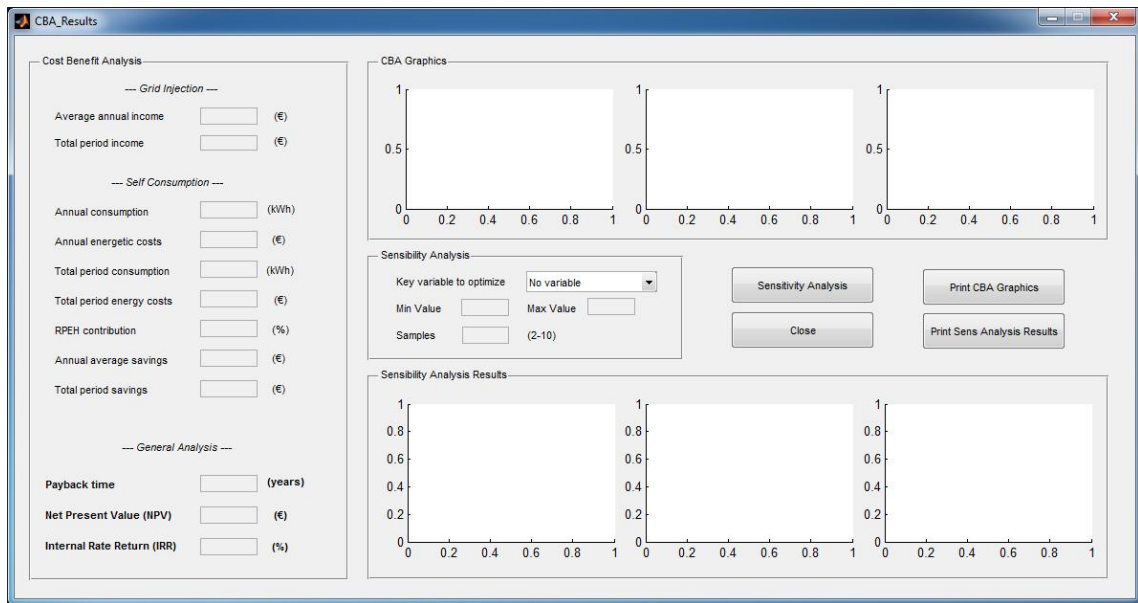


Figure 8.5- RETEES graphical user interface to present the outputs for the cost benefit analysis.

If the *Sensitivity Analysis* button is pressed, the model checks if any key variable is selected in the SA panel - if not, an error message is displayed. If a variable is selected, SA panel values are validated - if an error is detected, an error message is displayed, if not, the model proceeds with the SA, computing the previously model with the respective equations presented in the previous section, for the different key variable values, registering the outputs of each scenario. In the end, the results are presented graphically in the bottom panel of the GUI, with three graphics, each presenting an output result for the different key variable scenarios (Figure 8.6a).

If the *Print Sens Analysis Graphics* button is pressed, the model checks if any key variable is selected in the SA panel - if not, an error message is displayed. If a variable is selected, the model checks if the SA Results graphics are filled in - if not, an error message is displayed, if yes, the model proceeds by saving all the results in an Excel file, and then printing the graphical results in *jpeg* files (Figure 8.6b).

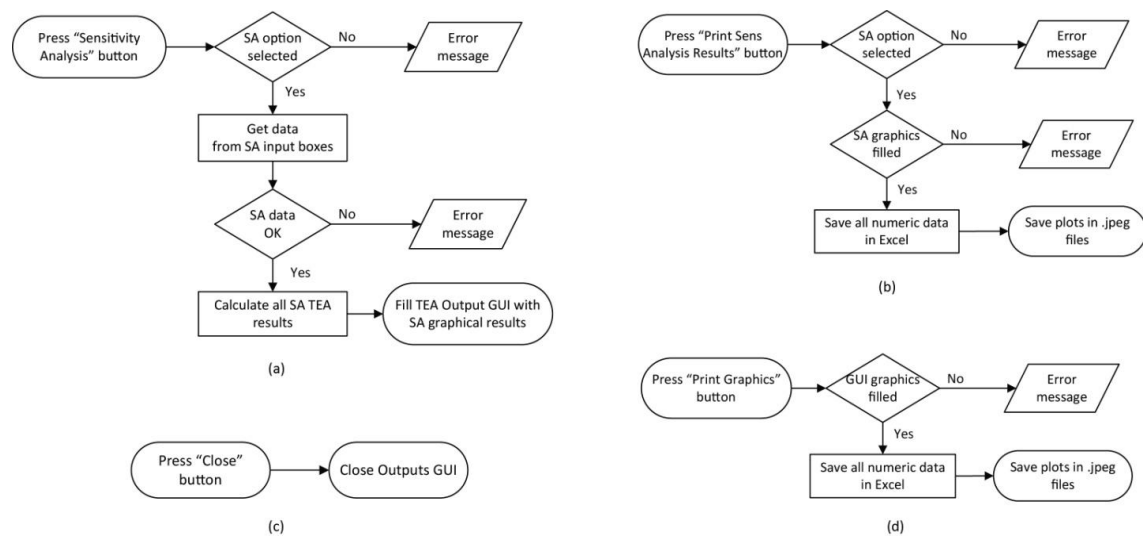


Figure 8.6- RETEES flowcharts from output GUI buttons: (a) press "Sensitivity Analysis" button; (b) press "Print Sens Analysis Results" button; (c) press "Close" button; (d) press "Print Graphics" button.

If the *Print Graphics* button is pressed, the model checks if the *TEA/CBA Graphics* are filled in - if not, an error message is displayed, if yes, the model proceeds by saving all the results in an Excel file, and then printing the graphical results in *jpeg* files (Figure 8.6c).

Finally, if the *Close* button is pressed, the GUI is automatically closed (Figure 8.6d).

8.3.4 Sensitivity analysis

The *Sensitivity Analysis* panel of the *TEA Output GUI* allows the user to select the key variables to optimize, with five key variables available - *AADT*, *IPM*, *PPM*, *YMP* and η . With the key variable selected, the user can define its minimum and maximum values, as well as the number of samples to be evaluated (only a number between 2 and 10 is accepted). The intermediate values of the key variable are determined in direct proportion between the minimum and maximum values, distributed by the number of

samples. For example, if the selected key variable is *AADT*, the minimum value is 10,000, the maximum value is 50,000 and the number of samples is 5, the model will evaluate five scenarios: 10 ,000; 20,000; 30,000; 40,000 and 50,000 vehicles/day (Figure 8.7).

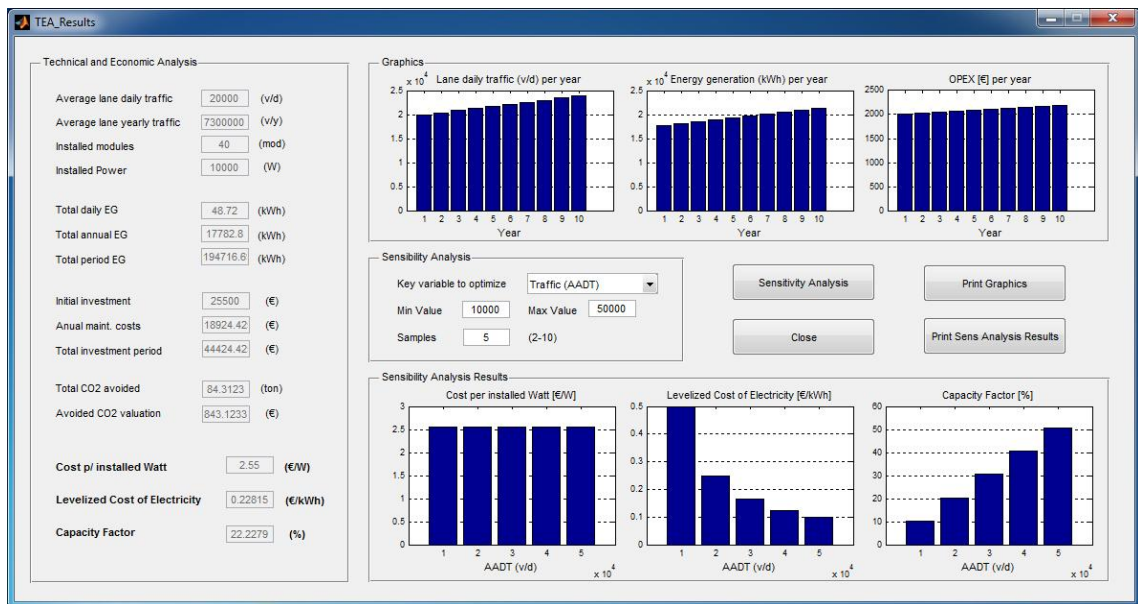


Figure 8.7- RETEES output GUI filled with TEA numerical and graphical results and with the SA graphical results.

The software uses all the data inserted in the *Input* GUI to perform the *SA*, changing only the key variable value in each scenario, registering the outputs. After computing all the key variable values, the results are presented graphically, in the *Sensitivity Analysis Results* panel, with one graphic for each output: *PPW*, *LCOE* and *CF* (Figure 8.7).

For the previously mentioned case with five different *AADT* values, Figure 8.7 presents the simulation results for the *SA*, with each graph having 5 bars, one for each scenario, making it possible to conclude that the *PPW* does not change with *AADT*, the *LCOE* decreases with the *AADT* increase, and the *CF* increases with the *AADT* increase.

Similarly, the *Sensitivity Analysis* panel of the *CBA Output* GUI allows the user to select the key variable to optimize, with six key variables available - *AADT*, *IPM*, *PPM*, *YMP*, *GIEP/SCEP* (depending on the energy application) and η . With the key variable selected, the user can define its minimum and maximum values, as well as the number of samples to be evaluated (only a number between 2 and 10 is accepted). The intermediate values of the key variable are determined in direct proportion between the minimum and maximum values, distributed by the number of samples.

The evaluation process of the cost benefit SA is similar to the technical and economical SA, with the results presented graphically in the *Sensitivity Analysis Results* panel, with one graph for each output: *ROC*, *NPV* and *IRR* (Figure 8.8).

Considering a case with 10 different *AADT* values, from 10,000 to 50,000 vehicles/day, Figure 8.8 presents the simulation results for the SA, with each graph having 10 bars, one for each scenario, making it possible to conclude that the *ROC* decreases with the increase in *AADT*, while the *NPV* and the *IRR* increase with the increase in *AADT*.

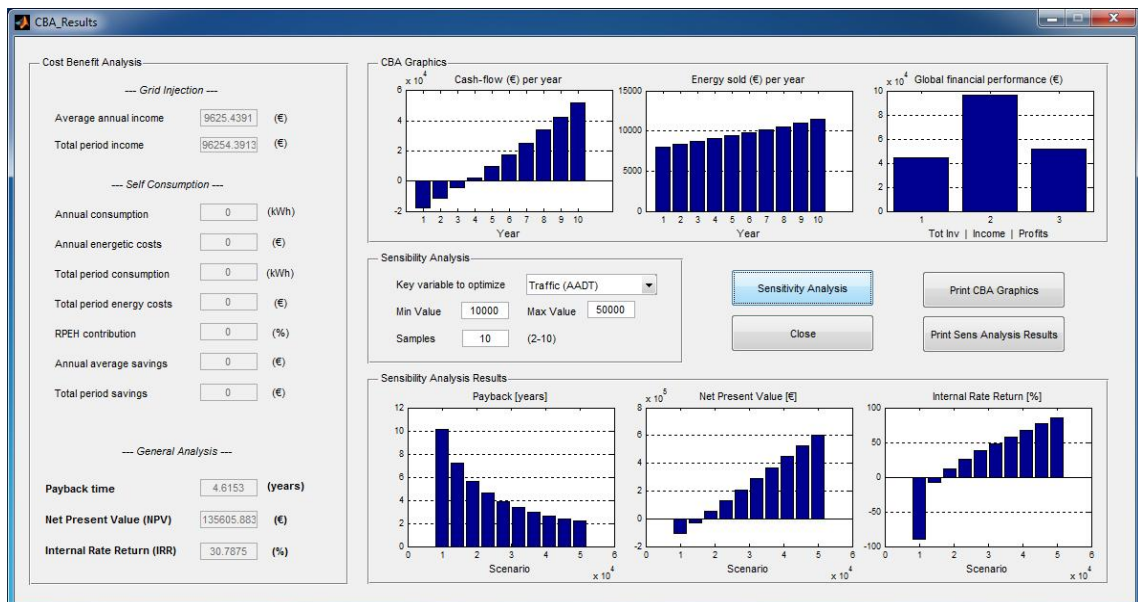


Figure 8.8- RETEES output GUI filled with CBA numerical and graphical results and with the SA graphical results.

8.4 Case Studies and Results

8.4.1 Introduction

The models being developed are used to evaluate a RPEH system application both technically and economically, as well as to perform a cost benefit analysis for an energy application of the RPEH system, and the results obtained from the case studies are discussed in this section.

First, the model inputs are presented and justified.

1. The road type considered for implementing the RPEH devices is a main distributor in an urban environment, where the traffic speed is 50 km/h, traffic volume is high enough to provide reasonable values of harvested energy and traffic speed reduction is required at its entrance, exit and in specific spots. The number of lanes of this road type can be two or four (AASHTO, 2001; Elvik *et al.*, 2009). In the present work, for simplification purposes, two lanes are considered, with the total *AADT* distributed equally over the two lanes.
2. To define the traffic data, typical values for urban mobility are considered, based on high density population cities (TRB, 2000). So, the initial value considered, for a two lane road, is 20,000 vehicles per day, which is changed in the sensitivity analysis.
3. The traffic distribution by vehicle category changes in relation to the country and the type of road. Considering a typical scenario of a main distribution road in an urban environment (TRB, 2000; AASHTO, 2001; Elvik *et al.*, 2009), the selected traffic profile is: TD_1 equal to 25%; TD_2 equal to 50%; TD_3 equal to 23%; and TD_4 equal to 2%.
4. To determine the energy released by each vehicle type (ERV_{1-4}) in relation to each traffic average speed (*TAS*), the software RoadVISS, presented in Chapter 3, was used. The results are presented in Table 8.1, for an EHW equal to 0.5 m.

Table 8.1- Average energy released by vehicle category in relation to the vehicle speed ($EHW = 0.25$ m).

TAS (km/h)	ERV ₁ (J)	ERV ₂ (J)	ERV ₃ (J)	ERV ₄ (J)
30	100	150	200	300
40	150	200	300	500
50	200	266	400	666
60	180	230	350	600
70	150	200	300	500

5. To define the energy conversion efficiency of a RPEH device, as well as its typical dimensions and installed power, the state-of-the-art study presented in Chapter 2 is used. From the different technologies under development, those which make use of electromechanical systems are the most efficient, reaching a maximum efficiency of 50% (currently). For this particular system (Duarte *et al.*, 2016), the module width is 0.7 m and the installed power per module is about 450 W. Despite the fact the module width is slightly more than 0.5 m, considered to determine the energy lost by the vehicle, the values of Table 8.1 are accepted for a module width of 0.7 m.
6. The considered values of CO₂ grams avoided for each kWh produced changes from country to country, depending on their energy production profile. An average value for OECD countries is 500 CO₂g/kWh (EEA, 2017), and this value is used in the present study. For USA, for example, this value is 480 CO₂g/kWh, while for Europe the average value is 290 CO₂g/kWh.
7. Valuation of CO₂, also known as carbon price, has been decreasing yearly. Currently, and as defined by the World Bank (Luckow *et al.*, 2015; The World Bank, 2017), a price of 10 €/ton can be considered a reference value.
8. The price per module is not defined in the existing studies regarding RPEH systems, as these are based on the technical performance of the systems under development. So, in this study, values are set in relation to the costs of the components used to produce the selected system (Duarte *et al.*, 2016). The

considered price of each module is 1,000 € and its installation cost is equal to 100 €. The extra equipment cost considered for a grid injection or self consumption application is 1,000 €, for a power inverter solution. Extra costs with certification and insurance are considered, giving a total cost of 500 €. The annual maintenance costs used are 50 € per RPEH unit.

9. To define the grid injection energy price, a subsidized regime is considered. Taking into consideration what has been done for other technologies in several countries (Haas *et al.*, 2004; Reiche and Bechberger, 2004; Alvarez *et al.*, 2009; Frondel *et al.*, 2009; Boomsma *et al.*, 2012; Schmalensee, 2012; Campoccia *et al.*, 2014), especially for solar PV, with several countries in Europe using feed-in tariff's higher than 0.50 €/kWh, a feed-in tariff of 0.65 €/kWh is considered in the present study, similarly to what was done to set up the solar energy program in Portugal, in 2007. This value is valid for a 10 year period (Portal Energia, 2017). This value was set initially to support the market's adoption of the technology and was then progressively reduced in order to follow the falling price of the technology.

The simulations input values are presented in Table 8.2.

8.4.2 Technical and economic analysis

Using the values presented in Table 8.2 to perform a TEA, the obtained results are presented in Table 8.3. One can conclude that the PPW is close to that of other renewable energy sources (Adaramola, 2014; Narbel *et al.*, 2014), but the LCOE is higher than current energy generation solutions, while the *CF* is too low. So, a sensitivity analysis was performed for different key variables to understand the impact of each variable in the technical and economic performance of the RPEH application.

Table 8.2- Initial values for the simulation variables.

	Variable name	Value	Unit
Traffic data	AADT	20,000	(vehicles/day)
	Number of road lanes	2	-
	Average speed	50	(km/h)
	Traffic distribution TD ₁₋₄	23 50 25 2	(%)
	Analysis: number of years	10	(Years)
	Annual traffic evolution	2	(%)
RPEH technical data	Number of installed meters	28	(m)
	Module width	0.7	(m)
	Power per RPEH module	450	(W)
	Conversion efficiency	50	(%)
	CO ₂ g/kWh	500	(g/kWh)
	CO ₂ valuation	10	(€/ton)
	Energy generation p/ vehicle type (EGM ₁₋₄)	Determined	(J)
RPEH economic data	Price per module	1,000	(€)
	Installation price per module	100	(€)
	Extra equipment price	1,000	(€)
	Other costs involved	500	(€)
	Yearly maintenance price per module	50	(€)
	Annual inflation	2	(%)
Energy application	Energy Application	GI	-
	GI: Energy price price evolution	0.65 0	(€/kWh) (%)
	SC: Energy cost Energy inflation	0 0	(€/kWh) (%)
	SC: Installed power Av. Hours/day	0 0	(W) (h)

The SA for different *AADT* values considers 5 values from 10,000 to 50,000 vehicles per day on the two road lanes and its results are presented in Figure 8.9a for the three key indicators. The SA for different values of η considers 5 values from 40 to 80% and the results are presented in Figure 8.9b. The SA for different *PPM* values considers 5 values from 500 to 1,500 € and its results are presented in Figure 8.9c. The SA for different *YMP* values considers 4 values from 20 to 100 € and its results are presented in Figure 8.9d.

Table 8.3- Results for a TEA to a RPEH application.

Variable	Value	Unit
Average lane daily traffic	10,000	(vehicles/day)
Average lane yearly traffic (Y1)	3,650,000	(vehicles /year)
Installed modules	40	-
Installed power	18,000	(W)
Daily energy generation	16.2	(kWh)
Annual energy generation (Y1)	5,926.6	(kWh)
Total (period) energy generation	64,905.6	(kWh)
Initial investment	45,500.0	(€)
Annual maintenance costs (Y2)	2,000.0	(€)
Total investment (period)	65,399.4	(€)
Total CO ₂ emissions avoided	32.4	(ton)
Value of CO ₂ emissions avoided	324.5	(€)
PPW	2.53	(€)
LCOE	1.01	(€/kWh)
CF	4.12	(%)

From the analysis of the SA results, one can conclude that the *AADT* variation does not have an impact on the *PPW*. However, this variable has a great impact on the *LCOE* and on the *CF*. When the *AADT* increases, there is a considerable reduction of the *LCOE* and a directly proportional increase of the *CF*. The same impact is obtained with the variation of the conversion efficiency of the RPEH system, leading us to conclude that these two variables have a great impact on the technical and economic performance of the system.

Also, from the analysis of the SA results one can conclude that neither the *PPM* nor the *YMP* affect the *CF*, but both have a direct impact on the *LCOE*, as this parameter rises with the increase of both variables. The *PPW* increases as the *PPM* increases, but it is not affected by the change to the *YMP*.

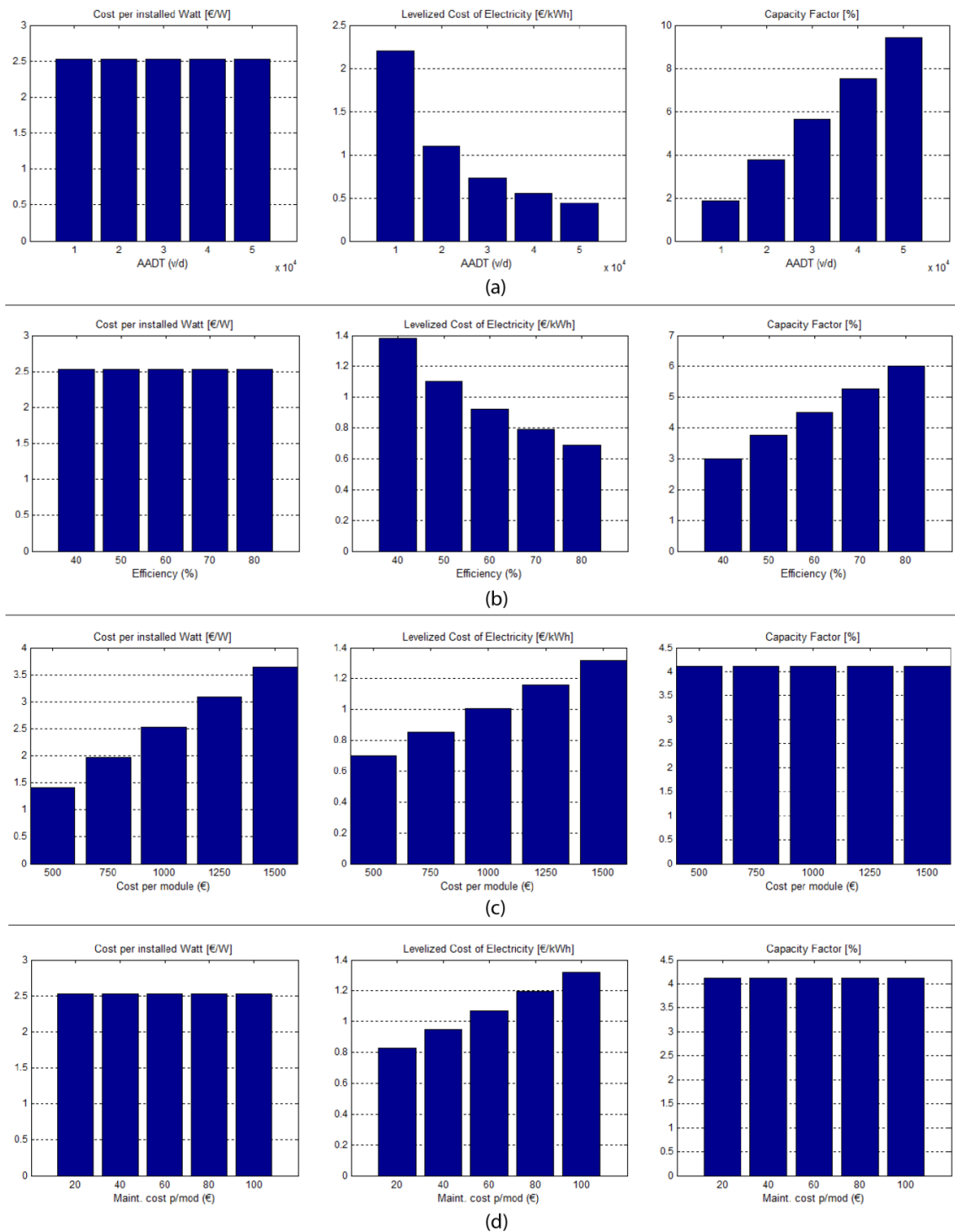


Figure 8.9- Sensitivity analysis results for the variation of the (a) AADT; (b) η ; (c) PPM; (d) YMP.

So, to optimize the technical and economic evaluation of the RPEH system application, the critical variables for consideration are the *AADT* and the η . With an SA performed on both variables simultaneously, the achieved results are presented in Table 8.4 and Figure 8.10 for the *LCOE* and the *CF* (*PPW* is not considered as this parameter does not change with these variables).

Table 8.4- Results of a multi-variable SA for a TEA to a RPEH application.

AADT (v/d)	η (%)	LCOE (€/kWh)	CF (%)
10,000	40	2.78	1.51
	50	2.22	1.92
	60	1.85	2.25
	70	1.61	2.66
	80	1.42	3.05
20,000	40	1.38	3.00
	50	1.10	3.76
	60	0.92	4.51
	70	0.79	5.26
	80	0.69	6.01
30,000	40	0.92	4.61
	50	0.74	5.64
	60	0.61	6.77
	70	0.52	7.90
	80	0.46	7.92
40,000	40	0.69	6.01
	50	0.55	7.52
	60	0.46	9.02
	70	0.39	10.53
	80	0.35	12.03
50,000	40	0.55	7.52
	50	0.44	9.40
	60	0.37	11.28
	70	0.31	13.16
	80	0.28	15.04

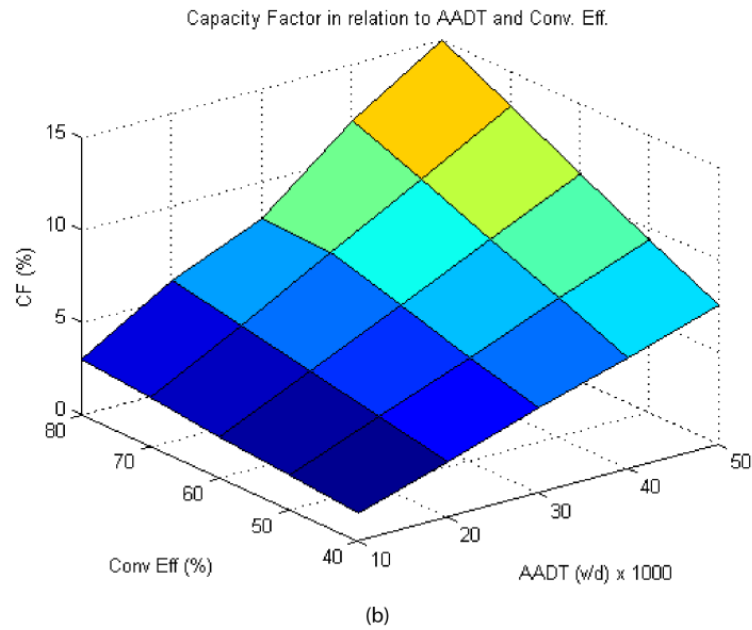
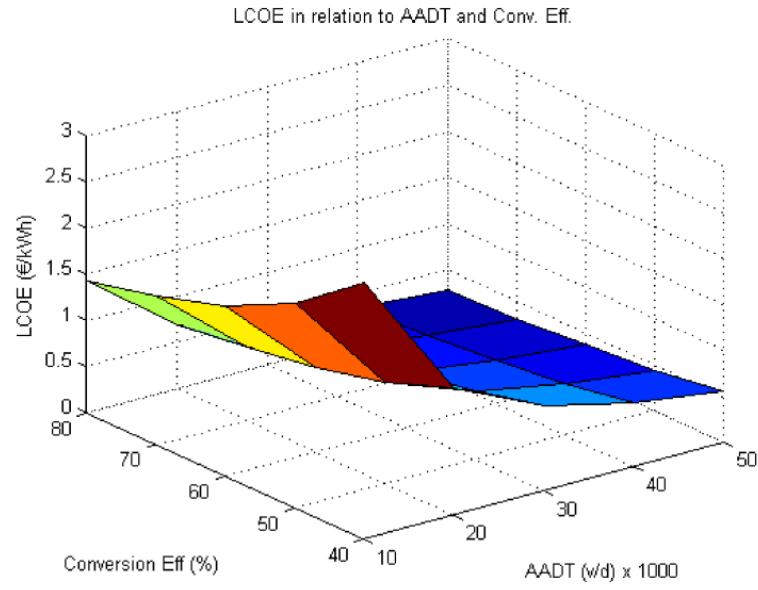


Figure 8.10- SA results for the simultaneous variation of the AADT and η to determine the: (a) LCOE and the (b) CF.

Analyzing the results, one can conclude that, as expected, the LCOE values decrease with the simultaneous increase of *AADT* and η , reaching for the tested values a minimum of 0.28 €/kWh, which might be considered enough for a technology launch, but still needs to be optimized to compete with other renewable energy sources. This can be achieved through the optimization of the *PPM* and *YMP*, through an industrial optimization process and a considerable market penetration that would lead to a decrease in production costs. Regarding the *CF*, it was also expected that this value would increase with the simultaneous increase of *AADT* and η , reaching for the tested values a maximum of 15%, which is considered competitive with other renewable energy sources. To increase this parameter, the best scenario would be the increase of the *AADT*, applying the RPEH system in places with higher *AADT* values.

8.4.3 Cost benefit analysis

The first energy application studied to perform a CBA on the RPEH system consists of a grid injection application and the values presented in Table 8.2 are used, with three changes resulting from the TEA: the *AADT* is increased to 30,000 vehicles per day, the η is increased to 60% and the *YMP* is reduced to 50 € per module. The obtained results are presented in Table 8.5 for two scenarios, with different periods: a 10-year study and a 15-year study. From these results one can conclude that, for the considered input data and for a 10-year study, the return of the investment is not positive, as although the return of capital is achieved after eight years, the *NPV* and the *IRR* are negative at the end of the period. However, when the study is extended to a 15 year period, the return of the investment becomes positive, but with a reduced *IRR*. In this study, one of the goals is to obtain positive viability for a 10 year period, so an SA is performed.

Table 8.5- Simulation results for a CBA on a GI application.

Variable	Period	10 years	15 years	Unit
		Value	Value	
Average annual income		7,593	7,995	(€)
Total income (period)		75,939	119,934	(€)
Total investment (period)		63,305	75,264	(€)
Total profits (period)		12,634	44,671	(€)
ROC		8.3	9.4	(Years)
NPV		-125,592	3,750	(€)
IRR		-27.9	1.8	(%)

For a 10-year study period, the SA for different *AADT* values considers 5 values from 10,000 to 50,000 vehicles per day on the two road lanes and its results are presented in Figure 8.11a for the three key indicators. The SA for different values of η considers 5 values from 40 to 80% and the results are presented in Figure 8.11b.

The SA for different *PPM* values considers 5 values from 500 to 1,500 € and its results are presented in Figure 8.11c. The SA for different *YMP* values considers 5 values from 20 to 100 € and its results are presented in Figure 8.11d. The SA for different *GIEP* values considers 5 values from 0.50 to 0.90 €/kWh and its results are presented in Figure 8.11e.

From the analysis of the SA results one can conclude that: the *ROC* decreases with the increase of the *AADT*, the η and the *GIEP* or with the decrease of the *PPM* and the *YMP*; the *NPV* and the *IRR* increase with the increase of the *AADT*, the η and the *GIEP* or with the decrease of the *PPM* and the *YMP*.

The two variables that present the greatest impact on the results are the *AADT* and the *GIEP*. So, an SA is performed for both variables simultaneously and the results obtained for the *ROC*, the *IRR* and the *NPV* are presented numerically in Table 8.6 and graphically in Figure 8.12.

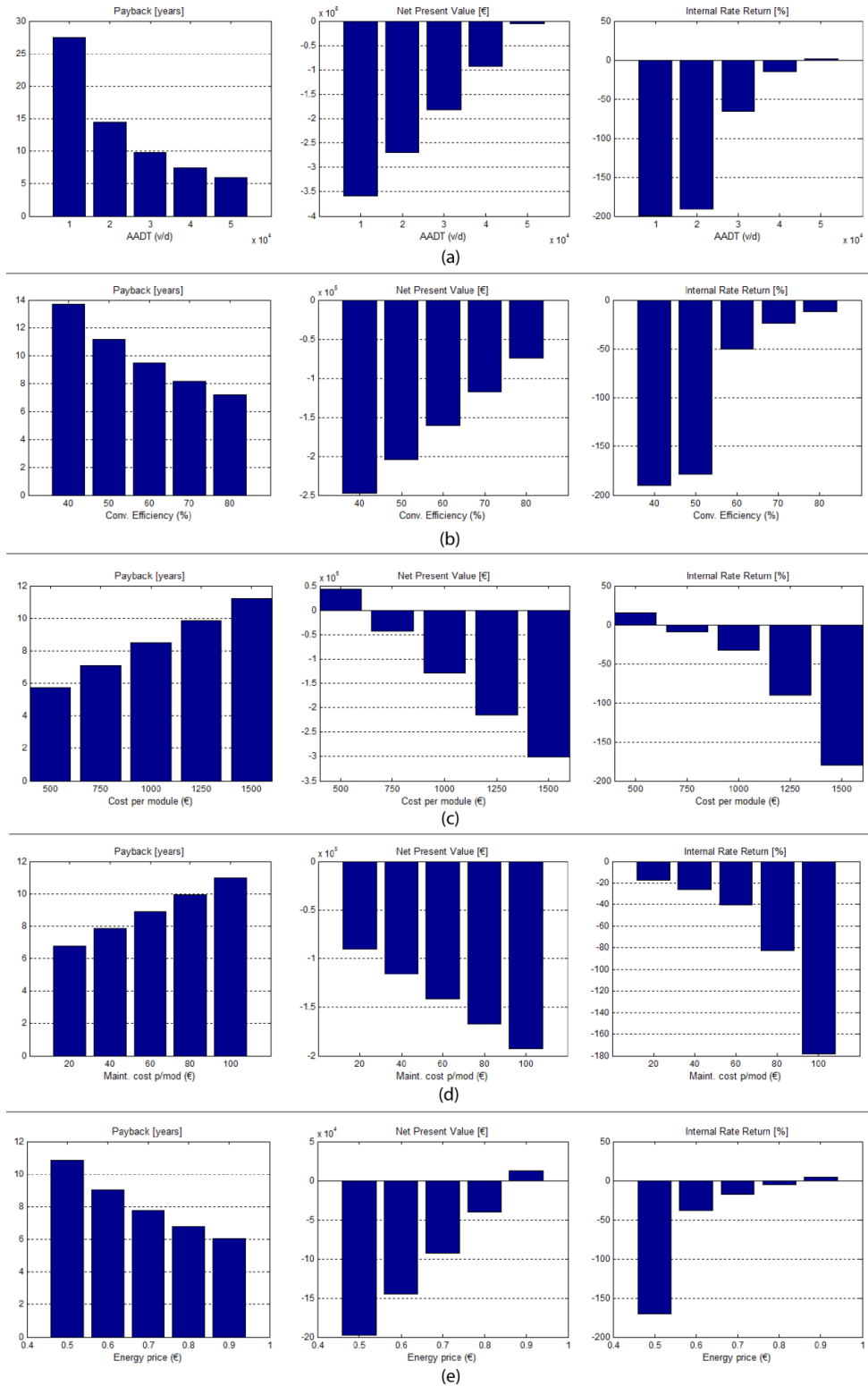


Figure 8.11- SA results of a CBA for a GI application, for the variation of the (a) AADT; (b) η ; (c) PPM; (d) YMP; (e) GIEP.

Table 8.6- Results of a multi-variable SA for a CBA to a RPEH system with a GI application.

AADT (v/d)	GIEP (€/kWh)	ROC (years)	NPV (€)	IRR (%)
10,000	0.5	32.5	-392,600	-200.1
	0.6	16.3	-298,970	-193.9
	0.7	10.8	-205,330	-172.5
	0.8	8.1	-111,700	-22.6
	0.9	6.5	-18,070	-1.5
20,000	0.5	27.1	-375,090	-199.2
	0.6	13.5	-262,730	-189.8
	0.7	9.0	-150,360	-39.6
	0.8	6.8	-38,000	-5.0
	0.9	5.4	74,360	12.6
30,000	0.5	23.2	-357,590	-198.2
	0.6	11.6	-226,500	-182.8
	0.7	7.7	-95,410	-17.9
	0.8	5.8	35,680	7.1
	0.9	4.6	166,790	24.7
40,000	0.5	20.3	-340,110	-197.1
	0.6	10.2	-190,300	-109.6
	0.7	6.8	-40,480	-5.5
	0.8	5.1	109,340	17.3
	0.9	4.0	259,150	36.1
50,000	0.5	18.0	-322,650	-195.9
	0.6	9.0	-154,110	-42.2
	0.7	6.0	14,430	3.9
	0.8	4.5	182,980	26.7
	0.9	3.6	351,520	47.6

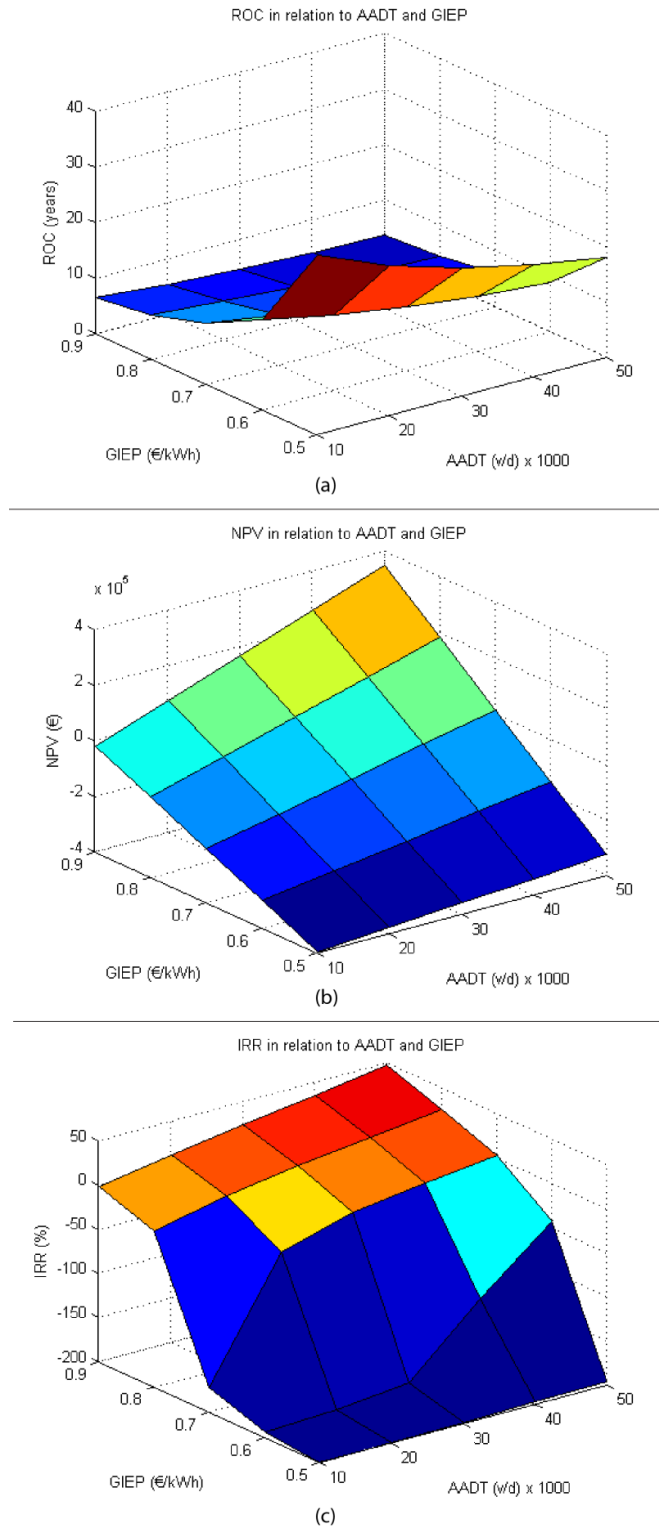


Figure 8.12- Results of a multi-variable SA for a CBA to a RPEH system with a GI application, for the (a) ROC; (b) NPV; (c) IRR.

Analyzing the results, one can conclude that, as expected, the *ROC* values decrease with the simultaneous increase of *AADT* and *GIEP*, reaching a minimum of 3.6 years for the tested values, which is considered very good for a technology launch and extremely competitive with other renewable energy sources. Additional optimizations can be performed, to the *PPM*, which will allow the *ROC* to be reduced. Regarding the *NPV* and the *IRR*, it was also expected that these indicators would increase with the simultaneous increase of *AADT* and *GIEP*, reaching a maximum of 351,520 € and 47.6%, respectively, for the tested values, which are very positive values for a 63,305 € investment. There are several scenarios where these indicators are considered positive, and others could become so by optimizing, for example, the *PPM*.

The second energy application studied to perform a CBA consists of a self-consumption application and the values presented in Table 8.2 are used, with an exception for the energy application values. Also, the *AADT* is increased to 30,000 vehicles per day and the η to 60%. Regarding the energy application, a *SCIP* of 3,500 W with a *SCAG* of 10 hours per day is considered. The considered *SCEP* is equal to the average EU energy price for the domestic sector, 0.22 €/kWh (Eurostat, 2017), with a *SCEI* of 2%.

The results for an SC energy application are presented in Table 8.7 for a 10-year period. From these results one can conclude that no indicator is positive, mainly due to the low value of the energy when compared with the investment made. Even after performing an SA and keeping the *SCEP* constant, no positive scenarios are verified. So, at the current energy prices, the application of RPEH systems for SC is not economically viable if these CBA parameters are considered.

Table 8.7- Simulation results for a CBA on a SC application.

Variable	Value	Unit
Annual energy consumption	12,775	(kWh)
Annual energy generation	11,682	(kWh)
RPEH system contribution	91.45	(%)
Average annual savings	2,814	(€)
Total period (period)	28,143	(€)
Total investment (period)	63,305	(€)
Total "profits" (period)	-35,162	(€)
ROC	22.5	(Years)
NPV	-355,430	(€)
IRR	-198	(%)

8.5 Summary and Conclusions

In this Chapter, a complete model for evaluating an RPEH system technically and economically was provided. Both the technical and economic analyses of renewable energy generation systems as well as their cost benefit analysis models are established and proven (Mathew, 2006; Bradford, 2008; Sorensen, 2011; Adaramola, 2014; Narbel *et al.*, 2014), with the values of the key parameters duly quantified and with the thresholds for positive viability defined. However, for new technologies under development, these models are not completely defined. Energy harvesting is a field which has recently gained the attention of both academia and companies and a set of new technologies are under development. RPEH is a field with some of these technologies under development and a model that allows proper technical and economic evaluation is needed.

The novelty of this Chapter lies in the definition of the complete model to evaluate an RPEH technically and economically, with all the technical and economic variables being presented, as well as the equations that allow all the key evaluation parameters to be determined, not only to perform a TEA, but also to perform a CBA for different energy applications. This model is applicable to different technologies that make use of the energy harvested from vehicles moving through the RPEH devices, allowing the

traffic and the RPEH system to be fully classified, considering piezoelectric, electromechanical, hydraulic and pneumatic technologies to be used in the presented model.

Then, a simulation software tool to evaluate RPEH applications both technically and economically, as well as for performing cost benefit analysis of the application of RPEH units on different energy applications was developed and presented.

The evaluation methodology proposed in this Chapter is based on existing methodologies for other renewable energy sources, with special emphasis on solar energy applications, being then adapted to RPEH systems. The simulation software tool also follows the analysis provided by other software that evaluates other energy sources, especially solar energy, allowing also sensitivity analyses to be performed to evaluate different values for user defined key variables.

From the case studies presented in this work one can conclude that there are specific conditions required for these technologies to achieve positive economic viability, and there is also a great dependency on the traffic affluence of the application spot. The *AADT* represents the most important variable to define the technical and economic viability of the RPEH system, as this parameter is directly related to the energy input into the system and from it results the total amount of generated energy and, consequently, the resulting economic value provided by the system. Other important variables with great influence on the viability of an RPEH system are the conversion efficiency of the technology, the price of each unit of the system and its maintenance costs. From the case studies one can also conclude that, for a grid injection scenario with a feed-in tariff being considered, an RPEH system can achieve positive economic viability with specific conditions, but for a self-consumption energy application, for the current average energy price in the European Union, no economic viability was achieved for the tested conditions.

8.6 References

- AASHTO (2001). *A Policy on Geometric Design of Highways and Streets*. American Association of State Highway and Transportation Officials, Washington, DC, USA.
- Adaramola, M. (2014). *Solar Energy: Application, Economics, and Public Perception*. CRC Press, Boca Raton, FL, USA.
- Alvarez, G., Jara, R., Julian, J. and Bielsa, J. (2009). *Study of the effects on employment of public aid to renewable energy sources*. Universidad Rey Juan Carlos, Madrid, Spain.
- Boccard, N. (2009). Capacity factor of wind power realized values vs. estimates. *Energy Policy*, 37(7): 2679-2688.
- Boomsma, T., Meade, N. and Fleten, S. (2012). Renewable energy investments under different support schemes: A real options approach. *European Journal of Operational Research*, 220(1): 225-237.
- Bradford, T. (2008). *Solar revolution: the economic transformation of the global energy industry*. MIT Press, Boston, MA, USA.
- Campoccia, A., Dusonchet, L., Telaretti, E. and Zizzo, G. (2014). An analysis of feed-in tariffs for solar PV in six representative countries of the European Union. *Solar Energy*, 107: 530-542
- Carley, S. (2009). State renewable energy electricity policies: An empirical evaluation of effectiveness. *Energy policy*, 37(8): 3071-3081.
- Diakoulaki, D. and Karangelis, F. (2007). Multi-criteria decision analysis and cost-benefit analysis of alternative scenarios for the power generation sector in Greece. *Renewable and Sustainable Energy Reviews*, 11(4): 716-727.
- Duarte, F., Champalimaud, J. and Ferreira, A. (2016). Waynergy Vehicles: an innovative pavement energy harvest system. *Proceedings of the Institution of Civil Engineers – Municipal Engineer*, 169(1): 13-18, <http://dx.doi.org/10.1680/muen.14.00021>.

- EEA (2017). *Climate change, impacts and vulnerability in Europe 2016 - An indicator-based report*. European Environment Agency, Copenhagen, Denmark. Available from: <https://www.eea.europa.eu/publications/climate-change-impacts-and-vulnerability-2016>. Accessed in June, 2017.
- Elvik, R., Vaa, T., Erke, A. and Sorensen, M. (2009). *The handbook of road safety measures*. Emerald, Bingley, UK.
- Eurostat (2017). http://ec.europa.eu/eurostat/statistics-explained/index.php/Energy_price_statistics. Accessed in June, 2017.
- Frondel, M., Ritter, N., Schmidt, C. and Vance, C. (2009). *Economic Impacts from the Promotion of Renewable Energy Technologies - The German Experience*. RUB, Bochum, Germany.
- GRHYSO (2017). <http://www.unizar.es/rdufo/grhyso.htm>. Accessed in January, 2017.
- Haas, R., Eichhammer, W., Huber, C., Langniss, O., Lorenzoni, A., ..., and Schleich, J. (2004). How to promote renewable energy systems successfully and effectively. *Energy Policy*, 32(6): 833-839.
- Harb, A. (2011). Energy Harvesting: State-of-the-art. *Renewable Energy*, 36(10): 2641-2654.
- HOGA (2017). <http://hoga-renewable.es.tl/>. Accessed in January, 2017.
- HOMER (2017). <http://www.homerenergy.com/>. Accessed in January 2017.
- HYBRID2 (2017). <https://www.umass.edu/windenergy/research/topics/tools/software/hybrid2>. Accessed in January, 2017.
- IEA (2015). *World Energy Outlook Special Report on Energy and Climate Change*, International Energy Agency, Paris, France. Available from: <https://www.iea.org/publications/freepublications/publication/WEO2015SpecialReportonEnergyandClimateChangeExecutiveSummaryUKversionWEB.PDF>. Accessed in June, 2017.
- IEA (2016). *Key world energy statistics 2016*, International Energy Agency, Paris, France. Available from:

<https://www.iea.org/publications/freepublications/publication/KeyWorld2016.pdf>.

Accessed in June, 2017.

INSEL (2017). <http://www.insel.eu/index.php?id=301&L=1>. Accessed in January, 2017.

Joskow, P. (2011). Comparing the costs of intermittent and dispatchable electricity generating technologies. *The American Economic Review*, 101(3): 238-241.

Kazmierski, T. and Beeby, S. (Eds.). (2009). *Energy harvesting Systems - Principles, Modeling and Applications*. Springer, New York, NY, USA.

Khaligh, A. and Onar, O. C. (2010). *Energy harvesting: solar, wind, and ocean energy conversion systems*. CRC Press Inc., Boca Raton, FL, USA.

Khatib, H. (2010). Review of OECD study into “Projected costs of generating electricity—2010 Edition”. *Energy Policy*, 38(10): 5403-5408.

KPMG (2015). *Taxes and incentives for renewable energy*. KPMG International Cooperative, Amstelveen, Netherlands.

Lewis, J. and Wiser, R. (2007). Fostering a renewable energy technology industry: An international comparison of wind industry policy support mechanisms. *Energy policy*, 35(3): 1844-1857.

Luckow, P., Stanton, E., Fields, S., Biewald, B., Jackson, S., Fisher, J. and Wilson, R. (2015). *Carbon Dioxide Price Forecast*. Synapse Energy Economics, Cambridge, MA, USA.

Mathew, S. (2006). *Wind energy: fundamentals, resource analysis and economics, vol. 1*. Springer, Heidelberg, Germany.

Narbel, P., Hansen, J. and Lien, J. (2014). *Energy technologies and economics*. Springer, Cham, Switzerland.

Polysun (2017). <http://www.polysunonline.com/PsoPublic/app/home/access>. Accessed in January, 2017.

Portal Energia (2017). <http://www.portal-energia.com/microgeracao-em-portugal/>. Accessed in June, 2017.

Priya, S., and Inman, D. J. (Eds.) (2009). *Energy harvesting technologies*. Springer, New York, NY, USA, vol. 21.

PV*SOL (2017). <http://www.valentin-software.com/en/products/photovoltaics/57/pvsol-premium>. Accessed in January, 2017.

- Reiche, D. and Bechberger, M. (2004). Policy differences in the promotion of renewable energies in the EU member states. *Energy policy*, 32(7): 843-849.
- RETSscreen. <https://www.nrcan.gc.ca/energy/software-tools/7465>. Accessed in January, 2017.
- Schmalensee, R. (2012). Evaluating policies to increase electricity generation from renewable energy. *Review of Environmental Economics and Policy*, 6(1): 45-64.
- Sinha, S. and Chandel, S. (2014). Review of software tools for hybrid renewable energy systems. *Renewable and Sustainable Energy Reviews*, 32: 192-205.
- SOLergo (2017). <http://hiperenergy.com.br/idc-portfolio/solergo/>. Accessed in January, 2017.
- Solterm (2017). <http://www.Ineg.pt/iedt/projectos/370/>. Accessed in January, 2017.
- Sorensen, B. (2011). *Renewable Energy: Physics, Engineering, Environmental Impacts, Economics & Planning*. Elsevier, Burlington, MA, USA.
- The World Bank (2017). *Leaders Step Up To Double the Wave on Carbon Pricing*. The World Bank, Washington, DC, USA. Available from:
<http://www.worldbank.org/en/news/feature/2017/01/17/leaders-step-up-to-double-the-wave-on-carbon-pricing>. Accessed in June, 2017.
- TRB (2000). *Highway Capacity Manual*. Transportation Research Board, Washington, DC, USA.
- TRNSYS (2017). <http://www.trnsys.com/>. Accessed in January 2017.
- Windsim (2017). <https://windsim.com/>. Accessed in January 2017.
- Yildiz, F. (2009). Potential ambient energy-harvesting sources and techniques. *Journal of Technology Studies*, 35(35): 40-48.

Chapter 9

Summary, Conclusions and Future Work

9.1 Summary and Conclusions

Over the last two centuries, our planet has witnessed three industrial revolutions that completely changed the way we live. The first industrial revolution used water and steam power to mechanize production. The second used electric power to promote mass production. The third used electronics and information technology to automate production. Now, a fourth industrial revolution is building on the third, the digital revolution, which has been going on since the middle of the last century. It is characterized by a fusion of technologies that is combining the physical, digital, and biological spheres (The World Bank, 2017).

This new industrial revolution will significantly alter the way we live, work, and relate to each other. Due to its scale and complexity, this change will have a greater impact on society than the previous industrial revolutions, and its effects are not known yet.

However, one thing that can be learnt from the previous industrial revolutions is that the planet was not respected during any of them. With all industrial revolutions, a great increase in the consumption of the planet's resources was verified, reaching an

unsustainable point in which mankind is consuming more resources than those the planet can provide year after year (WWF, 2017).

Energy, and in particular electrical energy, is one of the resources for which there has been a great increase in demand, and whose production has one of the most negative impacts on the environment, as almost 80% of the energy production comes from fossil fuels (IEA, 2016).

The transition that is about to happen must be built on more sustainable and environmentally friendly pillars so that it does not compromise the future of our planet and, consequently, our existence.

One of the key areas for ensuring a more sustainable planet is to change the paradigm for the production of electrical energy. Energy production must be based on renewable resources, decentralized, happen near to the point of consumption and, preferably, when it is needed. To achieve this goal, a combination of multiple energy sources will be needed, and every potential energy source that can be converted effectively into electrical energy should be used.

Renewable energy sources such as solar, wind and hydro have been developed in recent decades and have already reached a stage of maturity. Biomass and ocean energy have also been explored in the last few years and some technologies are being implemented on a considerable scale.

However, there are a number of other sources of energy that have not been exploited much and which, in specific places, would provide great potential for use and can significantly contribute to the promotion of self-sustaining electrical equipment. To accomplish this, energy harvesting has recently been adopted on a micro-scale, where it is possible to generate electrical energy from small energy variations, such as thermal gradients, pressure, vibrations, radiofrequency or electromagnetic radiation, among others (Khaligh and Onar, 2010).

Road pavements are continuously exposed to vehicle loads and, from this, it is possible to extract energy which, using specific technologies and equipment, can be converted

into electrical energy and supply the electrical devices near the road, such as public illumination, traffic lights, sensors and cameras, among others. Such devices are called RPEH devices.

In the last 15 years or so, several technologies have been developed in this field, but none have been successful to the extent that they have entered the market. The main goal of this research was the development of a new technology to convert mechanical energy from vehicles into electrical energy, which would be implemented in the road pavement to make use of a source of energy which is typically wasted.

Before the development of a new technology to be used in RPEH devices, a state-of-the-art study was performed, presented in Chapter 2, so that the existing technologies could be identified and evaluated, in order to draw some conclusions regarding their positive and negative aspects, and understand what should be done differently to succeed. In this study, not only were RPEH technologies analyzed, but also technologies for harvesting railway energy, since both are related to infrastructure applications and both make use of vehicles' mechanical energy to produce electrical energy.

From this study it was possible to conclude that several technologies have successfully achieved TRL 5, with a prototype validation in a relevant environment, but when they were implemented in a real environment most failed. One of the main reasons for this is related to the vehicle loads delivered to the device's surface, which were higher than expected and led to component failure.

The problem that was identified in these studies is related to a lack of understanding about how the vehicle's wheels interact with the RPEH device's surface, how loads are applied and how the vehicle's mechanical energy is delivered. With this in mind, it was decided that prior to the development of the new technology, a detailed study had to be performed to evaluate the VRI and to quantify the loads and energy delivered from vehicles to the pavement or an equipment applied in the pavement' surface precisely.

Also, from the state-of-the-art study, it was possible to analyze which are the most promising technologies and those which have achieved better results for both energy generation and energy conversion efficiency. In this field, electromechanical systems present the highest values, while hydraulic systems, despite slightly lower results, showed good potential for harvesting vehicle energy in multiple points and use only one electrical generator to convert all the mechanical energy into electrical energy. So, both types of systems should be considered and carefully evaluated when a new solution is designed.

The state-of-the-art evaluation contributed to a deeper understanding of the existing technologies both for RPEH and railway energy harvesting and their stage of development, and has introduced new concepts for the classification of systems, especially for different electromechanical devices, classifying them according to their input and output motion type. Also, the identification of the installation method has improved the existing knowledge of these types of technologies.

Based on the conclusions from Chapter 2, a detailed VRI study was performed in Chapter 3, identifying the most common vehicle models used in the literature, namely the quarter-car and bicycle-car models, and how loads are applied to the pavement surface. However, these models were unable to fully define the interaction of a moving vehicle and a RPEH device with a moving surface, as they are only related to the vehicle and do not take into account the changes in the vehicle's dynamics caused by the movement of the surface of the RPEH device. Taking this into account, two new models were developed to consider the interaction between a moving vehicle and a RPEH device with a moving surface, as presented in Chapter 3.

Typically the VRI models do not consider the tyre contact patch, as they consider only a resultant force applied on the pavement surface. For a typical VRI analysis, this approach is not incorrect, as the tyre contact patch is permanently in contact with the pavement surface, but when the interaction is related to a moving tyre and a specific surface, separated from the pavement surface, this common approach is not correct, as the tyre's contact patch does not establish total contact with the surface immediately,

but rather it makes progressive contact while the wheel is moving forward. This means that the tyre's force is progressively applied to the surface, as the tyre's contact patch establishes contact with it, and this has a huge impact on the quantification of the load applied to the surface of a RPEH device. As so, in Chapter 3 the equations are presented that allow the contact patch to be integrated into the vehicle dynamics models with a moving surface, allowing us to have more detailed and complete models to perform the evaluation of the interaction of a vehicle and a RPEH device.

Based on the developed models, a new software tool was developed and presented in Chapter 3, named RoadVISS, that allowed users to study the forces induced by a vehicle in motion onto the road pavement, an SRE or an RPEH device, as well as the energy lost by the vehicle, associated to the contact with the surface, and the energy received by that surface. This software tool was developed in MATLAB[®] environment, including a GUI where the user can select and define all the variables associated to the simulation, and another GUI where the results are presented. The software has an extensive database of considered variables, allowing a huge number of different combinations of values to be simulated, which means a great number of studies can be performed. The outputs of the system are focused on the forces and energy released by the vehicle and received by the pavement or by RPEH device' surface, but the computational model allows users to define new outputs and study other variables.

The existing software tools, mainly ADAMS[®] (MSC.Software, 2017) and AUTOSIM[®] (Carsim, 2017), already allow users to select all the vehicle characteristics and motion conditions, but the main differences of the developed software are evident: it allows us to obtain energetic outputs, select the pavement/SRE/RPEH device characteristics, dimensions and material, in a way that no other software tools do, and to compare the output, for both the vehicle and the pavement parameters, together or separately. The development of this software tool was a key milestone in the development of the remaining project as it allows us to have a more detailed and precise quantification of the loads and energy delivered from the vehicles' wheels to the RPEH surface and to have more realistic values during the project development stage of the RPEH device.

Using RoadVISS, a detailed study was performed of the interaction of different vehicles with equipment with a movable surface applied in the road pavement. This study has allowed us to come to conclusions not only about the energy lost by the vehicle and harvested by the equipment, but also about the low vertical acceleration induced to the vehicle body. Relating the achieved results with the international scale for the discomfort induced to the vehicle occupants by SRE, defined by ISO 2631-1 (ISO, 1997), it was possible to identify an opportunity to reduce the vehicle's speed by kinetic energy harvesting using a device applied in the road pavement surface, without affecting the ride comfort of the vehicle's occupants.

This conclusion led to a specific research goal of developing a solution to effectively contribute to the road safety promotion, by reducing the vehicle's speed without the need for driver action, such as breaking, and without affecting the ride comfort. Therefore, in Chapter 4 a study was conducted to optimize the energy extraction from vehicles with a minimum impact on ride comfort to promote road safety. In this Chapter, typical SRE equipment was studied and evaluated, allowing us to conclude that these devices induce extremely high levels of discomfort to the vehicle's occupants if the driver does not brake before reaching the device, but do not extract significant amounts of energy to the vehicles. Then, a new SRE was developed, with the physical models of the proposed solution being presented and incorporated into the RoadVISS software, allowing the user to perform computational simulations and evaluate their performance. It was concluded that this new solution is able to extract 81% more energy than a standard SRE, with 87% lower impact on the vehicle body for similar scenarios.

A prototype of the proposed solution was developed and tested, allowing us to get experimental results of its performance. From the analysis of results and the comparison between computational simulations and experimental results, it was possible to conclude that there is a small difference between the two of under 20% on average, which is a very satisfactory result, considering that the computational models include several vehicle parameters that we were not able to quantify precisely.

Considering the results achieved for the system presented in Chapter 4, we consider that the proposed solution may be effective in promoting road safety and is attractive both for the users (drivers) and beneficiaries (mainly pedestrians, but vulnerable road users in general), and there is great potential for application in the real world. With the developments in this thesis, the solution has reached TRL5, as the technology was validated in a relevant environment.

Following this study, and considering it as the first application of RoadVISS, the development of a RPEH device came next. The first novelty presented in this development was the approach that was defined and the methodology. The use of forces, kinematic and dynamic analysis, combined with an energetic analysis applied to all the device's components allowed us to identify the performance of each element and its impact on the end results of the entire system, so each component could be optimized and the efficiency of the entire system maximized. None of the existing studies in the literature, seen in Chapter 2, had implemented this methodology, which led to non-optimized systems.

This methodology was first applied to the most common electromechanical systems, namely the RAP system and the lever system, with these being modelled and then included in the software previously developed, allowing a new and more advanced software tool to be created for the development of RPEH devices. The results of the simulations for these systems agreed with the values of the systems evaluated in Chapter 2, allowing the models and the software to be considered accurate.

In Chapter 5, a new electromechanical system to implement in RPEH devices was presented. The development of this system was performed taking into account the limitations of the typical systems, in which the transmitted load and motion are physically limited by each other. The goal was to devise a system in which this relation was not direct, and in which the transmitted force could be maximized, while the displacement of components was not affected in direct proportion. To achieve this goal, a crank to slider system was proposed and its physical models were defined and included in the software tool. Several computational simulations were performed and,

based on the achieved results, several conclusions were drawn. The main conclusions in relation to typical electromechanical systems are that the new mechanical system proposed is the most efficient system regarding the mechanical energy transmission as, for the same pinion radius, it can double the efficiency of the RAP system which, in turn, is more efficient than the lever system. The maximum theoretical efficiency of the new proposed system is 74.3%, a much higher value than all systems studied and evaluated in Chapter 2.

After this validation, a prototype was developed and tested in a relevant environment, so that experimental results could be achieved and compared with the computational simulations results. During the prototype design some changes to the initial version of the system were made to avoid and prevent possible problems, but these led to an increase in the number of components which led to more energy loss. Some of the selected components have also proven to have higher friction coefficients than originally defined, inducing higher energy losses.

The experimental results were not as satisfactory as expected for the lower vehicle speed scenarios (20, 30 and 40 km/h), and there was a considerable difference in the electrical energy generation results. However, for the higher value of vehicle speed (50 km/h), the experimental results were closer to the computational simulation results, with the average difference being 11.9%, a very satisfactory result. For the 50 km/h tested scenarios, the maximum energy conversion efficiency of the device, from the mechanical energy harvested by the device's surface to the electrical energy generated and delivered to the electrical load was 60.5%, a value higher than all existing systems studied in Chapter 2, which proves that the proposed system has the potential to be more efficient than existing solutions. However, further developments should be made to increase the efficiency of the system for the lower vehicle speeds and to improve the global efficiency of the device, taking into account its theoretical energy conversion efficiency of higher than 70%.

Thinking of a possible product development in the future, this solution also has other technical advantages compared to the existing solutions studied in Chapter 2, as it is

smaller, which makes the installation process in the road pavement easier, and it is made of mainly high density and resistant plastic, a material that can be produced much more cheaply than iron and aluminium, the core materials typically used in the RPEH devices studied in Chapter 2. Altogether, this solution has more chance of breaking into the market than all the other solutions, as it is more efficient, simpler to install and costs less.

Although the achieved results with the RPEH device based on an electromechanical system were satisfactory, especially the computational simulations results, all electromechanical systems have one limitation in common - to keep the maximum efficiency of the system they all use one electromagnetic generator for each mechanical system, which may increase the total cost of a solution with multiple devices. This is where a hydraulic system may have an economic advantage as multiple hydraulic units can be connected to a single electromechanical converter.

A technical evaluation of typical hydraulic systems used in RPEH devices was conducted using the same methodology as used in the electromechanical systems, and the most common hydraulic system was modelled physically, and the model was incorporated in the software tool developed previously. The computational simulation results were examined in order to compare them with the study performed in Chapter 2, proving that a typical hydraulic system was not more efficient than an electromechanical system, as it has a maximum energy conversion efficiency of only 39.3%.

A new hydraulic system with a mechanical actuation was presented in Chapter 6, combining the electromechanical system presented in Chapter 5 with common hydraulic systems, to evaluate the performance of the combined system. The physical models of the solution were presented and integrated in the software tool, allowing us to perform computational simulations for the same scenarios as the previous systems. From the computational simulation results it was possible to conclude that this system can achieve a maximum energy conversion efficiency of 73.5%, a value close to the 74.3% of the electromechanical system, proving that a combined solution of a hydraulic system

with a mechanical actuation has the potential both technically and economically to be the best solution in the RPEH field. Experimental validation is needed to confirm these values, which is one of the next steps of the research.

Besides the connection of multiple devices to a single electromechanical converter, a hydraulic system also offers the possibility of storing the mechanical energy harvested from vehicles, transmitted through the mechanical and hydraulic system in the form of pressure, and actuating the electromechanical unit only when needed, thus increasing the number of potential applications of the electrical energy produced, especially at night.

In Chapter 7, a MES in the RPEH device based on hydraulic systems was included, and both a standard and the new proposed hydraulic system with mechanical actuation were studied. Following the same methodology as with the previous developments, the physical models of the MES systems were presented, as well as the complete models of the hydraulic systems with the proposed MES. These models were then integrated in the software tool and computational simulations were performed. The inclusion of a MES in a typical hydraulic system allows the global efficiency of the device to be increased to 43.0%, but it does not increase the efficiency of the hydraulic system with mechanical actuation, which has a maximum efficiency of 66.2%, lower than the 73.5% efficiency of the same system without storage. However, although the global efficiency of the system is decreased, the global efficiency of the system with MES is still higher than all existing solutions studied in Chapter 2, and the lower cost of this solution may compensate the lower efficiency of the device. Experimental validation is needed to confirm these values, which is one of the next steps of the research.

From Chapters 4 to 7, several technical developments were made leading to the development of four new solutions, one to promote a more effective speed reduction of vehicles without any driver action, one that consists of a RPEH device based on an electromechanical system, one that consists of a RPEH device based on a hydraulic system with a mechanical actuation without energy storage and another that is similar to the previous one but which includes a MES system. The first two solutions were

validated through prototypes and experimental tests, while the last two solutions were only evaluated based on computational simulations using the developed software. All the proposed solutions have presented better results than the state-of-the-art in their respective fields and have great potential for success in the future.

Besides the systems presented, the methodology used was also innovative and it can be used in other areas of research, especially related to the development of energy generation systems, as it allows researchers to identify the optimal characteristics of each component of the system.

Finally, following all the technical developments, in Chapter 8 a complete model to perform a technical and economic evaluation of RPEH applications was defined. Based on this model, a new software tool was created, called RETEES, and based on this tool several analyses were conducted to evaluate different applications. These analyses include both a TEA of a RPEH system, a CBA and also a SA, by changing the values of the most critical variables to define their impact on the achieved results.

The developed software tool has proved to be very useful in the technical and economic evaluation of RPEH applications, allowing us to understand the impact of each variable in the results. It is an important tool for defining the required traffic values for an application to be viable or for defining the production costs of the system so that it can be made viable, in relation to its energy generation potential. It can also be used by the potential users of RPEH devices to evaluate the economic benefits that can be achieved by investing in such solutions, or to define how many RPEH devices they need to implement in an application so that it can become completely energetically self-sufficient.

9.2 Future work

Three software tools were developed in Chapters 3, 5 and 8, one for the VRI analysis and the evaluation of the energy transfer from vehicles to the road pavement surface of specific devices applied on its surface (RoadVISS); one to evaluate the performance of RPEH devices from an energetic perspective and another to evaluate RPEH applications technically and economically (RETEES). All these solutions have been tested and some validations were made, but all can be improved and further developments should be performed.

First, the validation of vehicle parameters in the RoadVISS software tool can be improved through experimental tests with sensors applied in the vehicle body to compare the simulations results with experimental data. The developed models are validated for two-axle light vehicles. Additional developments will be performed to include multiple-axle light vehicles and heavy vehicles on the models, allowing the software applications and studies to be expanded.

Secondly, the upgraded version of RoadVISS, for the development of RPEH devices, has great potential to include more RPEH systems and components, not only electromechanical or hydraulic ones, but any type of technology that makes use of a vehicle's mechanical energy as an energy source. More experimental tests are needed to validate the performance of the hydraulic system, which should also include validating the hydraulic system with mechanical actuation presented in Chapter 6, as well as the same system with a MES unit presented in Chapter 7.

Thirdly, the RETEES software tool presented in Chapter 8 can also be used to perform TEA and CBA with other RPEH technologies, and the models can also be integrated with other existing software to evaluate different renewable energy sources technically and economically, so that RPEH systems can be considered as an alternative for electric energy production, especially in urban environments, where energy consumption continues to increase and more energy will be needed in the years to come with the growth of the electric mobility market. The RETEES software tool can also be upgraded

with new equations to determine the traffic distribution among several road lanes with better precision, as well as to adjust the maintenance costs to the traffic.

Regarding the four systems presented in this thesis, all have the potential for further developments, each with a different approach.

The system presented in Chapter 4, to be applied as a SRE, was successfully validated through a prototype in a relevant environment, allowing us to assume that a TRL 5 stage was achieved. However, more validations should be done. The next steps of this research work will consist of implementing a monitoring system in the vehicle, so that the vertical acceleration induced in the vehicle body can be measured, as well as enabling us to quantify the energy lost by the vehicle, allowing us to draw conclusions about the device's efficiency and the ride quality of the vehicle's occupants. Some developments should also be performed to prepare the system to resist to breaking actions from the vehicle and to water and snow conditions.

After this, a real scale pilot plant in an operational environment, such as an urban road, should be implemented to evaluate the system performance with several meters in the pavement and with real traffic.

Regarding the RPEH device based on an electromechanical system presented in Chapter 5, which presented a much higher energy conversion efficiency in relation to all existing RPEH systems studied in Chapter 2, based on the computational simulations performed, the developed prototype has only presented positive results for a vehicle speed of 50 km/h. So, further developments should be made to validate the simulation results for all the tested speeds and to conclude the experimental validation. Beside these improvements in the prototype, a monitoring system should also be implemented in the vehicle so that the vertical acceleration induced in the vehicle body can be measured, as well as making it possible to quantify the energy lost by the vehicle, allowing us to reach conclusions on the device's efficiency and the ride quality of the vehicle's occupants. As for the previous system, some developments should also be performed to prepare the system to resist to vehicle' breaking actions, as well as to resist to water and snow conditions.

After these validations and achieving TRL 5, the implementation of a real scale pilot plant in an operational environment, such as an urban road, will be performed to evaluate the system's performance with several meters implemented in the pavement and with real traffic.

Also, with the prototype construction and achieved results, an economic evaluation will be performed, allowing us to draw conclusions about the economic viability of the system, using the RETEES software tool, presented in Chapter 8.

Both the RPEH device based on a hydraulic system with a mechanical actuation presented in Chapter 6, and the same system with a MES unit presented in Chapter 7, have revealed a much higher energy conversion efficiency value than typical hydraulic systems, showing great potential for application in the real world. However, both systems were only validated through computational simulations and further research should be conducted to perform experimental validations. So, the next step of this research work will consist of designing and constructing a prototype of each system in order to test them in the laboratory and in a relevant environment and obtain experimental results. These will be compared to the theoretical results achieved by the computational simulations and will allow us to come to conclusions about the technical viability of these systems.

Based on the technical and economic data of the developed prototype, a TEA and a CBA can be performed, using the RETEES software tool presented in Chapter 8, allowing us to reach conclusions about the economic viability of these solutions.

With these systems developed and validated, a specific installation process in the road pavement should be designed. The four systems were designed to be as flat as possible, so that installation can be simple and avoid digging a huge hole in the pavement for the devices. However, a specific installation design should be developed, considering multiple assumptions: it should be simple and fast, have a minimum impact on the existing pavement and require a minimum amount of resources. It should take into account pavement engineering rules and respect the existing pavement design, so that it will not affect the pavement surrounding the RPEH device after its installation.

To sum up, the total or partial accomplishment of the research lines suggested above will provide more detailed validations of the systems developed in this thesis, increase the TRL of all systems and take them to a pre-market entrance stage. Ultimately, the accomplishment of these activities combined with an industrial development process will lead to the creation of innovative solutions in road safety, energy harvesting and smart cities, which, if successful, could be applied worldwide, contributing to a more sustainable planet, more cost-effective and self-sufficient electrical applications and to decrease the number of fatal accidents on the road, promoting road safety more effectively.

9.3 References

- Carsim (Mechanical Simulation Corporation) (2017). <http://www.carsim.com>. Accessed in July, 2017.
- IEA (2016a). *Key world energy statistics 2016*, International Energy Agency, Paris, France. Available from: <https://www.iea.org/publications/freepublications/publication/KeyWorld2016.pdf>. Accessed in June, 2017.
- ISO (1997). *Mechanical vibration and shock - Evaluation of human response to whole-body vibration. Part I: General requirements*. ISO 2631-1, Geneva, Switzerland.
- Khaligh, A. and Onar, O.C. (2010). *Energy Harvesting: Solar, Wind, and Ocean Energy Conversion Systems*. CRC Press Inc, Boca Raton, FL, USA.
- MSC.Software (Adams) (2017). <http://www.mscsoftware.com/product/adams>. Accessed in July, 2017.
- The World Bank (2017). *The Fourth Industrial Revolution: what it means, how to respond*. The World Bank, Washington, DC, USA. Available from: <https://www.weforum.org/agenda/2016/01/the-fourth-industrial-revolution-what-it-means-and-how-to-respond/>. Accessed in July, 2017.

WWF (2017). *Planning to succeed - how to build strong 2050 climate and energy development strategies*. World Wide Fund For Nature (WWF), Gland, Switzerland. Available from:
http://wwf.panda.org/about_our_earth/all_publications/?302651/Planning-to-Succeed---how-to-build-strong-2050-climate-and-energy-development-strategies#. Accessed in July, 2017.